

**Dynamic response of width- and thickness-tapered composite beams using Rayleigh-Ritz method and modal testing**

Vijay Kumar Badagi

A Thesis

In

The Department

Of

Mechanical and Industrial Engineering

Presented in Partial Fulfillment of the Requirements  
For the Degree of Master of Applied Science (Mechanical Engineering) at  
Concordia University  
Montreal, Quebec, Canada

September 2012

© Vijay Kumar Badagi, 2012

**CONCORDIA UNIVERSITY**

**SCHOOL OF GRADUATE STUDIES**

This is to certify that the Thesis prepared,

By: **Vijay Kumar BADAGI**

Entitled: **“Dynamic response of width- and thickness-tapered composite beams using Rayleigh-Ritz method and modal testing”**

and submitted in partial fulfillment of the requirements for the Degree of

**Master of Applied Science (Mechanical Engineering)**

complies with the regulations of this University and meets the accepted standards with respect to originality and quality.

Signed by the final Examining Committee:

\_\_\_\_\_ Chair  
Dr. M. Paraschivoiu

\_\_\_\_\_ Examiner  
Dr. S. V. Hoa

\_\_\_\_\_ Examiner  
Dr. R. Soleymani (External)

\_\_\_\_\_ Supervisor  
Dr. R. Ganesan

Approved by:

\_\_\_\_\_  
Dr. N.R.Sivakumar, MSc Program Director  
Department of Mechanical and Industrial Engineering

\_\_\_\_\_  
Dean Dr. Robin Drew  
Faculty of Engineering & Computer Science

Date: \_\_\_\_\_

## ABSTRACT

### **DYNAMIC RESPONSE OF WIDTH- AND THICKNESS-TAPERED COMPOSITE BEAMS USING RAYLEIGH-RITZ METHOD AND MODAL TESTING**

Vijay Kumar Badagi

Tapered composite beams formed by width-taper or by terminating or dropping-off some of the plies from the primary structure provide high stiffness to weight ratios, high modulus to weight ratios, damage tolerance and design tailoring capabilities. Since they are increasingly and widely being used in a variety of engineering applications such as robot arms, lightweight mechanical components, aircraft wings, space structures, helicopter blades and yokes, turbine blades, and civil infrastructures, it is important to ensure that their design is reliable and safe. Study of the dynamic response of the tapered composite beams helps to optimize the design and avoid future investments on repairs. It is, therefore, essential for design engineers to evaluate the dynamic characteristics of tapered composite beams effectively. In the present study, symmetric width-tapered and thickness- and width-tapered laminated composite beams are considered and their free and forced vibration response and the buckling response of tapered composite columns are investigated. Due to the variety of tapered beam configurations and the complexity of partial differential equations that govern their free and forced vibration response and their buckling response, no closed-form analytical solution can be obtained. Therefore, Rayleigh-Ritz method is used based on Kirchhoff one-dimensional laminated beam theory and the efficiency and accuracy are established very systematically. Width-tapered laminated composite beam samples are manufactured using NCT-301 graphite-epoxy

composite material. Experimental modal analysis using impact hammer testing is conducted for the determination of coherence function, time and auto-response function and Frequency Response Function (FRF) of width-tapered laminated composite beams. The natural frequencies obtained from experimental modal analysis are validated with that obtained Rayleigh-Ritz method. A detailed parametric study is conducted to investigate the effects of width ratio, taper configuration, taper angle, length ratio, boundary conditions, laminate configurations, static end-axial force, and damping on dynamic response. Free and forced vibration response results obtained using Rayleigh-Ritz method are also compared with that obtained using conventional finite element formulation in a separate but simultaneous study.

## **ACKNOWLEDGEMENT**

It is a great pleasure to thank many people who made this thesis possible.

First and foremost, I would like to thank my parents Mr. Prabhakar and Mrs.Savitri Prabhakar and my family members for all their love, encouragement and support to pursue my Masters degree.

Then, I offer my sincerest gratitude to my supervisor, Dr Rajamohan Ganesan, who has supported me, throughout my thesis research with his enthusiasm, inspiration, patience and immense knowledge. Throughout my thesis-writing period, he provided encouragement, sound advice, good teaching, and lots of good ideas.

I am grateful to Dr. S.V. Hoa for his support during the manufacturing of composite samples at Concordia Centre for Composites (CONCOM). I am thankful to Dr. Subhash Rakheja who supported me with the experimental equipments. I would also like to thank Dan Juras, Dr. Ming Xie, Heng Wang, Robert Oliver, Farjad Shadmehri and Ali Naghashpour for their time and guidance during my experimental work. I would like to thank the administrative staff at the Department of Mechanical and Industrial Engineering for their support.

I am thankful to National Research Council Canada (CNRC) and Dr. Alain Blouin at the CNRC who provided support in NDT inspection of the composite laminate.

I wish to thank my friends Dinesh Masilamani, Lakshmish Kowshik, Ramdas Satyan, Arunchandra, Swaroop Visweswaraiyah, Kshama Nargund, Krishnaprasad Balike, Anand Pranesh, Vasudevan Rajamohan, Balasubramanian Esakki, Nanduri Prasad Rao, Abhijit Dasgupta, Ashok Kaushal and Avinash Hebbar for all the support and caring they provided during my thesis research. My grateful thanks to Indrani Gorti for her support and encouragement provided to me during my thesis research.

I am thankful to all my friends at graduate research office EV 13.167 who supported me by sharing ideas and discussion during my research studies.

I gratefully acknowledge the funding sources for my Masters Thesis provided by the NSERC and Concordia University.

Thank You.

*Dedicated to*

## SHRI GAYATRI

ओम् । भूर्भुवस्सुवः । तत्सवितुर् वरेण्यम् ।  
भर्गो देवस्य धीमहि । धियो यो नः प्रचोदयात् ॥

MEANING IN FRENCH: NOUS MÉDITONS SUR L'ESPRIT SUPRÊME LE PLUS D'IMMENSE QUI DIRIGE ET INSPIRE NOTRE INTELLIGENCE ET NOTRE COMPRÉHENSION

MEANING IN ENGLISH: WE MEDITATE ON THE MOST IMMENSE SUPREME SPIRIT WHO DIRECTS AND INSPIRES OUR INTELLIGENCE AND UNDERSTANDING.

## **Table of contents**

|                 |       |
|-----------------|-------|
| List of Figures | xiv   |
| List of Tables  | xxii  |
| Nomenclature    | xxvii |

### CHAPTER 1

#### INTRODUCTION, LITERATURE SURVEY AND SCOPE OF THE THESIS

|      |   |    |
|------|---|----|
| 1.1  | Vibration analysis in mechanical design | 1  |
| 1.2  | Buckling analysis in mechanical design  | 3  |
| 1.3  | Composite materials and structures      | 4  |
| 1.4  | Energy method and Rayleigh-Ritz method  | 5  |
| 1.5  | Literature survey                       | 8  |
| 1.6  | Vibration response of composite beams   | 8  |
| 1.7  | Buckling response of composite beams    | 11 |
| 1.8  | Experimental modal testing              | 12 |
| 1.9  | Objectives of the thesis                | 14 |
| 1.10 | Layout of the thesis                    | 15 |

### CHAPTER 2

#### RAYLEIGH-RITZ FORMULATION FOR DYNAMIC RESPONSE OF WIDTH-TAPERED LAMINATED COMPOSITE BEAM

|     |   |    |
|-----|---|----|
| 2.1 | Introduction  | 18 |
| 2.2 | Elastic behavior of linear width-tapered laminated composite beam | 20 |

|         |   |    |
|---------|---|----|
| 2.3     | Energy formulation for dynamic response of width-tapered laminated composite beams based on one-dimensional laminated beam theory | 24 |
| 2.3.1   | System matrices   | 24 |
| 2.3.1.1 | Analysis using Rayleigh-Ritz method   | 29 |
| 2.3.2   | Free vibration response of width-tapered laminated composite beams  | 33 |
| 2.3.3   | Forced vibration response including static end-axial force  | 34 |
| 2.3.4   | Forced vibration response of composite beam including damping   | 36 |
| 2.3.5   | Buckling analysis of width-tapered composite columns  | 39 |
| 2.4     | First-ply failure analysis  | 40 |
| 2.4.1   | Tsai-Wu tensor theory   | 40 |
| 2.5     | Summary   | 41 |

## CHAPTER 3

### DYNAMIC RESPONSE OF WIDTH-TAPERED LAMINATED COMPOSITE BEAMS

|       |  |    |
|-------|--|----|
| 3.1   | Introduction   | 42 |
| 3.2   | Elastic behavior of width-tapered laminated composite beam   | 44 |
| 3.2.1 | Extensional and flexural stiffness distribution for linear width-tapered composite beam                | 45 |
| 3.3   | Free vibration response of width-tapered laminated composite beams                                     | 53 |
| 3.3.1 | Effect of width ratio ( $b_R/b_L$ ) on natural frequencies   | 53 |
| 3.3.2 | Effect of ply orientation and laminate configuration on natural frequencies                            | 56 |
| 3.3.3 | Effect of length ratio ( $L_1/L_3$ ) on natural frequencies  | 60 |
| 3.3.4 | Effect of boundary condition on natural frequencies  | 65 |
| 3.3.5 | Effect of end-axial forces on natural frequencies  | 67 |
| 3.3.6 | Effect of damping on natural frequencies   | 74 |
| 3.4   | Comparison of natural frequencies between Rayleigh-Ritz method and conventional finite element method. | 80 |
| 3.5   | Buckling response of linear width-tapered composite columns  | 86 |
| 3.5.1 | Effect of width ratio ( $b_R/b_L$ ) on critical buckling load ( $P_{cr}$ )                             | 86 |

|       |   |     |
|-------|---|-----|
| 3.5.2 | Effect of laminate configuration on critical buckling load ( $P_{cr}$ )   | 88  |
| 3.5.3 | Effect of length ratio ( $L_1/L_3$ ) on critical buckling load ( $P_{cr}$ )   | 90  |
| 3.5.4 | Effect of boundary conditions on critical buckling load ( $P_{cr}$ )  | 93  |
| 3.6   | First-ply failure load  | 94  |
| 3.6.1 | First-ply failure tensile and compressive loads for width-tapered beam  | 95  |
| 3.7   | Forced vibration analysis of width-tapered laminated composite beams  | 98  |
| 3.7.1 | Effect of width ratio ( $b_R/b_L$ ) on forced response in terms of sinusoidal transverse displacement   | 99  |
| 3.7.2 | Effect of laminate configuration on forced response in terms of sinusoidal transverse displacement  | 101 |
| 3.7.3 | Effect of length ratio ( $L_1/L_3$ ) on forced response in terms of sinusoidal transverse displacement  | 106 |
| 3.7.4 | Effect of boundary conditions on forced response in terms of sinusoidal transverse displacement   | 111 |
| 3.7.5 | Effect of axial forces on forced response in terms of sinusoidal transverse displacement  | 115 |
| 3.8   | Comparison of forced response in terms of sinusoidal transverse displacement between Rayleigh-Ritz method and conventional finite element method. | 124 |
| 3.9   | Summary   | 128 |

## CHAPTER 4

### EXPERIMENTAL VALIDATION FOR WIDTH-TAPERED COMPOSITE BEAMS

|       |  |     |
|-------|--|-----|
| 4.1   | Introduction   | 136 |
| 4.2   | Manufacturing of composite laminate                            | 138 |
| 4.2.1 | Fabrication  | 138 |
| 4.2.2 | Processing   | 142 |
| 4.3   | Inspection of NCT-301 graphite/epoxy panel by Laser ultrasonic | 145 |
| 4.4   | Water-cooled rotary-type diamond cutter                        | 149 |
| 4.5   | Experimental modal analysis                                    | 151 |

|         |  |     |
|---------|--|-----|
| 4.5.1   | Measurement equipments and apparatus   | 155 |
| 4.5.1.1 | Test fixture   | 155 |
| 4.5.1.2 | Signal analyzer  | 155 |
| 4.5.1.3 | Charge amplifiers  | 156 |
| 4.5.1.4 | Impact hammer  | 158 |
| 4.5.1.5 | Accelerometer  | 159 |
| 4.5.2   | Impact excitation  | 160 |
| 4.5.3   | Impact testing requirements  | 161 |
| 4.5.4   | Response transducer calibration  | 162 |
| 4.6     | Modal testing for damping factor   | 163 |
| 4.6.1   | Damping loss factor  | 163 |
| 4.7     | Experimental modal analysis results  | 165 |
| 4.7.1   | Coherence function at different excitation points for width-tapered composite beam   | 166 |
| 4.7.2   | Time response and autospectrum response at different excitation points for width-tapered composite beam                        | 170 |
| 4.7.3   | Frequency Response Function (FRF- $H_1$ ) at different excitation points for width-tapered composite beam                      | 177 |
| 4.7.4   | Comparison of natural frequencies between experimental modal testing and Rayleigh-Ritz method for width-tapered composite beam | 180 |
| 4.8     | Summary  | 183 |

## CHAPTER 5

### DYNAMIC RESPONSE OF THICKNESS- AND WIDTH-TAPERED LAMINATED COMPOSITE BEAMS USING RAYLEIGH-RITZ METHOD

|     |  |     |
|-----|--|-----|
| 5.1 | Introduction   | 186 |
| 5.2 | Energy formulation for dynamic response of thickness- and width-tapered laminated composite beams based on one-dimensional laminated beam theory | 189 |

|         |  |     |
|---------|--|-----|
| 5.2.1   | System matrices  | 189 |
| 5.2.1.1 | Properties of ply in the tapered laminate  | 190 |
| 5.2.2   | Analysis using Rayleigh-Ritz method  | 192 |
| 5.2.3   | Dynamic response of thickness- and width-tapered laminated composite beams   | 194 |
| 5.3     | Free vibration response of thickness- and width-tapered laminated composite beams  | 194 |
| 5.3.1   | Effect of angle of thickness-taper ( $\phi$ ) and width ratio ( $b_R/b_L$ ) on natural frequencies   | 196 |
| 5.3.2   | Effect of laminate configurations on natural frequencies   | 205 |
| 5.3.3   | Effect of boundary condition on natural frequencies  | 208 |
| 5.3.4   | Effects of end-axial forces on natural frequencies   | 210 |
| 5.3.5   | Effect of damping on natural frequencies   | 219 |
| 5.4     | Comparison of natural frequencies between Rayleigh-Ritz method and conventional finite element method  | 222 |
| 5.5     | Buckling response of thickness- and width-tapered laminated composite columns  | 234 |
| 5.5.1   | Effect of angle of thickness-taper ( $\phi$ ) and width ratio ( $b_R/b_L$ ) on critical buckling load  | 234 |
| 5.5.2   | Effect of laminate configuration on critical buckling load   | 241 |
| 5.5.3   | Effect of boundary condition on critical buckling load   | 243 |
| 5.6     | Comparison of forced response in terms of sinusoidal transverse displacement between Rayleigh-Ritz method and conventional finite element method | 246 |
| 5.7     | Summary  | 250 |

## CHAPTER 6

### CONCLUSIONS AND RECOMMENDATIONS

|     |                     |     |
|-----|---------------------|-----|
| 6.1 | Major contributions | 254 |
| 6.2 | Conclusions         | 256 |

|     |  |     |
|-----|--|-----|
| 6.3 | Recommendations for future work  | 261 |
|     | BIBLIOGRAPHY   | 263 |
|     | APPENDIX-A   | 274 |
|     | Flow chart for MATLAB <sup>®</sup> program for free and forced vibration and buckling response                       | 274 |
|     | Trial functions used for different boundary conditions   | 276 |
|     | APPENDIX-B   | 277 |
|     | Derivation for orthonormal modal matrix $[\tilde{P}]$  | 277 |
|     | Contribution of numerical computation for dynamic response of thickness- and width-tapered laminated composite beams | 282 |
|     | APPENDIX-C   | 283 |
|     | Cost estimation report of width-tapered composite beams  | 283 |

## List of Figures

|  |    |
|--|----|
| <b>Figure 2.1</b> Schematic illustration of linear width- tapered laminated composite beam and coordinate system.....                              | 21 |
| <b>Figure 3.1</b> Extensional stiffness distributions for linear width-tapered composite beam with a width ratio ( $b_R/b_L$ ) value of 0.01 ..... | 46 |
| <b>Figure 3.2</b> Extensional stiffness distributions for linear width-tapered composite beam with a width ratio ( $b_R/b_L$ ) value of 0.4.....   | 47 |
| <b>Figure 3.3</b> Extensional stiffness distributions for linear width-tapered composite beam with a width ratio ( $b_R/b_L$ ) value of 1 .....    | 48 |
| <b>Figure 3.4</b> Flexural stiffness distributions for linear width-tapered composite beam with a width ratio ( $b_R/b_L$ ) value of 0.01 .....    | 50 |
| <b>Figure 3.5</b> Flexural stiffness distributions for linear width-tapered composite beam with a width ratio ( $b_R/b_L$ ) value of 0.4.....      | 51 |
| <b>Figure 3.6</b> Flexural stiffness distributions for linear width-tapered composite beam with a width ratio ( $b_R/b_L$ ) value of 1 .....       | 52 |
| <b>Figure 3.7</b> Effect of width ratio ( $b_R/b_L$ ) on first natural frequency.....  | 54 |
| <b>Figure 3.8</b> Effect of width ratio ( $b_R/b_L$ ) on second natural frequency .....  | 55 |
| <b>Figure 3.9</b> Effect of width ratio ( $b_R/b_L$ ) on third natural frequency.....  | 55 |
| <b>Figure 3.10</b> Effect of ply orientation on first natural frequency for four boundary conditions.....  | 57 |

|   |    |
|---|----|
| <b>Figure 3.11</b> Effect of laminate configurations on natural frequencies.....  | 59 |
| <b>Figure 3.12</b> Schematic illustration of linear width- tapered laminated composite beam showing the length ratio.....                             | 61 |
| <b>Figure 3.13</b> Effect of length ratio ( $L_1/L_3$ ) on first natural frequency.....   | 62 |
| <b>Figure 3.14</b> Effect of length ratio ( $L_1/L_3$ ) on second natural frequency .....   | 63 |
| <b>Figure 3.15</b> Effect of length ratio ( $L_1/L_3$ ) on third natural frequency.....   | 64 |
| <b>Figure 3.16</b> Effect of boundary conditions on natural frequencies.....  | 66 |
| <b>Figure 3.17</b> Schematic illustration of linear width- tapered laminated composite beams with end axial force for three boundary conditions ..... | 67 |
| <b>Figure 3.18</b> Effect of damping on natural frequencies for simply-supported boundary condition .....   | 76 |
| <b>Figure 3.19</b> Effect of damping on natural frequencies for clamped-clamped boundary condition .....  | 77 |
| <b>Figure 3.20</b> Effect of damping on natural frequencies for clamped-free boundary condition .....   | 78 |
| <b>Figure 3.21</b> Effect of damping on natural frequencies for free-clamped boundary condition .....   | 79 |
| <b>Figure 3.22</b> Effect of width ratio ( $b_R/b_L$ ) on critical buckling load ( $P_{cr}$ ).....  | 87 |
| <b>Figure 3.23</b> Effect of laminate configuration on critical buckling load ( $P_{cr}$ ).....   | 89 |
| <b>Figure 3.24</b> Effect of length ratio ( $L_1/L_3$ ) on critical buckling load ( $P_{cr}$ ) .....  | 92 |
| <b>Figure 3.25</b> Effect of boundary conditions on critical buckling load ( $P_{cr}$ ) .....   | 93 |

|   |     |
|---|-----|
| <b>Figure 3.26</b> Schematic illustration of linear width- tapered laminated composite beams showing the excitation points.....         | 98  |
| <b>Figure 3.27</b> Effect of width ratio ( $b_R/b_L$ ) on frequency-displacement response .....   | 100 |
| <b>Figure 3.28</b> Effect of laminate configurations on frequency-amplitude response for width-ratio ( $b_R/b_L$ ) value of 0.2.....    | 103 |
| <b>Figure 3.29</b> Effect of laminate configurations on frequency-amplitude response for width-ratio ( $b_R/b_L$ ) value of 0.5.....    | 104 |
| <b>Figure 3.30</b> Effect of laminate configurations on frequency-amplitude response for width-ratio ( $b_R/b_L$ ) value of 1.....      | 105 |
| <b>Figure 3.31</b> Effect of length ratio ( $L_1/L_3$ ) on frequency-amplitude response for width-ratio ( $b_N/b_w$ ) value of 0.2..... | 108 |
| <b>Figure 3.32</b> Effect of length ratio ( $L_1/L_3$ ) on frequency-amplitude response for width-ratio ( $b_N/b_w$ ) value of 0.5..... | 109 |
| <b>Figure 3.33</b> Effect of length ratio ( $L_1/L_3$ ) on frequency-amplitude response for width-ratio ( $b_N/b_w$ ) value of 1.....   | 110 |
| <b>Figure 3.34</b> Effect of simply-supported boundary condition on frequency-amplitude response.....                                   | 112 |
| <b>Figure 3.35</b> Effect of clamped-free boundary condition on frequency-amplitude response .....                                      | 113 |
| <b>Figure 3.36</b> Effect of clamped-clamped boundary condition on frequency-amplitude response.....                                    | 114 |

|   |     |
|---|-----|
| <b>Figure 3.37</b> Schematic illustration of linear width- tapered laminated composite beams with end-axial static load .....   | 116 |
| <b>Figure 3.38</b> Effect of compressive end-axial static load on frequency-amplitude response for clamped-free boundary condition for width-ratio ( $b_R/b_L$ ) value of 0.2 ..... | 117 |
| <b>Figure 3.39</b> Effect of compressive end-axial static load on frequency-amplitude response for clamped-free boundary condition for width-ratio ( $b_R/b_L$ ) value of 0.5 ..... | 118 |
| <b>Figure 3.40</b> Effect of compressive end-axial static load on frequency-amplitude response for clamped-free boundary condition for width-ratio ( $b_R/b_L$ ) value of 1 .....   | 119 |
| <b>Figure 3.41</b> Effect of tensile end-axial static load on frequency-amplitude response for clamped-free boundary condition for width-ratio ( $b_R/b_L$ ) value of 0.2.....      | 121 |
| <b>Figure 3.42</b> Effect of tensile end-axial static load on frequency-amplitude response for clamped-free boundary condition for width-ratio ( $b_R/b_L$ ) value of 0.5.....      | 122 |
| <b>Figure 3.43</b> Effect of tensile end-axial static load on frequency-amplitude response for clamped-free boundary condition for width-ratio ( $b_R/b_L$ ) value of 1.....        | 123 |
| <b>Figure 3.44</b> Comparison of forced response in terms of sinusoidal transverse displacement- clamped-free boundary condition.....   | 125 |
| <b>Figure 3.45</b> Comparison of forced response in terms of sinusoidal transverse displacement- simply-supported boundary condition.....   | 126 |
| <b>Figure 3.46</b> Comparison of forced response in terms of sinusoidal transverse displacement- clamped-clamped boundary condition .....   | 127 |
| <b>Figure 4.1</b> Typical autoclave layup.....  | 140 |
| <b>Figure 4.2</b> Hand layup process of NCT-301 graphite/epoxy composite laminate.....  | 142 |

|  |     |
|--|-----|
| <b>Figure 4.3</b> Photograph of typical Autoclave for curing composite materials .....                             | 143 |
| <b>Figure 4.4</b> Photograph of NCT-301 graphite/epoxy composite laminate post autoclave curing .....              | 143 |
| <b>Figure 4.5</b> Cure cycle for NCT-301 graphite/epoxy composite material .....                                   | 145 |
| <b>Figure 4.6</b> Photograph of NCT-301 graphite/epoxy panel in a fixture .....                                    | 146 |
| <b>Figure 4.7</b> Photograph of NCT-301 graphite/epoxy panel - C scan .....  | 146 |
| <b>Figure 4.8</b> Photograph of NCT-301 graphite/epoxy panel- BY-Scan #59 .....                                    | 146 |
| <b>Figure 4.9</b> Photograph of NCT-301 graphite/epoxy panel- BY-Scan #111 .....                                   | 147 |
| <b>Figure 4.10</b> Photograph of NCT-301 graphite/epoxy panel- BY-Scan #220 .....                                  | 147 |
| <b>Figure 4.11</b> Photograph of NCT-301 graphite/epoxy panel- BX-Scan #91 .....                                   | 147 |
| <b>Figure 4.12</b> Pictorial representation of water cooled-rotary type diamond cutter and digital protractor..... | 149 |
| <b>Figure 4.13</b> Pictorial representation of composite beam fixture table and cutting position .....             | 150 |
| <b>Figure 4.14</b> Block diagram of experimental modal analysis instrumentation .....                              | 153 |
| <b>Figure 4.15</b> Photographs of NCT-301 graphite/epoxy composite beam specimens.....                             | 154 |
| <b>Figure 4.16</b> Photograph of B & K's PULSE™ front-end multi-analyzer type 3560.....                            | 156 |
| <b>Figure 4.17</b> Photograph of typical oscilloscope.....   | 156 |
| <b>Figure 4.18</b> Photograph of typical Dual mode amplifier .....   | 157 |
| <b>Figure 4.19</b> Photograph of piezoelectric charge amplifier.....   | 157 |

|   |     |
|---|-----|
| <b>Figure 4.20</b> Photograph of typical impact hammer.....   | 158 |
| <b>Figure 4.21</b> Photograph of typical response transducer mounted below width-tapered beam.....                              | 159 |
| <b>Figure 4.22</b> Photograph of experimental modal analysis test set-up .....  | 160 |
| <b>Figure 4.23</b> Schematic illustrations of composite beam with excitation points.....  | 165 |
| <b>Figure 4.24</b> Coherence function for width ratio ( $b_R/b_L$ ) of 0.2 at four excitation points                            | 167 |
| <b>Figure 4.25</b> Coherence function for width ratio ( $b_R/b_L$ ) of 0.4 at four excitation points                            | 168 |
| <b>Figure 4.26</b> Coherence function for width ratio ( $b_R/b_L$ ) of 0.6 at four excitation points                            | 168 |
| <b>Figure 4.27</b> Coherence function for width ratio ( $b_R/b_L$ ) of 0.8 at four excitation points                            | 169 |
| <b>Figure 4.28</b> Coherence function for width ratio ( $b_R/b_L$ ) of 1 at four excitation points ..                           | 169 |
| <b>Figure 4.29</b> Time response and autospectrum response for width ratio ( $b_R/b_L$ ) of 0.2 at four excitation points ..... | 172 |
| <b>Figure 4.30</b> Time response and autospectrum response for width ratio ( $b_R/b_L$ ) of 0.4 at four excitation points ..... | 173 |
| <b>Figure 4.31</b> Time response and autospectrum response for width ratio ( $b_R/b_L$ ) of 0.6 at four excitation points ..... | 174 |
| <b>Figure 4.32</b> Time response and autospectrum response for width ratio ( $b_R/b_L$ ) of 0.8 at four excitation points ..... | 175 |
| <b>Figure 4.33</b> Time response and autospectrum response for width ratio ( $b_R/b_L$ ) of 1 at four excitation points .....   | 176 |

|   |     |
|---|-----|
| <b>Figure 4.34</b> FRF $-H_1$ at four excitation points for width ratio ( $b_R/b_L$ ) values of 0.2, 0.4, 0.6, 0.8 and 1 .....  | 179 |
| <b>Figure 5.1</b> Schematic illustration of thickness- and width-tapered composite beam configurations .....  | 188 |
| <b>Figure 5.2</b> Schematic illustration of properties of typical thickness-tapered laminate ..   | 190 |
| <b>Figure 5.3</b> Effect of angle of thickness-taper and width ratio on the natural frequencies for simply-supported composite beam.....                                | 197 |
| <b>Figure 5.4</b> Effect of angle of thickness-taper and width ratio on the natural frequencies for clamped-clamped composite beam .....                                | 198 |
| <b>Figure 5.5</b> Effect of angle of thickness-taper and width ratio on the natural frequencies for clamped-free composite beam.....                                    | 199 |
| <b>Figure 5.6</b> Effect of width ratio for angle of thickness-taper ( $\phi$ ) of $0.57^0$ on natural frequencies (case 2) – simply-supported boundary condition ..... | 201 |
| <b>Figure 5.7</b> Effect of width ratio for angle of thickness-taper ( $\phi$ ) of $0.57^0$ on natural frequencies (case 2) - clamped-clamped boundary condition.....   | 202 |
| <b>Figure 5.8</b> Effect of width ratio for angle of thickness-taper ( $\phi$ ) of $0.57^0$ on natural frequencies (case 2) - clamped-free boundary condition.....      | 203 |
| <b>Figure 5.9</b> Effect of angle of thickness-taper ( $\phi$ ) and width ratio ( $b_R/b_L$ ) on critical buckling load for simply-supported boundary condition.....    | 236 |
| <b>Figure 5.10</b> Effect of angle of thickness-taper ( $\phi$ ) and width ratio ( $b_R/b_L$ ) on critical buckling load for clamped-clamped boundary condition.....    | 237 |
| <b>Figure 5.11</b> Effect of angle of thickness-taper ( $\phi$ ) and width ratio ( $b_R/b_L$ ) on critical buckling load for clamped-free boundary condition.....       | 238 |

|   |     |
|---|-----|
| <b>Figure 5.12</b> Effect of constant angle of thickness-taper ( $\phi$ ) of $0.57^\circ$ and width ratio ( $b_R/b_L$ ) (case 2) on critical buckling load..... | 239 |
| <b>Figure 5.13</b> Comparison of forced response in terms of sinusoidal transverse displacement- simply-supported boundary condition.....                       | 247 |
| <b>Figure 5.14</b> Comparison of forced response in terms of sinusoidal transverse displacement- clamped-clamped boundary condition .....                       | 248 |
| <b>Figure 5.15</b> Comparison of forced response in terms of sinusoidal transverse displacement- clamped-free boundary condition.....                           | 249 |

### List of Tables

|  |    |
|--|----|
| <b>Table 3.1</b> Mechanical properties of unidirectional NCT-301 graphite-epoxy prepreg [24]                                   | 43 |
| <b>Table 3.2</b> Mechanical properties of resin material [24]  | 44 |
| <b>Table 3.3</b> Geometric properties of width-tapered composite beam  | 44 |
| <b>Table 3.4</b> Effect of end axial compressive force on first three natural frequencies -simply supported boundary condition | 68 |
| <b>Table 3.5</b> Effect of end axial compressive force on first three natural frequencies – clamped-clamped boundary condition | 69 |
| <b>Table 3.6</b> Effect of end axial compressive force on first three natural frequencies – clamped-free boundary condition    | 70 |
| <b>Table 3.7</b> Effect of end axial tensile force on first three natural frequencies –simply-supported boundary condition     | 71 |
| <b>Table 3.8</b> Effect of end axial tensile force on first three natural frequencies –clamped-clamped boundary condition      | 72 |
| <b>Table 3.9</b> Effect of end axial tensile force on first three natural frequencies –clamped-free boundary condition         | 73 |
| <b>Table 3.10</b> Comparison of natural frequencies--Simply supported boundary condition                                       | 80 |
| <b>Table 3.11</b> Comparison of natural frequencies—Clamped-clamped boundary condition   | 81 |
| <b>Table 3.12</b> Comparison of natural frequencies—Clamped-free boundary condition  | 83 |

|   |     |
|---|-----|
| <b>Table 3.13</b> Comparison of natural frequencies—Free-clamped boundary condition   | 84  |
| <b>Table 3.14</b> Failure loads for 0° ply  | 96  |
| <b>Table 3.15</b> Failure loads for 90° ply   | 97  |
| <b>Table 4.1</b> Specifications of width-tapered composite beams  | 154 |
| <b>Table 4.2</b> Damping loss factor measurements   | 164 |
| <b>Table 4.3</b> Comparison of natural frequencies for width-tapered composite beams at four excitation points                    | 181 |
| <b>Table 5.1</b> Geometric properties of thickness- and width-tapered composite beam  | 195 |
| <b>Table 5.2</b> Angle of thickness-taper, length, length/height ratio and length/width at left section ratio                     | 195 |
| <b>Table 5.3</b> Cases for different thickness- and width-taper configurations  | 196 |
| <b>Table 5.4</b> Comparison of natural frequencies for the effect of laminate configuration - Simply-supported boundary condition | 205 |
| <b>Table 5.5</b> Comparison of natural frequencies for the effect of laminate configuration – clamped-clamped boundary condition  | 206 |
| <b>Table 5.6</b> Comparison of natural frequencies for the effect of laminate configuration – clamped-free boundary condition     | 207 |
| <b>Table 5.7</b> Comparison of natural frequencies-Simply-supported boundary condition  | 208 |
| <b>Table 5.8</b> Comparison of natural frequencies-Clamped-clamped boundary condition   | 209 |
| <b>Table 5.9</b> Comparison of natural frequencies-Clamped-free boundary condition  | 209 |

|   |     |
|---|-----|
| <b>Table 5.10</b> Effect of end-axial compressive force on natural frequencies -simply supported boundary condition | 211 |
| <b>Table 5.11</b> Effect of end-axial compressive force on natural frequencies- clamped-clamped boundary condition  | 212 |
| <b>Table 5.12</b> Effect of end-axial compressive force on natural frequencies- clamped-free boundary condition     | 214 |
| <b>Table 5.13</b> Effect of end-axial tensile force on natural frequencies -simply supported boundary condition     | 215 |
| <b>Table 5.14</b> Effect of end-axial tensile force on natural frequencies- clamped-clamped boundary condition      | 216 |
| <b>Table 5.15</b> Effect of end-axial tensile force on natural frequencies- clamped-free boundary condition         | 217 |
| <b>Table 5.16</b> Effect of damping on natural frequencies for simply-supported boundary condition.                 | 219 |
| <b>Table 5.17</b> Effect of damping on natural frequencies for clamped-clamped boundary condition                   | 220 |
| <b>Table 5.18</b> Effect of damping on natural frequencies for clamped-free boundary condition                      | 220 |
| <b>Table 5.19</b> Comparison of natural frequencies for configuration A-Simply supported boundary condition         | 222 |
| <b>Table 5.20</b> Comparison of natural frequencies for configuration A-Clamped-clamped boundary condition          | 223 |
| <b>Table 5.21</b> Comparison of natural frequencies for configuration A-Clamped-free boundary condition             | 224 |

|   |     |
|---|-----|
| <b>Table 5.22</b> Comparison of natural frequencies for configuration B-Simply-supported boundary condition | 225 |
| <b>Table 5.23</b> Comparison of natural frequencies for configuration B-Clamped-clamped boundary condition  | 226 |
| <b>Table 5.24</b> Comparison of natural frequencies for configuration B-Clamped-free boundary condition     | 227 |
| <b>Table 5.25</b> Comparison of natural frequencies for configuration C-Simply-supported boundary condition | 228 |
| <b>Table 5.26</b> Comparison of natural frequencies for configuration C-Clamped-clamped boundary condition  | 229 |
| <b>Table 5.27</b> Comparison of natural frequencies for configuration C-Clamped-free boundary condition     | 230 |
| <b>Table 5.28</b> Comparison of natural frequencies for configuration D-Simply-supported boundary condition | 231 |
| <b>Table 5.29</b> Comparison of natural frequencies for configuration D-Clamped-clamped boundary condition  | 232 |
| <b>Table 5.30</b> Comparison of natural frequencies for configuration D-Clamped-free boundary condition     | 233 |
| <b>Table 5.31</b> Comparison of critical buckling load-Simply-supported boundary condition                  | 241 |
| <b>Table 5.32</b> Comparison of critical buckling load -Clamped-clamped boundary condition                  | 242 |
| <b>Table 5.33</b> Comparison of critical buckling load - Clamped-free boundary condition                    | 242 |

|   |     |
|---|-----|
| <b>Table 5.34</b> Comparison of critical buckling load -Simply-supported boundary condition | 244 |
| <b>Table 5.35</b> Comparison of critical buckling load -Clamped-clamped boundary condition  | 244 |
| <b>Table 5.36</b> Comparison of critical buckling load -Clamped-free boundary condition     | 245 |
| <b>Table 10.1</b> Manufacturing cost of width-tapered composite beams                       | 283 |
| <b>Table 10.2</b> Dimension of composite laminate plate                                     | 284 |
| <b>Table 10.3</b> Vibration testing cost of composite beams                                 | 285 |

## Nomenclature

|                                    |   |
|------------------------------------|---|
| $H$                                | Height of the laminate  |
| $L$                                | Length of the beam  |
| $b$                                | Uniform width of the beam   |
| $u, v, w$                          | In-plane displacements  |
| $\varepsilon_z$                    | Transverse normal strain  |
| $N_x, N_y$                         | Normal force resultants in x and y-directions (N/m)                   |
| $N_{xy}$                           | Shear force resultants (N/m)  |
| $M_x, M_y$                         | Bending moment resultants in x and y-directions (N-m/m)               |
| $M_{xy}$                           | Twisting moment resultants (N-m/m)                                    |
| $P_x, P_y$                         | Normal forces on the laminate cross-section in x and y-directions (N) |
| $P_{xy}$                           | Shear force on the laminate cross-section (N)                         |
| $R_x, R_y$                         | Bending Moment on the laminate cross-section (N-m)                    |
| $R_{xy}$                           | Twisting moment on the laminate cross-section (N-m)                   |
| $\varepsilon_x^o, \varepsilon_y^o$ | Extensional strain of the reference surface in the x and y direction  |
| $\gamma_{xy}^o$                    | The reference surface in-plane shear strain                           |
| $k_x^o, k_y^o$                     | curvature of the reference surface in the x direction                 |

|                 |   |
|-----------------|---|
| $k_{xy}^o$      | The reference surface twisting curvature  |
| $[A],[B],[D]$   | Laminate stiffness matrices   |
| $b(x)$          | Width of the beam at coordinate x   |
| $b_L, b_R$      | Width of the beam at left and right end of the beam                                   |
| $D_{ij}^*$      | The coefficient of the inverse of variable bending stiffness matrix of composite beam |
| $U_{flexure}$   | The strain energy due to flexure of the beam  |
| $U_{axialload}$ | The work done due to applied static end-axial load                                    |
| $T$             | The kinetic energy of the beam  |
| $\rho_c$        | The density of composite material   |
| $\rho_r$        | The density of resin  |
| $w(x,t)$        | The transverse displacement of the beam   |
| $\omega$        | Natural frequency of the beam   |
| $c_i$           | The co-efficient of displacement  |
| $\phi_i(x)$     | Trial function  |
| $[K]$           | The stiffness matrix of the beam  |
| $[\bar{G}]$     | The geometric stiffness matrix of the beam  |
| $[M]$           | The mass matrix of the beam   |
| $[C]$           | The damping matrix of the beam  |
| $P$             | Static end-axial tensile load   |

|                          |  |
|--------------------------|--|
| $P_{cr}$                 | Critical buckling load                             |
| $\lambda$                | Eigenvalues  |
| $[\tilde{P}]$            | Ortho-normal modal matrix                          |
| $[\tilde{P}]^T$          | Transpose of ortho-normal modal matrix             |
| $[I]$                    | Identity matrix                                    |
| $[\Lambda]$              | The diagonal matrix of the eigenvalues             |
| $\{\tilde{f}\}$          | Orthonormal force vector                           |
| $\{f\}$                  | Force vector                                       |
| $\alpha$                 | mass-proportional constant                         |
| $\beta$                  | stiffness-proportional constant                    |
| $\zeta_i$                | Damping ratio                                      |
| $\eta$                   | Damping loss factor                                |
| $\omega_{di}$            | Damped natural frequency of the beam               |
| $\sigma_1, \sigma_2$     | Stresses in 1 and 2 directions                     |
| $\tau_{12}$              | The shear stress in 2-direction along 1-plane      |
| $\sigma_1^T, \sigma_2^T$ | Tensile failure stresses in 1 and 2 directions     |
| $\sigma_1^C, \sigma_2^C$ | Compressive failure stresses in 1 and 2 directions |
| $\tau_{12}^F$            | Failure due to positive shear stress               |
| $b_w$                    | width at wider side of beam                        |
| $b_N$                    | width at narrower side of beam                     |

|                    |  |
|--------------------|--|
| $c$                | The intercept of the centerline of the ply from the mid-plane  |
| $E$                | Modulus of elasticity of isotropic material  |
| $E_1$              | Modulus of elasticity in fiber direction   |
| $E_2$              | Modulus of elasticity in transverse direction  |
| $D_{11}$           | The first co-efficient of bending stiffness matrix of composite beam                                       |
| $D_{11}(x)$        | The first co-efficient of variable bending stiffness matrix of composite beam                              |
| $S$                | slope of thickness-tapered beam  |
| $h_k, h_{k-1}$     | height of the upper and lower surfaces of $k^{\text{th}}$ ply with respect to mid-plane                    |
| $h'_k, h'_{k-1}$   | height of the upper and lower surfaces of $k^{\text{th}}$ ply in thickness tapered beam from the mid-plane |
| $\theta$           | fiber orientation angle  |
| $\phi$             | angle of thickness-taper   |
| $x$                | Longitudinal direction of the laminated beam   |
| $y$                | Transverse direction of the laminated beam   |
| $z$                | Thickness direction of the laminated beam  |
| $H(x)$             | Height of the tapered laminate as the function of length of the beam                                       |
| $mV/N$             | Sensitivity of impact hammer, milli volt/newton  |
| $Npk$              | Measurement range of impact hammer,  |
| $pC/g$             | Sensitivity of response measurement accelerometer  |
| $\gamma(\omega)^2$ | The coherence function   |

|             |   |
|-------------|---|
| $G_{XF}$    | The cross spectrum between the force and response |
| $G_{XX}$    | The autospectra of the response                   |
| $G_{FF}$    | The autospectra of the force                      |
| $H(\omega)$ | The Frequency Response Function                   |
| $X(\omega)$ | Output or response spectrum                       |
| $F(\omega)$ | Input or force spectrum                           |

## CHAPTER 1

### INTRODUCTION, LITERATURE SURVEY AND SCOPE OF THE THESIS

#### 1.1 Vibration analysis in mechanical design

Vibration is the study of the repetitive motion of objects relative to a stationary frame of reference or nominal position (usually equilibrium). The vibration which occurs in most machines, vehicles, structures, buildings and dynamic systems is undesirable, not only because of the resulting unpleasant motions and the dynamic stresses which may lead to fatigue and failure of the structure or machine, and the energy losses and reduction in performance which accompany vibrations, but also because of the noise produced. Noise is generally considered to be unwanted sound, and since sound is produced by some source of motion or vibration causing pressure changes which propagate through the air or other transmitting medium, vibration control is of fundamental importance to sound attenuation. Vibration analysis of machines and structures is therefore often a necessary prerequisite for controlling not only vibration but also noise [1].

Until early 21<sup>st</sup> century, machines and structures usually had very high mass and damping, because heavy beams, timbers, castings and stonework were used in their construction. Since the vibration excitation sources were often small in magnitude, the dynamic response of these highly damped machines was low. However, with the development of strong lightweight materials, increased knowledge of material properties

and structural loading, and improved analysis and design techniques, the mass of machines and structures built to fulfill a particular function has decreased. Furthermore, the efficiency and speed of machinery have increased so that the vibration exciting forces are higher, and dynamic systems often contain high-energy sources, which can create intense noise and vibration problems. This process of increasing excitation with reducing machine mass and damping has continued at an increasing rate to the present day when few, if any, machines can be designed without carrying out the necessary vibration analysis, if their dynamic performance is to be acceptable. The demands made on machinery, structures, and dynamic systems are also increasing, so that the dynamic performance requirements are always rising [2].

There have been very many cases of systems failing or not meeting performance targets because of resonance, fatigue, excessive vibration of one component or another or high noise levels. Because of the very serious effects which unwanted vibrations can have on dynamic systems, it is essential that vibration analysis be carried out as an inherent part of their design, when necessary modifications can most easily be made to eliminate vibration or at least to reduce it as much as possible. However, it must also be recognized that it may sometimes be necessary to reduce the vibration of an existing machine, either because of inadequate initial design, or by a change in function of the machine, or by a change in environmental conditions or performance requirements, or by a revision of acceptable noise levels. Therefore techniques for the analysis of vibration in dynamic systems should be applicable to existing systems as well as those in the design stage; it is

the solution to the vibration or noise problem which may be different, depending on whether or not the system already exists.

## **1.2 Buckling analysis in mechanical design**

When analyzing a structure, in addition to looking at maximum deflections, maximum stresses and natural frequencies, one must investigate under what loading conditions instability can occur, which is generally referred to as buckling [2]. Change in the geometry of a structure or a mechanical component under compression results in the loss of its ability to resist loading. Stability of structures under compression can be grouped into two categories: (1) Instability associated with a bifurcation of equilibrium; (2) Instability that is associated with a limit of maximum load. The first category is characterized by the fact that as the compressive load increases, the member or system that originally deflects in the direction of applied force, suddenly deflects in a different direction. This phenomenon is called buckling. The point of transition from the usual deflection mode under load to an alternative deflection mode is referred to as the point of bifurcation of equilibrium. The lowest load at the point of bifurcation is called critical buckling load.

Buckling analysis is basically a subtopic of non-linear rather than linear mechanics. In linear mechanics of deformable solids, displacements are proportional to the loads. In buckling, disproportional increase in displacement occurs due to a small increase in the load. The instability due to buckling can lead to a catastrophic failure of a structure and it must be taken into account when one designs a structure.

### **1.3 Composite materials and structures**

Development and design of polymer composite materials and structures is the fastest growing segment of lightweight (durable and sustainable) construction and product engineering (in general 'moving and moved beings'). Since fifteen years for each five years period the world market volume of advanced polymer composites was doubled (100% growth per quinquennial). For the first decade of this millennium a growth of at least 700 % is foreseen (350% growth per quinquennial). The majority of structural parts in novel aircraft and space platform designs will be materialized in polymer composite materials. In case of fireproof interiors including floors and supporting structures (beams and brackets) the applied volume of composites are reaching the maximum of almost 100 % and for the high performance and durable exterior shell structures almost 80% by volume is within the reach [3].

The same trends and developments are true for inshore and offshore wind turbine blade designs (wing structures possessing a radius equal to the total span of a Boeing 747) and the development of the latest fast transport systems varying from trains, cars, ferries, and trucks to ships and yachts, show similar tendencies. In traditional metal structure design a proper mechanical behaviour as a response to 'loads' is realized by a sufficient volumetric distribution and combination of proper metallic materials (stress and stiffness level control). For today's and future designers of the ultimate lightweight structures in general (minimum material, minimum energy, and maximum performance) a change in attitude and design skills is indispensable. In addition to the volumetric distribution approach to sustain all kinds of stress and strain states, for composite

laminates a sophisticated distribution and control of coupled and uncoupled stress and strain phenomena, induced by both mechanical and physical loads, becomes necessary.

Compared to metals in composite structure design stiffness, strength and durability, resistance and tolerance with respect to impact events or proper scenarios to absorb impact energy are becoming true initial design parameters, from material to load path and structure design. The same is true for acoustic and thermo-insulating properties, stability, vibrations and aero-elasticity. Therefore in near future developments of advanced and cost effective structures would require a new generation of (scientific, academic) developers and designers capable of creating and using new design tools and rules and last but not least capable to create new paradigms in conceptual and structural design.

#### **1.4 Energy method and Rayleigh-Ritz method**

For simple mechanical systems, the vector methods provide an easy and direct way of deriving the equations. However, for complicated systems, the procedure becomes more cumbersome and intractable. In such cases, variational statements can be used to obtain governing equations, associated boundary conditions, and in certain simple cases, solutions for displacements and forces at selective points of a structure [4].

To obtain the governing differential equations and boundary conditions of various problems we need to apply the virtual-work principles or their derivatives. These principles involve setting the first variation of an approximate functional with respect to the dependent variables to zero. The procedure of the calculus of variations can then be applied to obtain the governing (Euler-Lagrange) equations of the problem. In contrast,

the method applied in this thesis seeks a solution in terms of adjustable parameters that are determined by substituting the assumed solutions into the functional and finding its stationary value with respect to the parameters. Such solution methods are called direct methods, because the approximate solutions are obtained directly by applying the same variational principle that was used to derive the governing equation. The assumed solutions in the variational methods are in the form of a finite linear combination of undetermined parameters with appropriately chosen functions. This amounts to representing a continuous function by a finite linear combination of functions. Since the solution of a continuum problem in general cannot be completely represented by a finite set of functions, error is introduced into the solution. Therefore, the solution obtained is an approximate of the true solution for the equations describing a physical problem. As a number of linearly independent terms in the assumed solution are increased, the error in the approximation will be reduced and the assumed solution converges to the desired solution of Euler's equations.

The equations governing a physical problem themselves are approximate. The approximations are introduced via several sources, including the geometry, the representation of specified loads and displacements, and the material constitution. In the present study, our primary concern is to determine accurate approximate solutions to appropriate analytical descriptions of physical problems.

The variational methods of approximation include those of Rayleigh-Ritz, Galerkin, Petrov-Galerkin (weighted-residuals), Kantorovitch, Treffiz, and the finite element method, which is a "piecewise" application of the Ritz-Galerkin method.

In the principle of virtual displacements, the Euler equations are the equilibrium equations, whereas in the principle of virtual forces, they are the compatibility equations. These Euler equations are in the form of differential equations that are not always tractable by exact methods of solution. A number of approximate methods exist for solving differential equations [e.g., finite-difference methods, perturbation methods, etc.]. The most direct methods bypass the derivation of the Euler equations and go directly from a variational statement of the problem to the solution of the Euler equations. One such direct method was proposed by Lord Rayleigh. A generalization of the method was proposed independently by Ritz (1878-1909) [6].

The Rayleigh-Ritz or Ritz method has found tremendous use during past three decades in obtaining accurate frequencies and mode shapes for the vibration of continuum system especially for problems not amendable to exact solution of the differential equations. This method is used frequently because of the increasing capability of digital computers to setup and solve the frequency determinants arising with the method. This method can be used to solve boundary value problem or eigen value problem by assuming a solution in the form of series of admissible functions (satisfying at least the geometric boundary conditions) each having an arbitrary co-efficient and minimizing the appropriate energy functional directly. In this thesis Rayleigh-Ritz method is employed to determine the free and forced vibration response of width-tapered and thickness- and width-tapered laminated composite beams and buckling response of tapered composite columns. Admissible functions are taken as series of products of beam mode shapes called trial functions.

## **1.5 Literature survey**

In this section, a comprehensive and up-to-date literature survey is presented on the relevant topics. Important works done on the dynamic response of uniform, width-tapered, thickness- and width-tapered composite beams including damping and axial load effects by Rayleigh-Ritz method and experimental modal testing method for composite beams are chronicled.

## **1.6 Vibration response of composite beams**

There is a wealth of literature available for the vibration and buckling analyses of laminated plates and shells. In comparison, study on the analysis of laminated beams has been scarce despite their applicability in important structures such as turbine blades, helicopter blades, robot arms, etc. Also, the works on vibration and buckling analyses of laminated beams are not sufficient especially on forced vibration.

Abarcar and Caniff [7] conducted the free vibration analysis of uniform laminated composite beams without considering the effects of shear deformation and rotary inertia. Miller and Adams [8] studied the vibration characteristics of the orthotropic clamped-free uniform beams using the classical lamination theory without including the effect of shear deformation. Vinson and Sierakowski [9] obtained the exact solutions for the natural frequencies of a simply-supported uniform composite beam based on classical lamination theory. Roy and Ganesan [10] have studied the response of a tapered composite beam with general boundary conditions. He et al. [11] have conducted a review of the works on

tapered laminated composite structures with focus on interlaminar failures and three-dimensional stress analyses. Steeves and Fleck [12] have studied the compressive strength of composite laminates with terminated internal plies. Aydogdu [13] have studied the vibration response of cross-ply laminated beams with general boundary conditions using the Ritz method. Boay and Wee [14] have studied the coupling effects in bending, buckling and free vibration of generally laminated composite beams. Hassan and Sabuncu [15] have conducted the stability analysis of a cantilever composite beam resting on elastic supports. Teoh and Huang [16] studied the vibration of beams of fibre reinforced materials. Krishnaswamy et al. [17] obtained analytical solutions to vibration of generally layered composite beams. Khdeir and Reddy [18] have studied the free vibration of cross-ply laminated beams with arbitrary boundary conditions. Abramovich and Livshits [19] established analytical solution of free vibration of non-symmetrical cross-ply laminated beams. Houmat [20] investigated the vibration of Timoshenko beams considering four-node element with variable degrees of freedom where he described element transverse displacement and cross-sectional rotations by cubic polynomial plus a variable number of trigonometric sine terms. Singh and Abdelnassar [21] examined the forced vibration response of composite beams considering a third order shear deformation theory. Thickness-tapered laminated composite beams have been studied for their dynamic response in the works of Ganesan and Zabihollah [22, 23] using an advanced finite element formulation and parametric study. Ahmed [24] has studied and conducted experiments for free and forced vibration response of tapered composite beams including the effects of axial force and damping. Chen [25] has studied the free vibration response of tapered composite beams using hierarchical finite element method

and Rayleigh-Ritz method. Amit and Yadav [26] investigated forced nonlinear random vibration of a simply supported cross-ply laminated composite plate analytically using Kirchhoff-Love plate theory and Von-Karman nonlinear strain displacement formulations. Asghar et al. [27] studied forced vibration analysis developed by the modal superposition technique and the layer wise theory of Reddy to study the low velocity impact response of laminated plates. Cheung et al. [28] proposed a computationally efficient and highly accurate numerical method to analyze the vibrations of symmetrically laminated rectangular composite plates with intermediate line supports. The governing eigen frequency equation is derived using Rayleigh-Ritz method. They developed a set of admissible functions from the static solutions of a beam with intermediate points of supports under a series of sinusoidal loads. Kadivar et al. [29] studied the forced vibration of an unsymmetrical laminated composite beam subjected to moving loads. They studied a one-dimensional element with 24 degrees of freedom, which included the effects of transverse shear deformation, rotary and higher order inertia to get the response. Beytullah et al. [30] investigated the dynamic behavior of composite cylindrical helical rods subjected to time dependent loads theoretically in the Laplace domain. Azrar et al. [31] studied the forced non-linear response of clamped-clamped and simply-supported beams using spectral analysis, Lagrange's equations and harmonic balanced method. They proposed a method to solve the multidimensional Duffing equation and obtained a set of non-linear algebraic equation whose numerical solution leads in each case to the basic function contribution co-efficient to the displacement response function based on harmonic balance method. These coefficients depend on the excitation frequency and the distribution of the applied loads. Faruk [32] analyzed free

and forced vibrations of non-uniform composite beams in the Laplace domain. He adopted Timoshenko beam theory in the derivation of governing equation.

## **1.7 Buckling response of composite beams**

There are few works available on buckling analysis of composite beams in the literature. Khdeir and Reddy [33] used various plate theories to study the buckling of laminated plates. Banerjee and Williams [34] obtained critical buckling loads for columns by considering shear deformation effects. Khdeir and Reddy [35] discussed buckling behavior of cross-ply rectangular composite beams with different boundary conditions. They presented analytical solution for composite beams with different boundary conditions. Song and Waas [36] discussed the effects of shear deformation on the buckling of composite beams. They are simple higher-order theory, which assumes a cubic distribution for the displacement field through the thickness of the beam. Chen and Peng [37] studied the stability of rotating composite beams subjected to axial compressive load. Kim et al. [38] conducted the buckling analysis of cross-ply laminate with one-dimensional through-the-width delaminations. Matsunaga [39] studied the buckling of multi-layer composite beams using higher-order deformation theories. Lee et al. [40] presented a general analytical model based on the classical laminate theory to study the lateral buckling of a laminated composite beam with I-section. They considered different laminate configurations and boundary conditions. The exact solutions for critical buckling loads based on classical laminate theory for different boundary

conditions are given by Bertholet [3], Reddy [6] and Whitney [41]. Abd El-Maksood [42] used an advanced finite element formulation to study the buckling of laminated beams. Recently, Cortinez and Piovan [43] discussed buckling of thin-walled composite beams. Lee and Kim [44] treated the lateral buckling of channel section composite beams.

## **1.8 Experimental modal testing**

It is always recommended to use the updated data of any materials for the analysis. In this thesis, NCT-301 graphite-epoxy is used for all analyses and parametric study. To get the idea about mechanical properties, it was found that Ibrahim [45] studied NCT-301 graphite epoxy material where he did some experimental work for determining notched and un-notched strengths of cross-ply laminates. He studied the effect of notch size on the reliability of composite laminates based on stochastic finite element analysis.

Damping analysis of fiber-reinforced composite has not been considered as a popular research area since composite materials are designed with stiffness to weight ratio, rather than damping. Damping in laminated composite materials, where laminae are bonded with adhesive joints of very low damping capacity, is mostly due to the inelastic or visco-elastic nature of matrix and to relative slipping at the fiber-matrix interfaces. The only reliable method for estimating damping in composite is by experimentation. Suarez et al. [46] used random and impulse techniques for measurement of damping in composite materials under flexural vibrations. They tested specimens of un-reinforced epoxy resin, graphite-epoxy and E-glass polyester composite in order to cover a range of damping

values from low (aluminium) to intermediate (composite) to high (epoxy). Morison [47] developed a model of material damping for a fiber reinforced polymer matrix composite and experimentally predicted the loss factor and the temperature and moisture dependant structural damping of an arbitrary laminate. Hoa and Oullette [48] proposed a rule of mixture for the calculation of the loss factor for hybrid laminate where they found the damping loss factor of individual laminate experimentally using logarithmic decrement method. Gibson [49] reviewed the progress in analytical and experimental characterization of dynamic properties of advanced materials. Adams and Bacon [50] performed a series of experiments on unidirectional fiber reinforced beams under longitudinal shear and flexural loading conditions to determine the specific damping capacity. Zabarar et al. [51] studied viscous damping approximation and transient response of laminated composite plates using finite element method. Wei and Kukureka [52] evaluated the damping and elastic properties of composite material and composite structures experimentally by the resonance method. Adams and Maheri [53] investigated the damping capacity of fiber-reinforced plastic and developed a damping energy equation for analysis. Damping capacity and frequency of cross ply fiber reinforced plastic composite plates were compared at room temperature by using finite element method, Rayleigh-Ritz method and an experimental method. Sefrani and Bertholet [54] analyzed the effect of temperature on the damping properties of unidirectional glass fiber composite as a function of the frequency and fiber orientation using a cantilever beam test specimen and an impulse technique. Colakoglu [55] studied damping and vibration analysis of polyethylene fiber composite under varied temperature where he analyzed

temperature dependent frequency response experimentally using a damping monitoring technique.

Eslimy-Isfahay et al. [56] studied the dynamic response of composite beams with application to aircraft wings. Ewins [57] presented the techniques for experimental modal analysis. He et al. [58] studied the stress distributions in tapered beams made of composite materials. Koo and Lee [59] studied the dynamic behavior of thick composite beams. McConnell and Varato [60] presented the basic concepts and principles underlying dynamic testing. Tsai and Hahn [61] presented the principles governing the mechanical behavior of composite materials and the unique features in their design. Halvorsen and Brown [62] studied the impulse technique for structural frequency response testing. Klosterman [63] conducted the experimental determination and use of modal representations of dynamic characteristics. Potter [64] studied a general theory of modal analysis for linear systems.

## **1.9 Objectives of the thesis**

The present thesis is concerned with the dynamic response of tapered laminated composite beams. The beams are either width-tapered or both thickness- and width-tapered. The objectives of the work are: 1) To investigate the free and forced vibration response and buckling response of tapered laminated composite beams using Rayleigh-Ritz method and to conduct a detailed parametric study for the effects of width ratio, taper configuration, thickness taper angle, length ratio, boundary conditions, and laminate

configurations; 2) To investigate the effects of static end-axial compressive and tensile loads on natural frequencies and forced response of tapered laminated composite beams; 3) To conduct the modal testing of width-tapered composite beams and to compare the natural frequencies with those obtained using the Rayleigh-Ritz method; and, 4) To compare the free and forced vibration response of tapered laminated composite beams obtained using Rayleigh-Ritz method with that obtained using conventional finite element method [81].

The dynamic response of width-tapered and thickness- and width-tapered laminated composite beams is developed based on classical laminate theory by using approximate Rayleigh-Ritz solution. The developed methodology gives accurate and converging results, and is advantageous in the analysis of composite beam structures.

## **1.10 Layout of the thesis**

The present chapter provided a brief introduction and literature survey on free and forced vibration of tapered laminated composite beams and buckling response of tapered composite columns using Rayleigh-Ritz method and experimental modal testing for determination of Frequency Response Function (FRF) of composite beams.

In chapter 2, elastic behaviour of linear width-tapered composite beam is determined. Energy formulation for dynamic response of width-tapered laminated composite beam is developed based on Kirchhoff one dimensional laminated beam theory using Rayleigh-

Ritz method. Trial functions for different boundary conditions are given in Appendix A. Free and forced vibration responses are determined including damping and axial force effects. The first-ply failure analysis using Tsai-Wu failure criterion is conducted to understand the effect of tensile static end-axial force on width-tapered laminated composite beams.

In chapter 3, numerical results on the dynamic response of width-tapered laminated composite beams are considered. Rayleigh-Ritz method is used to find the natural frequencies, forced response and critical buckling loads for width-tapered laminated composite beams. The extensional and flexural stiffness distribution for linear width-tapered composite beams is shown. The effects of width ratio, length ratio, boundary conditions, and laminate configurations on natural frequencies, maximum transverse amplitude of tapered composite beams and critical buckling loads of tapered composite columns are determined. The effects of static end-axial load and damping on the natural frequencies and forced response of width-tapered composite beams have been investigated. The first ply failure load of width-tapered beam is obtained to find the effects of end-axial tensile load on natural frequencies and maximum transverse amplitude of tapered composite beams.

In chapter 4, experimental validation for width-tapered composite beams has been carried out. The manufacturing of composite laminate is discussed with fabrication and processing. Experimental modal testing is discussed using impact hammer excitation. The experimental modal testing results like Coherence function, time and auto response function and Frequency response Function (FRF) for different width ratios of width-

tapered composite beams are determined. Comparison of natural frequencies obtained using experimental modal testing with that obtained using analytical results for width-tapered composite beams are shown.

In chapter 5, free vibration and buckling response of thickness- and width-tapered laminated composite beams are considered using Rayleigh-Ritz method. Natural frequencies and critical buckling loads are determined for the combination of different angles of thickness-taper and width ratios, laminate configurations, and boundary conditions. The effects of applied static end-axial force and damping on natural frequencies of thickness- and width-tapered composite beams have been investigated. Finally a detailed comparison is arranged in tables to compare the natural frequencies obtained by Rayleigh-Ritz method from the current thesis with conventional finite element method obtained from the separate work [81] and graphical plots of forced response in terms of sinusoidal transverse displacement.

The thesis ends with chapter 6, which provides the overall conclusions of the present work and some recommendations for future work.

## CHAPTER 2

### RAYLEIGH-RITZ FORMULATION FOR DYNAMIC RESPONSE OF WIDTH-TAPERED LAMINATED COMPOSITE BEAM

#### 2.1 Introduction

The design of mechanical structures requires the development of necessary tools for modeling the mechanical behavior in design and analysis. Laminated composite beams are increasingly being used as load-carrying elements especially in high-performance mechanical, aerospace, aircraft, naval, and civil applications, where high-strength- and high-stiffness-to-weight ratios are desired. In these areas, the dynamic and static instabilities show themselves as a problem of elastic instability. When their behavior is to be predicted under various loadings, there is a need for accurate analysis of the loading effects. The practical loadings on aerospace and automobile structures are mostly dynamic in nature. Therefore, advanced analytical and numerical techniques are required for the calculation of the dynamic response characteristics of structures in order that they can be designed against failure due to dynamic loads. In this chapter, free and forced vibration and buckling response of width-tapered laminated composite beams are conducted using Rayleigh-Ritz formulation to obtain the equation of motion.

Elastic behavior of linear-width-tapered laminated composite beam is determined in section 2.2. In section 2.3, energy formulation for dynamic response of width-tapered

laminated composite beam based on Kirchhoff one-dimensional laminated beam theory is developed. In section 2.3.1 system matrices are formed using Rayleigh-Ritz method for free and forced vibration and buckling response of width-tapered laminated composite beams. Free undamped vibration of width-tapered composite beams is shown in section 2.3.2. Forced vibration response including static end-axial force is discussed in section 2.3.3. Forced vibration response considering damping properties are determined in section 2.3.4. In section 2.3.5, the formulation based on Rayleigh-Ritz method for buckling response is carried out for width-tapered composite columns. In section 2.4 the formulation for first-ply failure of the laminate using Tsai-Wu tensor theory is carried out.

A beam is a solid structural member most commonly used in mechanical structures or systems. In practical structures, it can take up a great variety of loads such as transverse load applied between its supports, transverse shear, bi-plane bending and even torsion. A plane beam resists primarily loading applied in one plane and has cross-section that is symmetric with respect to that plane. One-dimensional mathematical model of plane beam is considered on the basis of beam theories. The stiffness co-efficients of the laminated beam are determined based on classical laminate theory (corresponding to the Euler-Bernoulli beam theory) [1].

## 2.2 Elastic behavior of linear width-tapered laminated composite beam

Many structures made of composite materials are composed of numerous laminae, which are bonded and/or cured together. The superior properties in strength and stiffness that composites possess, and the ability to stack laminae one on the other in a varied but unique fashion to result in the optimum laminate properties for a given structural size and set of loadings are major advantages that composite structures have over more conventional structures. The focus has been on the stress-strain or constitutive relations [80].

For width-tapered laminated composite beam as shown in Figure 2.1, few basic assumptions are imposed:

1. The beam is constructed of an arbitrary number of layers of orthotropic sheets bonded together. However, the orthotropic axes of material symmetry of an individual layer need not coincide with the xyz axes of the beam.
2. The beam is thin, i.e the thickness  $H$  is much smaller than the length  $L$  and width  $b$ .
3. The height of the beam is constant, whereas the width is tapered.
4. Transverse shear strains  $\gamma_{xz}$  and  $\gamma_{yz}$  are negligible.
5. In-plane displacements  $u$  and  $v$  are linear functions of the  $z$  coordinate.
6. The transverse normal strain  $\varepsilon_z$  is negligible.

7. Each ply obeys Hooke's law.
8. The rotatory inertia caused by the rotational acceleration is negligible.
9. There are no body forces.
10. Transverse shear stresses  $\tau_{xz}$  and  $\tau_{yz}$  vanish on the surfaces  $z = \pm H/2$ .

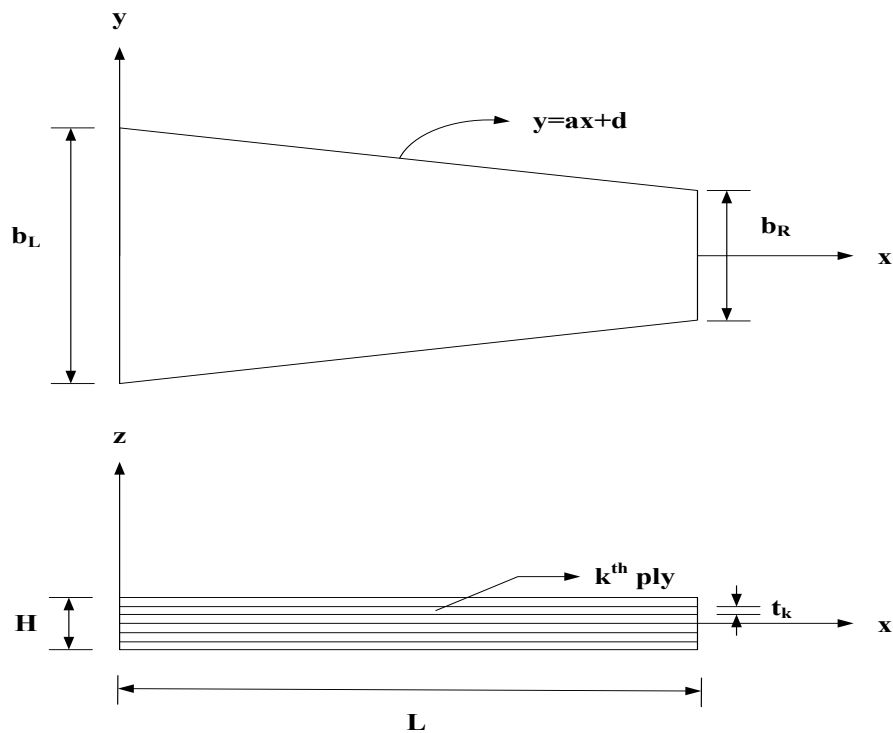


**Figure 2.1** Schematic illustration of linear width- tapered laminated composite beam and coordinate system

In this work, Classical Laminate Theory (CLT) is applied to width-tapered laminated composite beam.

The constitutive relation between the force and moment resultants and the midsurface strains and curvatures are given by [3]:

$$\begin{Bmatrix} N_x \\ N_y \\ N_{xy} \\ M_x \\ M_y \\ M_{xy} \end{Bmatrix} = \begin{bmatrix} A_{11} & A_{12} & A_{16} & B_{11} & B_{12} & B_{16} \\ A_{12} & A_{22} & A_{26} & B_{12} & B_{22} & B_{26} \\ A_{16} & A_{26} & A_{66} & B_{16} & B_{26} & B_{66} \\ B_{11} & B_{12} & B_{16} & D_{11} & D_{12} & D_{16} \\ B_{12} & B_{22} & B_{26} & D_{12} & D_{22} & D_{26} \\ B_{16} & B_{26} & B_{66} & D_{16} & D_{26} & D_{66} \end{bmatrix} \begin{Bmatrix} \varepsilon_x \\ \varepsilon_y \\ \gamma_{xy} \\ k_x \\ k_y \\ k_{xy} \end{Bmatrix} \quad (2.1)$$

where,

$$A_{ij} = \int_{-\frac{H}{2}}^{\frac{H}{2}} \bar{Q}_{ij} dz \quad (2.2a)$$

$$B_{ij} = \int_{-\frac{H}{2}}^{\frac{H}{2}} \bar{Q}_{ij} z dz \quad (2.2b)$$

$$D_{ij} = \int_{-\frac{H}{2}}^{\frac{H}{2}} \bar{Q}_{ij} z^2 dz \quad (2.2c)$$

with  $i, j = 1, 2, 6$ .

It should be noted that in the Equation (2.1), the  $N_x$  and  $M_x$  were originally defined for plate type structures and correspond to unit width in the y-direction, and hence apply directly to a beam of ‘unit’ width. In the present thesis, since the width varies along the x-direction, it is convenient to multiply all of the above equations by the beam width  $b(x)$ .

The resulting force and moment equations are expressed as:

$$P_x(x) = N_x \times b(x), P_y(x) = N_y \times b(x), P_{xy}(x) = N_{xy} \times b(x) \quad (2.3)$$

$$R_x(x) = M_x \times b(x), R_y(x) = M_y \times b(x), R_{xy}(x) = M_{xy} \times b(x) \quad (2.4)$$

The Equations (2.3) and (2.4) are shown as:

$$\begin{Bmatrix} P_x \\ P_y \\ P_{xy} \\ R_x \\ R_y \\ R_{xy} \end{Bmatrix} = b(x) \times \begin{bmatrix} A_{11} & A_{12} & A_{16} & B_{11} & B_{12} & B_{16} \\ A_{12} & A_{22} & A_{26} & B_{12} & B_{22} & B_{26} \\ A_{16} & A_{26} & A_{66} & B_{16} & B_{26} & B_{66} \\ B_{11} & B_{12} & B_{16} & D_{11} & D_{12} & D_{16} \\ B_{12} & B_{22} & B_{26} & D_{12} & D_{22} & D_{26} \\ B_{16} & B_{26} & B_{66} & D_{16} & D_{26} & D_{66} \end{bmatrix} \begin{Bmatrix} \varepsilon_x \\ \varepsilon_y \\ \gamma_{xy} \\ k_x \\ k_y \\ k_{xy} \end{Bmatrix} \quad (2.5)$$

It is to be noted in the Equation (2.5), the effect of change in width is considered in the matrix of stiffness elements.

For linear width taper, at any arbitrary position ‘x’ of the beam as shown in Figure 2.1,  $b(x)$  is given as:

$$b(x) = b_L - \left( \frac{b_L - b_R}{L} \right) x \quad (2.6)$$

## 2.3 Energy formulation for dynamic response of width-tapered laminated composite beams based on one-dimensional laminated beam theory

Euler-Bernoulli beam theory is also defined as classical beam theory. This beam model accounts for bending moment effects on stress and deformation. Transverse shear forces are recovered from equilibrium but their effect on beam deformation is neglected [24].

### 2.3.1 System matrices

Classical Laminated Plate Theory (CLPT) states that the transverse shear stresses through the thickness of the laminate are negligible and further, the normal to the middle plane remains normal after deformation [5]. Here we consider pure bending of symmetrically laminated beams according to CLPT. For symmetric laminates, the equations for bending deflection are uncoupled from those of the stretching displacements. If the in-plane forces are zero, the in-plane displacements are zero, and the problem is reduced to solving for bending deflection.

In the case of pure bending of a symmetric laminate the constitutive equation (2.5) reduces to:

$$\begin{Bmatrix} R_x \\ R_y \\ R_{xy} \end{Bmatrix} = \begin{bmatrix} b(x) \times D_{11}(x) & b(x) \times D_{12}(x) & b(x) \times D_{16}(x) \\ b(x) \times D_{12}(x) & b(x) \times D_{22}(x) & b(x) \times D_{26}(x) \\ b(x) \times D_{16}(x) & b(x) \times D_{26}(x) & b(x) \times D_{66}(x) \end{bmatrix} \begin{Bmatrix} \circ k_x \\ \circ k_y \\ \circ k_{xy} \end{Bmatrix} \quad (2.7)$$

In deriving one-dimensional laminated beam theory, the Equation (2.7) is represented in the inverse form as:

$$\begin{Bmatrix} {}^o k_x \\ {}^o k_y \\ {}^o k_{xy} \end{Bmatrix} = \begin{bmatrix} b(x) \times D_{11}(x) & b(x) \times D_{12}(x) & b(x) \times D_{16}(x) \\ b(x) \times D_{12}(x) & b(x) \times D_{22}(x) & b(x) \times D_{26}(x) \\ b(x) \times D_{16}(x) & b(x) \times D_{26}(x) & b(x) \times D_{66}(x) \end{bmatrix}^{-1} \begin{Bmatrix} R_x \\ R_y \\ R_{xy} \end{Bmatrix} \quad (2.8)$$

The Equation (2.8) is given as:

$$\begin{Bmatrix} {}^o k_x \\ {}^o k_y \\ {}^o k_{xy} \end{Bmatrix} = \begin{bmatrix} D_{11}^*(x) & D_{12}^*(x) & D_{16}^*(x) \\ D_{12}^*(x) & D_{22}^*(x) & D_{26}^*(x) \\ D_{16}^*(x) & D_{26}^*(x) & D_{66}^*(x) \end{bmatrix} \begin{Bmatrix} R_x \\ R_y \\ R_{xy} \end{Bmatrix} \quad (2.9)$$

In deriving one-dimensional laminated beam theory, here it is assumed that the moments  $R_y$  and  $R_{xy}$  are equal to zero.

The inverse form of the relation between curvatures to bending moments as shown in the Equation (2.9) is represented as:

$${}^o k_x = -\frac{\partial^2 w}{\partial x^2} = D_{11}^*(x) \times R_x \quad (2.10a)$$

$${}^o k_y = -\frac{\partial^2 w}{\partial y^2} = D_{12}^*(x) \times R_x \quad (2.10b)$$

$${}^o k_{xy} = -2 \frac{\partial^2 w}{\partial x \partial y} = D_{16}^*(x) \times R_x \quad (2.10c)$$

The above relations (2.10a) to (2.10c) show that the deflection ‘w’ cannot be strictly independent of the variable ‘y’. The bending and twisting induced by the terms  $D_{12}^*$  and  $D_{16}^*$  can cause the beam to lift off its supports. This effect is negligible where the length to width (L/b) ratio of the beam is sufficiently high.

Neglecting the bending and twisting induced by the terms  $D_{12}^*$  and  $D_{16}^*$  in the Equations (2.10b) and (2.10c),  $\overset{o}{k}_y$  and  $\overset{o}{k}_y$  are neglected.

The Equation (2.10a) is rewritten as:

$$R_x = - \left( \frac{1}{D_{11}^*} \right) \frac{\partial^2 w}{\partial x^2} \quad (2.11)$$

From the reference [24], the potential energy for uniform width composite beam according to classical laminated beam theory and cylindrical bending theory is given as:

$$U = \frac{1}{2} \int_0^L b D_{11} \left( \frac{\partial^2 w}{\partial x^2} \right)^2 dx \quad (2.12)$$

The above Equation (2.12) is given for finite uniform width of the composite laminated beam. As the scale factor for the beam width increases such that it satisfies the Euler-Bernoulli beam theory, the width ‘b’ is multiplied in the strain energy as shown in the Equation (2.12).

For width-tapered laminated composite beam, the term  $b(x)$  is multiplied in the stiffness elements as shown in the Equation (2.5).

The strain energy due to flexure of the beam which is given in Equation (2.12) can be represented according to one-dimensional beam theory as:

$$U_{flexure} = \frac{1}{2} \int_0^L \left( \frac{1}{D_{11}^*(x)} \right) \left( \frac{\partial^2 w}{\partial x^2} \right)^2 dx \quad (2.13)$$

It is to be noted that, in the above Equation (2.13), the term  $b(x)$  is integrated in the matrix of stiffness and compliance elements. This is one of the prime contributions of the present formulation.

The work done due to applied static end-axial load on the width-tapered laminated beam is represented as follows [3]:

$$U_{axialload} = \frac{1}{2} P \int_0^L \left[ \left( \frac{\partial w}{\partial x} \right)^2 dx \right] \quad (2.14)$$

Therefore, the total strain energy  $U_{total}$  which is the sum of  $U_{flexure}$  and  $U_{axialload}$  is given as:

$$U_{total} = \frac{1}{2} \int_0^L \left( \frac{1}{D_{11}^*(x)} \right) \left( \frac{\partial^2 w}{\partial x^2} \right)^2 dx + \frac{1}{2} P \int_0^L \left( \frac{\partial w}{\partial x} \right)^2 dx \quad (2.15)$$

In the above Equation (2.15), the static end-axial load applied is tensile load. If the applied load is compressive load, then  $P < P_{cr}$ , where  $P_{cr}$  is the critical buckling load and the sign of P will be negative.

The kinetic energy denoted as 'T' of an elastic body in terms of xyz coordinates is given as [24]:

$$T = \frac{1}{2} \iiint_V \rho_c \left( \left( \frac{\partial u}{\partial t} \right)^2 + \left( \frac{\partial v}{\partial t} \right)^2 + \left( \frac{\partial w}{\partial t} \right)^2 \right) dx dy dz. \quad (2.16)$$

where,  $\rho_c$  is the density of composite material at the point xyz.

The displacements u, v and w are given by:

$$u = \left( -z \left( \frac{\partial w(x)}{\partial x} \right) \right) \quad (2.17a)$$

$$v = 0 \quad (2.17b)$$

$$w = w(x, t) \quad (2.17c)$$

Substituting Equation (2.17) in Equation (2.16),

$$T = \frac{1}{2} \iiint_V \rho_c \left( \left( -z \frac{\partial^2 w(x)}{\partial x \partial t} \right)^2 + \left( \frac{\partial w}{\partial t} \right)^2 \right) dx dy dz. \quad (2.18)$$

The first term of Equation (2.18) arises due to the change in slope of the deflection curve (or the angle of rotation) with time and is related to the rotational kinetic energy. According to Euler-Bernoulli beam or thin-beam theory [1], the rotatory inertia caused by the rotational acceleration of a beam element is negligible; hence the first term is neglected in Equation (2.18). The equation for kinetic energy of the width-tapered laminated beam reduces to:

$$T = \frac{1}{2} \int_0^L \rho_c \cdot b(x) \cdot H \cdot \left( \frac{\partial w}{\partial t} \right)^2 dx \quad (2.19)$$

where,  $H$  is the height of the laminate.

### 2.3.1.1 Analysis using Rayleigh-Ritz method

There exist no exact solutions for the natural frequencies and forced responses for general non-uniform composite beams. Even if they exist for more idealized cases they are often cumbersome to use, often requiring solution for transcendental equations to determine the natural frequencies and subsequent evaluation of infinite series to evaluate the system response. Therefore, approximate solution based on Rayleigh-Ritz method is developed to find the natural frequencies and forced response of tapered laminated composite beams and critical buckling load of tapered laminated composite columns. In this section, the formulations based on Rayleigh-Ritz method for width-tapered laminated composite beams are derived using classical laminate theory.

From the reference [4], the Rayleigh equation is given as:

$$\omega^2 = \frac{U_{total\max}}{T_{\max}^*} \quad (2.20)$$

where the kinetic energy ‘ $T_{\max}$ ’ is expressed as  $\omega^2 T_{\max}^*$ . In Rayleigh-Ritz method, the assumed deflection to be the sum of several functions multiplied by constants is given as follows:

$$w(x,t) = c_1\phi_1(x) + c_2\phi_2(x) + \dots + c_i\phi_i(x) + \dots + c_n\phi_n(x) \quad (2.21)$$

where  $c_i$  are the undetermined coefficients and  $\phi_i(x)$  are any admissible functions satisfying the geometric boundary conditions.

$U_{total\max}$  and  $T_{\max}^*$  are expressed as:

$$U_{total\max} = \frac{1}{2} \sum_{i=1}^n \sum_{j=1}^n K_{ij} \cdot c_i c_j + \frac{1}{2} \sum_{i=1}^n \sum_{j=1}^n P \cdot \bar{G}_{ij} \cdot c_i c_j \quad (2.22)$$

$$T_{\max}^* = \frac{1}{2} \sum_{i=1}^n \sum_{j=1}^n M_{ij} \cdot c_i c_j \quad (2.23)$$

where the coefficients are derived as:

$$K_{ij} = \int_0^L \left( \frac{1}{D_{11}(x)} \right) \cdot \phi_i''(x) \cdot \phi_j''(x) \cdot dx \quad (2.24)$$

$$\overline{G}_{ij} = \int_0^L \phi_i'(x) \cdot \phi_j'(x) dx \quad (2.25)$$

$$M_{ij} = \int_0^L \rho_c \cdot b(x) \cdot H \cdot \phi_i(x) \cdot \phi_j(x) dx \quad (2.26)$$

If the Rayleigh's proportional damping model is used,

$$C_{ij} = \alpha(M_{ij}) + \beta(K_{ij}) \quad (2.27)$$

In the above Equation (2.27),  $C_{ij}$  is the coefficient of Rayleigh's proportional damping [4].

Minimizing  $\omega^2$  by differentiating it with respect to each of the constants, the derivative of  $\omega^2$  with respect to  $c_i$  is given as:

$$\frac{\partial \omega^2}{\partial c_i} = \frac{\partial}{\partial c_i} \left( \frac{U_{totalmax}}{T_{max}^*} \right) = \frac{T_{max}^* \cdot \frac{\partial U_{totalmax}}{\partial c_i} - U_{totalmax} \frac{\partial T_{max}^*}{\partial c_i}}{T_{max}^{*2}} = 0 \quad (2.28)$$

The above Equation (2.28) is satisfied by:

$$\frac{\partial U_{totalmax}}{\partial c_i} - \omega^2 \frac{\partial T_{max}^*}{\partial c_i} = 0 \quad (2.29)$$

The two terms of the Equation (2.29) are shown as:

$$\frac{\partial U_{totalmax}}{\partial c_i} = \sum_{j=1}^n (K_{ij} + P.\bar{G}_{ij})c_j \quad (2.30)$$

$$\frac{\partial T^*_{max}}{\partial c_i} = \sum_{j=1}^n M_{ij}.c_j \quad (2.31)$$

Therefore, Equations (2.30) and (2.31) become:

$$c_1((K_{i1} + P.\bar{G}_{i1}) - \omega^2 M_{i1}) + c_2((K_{i2} + P.\bar{G}_{i2}) - \omega^2 M_{i2}) + \dots + c_n((K_{in} + P.\bar{G}_{in}) - \omega^2 M_{in}) = 0 \quad (2.32)$$

From the Equation (2.32), with 'i' varying from 1 to n, there will be n such equations, which are arranged in the matrix form as:

$$\begin{bmatrix} (K_{11} + P.\bar{G}_{11}) - \omega^2 M_{11} & (K_{12} + P.\bar{G}_{12}) - \omega^2 M_{12} & \bullet & \bullet & (K_{1n} + P.\bar{G}_{1n}) - \omega^2 M_{1n} \\ (K_{21} + P.\bar{G}_{21}) - \omega^2 M_{21} & \bullet & \bullet & \bullet & \bullet \\ \bullet & \bullet & \bullet & \bullet & \bullet \\ \bullet & \bullet & \bullet & \bullet & \bullet \\ (K_{n1} + P.\bar{G}_{n1}) - \omega^2 M_{n1} & \bullet & \bullet & \bullet & (K_{nn} + P.\bar{G}_{nn}) - \omega^2 M_{nn} \end{bmatrix} \begin{Bmatrix} c_1 \\ c_2 \\ \bullet \\ \bullet \\ c_n \end{Bmatrix} = \{0\} \quad (2.33)$$

The determinant of the Equation (2.33) is an n degree algebraic equation in  $\omega^2$ , and its solution results in n eigenvalues.

### 2.3.2 Free vibration response of width-tapered laminated composite beams

All systems possessing mass and elasticity are capable of free vibration, or vibration that takes place in the absence of external excitation. Of primary interest for such a system is its natural frequency of vibration.

There are many ways to connect the solution of the vibration problems with that of the algebraic eigenvalue problem. The most productive approach is to cast the vibration problem as a systematic eigenvalue problem because of the special properties associated with symmetry. The physical nature of mass and stiffness matrices is that they are usually symmetric [65].

The equation (2.33) can be written in the matrix form of equation of motion using Newton's second law of motion [1] including forced excitation and damping as follows:

$$[M]\{\ddot{c}\} + [C]\{\dot{c}\} + ([K] + P[\bar{G}])\{c\} = \{F\} \quad (2.34)$$

For undamped free vibration without static end-axial load, the Equation (2.34) can be written as:

$$[M]\{\ddot{c}\} + [K]\{c\} = \{0\} \quad (2.35)$$

For free vibration the Equation (2.35) becomes:

$$([K] - \omega^2 [M])\{c\} = \{0\} \quad (2.36)$$

From the above Equation (2.36),  $\omega$  represents the natural frequencies. Replacing  $\lambda = \omega^2$  in equation (2.36) which becomes,

$$([K] - \lambda[M])\{c\} = \{0\} \quad (2.37)$$

The above Equation (2.37) is a classical eigenvalue problem, where  $\lambda$  are eigenvalues and  $\{c\}$  are mode shapes.

### 2.3.3 Forced vibration response including static end-axial force

The forced vibration response with reference to finite number of nodal coordinates of the composite beam is determined in this section.

Considering static end-axial force, the Equation (2.34) can be re-written for undamped forced vibration as:

$$[M]\{\ddot{c}\} + ([K] + P[\bar{G}])\{c\} = \{F\} \quad (2.38)$$

$[M]$ ,  $[K]$ ,  $[\bar{G}]$ ,  $\{F\}$  and  $\{c\}$  are the mass matrix, stiffness matrix, geometric stiffness matrix, force vector and displacement vector of the beam respectively. In the Equation (2.38),  $P$  is the prescribed static end-axial tensile load. Mode superposition method is considered for forced vibration of laminated composite beam. By making the coordinate transformation [4], one can write,

$$\{c\} = [\tilde{P}]\{y\} \quad (2.39)$$

where  $[\tilde{P}]$  denotes the orthonormal modal matrix. The formation for  $[\tilde{P}]$  is shown in Appendix-B. Substituting Equation (2.39) in (2.40) and pre-multiplying by  $[\tilde{P}]^T$  on both sides of Equation (2.38), leads to

$$[\tilde{P}]^T [M][\tilde{P}]\{\ddot{y}\} + [\tilde{P}]^T [K][\tilde{P}]\{y\} + [\tilde{P}]^T P[\bar{G}][\tilde{P}]\{y\} = [\tilde{P}]^T \{F\} \quad (2.40)$$

The normal modes or eigenvectors of the system can be shown to be orthogonal with respect to the mass, stiffness and geometric stiffness matrices [4].

It can be shown from the above equation (2.40), the orthogonality relationships are [4]:

$$[\tilde{P}]^T [M][\tilde{P}] = [I] \quad (2.41)$$

$$[\tilde{P}]^T [K][\tilde{P}] = [\Lambda] \quad (2.42)$$

where,  $[I]$  is the unit matrix and  $[\Lambda]$  is a diagonal matrix of the eigenvalues which is given as:

$$\Lambda = \begin{bmatrix} \omega_1^2 & & & \\ & \omega_2^2 & & \\ & & \ddots & \\ & & & \omega_n^2 \end{bmatrix} \quad (2.43)$$

By taking the advantages of orthogonal property, the above Equation (2.40) can be written as a set of decoupled 2<sup>nd</sup> order differential equations as:

$$\{\ddot{y}\}_i + \text{diag}(\omega)_i^2 \{y\}_i = \{\tilde{f}\}_i \quad (2.44)$$

The new equations in terms of  $y$  are uncoupled and they can be solved as a set of single degree of freedom systems.

The solution for  $y_i(t)$  are in the form:

$$y_i = y_i(0) \cos \omega_i t + \frac{\dot{y}_i(0)}{\omega_i} \sin \omega_i t + \frac{\tilde{f}_i(t) \sin \omega t}{1 - \left(\frac{\omega}{\omega_i}\right)^2} \quad (2.45)$$

Substituting the value of  $y_i$  from Equation (2.45) in Equation (2.39), and representing in the form of equation (2.21), one can get forced vibration response including end-axial force.

#### 2.3.4 Forced vibration response of composite beam including damping

The definition of composite materials is mostly based on the macroscopic response rather than the microscopic mechanisms governing the energy dissipation process [3]. To investigate the concept of an equivalent viscous damping mechanism for a multiple degree of freedom system that is damped by a non-viscous process, the Equation (2.38) is extended as:

$$[M]\{\ddot{c}\} + [C]\{\dot{c}\} + ([K] + P[\bar{G}])\{c\} = \{F\} \quad (2.46)$$

By making the coordinate transformation as shown in Equation (2.39) and by taking advantage of orthogonal properties, substituting Equation (2.39) in Equation (2.46) and

pre-multiplying by  $[\tilde{P}]^T$  on both sides of Equation (2.46), the Equation (2.46) can be written as:

$$[\tilde{P}]^T [M][\tilde{P}]\{\ddot{y}\} + [\tilde{P}]^T [C][\tilde{P}]\{\dot{y}\} + [\tilde{P}]^T [K][\tilde{P}]\{y\} + [\tilde{P}]^T P[\bar{G}][\tilde{P}]\{y\} = [\tilde{P}]^T \{F\} \quad (2.47)$$

It is shown in Ref. [4] that  $[\tilde{P}]^T [M][\tilde{P}]$  and  $[\tilde{P}]^T [K][\tilde{P}]$  are diagonal matrices but  $[\tilde{P}]^T [C][\tilde{P}]$  is not diagonal and the preceding Equation (2.47) is coupled by the damping matrix. The difficulty with modeling damping in this fashion is that modal analysis cannot in general be used to solve Equation (2.47), because damping provides additional coupling between the equations of motion. As a result, this cannot be always decoupled by the modal transformation. Modal analysis can be used to directly solve Equation (2.47), if the damping matrix  $[C]$  can be written as a linear combination of the mass and stiffness matrices [24].

By using Rayleigh's proportional damping which is given as:

$$[C] = \alpha[M] + \beta[K] \quad (2.48)$$

where  $\alpha$  and  $\beta$  are mass-proportional and stiffness-proportional constants. Substitution of Equation (2.48) into Equation (2.47) yields,

$$[\tilde{P}]^T [M][\tilde{P}]\{\ddot{y}\} + [\tilde{P}]^T (\alpha[M] + \beta[K])[\tilde{P}]\{\dot{y}\} + [\tilde{P}]^T [K][\tilde{P}]\{y\} + [\tilde{P}]^T P[\bar{G}][\tilde{P}]\{y\} = [\tilde{P}]^T \{F\} \quad (2.49)$$

The Equation (2.49) is completely uncoupled and will have the form:

$$\ddot{y}_i + 2\zeta_i\omega_i\dot{y}_i + \omega_i^2 y_i = \tilde{f}(t) \quad (2.50)$$

where the modal damping is given as:

$$2\zeta_i\omega_i = \alpha + \beta\omega_i^2 \quad (2.51)$$

This corresponds to the n decoupled modal equations as:

$$\ddot{y}_i + (\alpha + \beta\omega_i^2)\dot{y}_i + \omega_i^2 y_i = \tilde{f}(t) \quad (2.52)$$

Considering the response of Equation (2.52) as viscously-damped single-degree-of-freedom system subject to harmonic excitation, the solution for Equation (2.52) will be

$$y_i = e^{-\zeta_i\omega_{di}t} \left[ \frac{\dot{y}(0) + \zeta_i\omega_i}{\omega_{di}} \sin \omega_{di}t + y(0) \cos \omega_{di}t \right] + \frac{\tilde{f}_0}{\sqrt{(\omega_{ni}^2 - \omega^2)^2 + (2\zeta_i\omega_{ni}\omega)^2}} \sin(\omega t - \tan^{-1} \frac{2\zeta_i\omega_{ni}\omega}{\omega_{ni}^2 - \omega^2}) \quad (2.53)$$

where,

$$\omega_{di} = \omega_{ni} \sqrt{1 - \zeta_i^2} \quad (2.54)$$

Substituting the value of  $y_i$  from Equation (2.53) in Equation (2.39), and representing in the form of Equation (2.21), the forced vibration response with damping effects is obtained considering static end-axial force.

### 2.3.5 Buckling analysis of width-tapered composite columns

It is important in analyzing a structure, in addition to looking at maximum deflections, and natural frequencies, one must investigate under what loading conditions instability can occur, this instability is referred to as buckling.

In this work, the equation for total strain energy which is the sum of strain energy due to flexure and work done due to applied static end-axial load is given in the equation (2.22). Considering the applied static end-axial compressive load, the equation (2.22) is re-written for buckling response of width-tapered laminated columns as:

$$U_{Total} = \frac{1}{2} \sum_{i=1}^n \sum_{j=1}^n K_{ij} \cdot c_i c_j - \frac{1}{2} \sum_{i=1}^n \sum_{j=1}^n P \cdot \bar{G}_{ij} \cdot c_i c_j \quad (2.55)$$

The Equation (2.56) can be written in the matrix form as:

$$([K] - P[\bar{G}])\{c\} = \{0\} \quad (2.56)$$

The above Equation (2.56) is an eigenvalue problem, where 'P' represents the eigenvalue. The system represented by Equation (2.56) has 'n' eigenvalues where 'n' represents the total number of degrees of freedom. The smallest eigenvalue will be the critical buckling load which is represented as  $P_{cr}$ .

## 2.4 First-ply failure analysis

A laminate will fail under increasing mechanical and thermal loads. The laminate failure, however, may not be catastrophic. It is possible that some layer fails and the composite continue to take more loads until all the plies fail. Failed plies may still contribute to the stiffness and strength of the laminate. Since polymer-matrix composites are stronger in the fiber direction relative to the other directions, it is clear that failure must be a function of the direction of the applied stress relative to the direction of the fibers. Causing failure of an element of material in the fiber direction requires significantly more stress than causing failure perpendicular to the fibers. Tensile failure in the fiber direction is controlled by fiber strength, while tensile failure perpendicular to the fibers is controlled by the strength of the bond between the fiber and matrix, and by the strength of the matrix itself.

### 2.4.1 Tsai-Wu tensor theory

The Tsai-Wu failure criterion is widely used as suggested in [67] to predict the first-ply failure of laminate. The first-ply tensile failure load is calculated to understand the effect of tensile end-axial load on the dynamic response of width-tapered laminated composite beams.

The Tsai-Wu failure criterion reduces to [80]:

$$F_1\sigma_1 + F_2\sigma_2 + F_6\tau_{12} + F_{11}\sigma_1^2 + F_{22}\sigma_2^2 + F_{66}\tau_{12}^2 - \sqrt{F_{11}F_{22}}\sigma_1\sigma_2 < 1 \quad (2.57)$$

The failure constants are given by:

$$F_1 = \frac{1}{\sigma_1^T} + \frac{1}{\sigma_1^C}, F_{11} = -\frac{1}{\sigma_1^T \sigma_1^C}, F_2 = \frac{1}{\sigma_2^T} + \frac{1}{\sigma_2^C}, F_{22} = -\frac{1}{\sigma_2^T \sigma_2^C}, F_6 = 0, F_{66} = \left( \frac{1}{\tau_{12}^F} \right)^2 \quad (2.58)$$

## 2.5 Summary

In this chapter, Rayleigh-Ritz method is used for the dynamic response of width-tapered laminated composite beams. The resulting force and moment equations for width-tapered composite beams are derived. Energy formulation for dynamic response of width-tapered laminated composite beams is described based on one-dimensional laminated beam theory. Formulations for free and forced vibration response of width-tapered laminated composite beams considering end-axial force and damping are derived. Buckling response of width-tapered laminated composite columns is determined. First-ply failure analysis using Tsai-Wu tensor theory is shown.

## CHAPTER 3

### DYNAMIC RESPONSE OF WIDTH-TAPERED LAMINATED COMPOSITE BEAMS

#### 3.1 Introduction

In the previous chapter, energy formulations based on Euler-Bernoulli beam theory using Rayleigh-Ritz method were described for the dynamic response of width-tapered laminated composite beams. First, the system matrices for energy formulation of width-tapered laminated composite beam based on one-dimensional laminated beam theory was considered. Second, the Rayleigh-Ritz method is used assuming the deflection to be a sum of several functions multiplied by coefficients. The coefficients of matrices were developed for width-tapered laminated composite beams. Next, the Rayleigh-Ritz formulation is used for free and forced vibration response of composite beams including the effects of end-axial force and damping properties and for buckling response of width-tapered laminated columns. The first-ply failure analysis for width-tapered composite beam was conducted using Tsai-Wu tensor theory. The formulations are used in the present chapter for a comprehensive parametric study for free and forced vibration response of width-tapered laminated composite beams and buckling response of width-tapered laminated columns.

The material chosen is NCT-301 graphite-epoxy that is available in the laboratory of Concordia Centre for Composites (CONCOM). The mechanical properties of the fiber

and the resin are given in the Tables 3.1 and 3.2 respectively. The geometric properties are given in detail in Table 3.3. Symmetric laminate is considered in all problems.

The results are summarized in plots to interpret the results. Each subsection is ended with a short interpretation. Finally, overall summary is provided at the end of the chapter.

**Table 3.1** Mechanical properties of unidirectional NCT-301 graphite-epoxy prepreg [24]

|   |                        |
|---|------------------------|
| Longitudinal modulus ( $E_1$ )          | 113.9 GPa              |
| Transverse modulus ( $E_2$ )            | 7.985 GPa              |
| $E_3=E_2$                               | 7.985 GPa              |
| In-plane shear modulus ( $G_{12}$ )     | 3.137 GPa              |
| Out-of-plane shear modulus ( $G_{23}$ ) | 2.852 GPa              |
| Density of fiber ( $\rho_k$ )           | 1480 kg/m <sup>3</sup> |
| Major Poisson's ratio ( $\nu_{12}$ )    | 0.288                  |
| Minor Poisson's ratio ( $\nu_{21}$ )    | 0.018                  |

**Table 3.2** Mechanical properties of resin material [24]

|                               |                        |
|-------------------------------|------------------------|
| Elastic modulus (E)           | 3.93 GPa               |
| Shear modulus (G)             | 1.034 GPa              |
| Density of resin ( $\rho_r$ ) | 1000 kg/m <sup>3</sup> |
| Poisson's ratio ( $\nu$ )     | 0.37                   |

**Table 3.3** Geometric properties of width-tapered composite beam

|                                 |  |
|---------------------------------|--|
| Length (L)                      | 0.25 m                                       |
| Width at left section ( $b_L$ ) | 0.016 m                                      |
| Width ratio ( $b_R/b_L$ )       | 0.01, 0.02, 0.05, 0.1, 0.2, 0.4, 0.6, 0.8, 1 |
| Individual ply thickness (t)    | 0.000125 m                                   |
| Height of the laminate (H)      | 0.0045 m                                     |

### 3.2 Elastic behavior of width-tapered laminated composite beam

The design of a tapered structure involves consideration of stiffness, static strength, dynamic stability and damage tolerance. For designing a width-tapered composite beam, the stiffness distribution, laminate configuration, ply orientation and width ratio are major considerations. The extensional and flexural stiffness distribution plays an important role in the dynamic response of composite beams.

### 3.2.1 Extensional and flexural stiffness distribution for linear width-tapered composite beam

The linear width-tapered composite beam shown in the Figure 2.1 is considered to analyze the extensional and flexural stiffness distribution. The laminate configurations considered are, 1) LC1 which is the laminate with  $([0/90]_9)_s$  configuration, 2) LC2 which is the laminate with  $([\pm 45]_9)_s$  configuration, 3) LC3 which is the laminate with  $([0_4/\pm 45_7])_s$  configuration, and 4) LC4 which is the laminate with  $([0/\pm 60]_6)_s$  configuration.

The extensional and flexural stiffness distributions of linear width-tapered composite beams across the length of the beam for width ratio  $(b_R/b_L)$  values of 0.01, 0.4 and 1 are determined and are given in the Figures 3.1-3.3 for laminate configurations LC1, LC2, LC3 and LC4. The extensional and flexural stiffnesses are represented in semi-log plot.

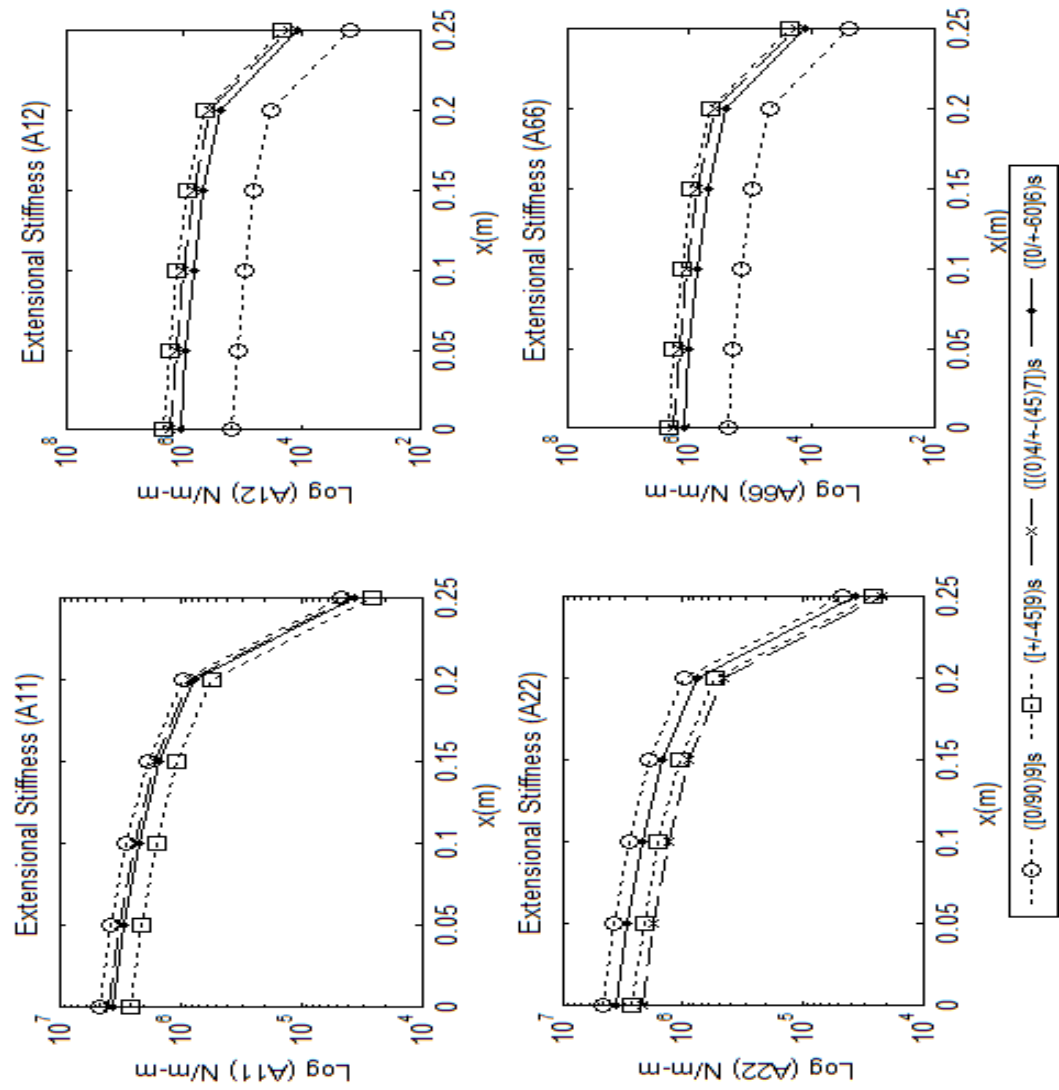


**Figure 3.1** Extensional stiffness distributions for linear width-tapered composite beam with a width ratio ( $b_R/b_L$ ) value of 0.01

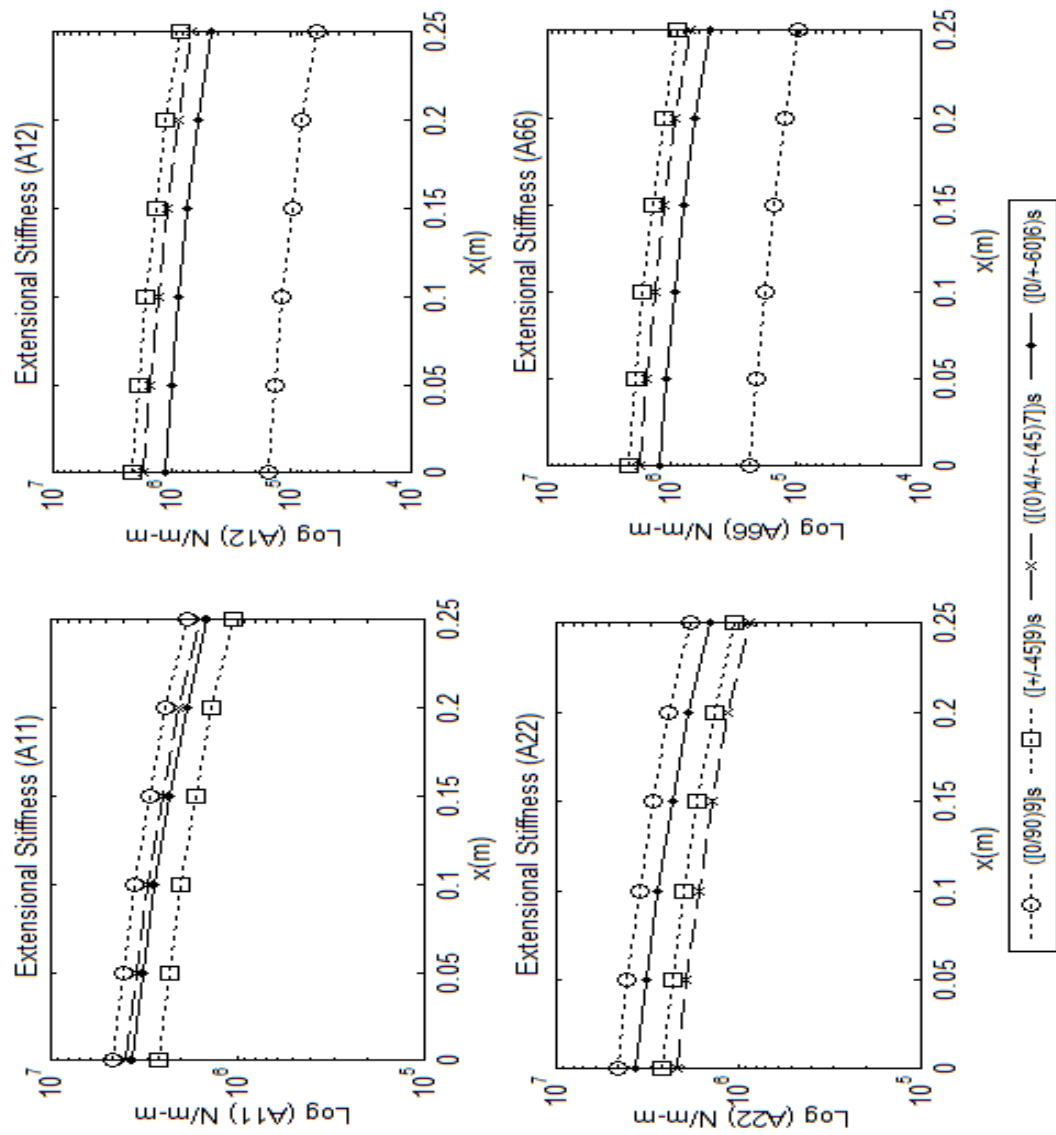


**Figure 3.2** Extensional stiffness distributions for linear width-tapered composite beam with a width ratio ( $b_R/b_L$ ) value of 0.4

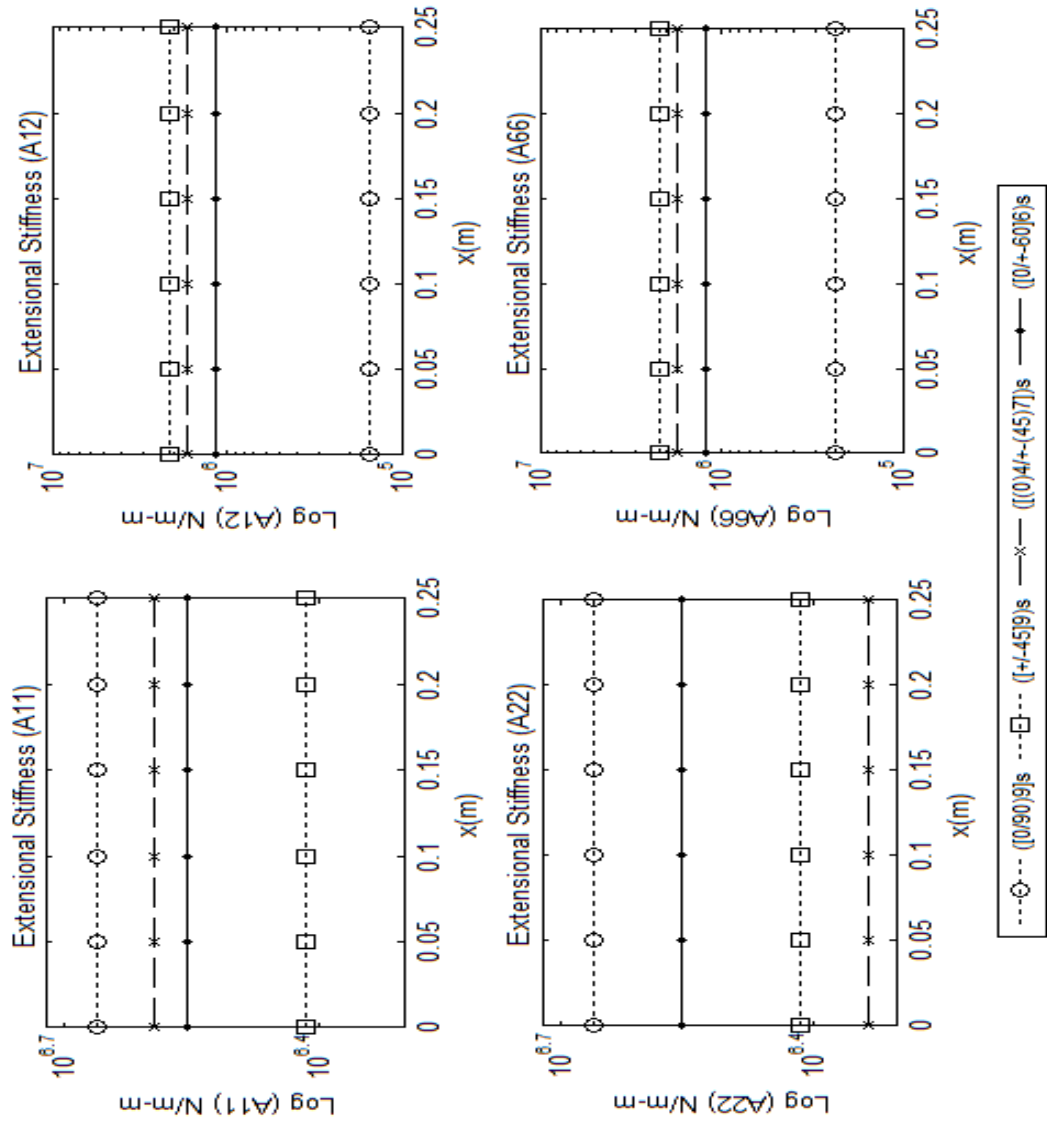


**Figure 3.3** Extensional stiffness distributions for linear width-tapered composite beam with a width ratio ( $b_R/b_L$ ) value of 1

Figures 3.1-3.3 show the extensional stiffness distribution on laminate configurations for width ratio ( $b_R/b_L$ ) values of 0.01, 0.4 and 1. From the Figure 3.1, it can be observed that the laminate configuration LC1 is strongest in terms of extensional stiffness coefficients  $A_{11}$  and  $A_{22}$ . It is fairly evident that from the laminate configurations considered, most of the  $0^\circ$  fibers are oriented along the length of the beam for laminate configuration LC1. Hence values of  $A_{12}$  and  $A_{66}$  are the least. The laminate configuration LC2 is strongest in terms of extensional stiffness coefficients  $A_{12}$  and  $A_{66}$ . This is because  $\pm 45^\circ$  laminate configuration has higher laminate shear modulus compared to that of LC1, LC3 and LC4. The laminate configuration LC3 is second largest for extensional stiffness coefficients  $A_{11}$ ,  $A_{12}$  and  $A_{66}$  and lowest for  $A_{22}$ . The laminate configuration LC4 is third largest for extensional stiffness coefficients  $A_{11}$ ,  $A_{12}$  and  $A_{66}$  but second largest for  $A_{22}$ . From the Figure 3.2, the extensional stiffness distribution is similar to the Figure 3.1, except that the change in the extensional stiffnesses at  $x=0$  and at  $x=0.25$  is smaller, whereas in the Figure 3.3 the stiffness distribution is uniform since the beam is uniform. One can observe from Figures 3.1-3.3, that the laminate configuration LC1 is weakest in terms of extensional stiffness coefficients  $A_{12}$  and  $A_{66}$  compared to the laminate configurations LC2, LC3 and LC4 because LC1 has lower Poisson's ratio and lower shear coupling coefficient [82].

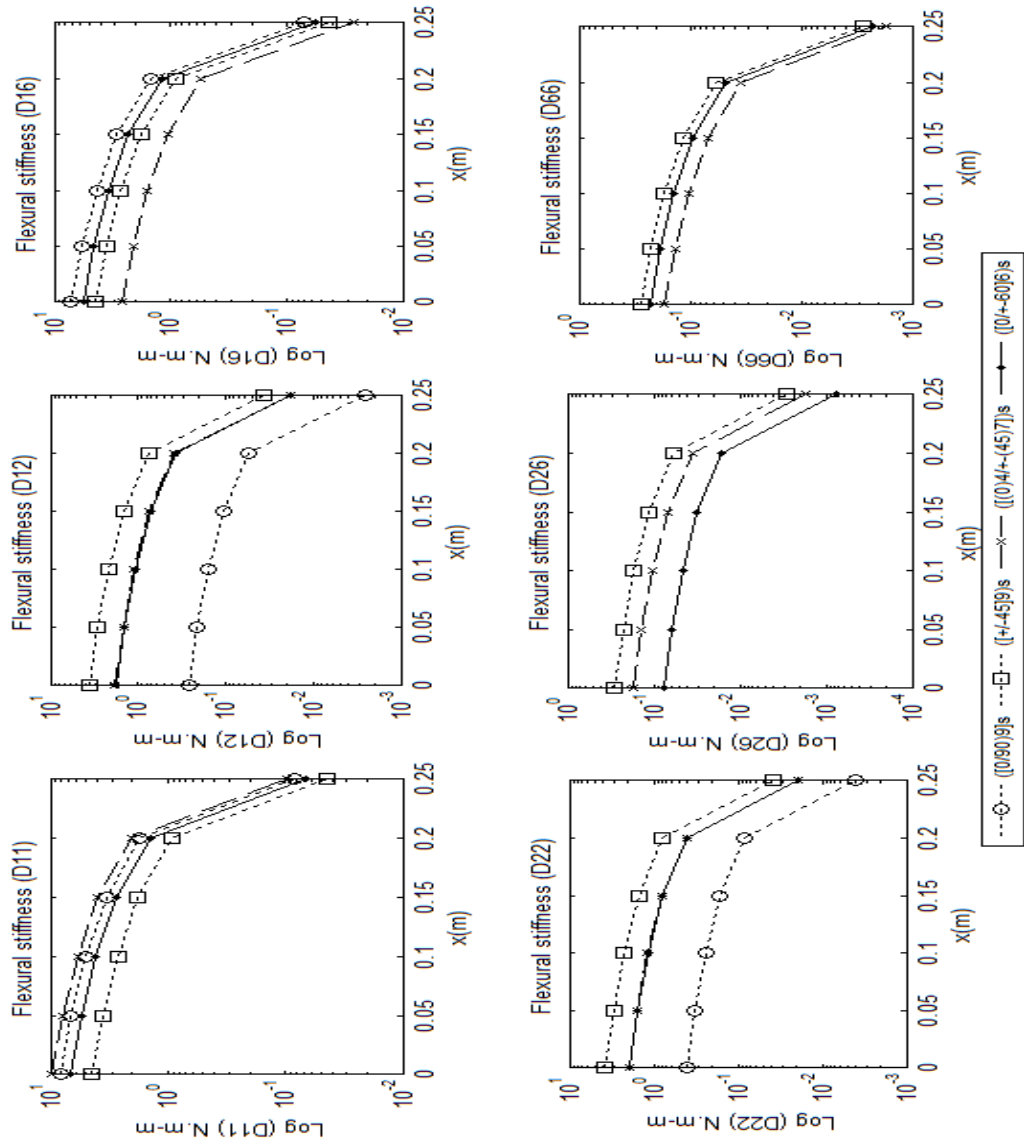


**Figure 3.4** Flexural stiffness distributions for linear width-tapered composite beam with a width ratio ( $b_R/b_L$ ) value of 0.01

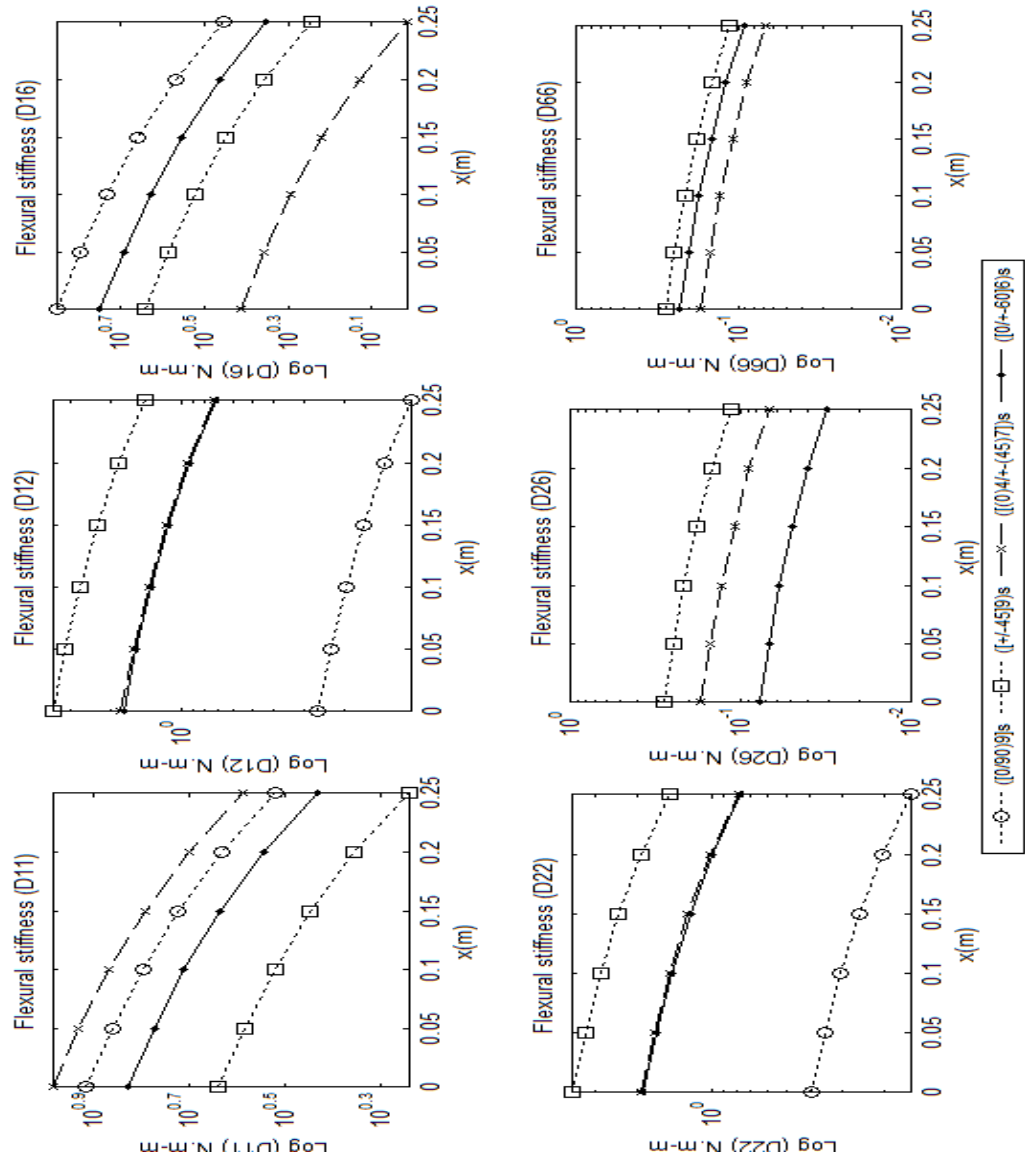


**Figure 3.5** Flexural stiffness distributions for linear width-tapered composite beam with a width ratio ( $b_R/b_L$ ) value of 0.4

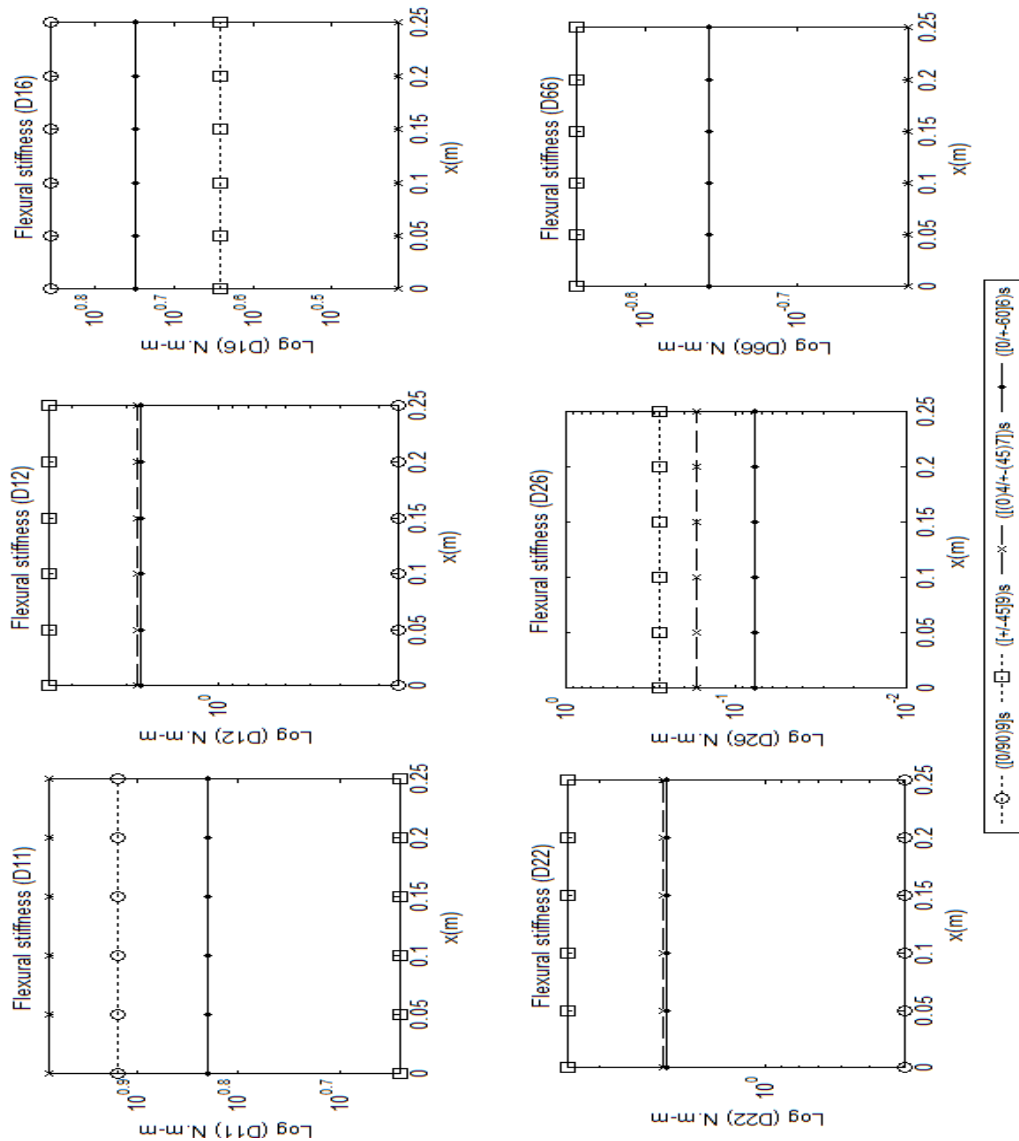


**Figure 3.6** Flexural stiffness distributions for linear width-tapered composite beam with a width ratio ( $b_R/b_L$ ) value of 1

Figures 3.4-3.6 show the flexural stiffness distribution on laminate configurations for width ratio ( $b_R/b_L$ ) values of 0.01, 0.4 and 1. From the Figure 3.4, the laminate configuration LC3 is strongest in terms of flexural stiffness coefficient  $D_{11}$ . The laminate configuration LC1 is second largest, LC4 and LC2 are third and fourth largest

respectively. This is since most of the  $0^0$  fibers are oriented along the length of the beam for the laminate configuration LC3,  $0^0$  fibers have highest  $E_1$  compared to other fiber direction which is the direction of the bending loads, whereas the laminate configuration LC2 is strongest in terms of flexural stiffness coefficients  $D_{12}$ ,  $D_{22}$ ,  $D_{26}$  and  $D_{66}$ . But the laminate configuration LC1 is strongest in terms of flexural stiffness coefficient  $D_{12}$ , the laminate configuration LC2 is strongest in terms of flexural stiffness coefficient  $D_{16}$ . From the Figure 3.5, the stiffness distribution is similar to the Figure 3.4 except that the change in the stiffnesses between the length of the beam ( $x=0$  and  $x=0.25\text{m}$ ) is smaller. From the Figure 3.6, the flexural stiffness distribution is uniform.

### **3.3 Free vibration response of width-tapered laminated composite beams**

In this section, free vibration response of width-tapered laminated composite beams is considered for simply-supported, clamped-clamped, clamped-free, and free-clamped boundary conditions. Rayleigh-Ritz method is used to find the natural frequencies of width-tapered composite beams. Comprehensive parametric studies for natural frequencies of width-tapered composite beams have been shown through plots.

#### **3.3.1 Effect of width ratio ( $b_R/b_L$ ) on natural frequencies**

To study the effect of width ratio ( $b_R/b_L$ ) on first three natural frequencies, the linear width-tapered composite beams with four boundary conditions are considered. The

boundary conditions considered are: a) SS (Simply-supported), b) CC (Clamped-clamped), c) CF (Clamped-free) and d) FC (Free-clamped). The width ratio values considered are 0.01, 0.02, 0.05, 0.1, 0.2, 0.4, 0.6, 0.8 and 1, to investigate the effects on natural frequencies. The laminate configuration considered is  $([0/90]_9)_s$ . The thickness of the beam is constant. The problems are solved using Rayleigh-Ritz method. The results are summarized in the Figures 3.7, 3.8 and 3.9 to interpret the results.

By using the properties given in the Tables 3.1, 3.2 and 3.3, the current section is focused to find the effect of width ratio ( $b_R/b_L$ ) on first three natural frequencies for four boundary conditions. The natural frequencies are in rad/sec.

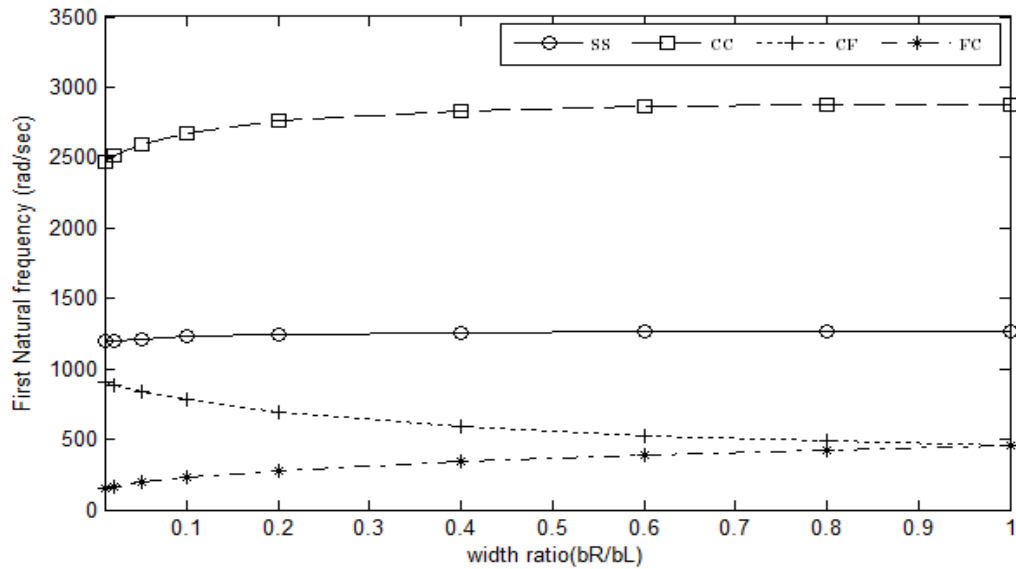


**Figure 3.7** Effect of width ratio ( $b_R/b_L$ ) on first natural frequency

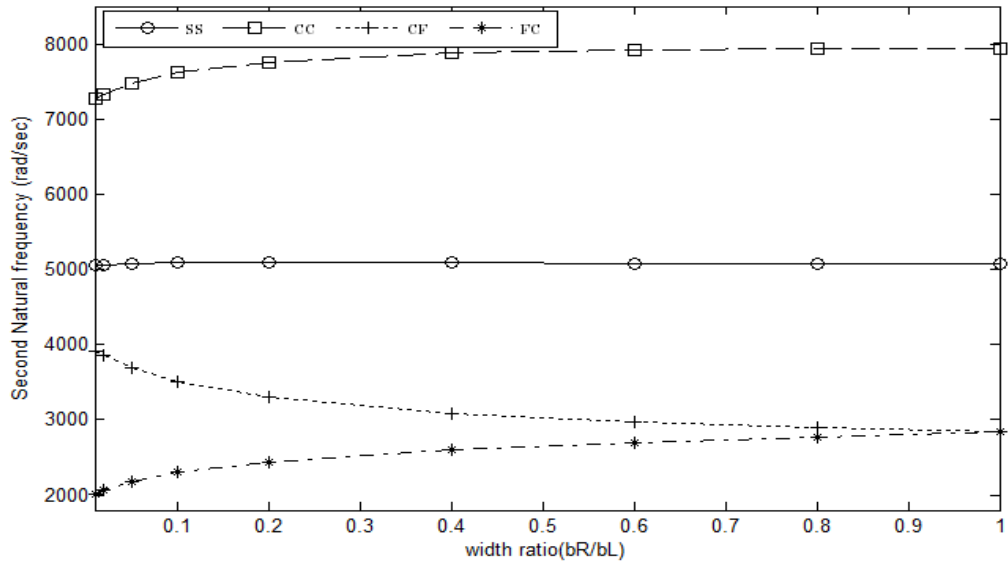


**Figure 3.8** Effect of width ratio ( $b_R/b_L$ ) on second natural frequency

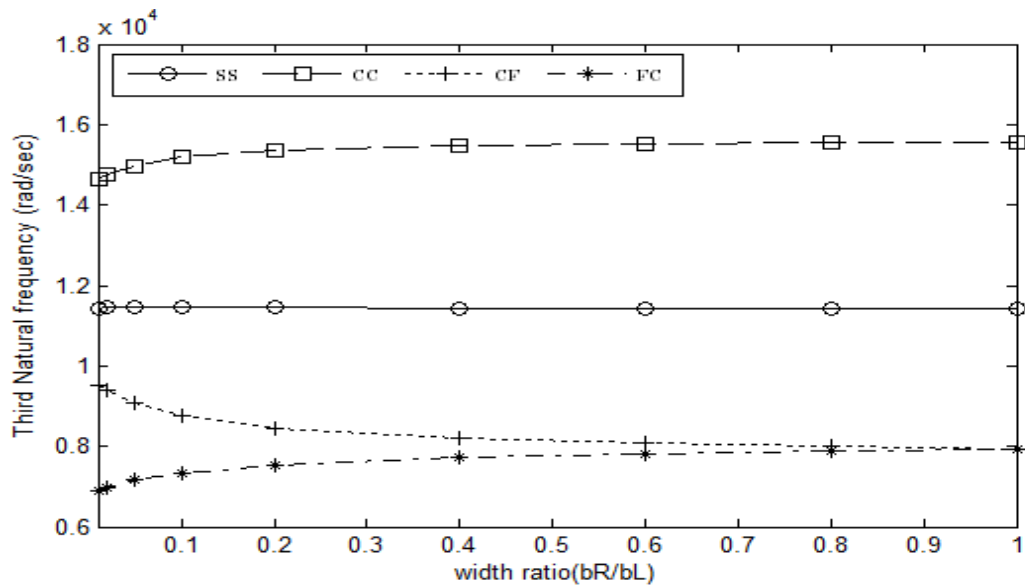


**Figure 3.9** Effect of width ratio ( $b_R/b_L$ ) on third natural frequency

Figures 3.7-3.9 show the effect of width ratio ( $b_R/b_L$ ) on three natural frequencies with four boundary conditions. It can be observed that as the width ratio ( $b_R/b_L$ ) values increase, all three natural frequencies increase for simply-supported, clamped-clamped and free-clamped boundary conditions. Increasing the width ratio ( $b_R/b_L$ ) values results in increase in the value of x-directional bending stiffness term  $\left(\frac{1}{D_{11}^*(x)}\right)$  as can be seen from the Equation (2.11), which in turn results in increase in stiffness matrix coefficients. But all three natural frequencies decrease for clamped-free boundary condition as the width ratio ( $b_R/b_L$ ) increase along the length of the beam. This is because of the change in the value of  $\left(\frac{1}{D_{11}^*(x)}\right)$ . Also the stiffness values coincide for clamped-free and free-clamped boundary conditions at width-ratio ( $b_R/b_L$ ) =1 as it should be.

### 3.3.2 Effect of ply orientation and laminate configuration on natural frequencies

To investigate the effects of laminate orientation on first three natural frequencies, the linear width-tapered beam with width ratio ( $b_R/b_L$ ) values mentioned previously in the section 3.3.1 along with four boundary conditions are considered. The laminate configuration considered is  $([\pm\theta]_9)_s$  ply group. The beam is made of 36 plies. The laminate configurations considered for the effect on natural frequencies are: 1)  $([0/90]_9)_s$  denoted as ‘LC1’, 2)  $([\pm 45]_9)_s$  denoted as ‘LC2’, 3)  $([0_4/\pm 45_7])_s$  denoted as ‘LC3’, and 4)  $([0/\pm 60]_6)_s$  denoted as ‘LC4’.

By using the properties given in the Tables 3.1, 3.2 and 3.3, the current section is analyzed to find the effect of ply orientation on fundamental natural frequency and the effect of laminate configurations on first three natural frequencies of width-tapered composite beams. The plots 3.10 and 3.11 are showing the variations of natural frequencies for simply-supported, clamped-clamped, clamped-free and free-clamped boundary conditions for uniform and width-tapered beam. The width ratio ( $b_R/b_L$ ) value of 0.5 is considered for width-tapered beam to find the effect of ply orientation on fundamental natural frequency.

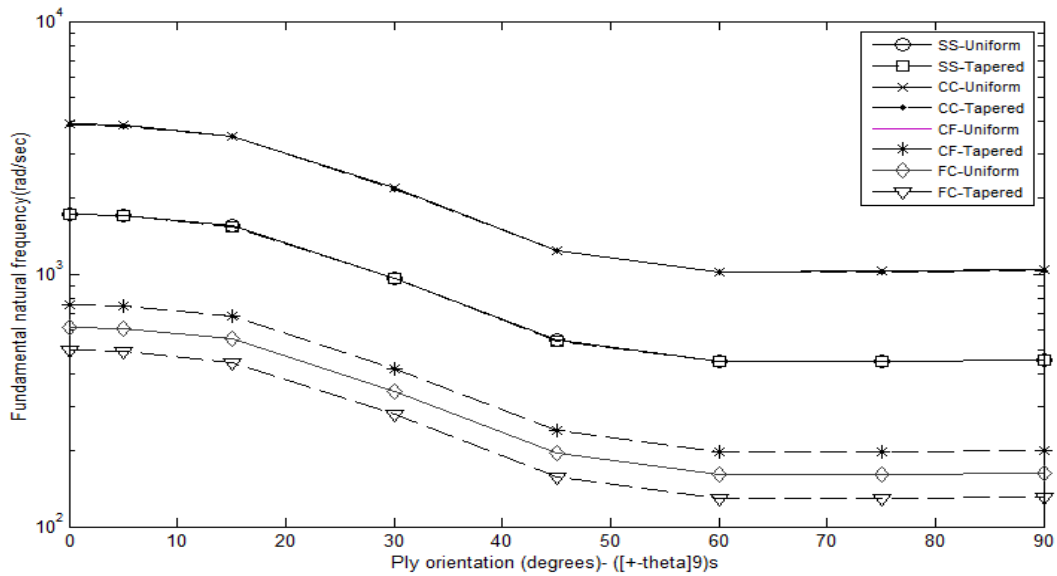


**Figure 3.10** Effect of ply orientation on first natural frequency for four boundary conditions

Figure 3.10 shows the effect of ply orientation on first natural frequency (rad/sec) for four boundary conditions of uniform and width-tapered beams. From the figure 3.10 it can be observed that the fundamental natural frequency is largest for clamped-clamped

boundary condition of uniform beam compared to the width-tapered beam. The second, third and fourth largest for simply-supported, clamped-free and free-clamped boundary conditions. The change in the fundamental natural frequency corresponds to different ply orientations of the laminate. As one can observe that the fundamental natural frequency drops significantly for orientation greater than  $10^0$ . In semi-log plot shown in Figure 3.10, only 5 out of 8 lines in the legend appear to be distinguishable. This is because the differences in the fundamental natural frequencies among the uniform and width-tapered beams for SS, CC and CF boundary conditions is small on the one hand and a logarithmic scale is used for the ordinate representing the frequency, on the other hand. It may also be noted that the difference in the fundamental natural frequency between the uniform and width-tapered beams for FC boundary condition is larger than that for SS, CC and CF boundary conditions because of the change in cross-sectional stiffness values due to the restrained condition. The fundamental natural frequency is second largest for simply-supported, third largest for clamped-free and fourth largest for free-clamped condition.

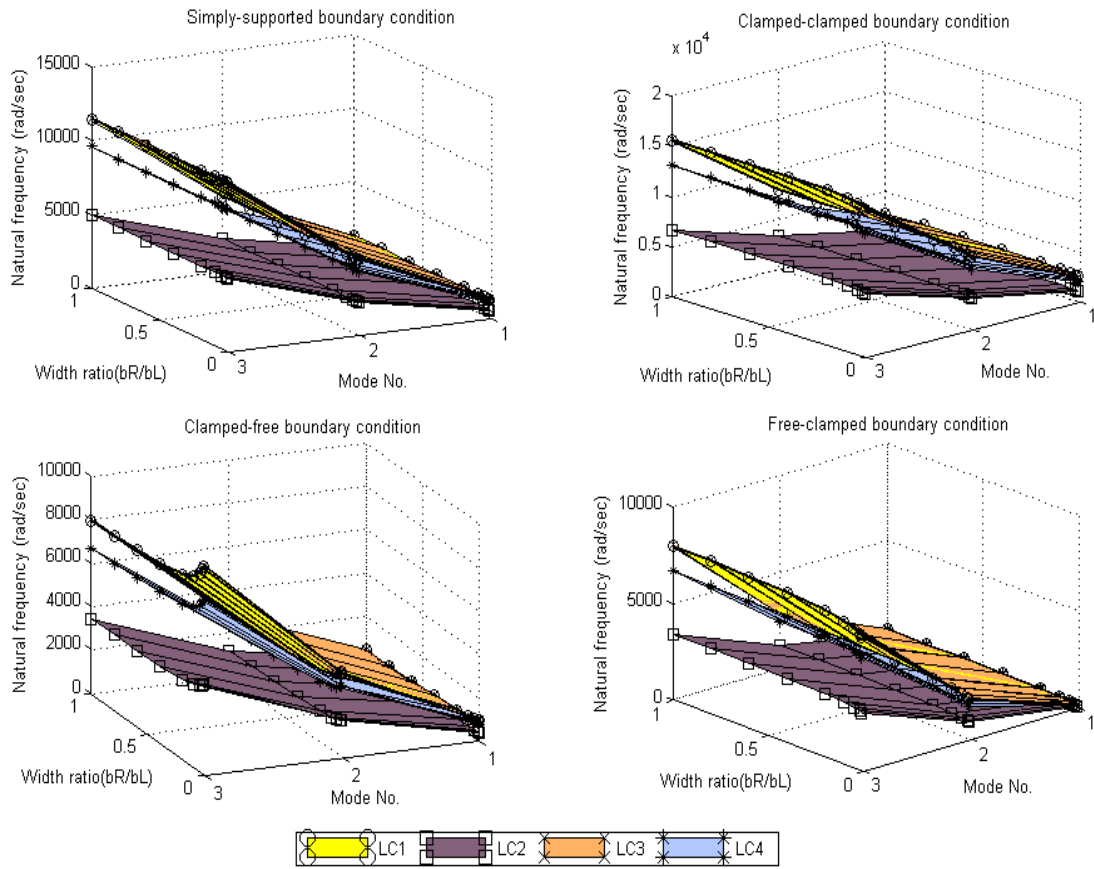


**Figure 3.11** Effect of laminate configurations on natural frequencies

Figure 3.11 shows the effect of laminate configuration on first three natural frequencies of width-tapered composite beams for four boundary conditions. From the Figure 3.11 one can observe that the natural frequencies are largest for laminate configuration LC3, second largest for LC1, third largest for LC4 and fourth largest for LC2. This difference in natural frequencies is expected for different laminate configurations because the different laminate configurations depend on the stiffness of

the beam. The stiffness of the beam depends on  $\left( \frac{1}{D_{11}^*(x)} \right)$  which is directly related with  $Q_{11}$  of the ply. Also, as the width ratio ( $b_R/b_L$ ) value increases from 0.01 to 1, the natural frequencies increase for simply-supported, clamped-clamped and free-clamped boundary conditions. But they decrease for clamped-free boundary condition.

### 3.3.3 Effect of length ratio ( $L_1/L_3$ ) on natural frequencies

To study the effect of length ratio ( $L_1/L_3$ ) on natural frequencies, the width-tapered composite beams of width ratio ( $b_N/b_w$ ) with length ratio ( $L_1/L_3$ ) as shown in the Figure 3.12 for four boundary conditions are considered. The plies of  $([0/90]_9)_s$  composite beam is made of NCT-301 graphite-epoxy. The geometric properties of the beam are: the beam is considered with 36 plies, the height of the beam is 0.0045 m, and individual ply thickness ( $t_k$ ) is 0.000125 m. From the Figure 3.12 ‘ $b_w$ ’ represents the wider section of the beam and ‘ $b_N$ ’ represents the narrower section of the beam. ‘ $L_1$ ’ represents the length of the beam at wider section, ‘ $L_2$ ’ represents the length of the beam at width-tapered section, and ‘ $L_3$ ’ represents the length of the beam at narrower section. The total length of the beam is kept constant. Changing the length ratio is by changing length of the beam at wider and narrower sections to achieve different length ratios. When the length ratio ( $L_1/L_3$ ) is 2, it is that the length of wider section is twice that of narrower section of the beam. When the length ratio ( $L_1/L_3$ ) is  $1/2$ , it is that the length of

wider section is half of the length of narrower section of the beam whereas, when the length ratio is 1, the length of wider section is equal to the length of narrower section.

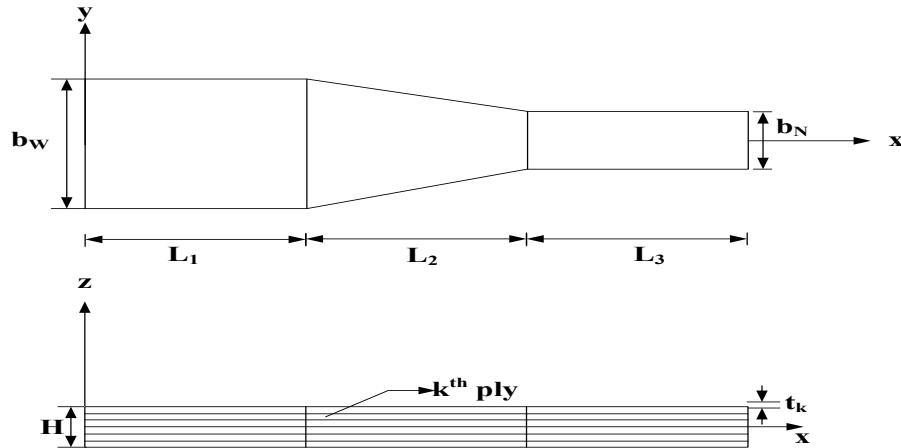


**Figure 3.12** Schematic illustration of linear width- tapered laminated composite beam showing the length ratio

By using the properties given in the Tables 3.1, 3.2 and 3.3, the section 3.3.3 is carried out to find the effect of length ratio ( $L_1/L_3$ ) on first three natural frequencies with width ratio ( $b_N/b_w$ ) values of 0.01, 0.02, 0.05, 0.1, 0.2, 0.4, 0.6, 0.8 and 1 considered for four boundary conditions. The first three natural frequencies for all boundary conditions are obtained using Rayleigh-Ritz method.

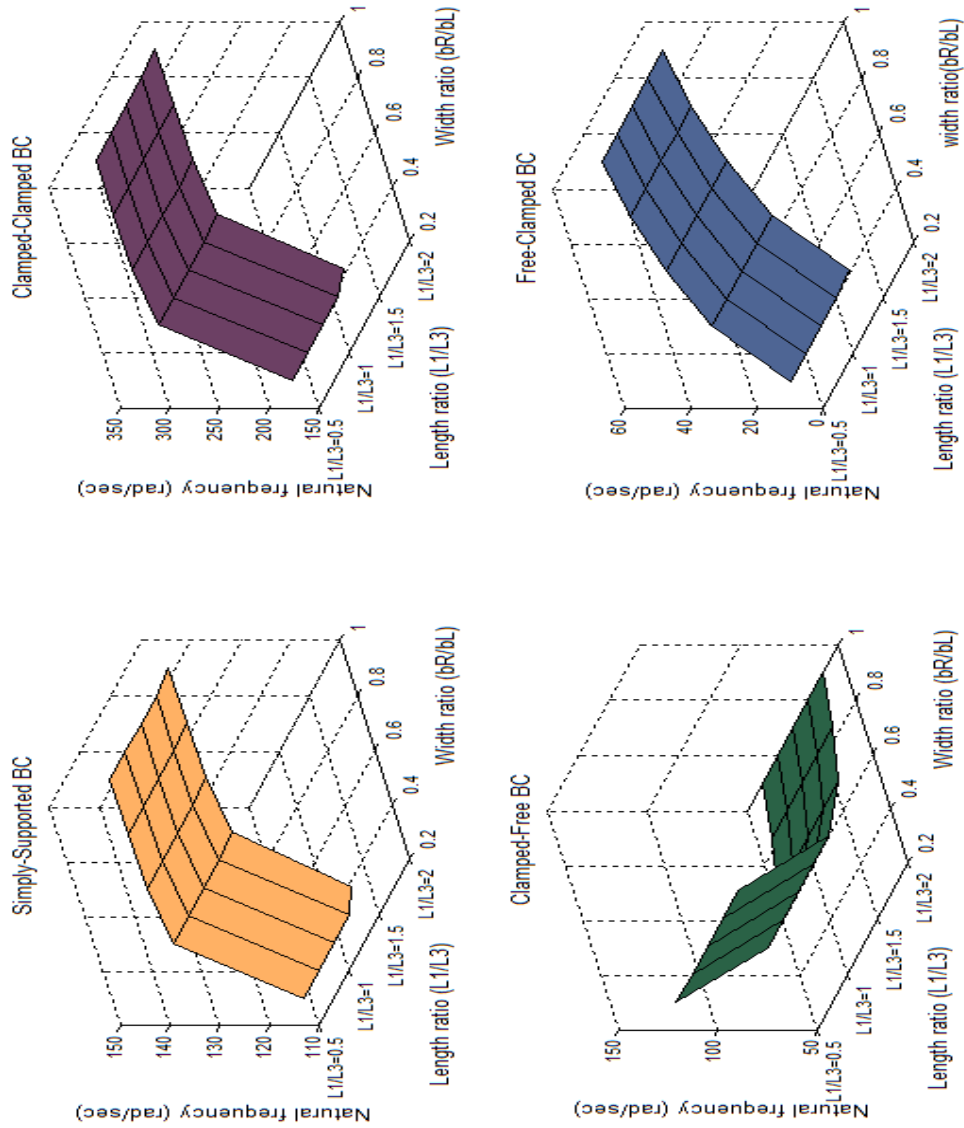


**Figure 3.13** Effect of length ratio ( $L_1/L_3$ ) on first natural frequency

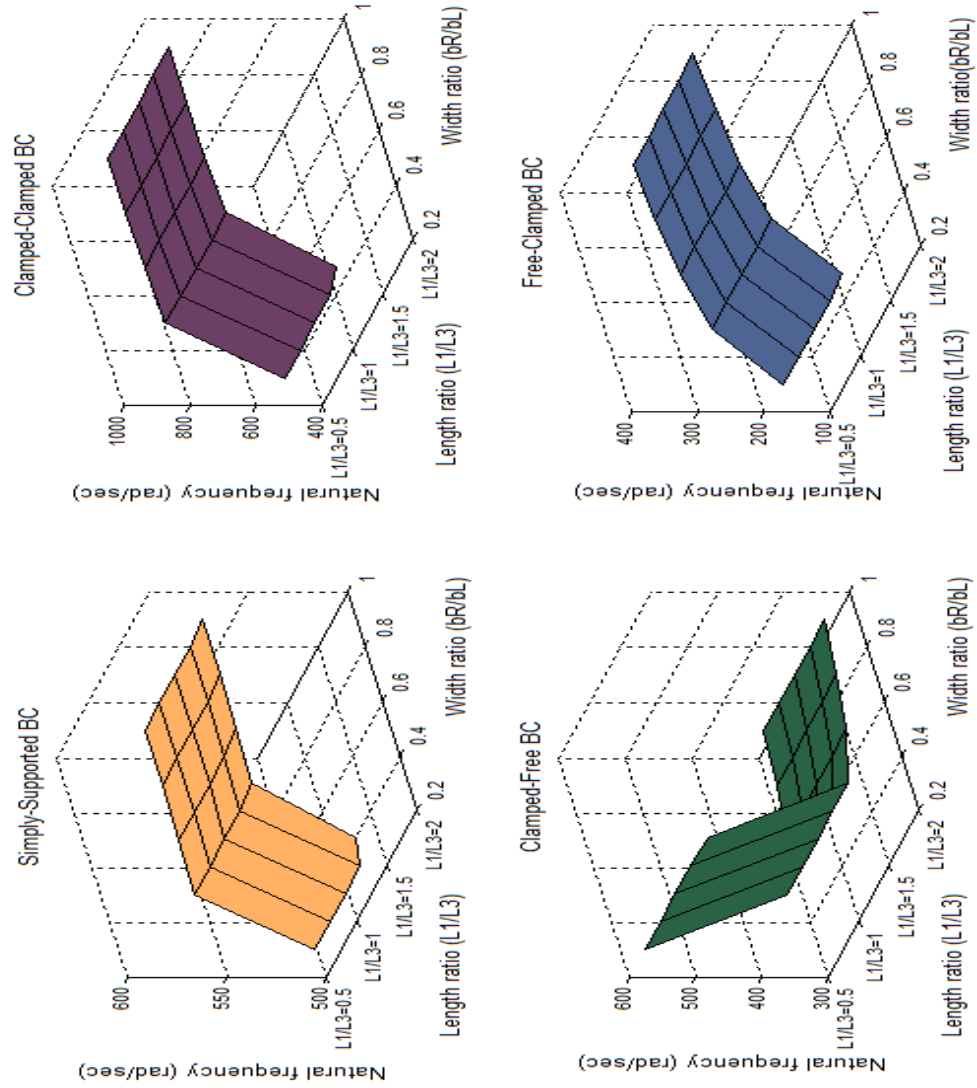


**Figure 3.14** Effect of length ratio ( $L_1/L_3$ ) on second natural frequency

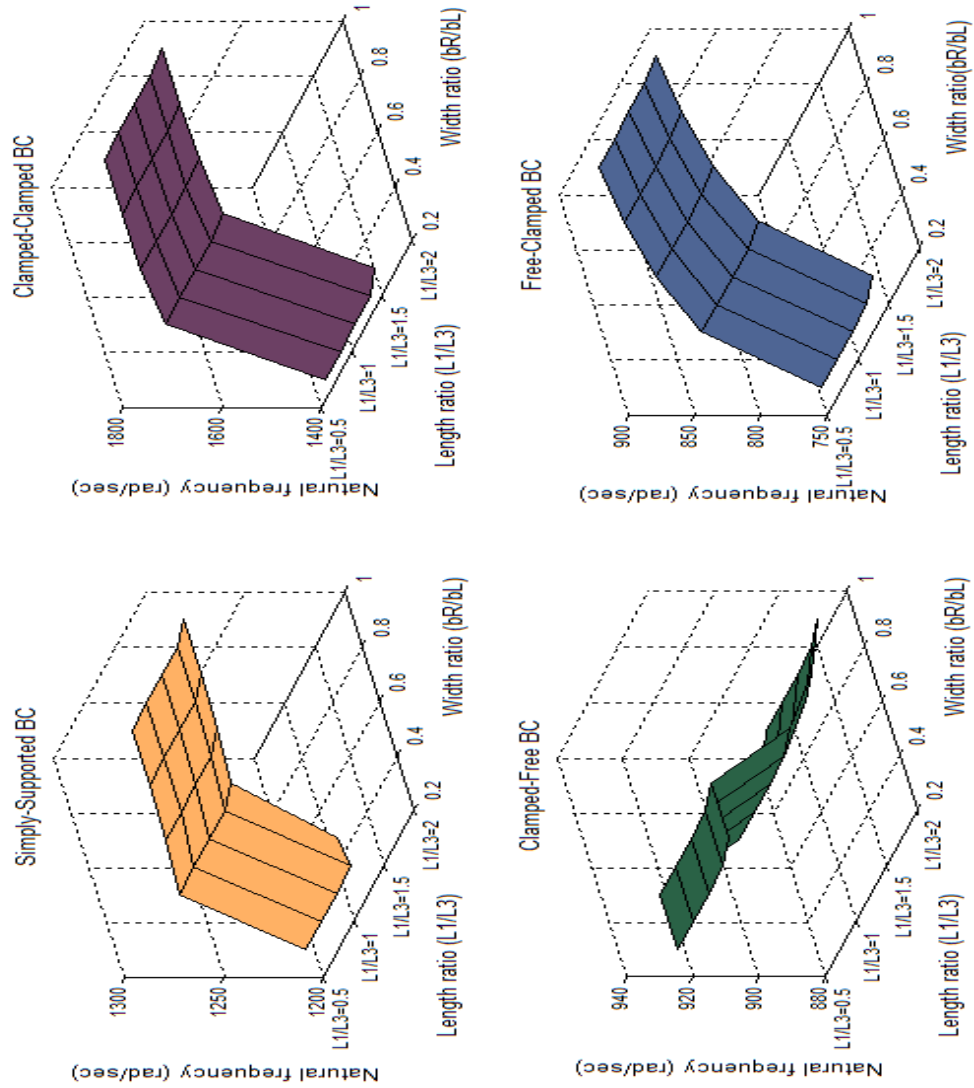


**Figure 3.15** Effect of length ratio ( $L_1/L_3$ ) on third natural frequency

Figures 3.13-3.15 show the effect of length ratio ( $L_1/L_3$ ) on three natural frequencies for all four boundary conditions. From the Figures 3.13-3.15, it can be observed that as the length ratio ( $L_1/L_3$ ) increases, all the three natural frequencies increase because as the

length on the wider section of beam is increased the stiffness of the beam increases. Also the three natural frequencies increase as the width ratio ( $b_R/b_L$ ) value increases for SS, CC and FC boundary conditions, but decrease for CF boundary condition. Another important observation that can be made is the first, second and third natural frequencies increase for width ratio ( $b_R/b_L$ ) values from 0.2 to 0.4 but the natural frequencies remain unchanged with the increase in width ratio ( $b_R/b_L$ ) values beyond 0.4 upto 1. This is because when the length of the wider section is bigger than that of the narrower section, the increase in width ratio ( $b_R/b_L$ ) has no change in the natural frequencies for SS and CC boundary condition. But the natural frequencies gradually increase as the width ratio ( $b_R/b_L$ ) values increase from 0.2 to 1 for FC boundary condition, while the natural frequencies decrease for CF boundary condition.

### **3.3.4 Effect of boundary condition on natural frequencies**

To study the effect of boundary condition on first three natural frequencies, the tapered beam of width ratio ( $b_R/b_L$ ) values mentioned in the section 3.3.1 for simply-supported, clamped-clamped, clamped-free, and free-clamped boundary conditions are considered. The different boundary conditions are considered to investigate the degree of restraint and the position of restraint on the natural frequencies. The plies of  $([0/90]_9)_s$  composite beam is considered. By using the properties given in the Tables 3.1, 3.2 and

3.3, the effect of boundary condition on first three natural frequencies for different width ratio ( $b_R/b_L$ ) values is obtained using Rayleigh-Ritz method.

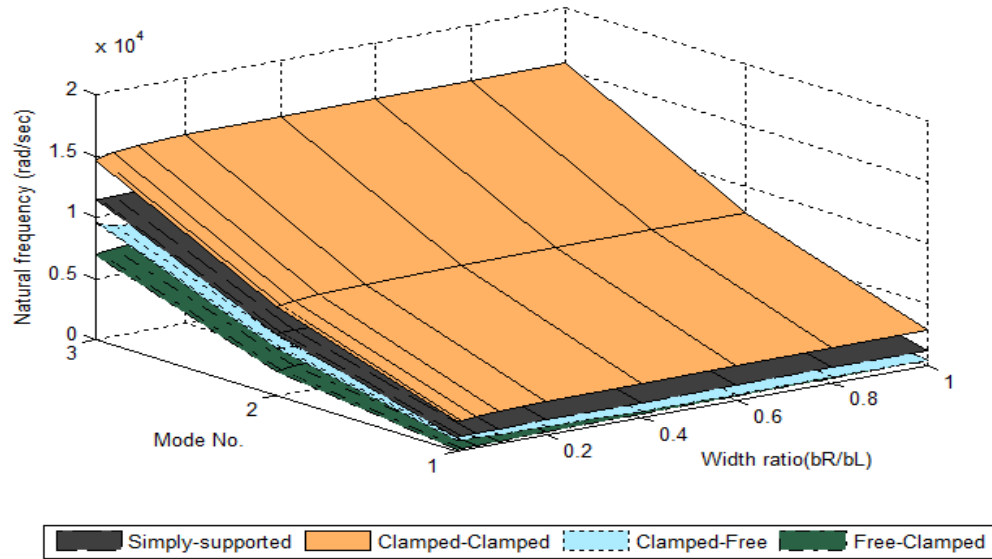


**Figure 3.16** Effect of boundary conditions on natural frequencies

Figure 3.16 shows the effect of boundary conditions on first three natural frequencies for  $[(0/90)_9]_s$  width-tapered composite beam. From the Figure 3.16, it can be observed that the natural frequencies increase as the width ratio ( $b_R/b_L$ ) values increase from 0.01 to 1 for SS, CC and FC boundary condition, but decrease for CF boundary conditions. One can observe that for clamped-clamped boundary condition, the beam has highest natural frequencies compared to other boundary conditions as the beam becomes stiffer. Beam with free-clamped boundary condition has lowest natural frequencies because the beam has lowest stiffness. Then beam with simply-supported and clamped-free boundary conditions are second highest and third highest in natural frequencies respectively.

### 3.3.5 Effect of end-axial forces on natural frequencies

To investigate the effects of applied end-axial (static) forces on first three natural frequencies, the linear width-tapered beam with width ratio ( $b_R/b_L$ ) values of 0.01, 0.02, 0.05, 0.1, 0.2, 0.4, 0.6, 0.8 and 1 along with four boundary conditions are considered as shown in the Figure 3.17. The plies of  $[[0/90]_9)_s$  composite beam which is made by NCT-301 graphite-epoxy is considered.

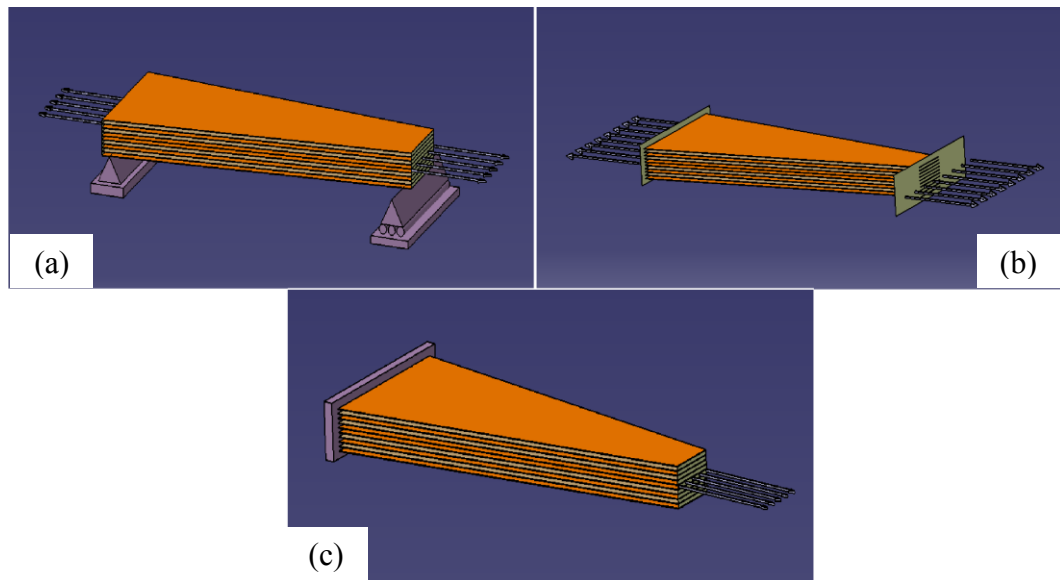


**Figure 3.17** Schematic illustration of linear width- tapered laminated composite beams with end axial force for three boundary conditions

Static -end axial compressive and tensile forces are applied at both ends of the beam as shown in the Figure 3.17. From the Figure 3.17, ‘a’ represents simply-supported, ‘b’ represents clamped-clamped and ‘c’ represents clamped-free boundary condition. The

natural frequencies are calculated for simply-supported, clamped-clamped and clamped-free boundary conditions. The critical buckling load and first-ply tensile failure loads are determined in the sections 3.5.1 and 3.6.1 respectively. The end-axial compressive and tensile forces which are applied as the percentage of the critical buckling load ( $P_{cr}$ ) and first-ply tensile failure load ( $P_1$ ) in the current section to find the effect of axial forces on natural frequencies.

By using the properties given in the Tables 3.1, 3.2 and 3.3, the effect of applied static end-axial compressive and tensile forces on first three natural frequencies for three boundary conditions are determined in the current section. The first three natural frequencies are obtained using Rayleigh-Ritz method.

**Table 3.4** Effect of end axial compressive force on first three natural frequencies -simply supported boundary condition

| % Pcr | Mode No.   | Width ratio ( $b_R/b_L$ ) |       |       |       |       |       |       |       |       |
|-------|------------|---------------------------|-------|-------|-------|-------|-------|-------|-------|-------|
|       |            | 0.01                      | 0.02  | 0.05  | 0.1   | 0.2   | 0.4   | 0.6   | 0.8   | 1     |
| 0     | 1          | 1199                      | 1203  | 1214  | 1227  | 1244  | 1260  | 1267  | 1269  | 1270  |
|       | 2          | 5056                      | 5063  | 5077  | 5088  | 5091  | 5086  | 5082  | 5080  | 5080  |
|       | 3          | 11438                     | 11446 | 11460 | 11464 | 11456 | 11439 | 11432 | 11429 | 11430 |
| 50    | 1          | 1017                      | 1020  | 1028  | 1038  | 1053  | 1064  | 1070  | 1074  | 1076  |
|       | % decrease | 15                        | 15    | 15    | 15    | 15    | 16    | 15    | 15    | 15    |

|    |            |       |       |       |       |       |       |       |       |       |
|----|------------|-------|-------|-------|-------|-------|-------|-------|-------|-------|
|    | 2          | 4888  | 4895  | 4906  | 4912  | 4913  | 4902  | 4897  | 4896  | 4898  |
|    | % decrease | 3     | 3     | 3     | 3     | 3     | 4     | 4     | 4     | 4     |
|    | 3          | 11269 | 11276 | 11287 | 11288 | 11278 | 11257 | 11249 | 11248 | 11250 |
|    | % decrease | 1     | 1     | 2     | 2     | 2     | 2     | 2     | 2     | 2     |
| 95 | 1          | 818   | 820   | 825   | 830   | 845   | 849   | 856   | 861   | 865   |
|    | % decrease | 32    | 32    | 32    | 32    | 32    | 33    | 32    | 32    | 32    |
|    | 2          | 4733  | 4738  | 4746  | 4748  | 4747  | 4730  | 4725  | 4725  | 4728  |
|    | % decrease | 6     | 6     | 7     | 7     | 7     | 7     | 7     | 7     | 7     |
|    | 3          | 11115 | 11121 | 11129 | 11127 | 11116 | 11090 | 11082 | 11082 | 11085 |
|    | % decrease | 3     | 3     | 3     | 3     | 3     | 3     | 3     | 3     | 3     |

**Table 3.5** Effect of end axial compressive force on first three natural frequencies – clamped-clamped boundary condition

| % Pcr | Mode No.   | Width ratio ( $b_R/b_L$ ) |       |       |       |       |       |       |       |       |
|-------|------------|---------------------------|-------|-------|-------|-------|-------|-------|-------|-------|
|       |            | 0.01                      | 0.02  | 0.05  | 0.1   | 0.2   | 0.4   | 0.6   | 0.8   | 1     |
| 0     | 1          | 2475                      | 2511  | 2591  | 2674  | 2761  | 2836  | 2865  | 2876  | 2879  |
|       | 2          | 7264                      | 7328  | 7470  | 7614  | 7759  | 7874  | 7915  | 7931  | 7936  |
|       | 3          | 14657                     | 14754 | 14971 | 15188 | 15348 | 15485 | 15533 | 15552 | 15558 |
| 50    | 1          | 2023                      | 2079  | 2179  | 2267  | 2358  | 2433  | 2463  | 2474  | 2477  |
|       | % decrease | 18                        | 17    | 16    | 15    | 15    | 14    | 14    | 14    | 14    |
|       | 2          | 6610                      | 6722  | 6915  | 7077  | 7231  | 7349  | 7392  | 7408  | 7413  |
|       | % decrease | 9                         | 8     | 7     | 7     | 7     | 7     | 7     | 7     | 7     |
|       | 3          | 13913                     | 14080 | 14361 | 14586 | 14782 | 14921 | 14970 | 14989 | 14995 |
|       | % decrease | 5                         | 5     | 4     | 4     | 4     | 4     | 4     | 4     | 4     |

|    |            |       |       |       |       |       |       |       |       |       |
|----|------------|-------|-------|-------|-------|-------|-------|-------|-------|-------|
| 95 | 1          | 1550  | 1613  | 1723  | 1819  | 1916  | 1996  | 2027  | 2039  | 2042  |
|    | % decrease | 37    | 36    | 34    | 32    | 31    | 30    | 29    | 29    | 29    |
|    | 2          | 6079  | 6194  | 6392  | 6560  | 6718  | 6840  | 6885  | 6902  | 6906  |
|    | % decrease | 16    | 15    | 14    | 14    | 13    | 13    | 13    | 13    | 13    |
|    | 3          | 13373 | 13542 | 13826 | 14053 | 14253 | 14394 | 14444 | 14463 | 14469 |
|    | % decrease | 9     | 8     | 8     | 7     | 7     | 7     | 7     | 7     | 7     |

**Table 3.6** Effect of end axial compressive force on first three natural frequencies – clamped-free boundary condition

| % Per | Mode No.   | Width ratio ( $b_R/b_L$ ) |      |      |      |      |      |      |      |      |
|-------|------------|---------------------------|------|------|------|------|------|------|------|------|
|       |            | 0.01                      | 0.02 | 0.05 | 0.1  | 0.2  | 0.4  | 0.6  | 0.8  | 1    |
| 0     | 1          | 902                       | 886  | 841  | 781  | 694  | 590  | 527  | 484  | 452  |
|       | 2          | 3917                      | 3851 | 3692 | 3511 | 3300 | 3090 | 2974 | 2895 | 2835 |
|       | 3          | 9531                      | 9385 | 9068 | 8760 | 8456 | 8200 | 8076 | 7997 | 7939 |
| 50    | 1          | 787                       | 772  | 733  | 681  | 606  | 515  | 461  | 423  | 396  |
|       | % decrease | 13                        | 13   | 13   | 13   | 13   | 13   | 13   | 13   | 13   |
|       | 2          | 3806                      | 3741 | 3587 | 3413 | 3212 | 3014 | 2906 | 2832 | 2776 |
|       | % decrease | 3                         | 3    | 3    | 3    | 3    | 2    | 2    | 2    | 2    |
|       | 3          | 9427                      | 9283 | 8971 | 8669 | 8375 | 8132 | 8016 | 7943 | 7889 |
|       | % decrease | 1                         | 1    | 1    | 1    | 1    | 1    | 1    | 1    | 1    |
| 95    | 1          | 663                       | 651  | 618  | 574  | 511  | 435  | 389  | 357  | 334  |
|       | % decrease | 27                        | 27   | 27   | 26   | 26   | 26   | 26   | 26   | 26   |
|       | 2          | 3702                      | 3640 | 3491 | 3323 | 3131 | 2944 | 2843 | 2774 | 2722 |
|       | % decrease | 5                         | 5    | 5    | 5    | 5    | 5    | 4    | 4    | 4    |

|  |            |      |      |      |      |      |      |      |      |      |
|--|------------|------|------|------|------|------|------|------|------|------|
|  | 3          | 9333 | 9191 | 8883 | 8587 | 8302 | 8071 | 7962 | 7893 | 7844 |
|  | % decrease | 2    | 2    | 2    | 2    | 2    | 2    | 1    | 1    | 1    |

Tables 3.4-3.6 show the effect of end axial compressive forces on first three natural frequencies for simply-supported, clamped-clamped and clamped-free boundary conditions. The compressive axial load is applied as % of critical buckling load. From the Tables 3.4-3.6, one can observe that as the axial compressive load is increased from 0 to 95 % of critical buckling load, the natural frequencies decrease. This is because as the axial compressive load is applied at the end of the beam, the beam becomes less stiff which results in decrease in the natural frequencies. The % of decrease in the natural frequencies due to the application of end-axial compressive loads is shown

**Table 3.7** Effect of end axial tensile force on first three natural frequencies –simply-supported boundary condition

| % $P_1$ | Mode No.   | Width ratio ( $b_R/b_L$ ) |       |       |       |       |       |       |       |       |
|---------|------------|---------------------------|-------|-------|-------|-------|-------|-------|-------|-------|
|         |            | 0.01                      | 0.02  | 0.05  | 0.1   | 0.2   | 0.4   | 0.6   | 0.8   | 1     |
| 0       | 1          | 1199                      | 1203  | 1214  | 1227  | 1244  | 1260  | 1267  | 1269  | 1270  |
|         | 2          | 5056                      | 5063  | 5077  | 5088  | 5091  | 5086  | 5082  | 5080  | 5080  |
|         | 3          | 11438                     | 11446 | 11460 | 11464 | 11456 | 11439 | 11432 | 11429 | 11430 |
| 50      | 1          | 4234                      | 4259  | 4317  | 4382  | 4457  | 4525  | 4552  | 4579  | 4606  |
|         | % increase | 253                       | 254   | 256   | 257   | 258   | 259   | 259   | 261   | 263   |

|    |            |       |       |       |       |       |       |       |       |       |
|----|------------|-------|-------|-------|-------|-------|-------|-------|-------|-------|
|    | 2          | 9890  | 9916  | 9974  | 10030 | 10082 | 10118 | 10129 | 10140 | 10151 |
|    | % increase | 96    | 96    | 96    | 97    | 98    | 99    | 99    | 100   | 100   |
|    | 3          | 17257 | 17282 | 17332 | 17374 | 17405 | 17419 | 17423 | 17427 | 17431 |
|    | % increase | 51    | 51    | 51    | 52    | 52    | 52    | 52    | 52    | 53    |
| 95 | 1          | 5682  | 5721  | 5811  | 5909  | 6020  | 6118  | 6157  | 6192  | 6231  |
|    | % increase | 374   | 376   | 379   | 381   | 384   | 386   | 386   | 388   | 391   |
|    | 2          | 12741 | 12780 | 12865 | 12949 | 13029 | 13085 | 13103 | 13146 | 13164 |
|    | % increase | 152   | 152   | 153   | 155   | 156   | 157   | 158   | 159   | 159   |
|    | 3          | 21161 | 21197 | 21270 | 21335 | 21388 | 21419 | 21428 | 21459 | 21468 |
|    | % increase | 85    | 85    | 86    | 86    | 87    | 87    | 87    | 88    | 88    |

**Table 3.8** Effect of end axial tensile force on first three natural frequencies –clamped-clamped boundary condition

| % $P_1$ | Mode No.   | Width ratio ( $b_R/b_L$ ) |       |       |       |       |       |       |       |       |
|---------|------------|---------------------------|-------|-------|-------|-------|-------|-------|-------|-------|
|         |            | 0.01                      | 0.02  | 0.05  | 0.1   | 0.2   | 0.4   | 0.6   | 0.8   | 1     |
| 0       | 1          | 2475                      | 2511  | 2591  | 2674  | 2761  | 2836  | 2865  | 2876  | 2879  |
|         | 2          | 7264                      | 7328  | 7470  | 7614  | 7759  | 7874  | 7915  | 7931  | 7936  |
|         | 3          | 14657                     | 14754 | 14971 | 15188 | 15348 | 15485 | 15533 | 15552 | 15558 |
| 50      | 1          | 5021                      | 5086  | 5206  | 5316  | 5430  | 5526  | 5564  | 5578  | 5582  |
|         | % increase | 103                       | 103   | 101   | 99    | 97    | 95    | 94    | 94    | 94    |
|         | 2          | 11516                     | 11625 | 11815 | 11974 | 12120 | 12228 | 12266 | 12281 | 12285 |
|         | % increase | 59                        | 59    | 58    | 57    | 56    | 55    | 55    | 55    | 55    |
|         | 3          | 19814                     | 19972 | 20239 | 20451 | 20632 | 20757 | 20800 | 20817 | 20823 |

|    |            |       |       |       |       |       |       |       |       |       |
|----|------------|-------|-------|-------|-------|-------|-------|-------|-------|-------|
|    | % increase | 35    | 35    | 35    | 35    | 34    | 34    | 34    | 34    | 34    |
| 95 | 1          | 6446  | 6524  | 6668  | 6802  | 6942  | 7059  | 7105  | 7123  | 7128  |
|    | % increase | 160   | 160   | 157   | 154   | 151   | 149   | 148   | 148   | 148   |
|    | 2          | 14281 | 14398 | 14603 | 14775 | 14931 | 15045 | 15084 | 15099 | 15104 |
|    | % increase | 97    | 96    | 95    | 94    | 92    | 91    | 91    | 90    | 90    |
|    | 3          | 23562 | 23722 | 23995 | 24209 | 24391 | 24515 | 24557 | 24573 | 24579 |
|    | % increase | 61    | 61    | 60    | 59    | 59    | 58    | 58    | 58    | 58    |

**Table 3.9** Effect of end axial tensile force on first three natural frequencies –clamped-free boundary condition

| % P <sub>1</sub> | Mode No.   | Width ratio (b <sub>R</sub> /b <sub>L</sub> ) |       |       |       |       |       |       |       |       |
|------------------|------------|---|-------|-------|-------|-------|-------|-------|-------|-------|
|                  |            | 0.01  | 0.02  | 0.05  | 0.1   | 0.2   | 0.4   | 0.6   | 0.8   | 1     |
| 0                | 1          | 902   | 886   | 841   | 781   | 694   | 590   | 527   | 484   | 452   |
|                  | 2          | 3917  | 3851  | 3692  | 3511  | 3300  | 3090  | 2974  | 2895  | 2835  |
|                  | 3          | 9531  | 9385  | 9068  | 8760  | 8456  | 8200  | 8076  | 7997  | 7939  |
| 50               | 1          | 3694  | 3655  | 3547  | 3396  | 3166  | 2866  | 2674  | 2538  | 2434  |
|                  | % increase | 309   | 313   | 322   | 335   | 356   | 386   | 407   | 424   | 438   |
|                  | 2          | 9045  | 8951  | 8725  | 8472  | 8196  | 7961  | 7856  | 7794  | 7750  |
|                  | % increase | 131   | 132   | 136   | 141   | 148   | 158   | 164   | 169   | 173   |
|                  | 3          | 15818   | 15653 | 15301 | 14976 | 14687 | 14479 | 14392 | 14339 | 14302 |
|                  | % increase | 66  | 67    | 69    | 71    | 74    | 77    | 78    | 79    | 80    |
| 95               | 1          | 4933  | 4883  | 4743  | 4545  | 4239  | 3838  | 3579  | 3394  | 3254  |
|                  | % increase | 447   | 451   | 464   | 482   | 511   | 551   | 579   | 601   | 619   |

|  |            |       |       |       |       |       |       |       |       |       |
|--|------------|-------|-------|-------|-------|-------|-------|-------|-------|-------|
|  | 2          | 11759 | 11643 | 11361 | 11041 | 10685 | 10382 | 10247 | 10168 | 10115 |
|  | % increase | 200   | 202   | 208   | 214   | 224   | 236   | 245   | 251   | 257   |
|  | 3          | 19721 | 19531 | 19122 | 18741 | 18401 | 18163 | 18065 | 18009 | 17970 |
|  | % increase | 107   | 108   | 111   | 114   | 118   | 121   | 124   | 125   | 126   |

Tables 3.7-3.9 show the effect of end axial tensile force on first three natural frequencies for four boundary conditions. The tensile axial load is applied as % of tensile failure load. From the Tables 3.7-3.9, one can observe that as the tensile axial load is increased from 0% to 95 % of tensile failure load, the natural frequencies increase. This is because as the axial tensile load is applied the beam becomes stiffer thereby increasing the natural frequencies. It may be noted that the percentage increase in the natural frequencies is higher for applied end-axial tensile load compared to the case of percentage decrease in the natural frequencies due to applied end-axial compressive load, because the magnitudes of tensile failure loads are higher than the critical buckling load.

### 3.3.6 Effect of damping on natural frequencies

To investigate the effect of damping on first three natural frequencies, the linear width-tapered beam with width ratio ( $b_R/b_L$ ) values of 0.01, 0.02, 0.05, 0.1, 0.2, 0.4, 0.6, 0.8 and 1 for four boundary conditions are considered. The plies of  $([0/90]_9)_s$  composite beam which is made by using NCT-301 graphite-epoxy is considered.

The mass proportional constant ( $\alpha$ ) and stiffness proportional constant ( $\beta$ ) are 3.753 and  $4.83 \times 10^{-5}$  respectively which are obtained through experimental modal testing is described in the section 4.6.1.

By using the properties given in the Tables 3.1, 3.2 and 3.3, the effect of damping on first three natural frequencies for four boundary conditions are carried out in the current section. The first three natural frequencies corresponding to the effects of damped and undamped conditions are obtained using Rayleigh-Ritz method.

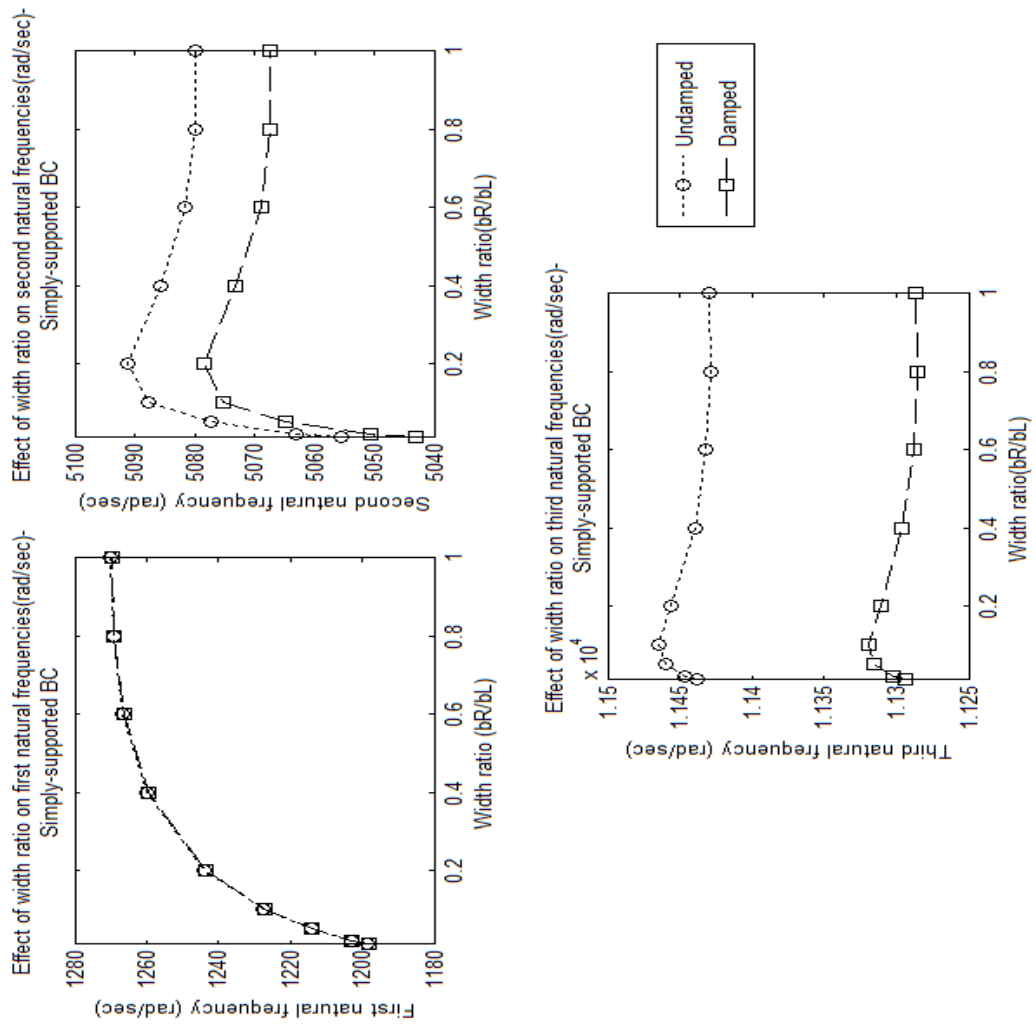


**Figure 3.18** Effect of damping on natural frequencies for simply-supported boundary condition

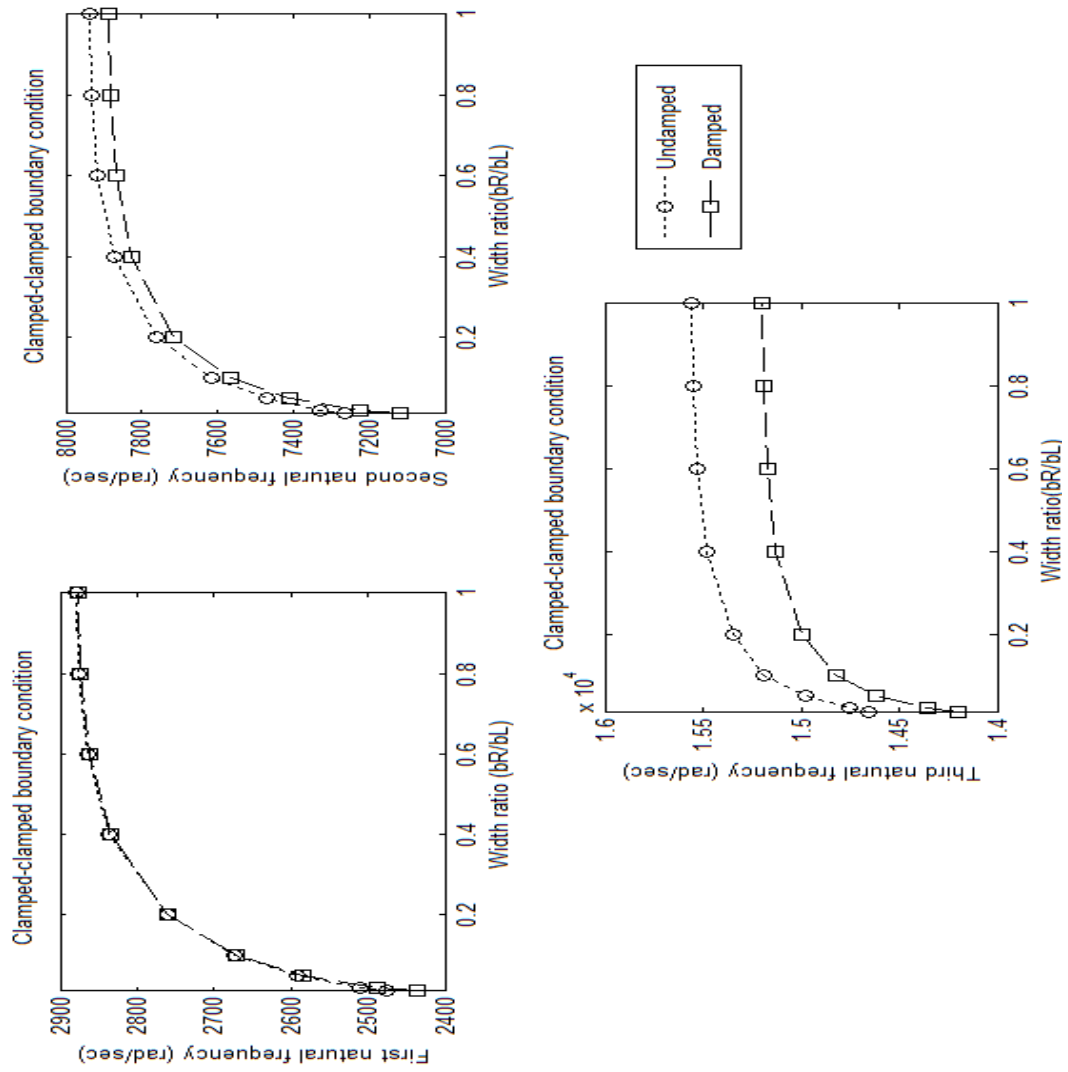


**Figure 3.19** Effect of damping on natural frequencies for clamped-clamped boundary condition

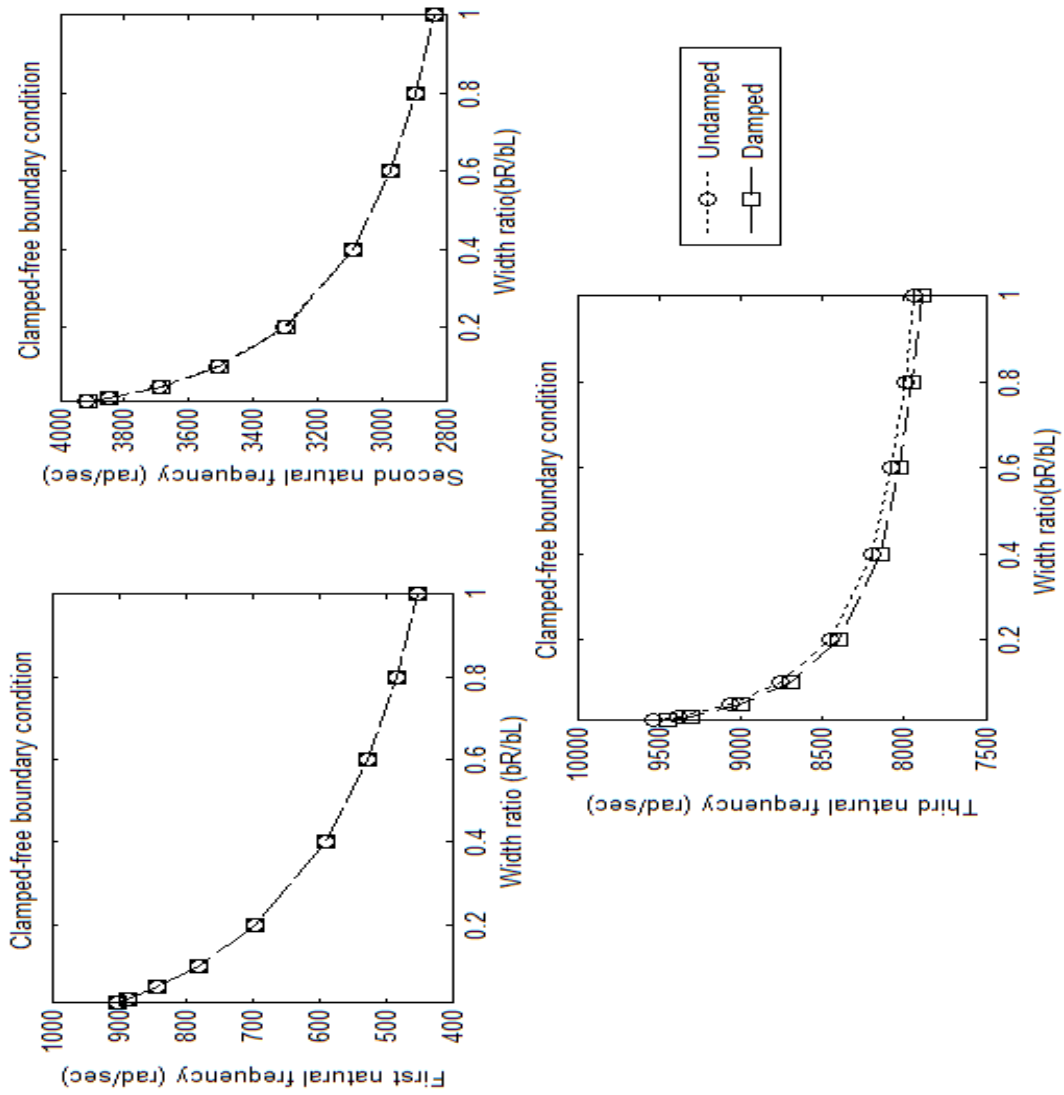


**Figure 3.20** Effect of damping on natural frequencies for clamped-free boundary condition

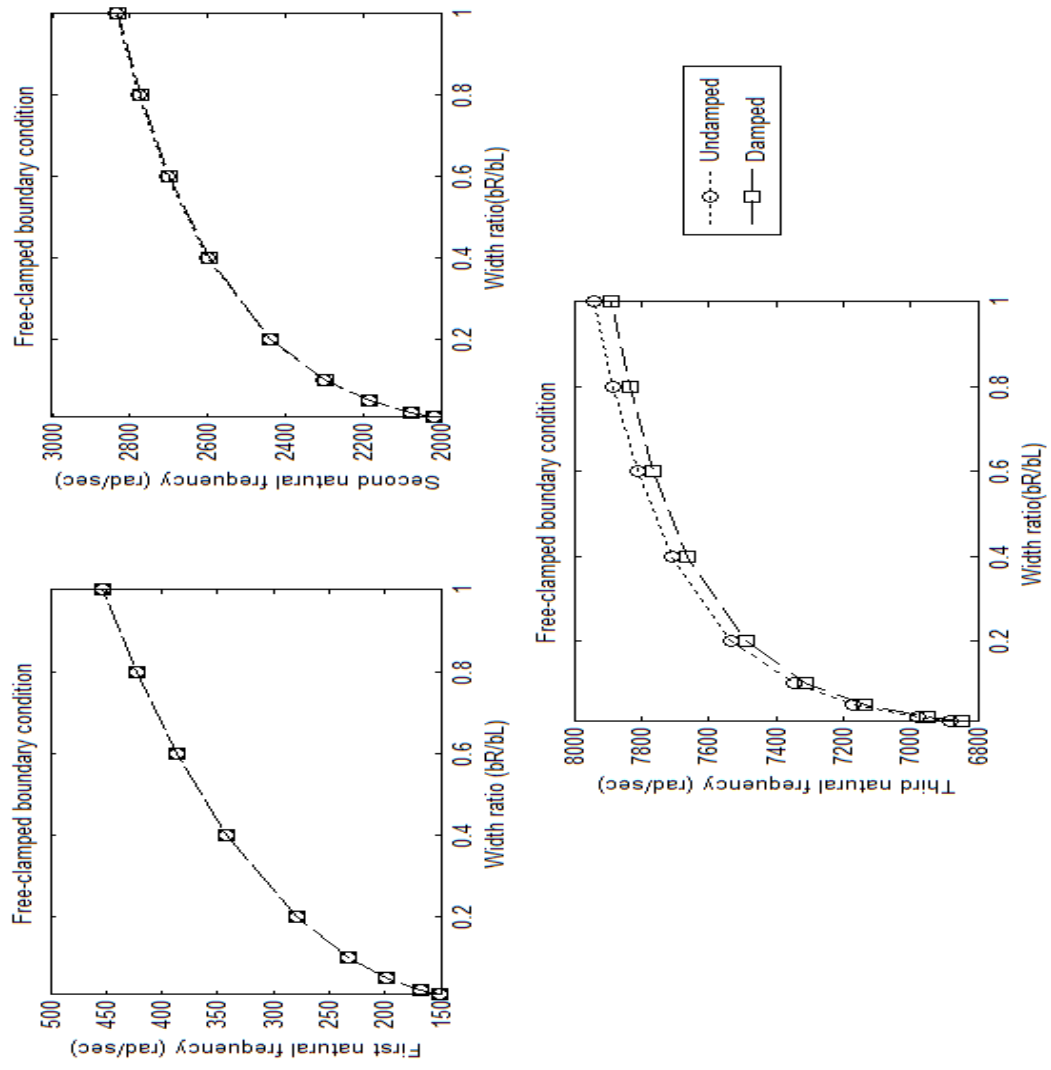


**Figure 3.21** Effect of damping on natural frequencies for free-clamped boundary condition

Figures 3.18-3.21 show the effect of damping on first three natural frequencies for all four boundary conditions. From the Figures 3.18-3.21, it can be observed that the natural frequencies decrease for damped condition compared to that obtained for un-damped condition. The difference between the undamped and damped natural frequencies is small because of low values of damping.

### 3.4 Comparison of natural frequencies between Rayleigh-Ritz method and conventional finite element method.

By using the properties given in the Tables 3.1, 3.2 and 3.3, the current section presents the comparison of first three natural frequencies for simply-supported, clamped-clamped, clamped-free and free-clamped boundary conditions of width-tapered composite beams obtained by using Rayleigh-Ritz method with that obtained using conventional finite element method [81]. The compared results are summarized in the Tables 3.10-3.13 below.

**Table 3.10** Comparison of natural frequencies--Simply supported boundary condition

| Width ratio<br>( $b_R/b_L$ ) | Mode<br>No. | Rayleigh-Ritz<br>Method | Conventional finite<br>element method | %<br>difference |
|------------------------------|-------------|-------------------------|---------------------------------------|-----------------|
| 0.01                         | $\omega_1$  | 1199                    | 1199                                  | 0.07            |
|                              | $\omega_2$  | 5056                    | 5055                                  | 0.00            |
|                              | $\omega_3$  | 11438                   | 11428                                 | 0.09            |
| 0.02                         | $\omega_1$  | 1203                    | 1204                                  | 0.10            |
|                              | $\omega_2$  | 5063                    | 5065                                  | 0.05            |

|      |            |       |       |      |
|------|------------|-------|-------|------|
|      | $\omega_3$ | 11446 | 11446 | 0.00 |
| 0.05 | $\omega_1$ | 1214  | 1216  | 0.13 |
|      | $\omega_2$ | 5077  | 5083  | 0.11 |
|      | $\omega_3$ | 11460 | 11470 | 0.08 |
| 0.1  | $\omega_1$ | 1227  | 1229  | 0.14 |
|      | $\omega_2$ | 5088  | 5094  | 0.13 |
|      | $\omega_3$ | 11464 | 11478 | 0.12 |
| 0.2  | $\omega_1$ | 1244  | 1246  | 0.14 |
|      | $\omega_2$ | 5091  | 5098  | 0.13 |
|      | $\omega_3$ | 11456 | 11471 | 0.13 |
| 0.4  | $\omega_1$ | 1260  | 1261  | 0.12 |
|      | $\omega_2$ | 5086  | 5092  | 0.12 |
|      | $\omega_3$ | 11439 | 11453 | 0.12 |
| 0.6  | $\omega_1$ | 1267  | 1268  | 0.11 |
|      | $\omega_2$ | 5082  | 5087  | 0.11 |
|      | $\omega_3$ | 11432 | 11444 | 0.11 |
| 0.8  | $\omega_1$ | 1269  | 1270  | 0.10 |
|      | $\omega_2$ | 5080  | 5085  | 0.10 |
|      | $\omega_3$ | 11429 | 11440 | 0.10 |
| 1    | $\omega_1$ | 1270  | 1271  | 0.08 |
|      | $\omega_2$ | 5080  | 5084  | 0.08 |
|      | $\omega_3$ | 11430 | 11440 | 0.08 |

**Table 3.11** Comparison of natural frequencies—Clamped-clamped boundary condition

| Width ratio<br>( $b_R/b_L$ ) | Mode<br>No. | Rayleigh-Ritz<br>Method | Conventional finite<br>element method | %<br>difference |
|------------------------------|-------------|-------------------------|---------------------------------------|-----------------|
|------------------------------|-------------|-------------------------|---------------------------------------|-----------------|

|      |            |       |       |      |
|------|------------|-------|-------|------|
| 0.01 | $\omega_1$ | 2475  | 2439  | 1.45 |
|      | $\omega_2$ | 7264  | 7159  | 1.45 |
|      | $\omega_3$ | 14657 | 14505 | 1.04 |
| 0.02 | $\omega_1$ | 2511  | 2495  | 0.65 |
|      | $\omega_2$ | 7328  | 7273  | 0.75 |
|      | $\omega_3$ | 14754 | 14679 | 0.51 |
| 0.05 | $\omega_1$ | 2591  | 2591  | 0.01 |
|      | $\omega_2$ | 7470  | 7462  | 0.11 |
|      | $\omega_3$ | 14971 | 14958 | 0.08 |
| 0.1  | $\omega_1$ | 2674  | 2677  | 0.13 |
|      | $\omega_2$ | 7614  | 7621  | 0.08 |
|      | $\omega_3$ | 15188 | 15178 | 0.07 |
| 0.2  | $\omega_1$ | 2761  | 2765  | 0.14 |
|      | $\omega_2$ | 7759  | 7770  | 0.14 |
|      | $\omega_3$ | 15348 | 15370 | 0.14 |
| 0.4  | $\omega_1$ | 2836  | 2839  | 0.12 |
|      | $\omega_2$ | 7874  | 7883  | 0.12 |
|      | $\omega_3$ | 15485 | 15504 | 0.13 |
| 0.6  | $\omega_1$ | 2865  | 2868  | 0.11 |
|      | $\omega_2$ | 7915  | 7924  | 0.11 |
|      | $\omega_3$ | 15533 | 15550 | 0.11 |
| 0.8  | $\omega_1$ | 2876  | 2879  | 0.10 |
|      | $\omega_2$ | 7931  | 7939  | 0.10 |
|      | $\omega_3$ | 15552 | 15567 | 0.09 |
| 1    | $\omega_1$ | 2879  | 2881  | 0.08 |
|      | $\omega_2$ | 7936  | 7943  | 0.08 |
|      | $\omega_3$ | 15558 | 15571 | 0.08 |

**Table 3.12** Comparison of natural frequencies—Clamped-free boundary condition

| Width ratio<br>( $b_R/b_L$ ) | Mode<br>No. | Rayleigh-Ritz<br>Method | Conventional finite<br>element method | %<br>difference |
|------------------------------|-------------|-------------------------|---------------------------------------|-----------------|
| 0.01                         | $\omega_1$  | 902                     | 904                                   | 0.14            |
|                              | $\omega_2$  | 3917                    | 3922                                  | 0.13            |
|                              | $\omega_3$  | 9531                    | 9542                                  | 0.12            |
| 0.02                         | $\omega_1$  | 886                     | 887                                   | 0.14            |
|                              | $\omega_2$  | 3851                    | 3855                                  | 0.13            |
|                              | $\omega_3$  | 9385                    | 9396                                  | 0.12            |
| 0.05                         | $\omega_1$  | 841                     | 842                                   | 0.14            |
|                              | $\omega_2$  | 3692                    | 3696                                  | 0.13            |
|                              | $\omega_3$  | 9068                    | 9079                                  | 0.12            |
| 0.1                          | $\omega_1$  | 781                     | 782                                   | 0.14            |
|                              | $\omega_2$  | 3511                    | 3515                                  | 0.13            |
|                              | $\omega_3$  | 8760                    | 8771                                  | 0.13            |
| 0.2                          | $\omega_1$  | 694                     | 695                                   | 0.13            |
|                              | $\omega_2$  | 3300                    | 3304                                  | 0.13            |
|                              | $\omega_3$  | 8456                    | 8467                                  | 0.13            |
| 0.4                          | $\omega_1$  | 590                     | 591                                   | 0.12            |
|                              | $\omega_2$  | 3090                    | 3093                                  | 0.12            |
|                              | $\omega_3$  | 8200                    | 8210                                  | 0.12            |
| 0.6                          | $\omega_1$  | 527                     | 528                                   | 0.11            |
|                              | $\omega_2$  | 2974                    | 2977                                  | 0.11            |
|                              | $\omega_3$  | 8076                    | 8084                                  | 0.11            |
| 0.8                          | $\omega_1$  | 484                     | 485                                   | 0.10            |
|                              | $\omega_2$  | 2895                    | 2898                                  | 0.10            |
|                              | $\omega_3$  | 7997                    | 8004                                  | 0.10            |

|   |            |      |      |      |
|---|------------|------|------|------|
| 1 | $\omega_1$ | 452  | 453  | 0.08 |
|   | $\omega_2$ | 2835 | 2838 | 0.08 |
|   | $\omega_3$ | 7939 | 7946 | 0.08 |

**Table 3.13** Comparison of natural frequencies—Free-clamped boundary condition

| Width ratio<br>( $b_R/b_L$ ) | Mode<br>No. | Rayleigh-Ritz<br>Method | Conventional finite<br>element method | %<br>difference |
|------------------------------|-------------|-------------------------|---------------------------------------|-----------------|
| 0.01                         | $\omega_1$  | 151                     | 150                                   | 0.66            |
|                              | $\omega_2$  | 2019                    | 2015                                  | 0.22            |
|                              | $\omega_3$  | 6879                    | 6868                                  | 0.16            |
| 0.02                         | $\omega_1$  | 167                     | 167                                   | 0.04            |
|                              | $\omega_2$  | 2075                    | 2076                                  | 0.07            |
|                              | $\omega_3$  | 6981                    | 6985                                  | 0.07            |
| 0.05                         | $\omega_1$  | 199                     | 199                                   | 0.19            |
|                              | $\omega_2$  | 2186                    | 2190                                  | 0.17            |
|                              | $\omega_3$  | 7173                    | 7184                                  | 0.16            |
| 0.1                          | $\omega_1$  | 233                     | 233                                   | 0.16            |
|                              | $\omega_2$  | 2300                    | 2303                                  | 0.16            |
|                              | $\omega_3$  | 7348                    | 7359                                  | 0.16            |
| 0.2                          | $\omega_1$  | 279                     | 280                                   | 0.15            |
|                              | $\omega_2$  | 2438                    | 2442                                  | 0.14            |
|                              | $\omega_3$  | 7531                    | 7542                                  | 0.14            |
| 0.4                          | $\omega_1$  | 341                     | 342                                   | 0.13            |
|                              | $\omega_2$  | 2599                    | 2603                                  | 0.12            |
|                              | $\omega_3$  | 7709                    | 7719                                  | 0.13            |
| 0.6                          | $\omega_1$  | 386                     | 387                                   | 0.11            |

|     |            |      |      |      |
|-----|------------|------|------|------|
|     | $\omega_2$ | 2701 | 2704 | 0.11 |
|     | $\omega_3$ | 7810 | 7818 | 0.11 |
| 0.8 | $\omega_1$ | 422  | 423  | 0.10 |
|     | $\omega_2$ | 2776 | 2779 | 0.10 |
|     | $\omega_3$ | 7882 | 7889 | 0.10 |
| 1   | $\omega_1$ | 452  | 453  | 0.08 |
|     | $\omega_2$ | 2835 | 2838 | 0.08 |
|     | $\omega_3$ | 7939 | 7946 | 0.08 |

Tables 3.10-3.13 show the comparison of three natural frequencies for simply-supported, clamped-clamped, clamped-free and free-clamped boundary conditions of width-tapered composite beams for width-ratio values of 0.01, 0.02, 0.05, 0.1, 0.2, 0.4, 0.6, 0.8 and 1. The comparisons of natural frequencies were made between Rayleigh-Ritz method and conventional finite element method [81] for validation purpose. From the above table, the comparison differences for simply-supported boundary condition is <0.2%, for clamped-clamped boundary condition it is <1.5%, for clamped-free boundary condition it is <0.15% and for free-clamped boundary condition it is <0.7%. The comparison differences in natural frequencies from the above tables are well accepted.

### **3.5 Buckling response of linear width-tapered composite columns**

In this section, buckling response of width-tapered laminated composite columns is considered for simply-supported, clamped-clamped, clamped-free and free-clamped boundary conditions. Rayleigh-Ritz method is used to find the critical buckling load for width-tapered composite columns. The effects of width ratio ( $b_R/b_L$ ), laminate configuration, length ratio and boundary conditions on critical buckling loads for width-tapered composite columns have been shown through graphical plots.

#### **3.5.1 Effect of width ratio ( $b_R/b_L$ ) on critical buckling load ( $P_{cr}$ )**

To study the effect of width ratio ( $b_R/b_L$ ) on critical buckling load ( $P_{cr}$ ), the linear width-tapered composite columns with SS (simply-supported), CC (clamped-clamped), CF (clamped-free) and FC (free-clamped) boundary conditions are considered. The width ratio ( $b_R/b_L$ ) values of 0.01, 0.02, 0.05, 0.1, 0.2, 0.4, 0.6, 0.8 and 1 are considered to investigate the effects on critical buckling load ( $P_{cr}$ ). The plies of  $([0/90]_9)_s$  composite beam which is made up of NCT-301 graphite-epoxy is considered to find the critical buckling loads.

By using the properties given in the Tables 3.1, 3.2 and 3.3, the effect of width ratio ( $b_R/b_L$ ) on critical buckling load ( $P_{cr}$ ) for four boundary conditions is carried out in the current section.

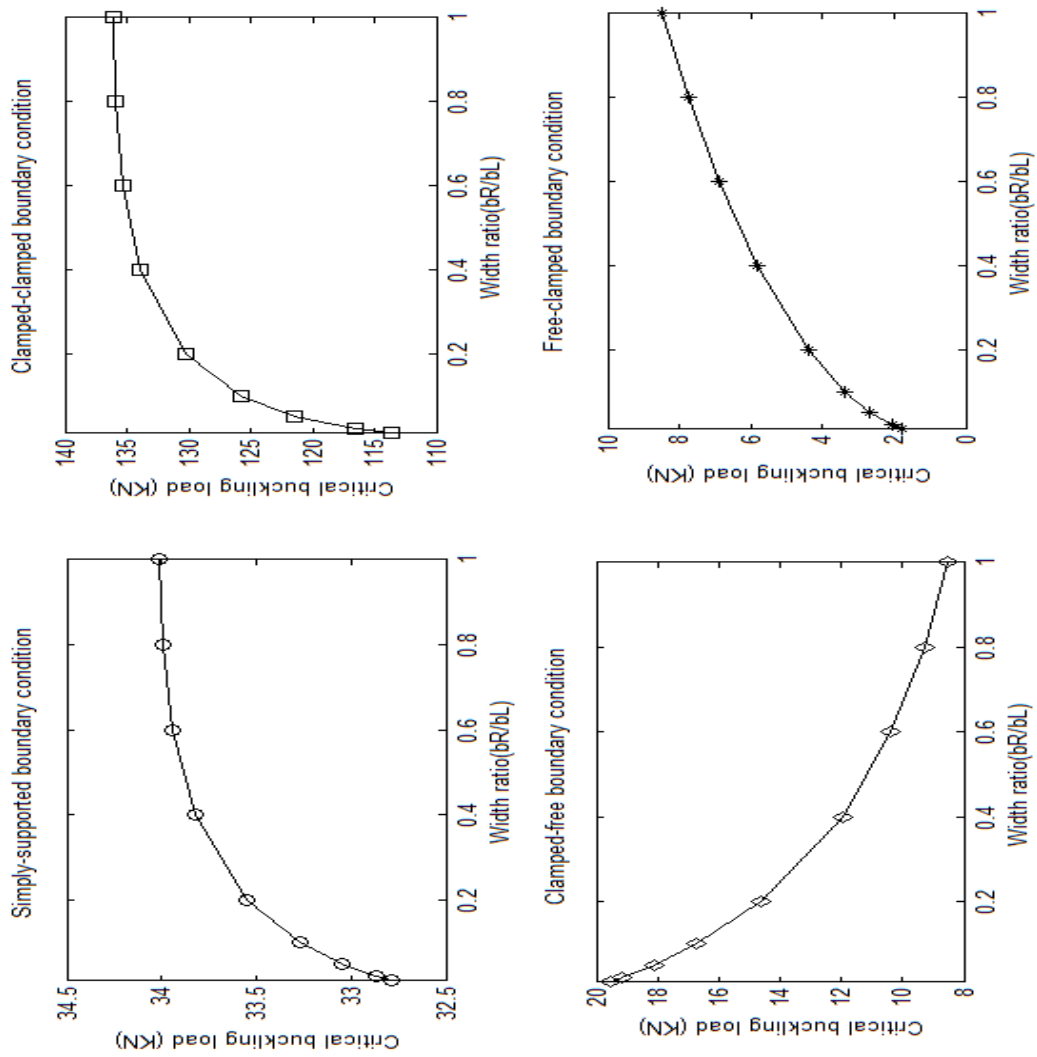


**Figure 3.22** Effect of width ratio ( $b_R/b_L$ ) on critical buckling load (Per)

Figure 3.22 shows the effect of width ratio ( $b_R/b_L$ ) on critical buckling load ( $P_{cr}$ ) for all four boundary conditions. It can be observed that as the width ratio values increase the critical buckling load increases for SS, CC and FC boundary conditions, but decreases for CF boundary condition. This is because the critical buckling load ( $P_{cr}$ ) depends on the restrained condition at both ends of the beam. The degree of restraint and the position of restraint affect the value of stiffness of the beam. In clamped-free boundary condition, the beam is fixed at the wider section and free at the narrower section. The critical buckling load is highest for clamped-clamped boundary condition and lowest for free-clamped boundary condition. The critical buckling load is second and third highest for simply-supported and clamped-free boundary conditions respectively.

### 3.5.2 Effect of laminate configuration on critical buckling load ( $P_{cr}$ )

To investigate the effect of laminate configurations on critical buckling load ( $P_{cr}$ ), the linear width-tapered column with width ratio ( $b_R/b_L$ ) values mentioned above in section 3.5.1 with four boundary conditions are considered. The ply of composite column is made up of NCT-301 graphite-epoxy and consists of 36 plies. The laminate configurations considered are: 1)  $([0/90]_9)_s$  denoted as ‘LC1’, 2)  $([\pm 45]_9)_s$  denoted as ‘LC2’, 3)  $([0_4/\pm 45_7])_s$  denoted as ‘LC3’, and 4)  $([0/\pm 60]_6)_s$  denoted as ‘LC4’.

By using the properties given in the Tables 3.1, 3.2 and 3.3, the effect of laminate configurations on critical buckling load ( $P_{cr}$ ) for width ratio ( $b_R/b_L$ ) values of 0.01, 0.02,

0.05, 0.1, 0.2, 0.4, 0.6, 0.8 and 1 which is obtained using Rayleigh-Ritz method is carried out in the current section.

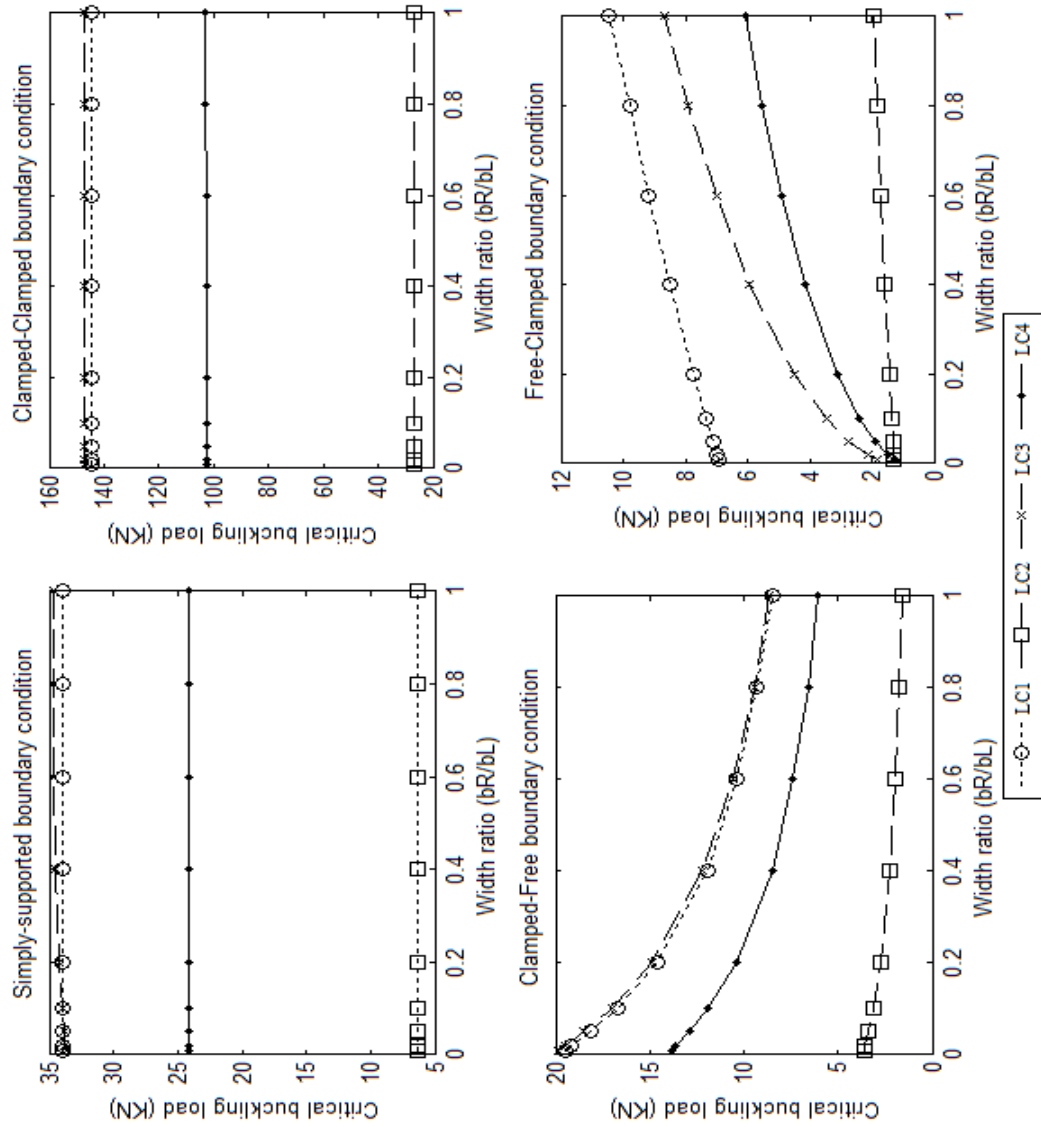


**Figure 3.23** Effect of laminate configuration on critical buckling load ( $P_{cr}$ )

Figure 3.23 shows the effect of laminate configuration on critical buckling load for all four boundary conditions. From the Figure 3.23 one can observe that the critical buckling load for variation of width ratio ( $b_R/b_L$ ) values is largest for laminate configuration LC3, second largest for LC1, third largest for LC4 and fourth largest for LC2. This difference in critical buckling load is expected for different laminate configurations because the stiffness of the column depends on bending stiffness term

$\left( \frac{1}{D_{11}(x)} \right)$  which is directly related with  $Q_{11}$  of the ply.

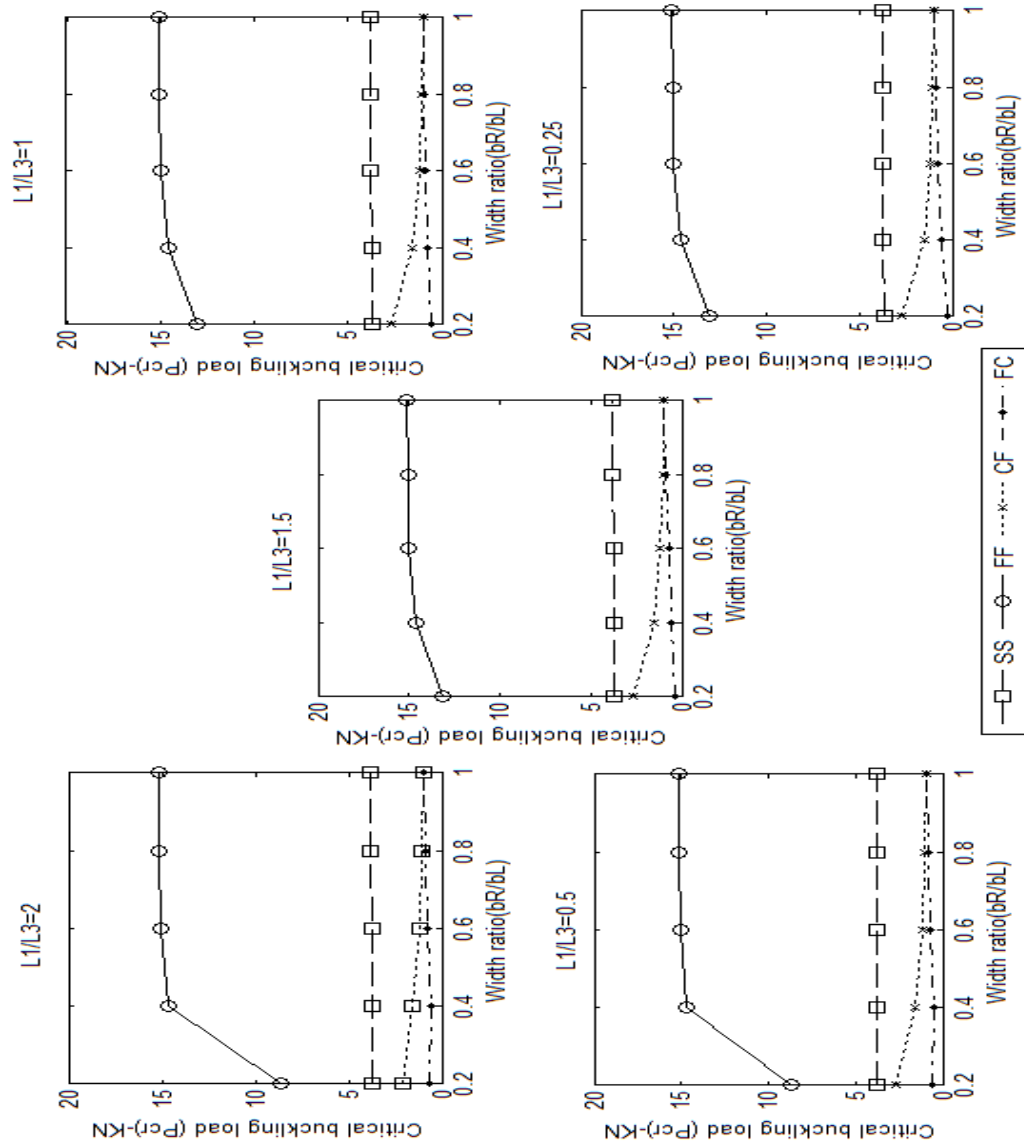
### 3.5.3 Effect of length ratio ( $L_1/L_3$ ) on critical buckling load ( $P_{cr}$ )

To study the effect of length ratio ( $L_1/L_3$ ) on critical buckling load ( $P_{cr}$ ), the tapered column of width ratio ( $b_R/b_L$ ) values mentioned in section 3.5.1 for four boundary conditions are considered. The plies of  $([0/90]_9)_s$  composite beam which is made up of NCT-301 graphite-epoxy is considered.

The geometric properties of the column considered are: the height of the column is 0.0045 m and individual ply thickness ( $t_k$ ) is 0.000125 m. The column at wider section and narrower section is shown in the Figure 3.12. ' $b_w$ ' and ' $b_N$ ' represents the wider and narrower sections of the column respectively. ' $L_1$ ' represents the length of the column at wider section, ' $L_2$ ' represents the length at width-tapered section of the column, and ' $L_3$ ' represents the length of the column at narrower section. The total length of the column is

kept constant. Changing the length ratio is by changing lengths of the column at wider and narrower sections to achieve different length ratios. When the length ratio is 2, the length of wider section is twice that of narrower section of the column. When the length ratio is  $\frac{1}{2}$ , the length of wider section is half of the length of narrower section of the column. When the length ratio is 1, the length of wider section is equal to the length of narrower section.

By using the properties given in the Tables 3.1, 3.2 and 3.3, the effect of length ratio ( $L_1/L_3$ ) on critical buckling load ( $P_{cr}$ ) with different width ratio ( $b_R/b_L$ ) values for four boundary conditions is carried out in the current section. The critical buckling loads ( $P_{cr}$ ) for all boundary conditions are obtained using Rayleigh-Ritz method.



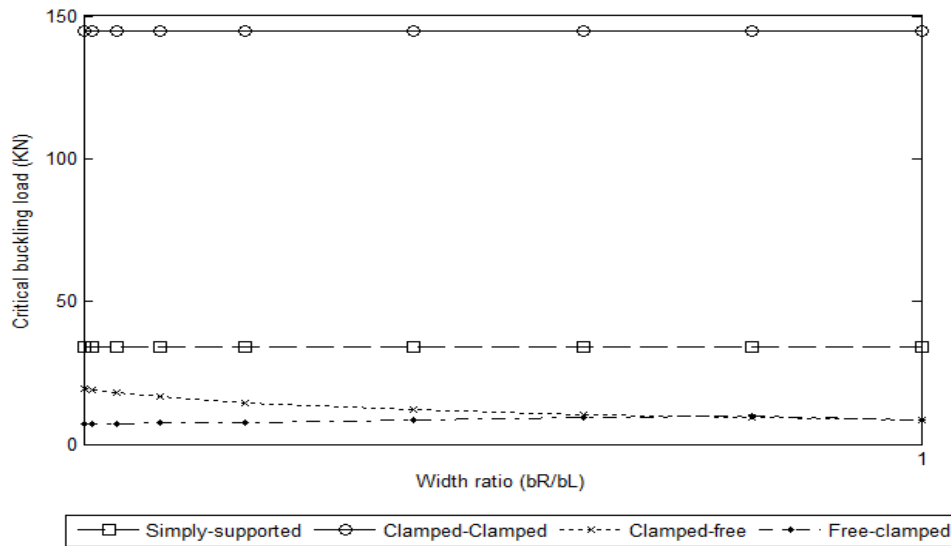
**Figure 3.24** Effect of length ratio ( $L_1/L_3$ ) on critical buckling load ( $P_{cr}$ )

Figure 3.24 shows the effect of length ratio ( $L_1/L_3$ ) on critical buckling load for all four boundary conditions. The critical buckling load is highest for length ratio ( $L_1/L_3$ ) of 2 and least for length ratio 0.25. Another observation can be made is that as the width ratio ( $b_R/b_L$ ) increases from 0.2 to 1, the critical buckling load increases for simply-

supported, clamped-clamped and free-clamped boundary condition but decreases for clamped-free boundary condition.

### 3.5.4 Effect of boundary conditions on critical buckling load ( $P_{cr}$ )

To study the effect of boundary conditions on critical buckling load ( $P_{cr}$ ) the tapered composite column with width ratio ( $b_R/b_L$ ) values mentioned in the section 3.5.1 for four boundary conditions are considered. The plies of  $([0/90]_9)_s$  composite columns which consists of 36 plies made of NCT-301 graphite-epoxy. By using the properties given in the Tables 3.1, 3.2 and 3.3, the effect of boundary condition on critical buckling load ( $P_{cr}$ ) with width ratio ( $b_R/b_L$ ) values of 0.01, 0.02, 0.05, 0.1, 0.2, 0.4, 0.6, 0.8 and 1 for four boundary conditions is carried out in the current section.



**Figure 3.25** Effect of boundary conditions on critical buckling load ( $P_{cr}$ )

Figure 3.25 shows the effect of boundary conditions on critical buckling load. It can be observed that the critical buckling load is highest for clamped-clamped boundary condition since the column is stiffer and least for free-clamped boundary condition. Another observation can be made is that as the width ratio ( $b_R/b_L$ ) values increase from 0.01 to 1, the critical buckling load increases for SS, CC and FC boundary conditions, but decreases for CF boundary condition.

### **3.6 First-ply failure load**

A laminate will fail under increasing mechanical and thermal loads. The laminate failure, however, may not be catastrophic. It is possible that some layer fails first and that the composite continues to take more loads until all the plies fail [79]. When a ply fails, it may have cracks parallel to the fibers. This ply is still capable of taking load parallel to the fibers. Here, the cracked ply can be replaced by a hypothetical ply that has no transverse stiffness, transverse tensile strength, and shear strength. The longitudinal modulus and strength remain unchanged. When a ply fails, fully discount the ply and replace the ply of near zero stiffness and strength. Near zero values avoid singularities in stiffness and compliance matrices.

In order to find the effect of static end-axial tensile force on natural frequencies and forced response of width-tapered composite beam, the first-ply failure load for beams of width ratio ( $b_R/b_L$ ) values mentioned in the section 3.5.1 is calculated.

The ply of composite beam is made of NCT-301 graphite-epoxy. The laminate configuration considered is  $([0/90]_9)_s$ . The first-ply failure load for  $0^\circ$  and  $90^\circ$  plies in the laminate are obtained using Tsai–Wu failure theory. The geometric properties of the beam considered are given in Table 3.3.

### 3.6.1 First-ply failure tensile and compressive loads for width-tapered beam

By using the properties given in the Tables 3.1, 3.2 and 3.3, the first-ply failure load for beams of width ratio  $(b_R/b_L)$  values of 0.01, 0.02, 0.05, 0.1, 0.2, 0.4, 0.6, 0.8 and 1 is carried out in the current section. The tensile and compressive failure loads for  $0^\circ$  and  $90^\circ$  plies are obtained by Tsai-Wu failure criterion. The method to find the first-ply failure load using Tsai-Wu failure criterion is given as:

- The load applied is axial load, hence only the extensional stiffness matrix is required. The extensional compliance matrix is calculated for  $([0/90]_9)_s$  laminate
- The midplane strains for symmetric laminates subjected to  $P_x = 1$  N are calculated
- The midplane curvatures are zero because the laminate is symmetric and no bending and no twisting loads are applied. The global strain for  $0^\circ$  ply is found by transformation relation. One can find the global stress for  $0^\circ$  ply using constitutive relation.
- Using the transformation relation the local stresses are found.
- The Tsai–Wu failure theory is applied for  $0^\circ$  ply.

- Using the parameters  $F_1$ ,  $F_2$ ,  $F_6$ ,  $F_{11}$ ,  $F_{22}$ ,  $F_{66}$ , and  $F_{12}$ , the Tsai–Wu failure theory gives the failure load for  $0^\circ$  ply.
- The above steps are followed for  $90^\circ$  plies
- The tensile and compressive failure loads for  $0^\circ$  and  $90^\circ$  plies in the laminate are summarized in Tables 3.8 and 3.9 respectively.

**Table 3.14** Failure loads for  $0^\circ$  ply

| Width ratio<br>( $b_R/b_L$ ) | Tensile failure load<br>(MN) | Compressive failure<br>load (MN) |
|------------------------------|------------------------------|----------------------------------|
| 0.01                         | 3.1456                       | 2.7531                           |
| 0.02                         | 3.1456                       | 2.7532                           |
| 0.05                         | 3.1457                       | 2.7533                           |
| 0.1                          | 3.1459                       | 2.7534                           |
| 0.2                          | 3.1463                       | 2.7540                           |
| 0.4                          | 3.1471                       | 2.7547                           |
| 0.6                          | 3.1479                       | 2.7553                           |
| 0.8                          | 3.1486                       | 2.7560                           |
| 1                            | 3.1494                       | 2.7566                           |

**Table 3.15** Failure loads for 90° ply

| Width ratio<br>( $b_R/b_L$ ) | Tensile failure<br>load (MN) | Compressive failure<br>load (MN) |
|------------------------------|------------------------------|----------------------------------|
| 0.01                         | 1.6198                       | 0.926526                         |
| 0.02                         | 1.6198                       | 0.926537                         |
| 0.05                         | 1.6199                       | 0.926571                         |
| 0.1                          | 1.6200                       | 0.926641                         |
| 0.2                          | 1.6202                       | 0.926754                         |
| 0.4                          | 1.6206                       | 0.926981                         |
| 0.6                          | 1.6210                       | 0.927207                         |
| 0.8                          | 1.6214                       | 0.927432                         |
| 1                            | 1.6218                       | 0.927658                         |

Tables 3.14-3.15 show the tensile and compressive failure loads of linear width-tapered composite beam at right most end of the beam. The first-ply failure load varies for different width ratio values of width-tapered composite beams. From the Tables 3.14-3.15 using the Tsai-Wu theory it can be found that the failure load is minimum for the 90° ply compared to 0° ply. This is considered as first-ply failure load for  $([0/90]_9)_s$  laminate. The failure loads (tensile and compressive) for both 0° and 90° plies are least for width ratio value of 0.01 and highest for 1, this is because of the change in the cross-section of the beam. The first-ply failure load is used to find the natural frequencies and

forced response including effect of static end-axial load. The load applied is less than the failure load in tensile condition and lesser than the buckling load for compressive load condition.

### 3.7 Forced vibration analysis of width-tapered laminated composite beams

In this section, a sinusoidal force with excitation frequency  $\omega$  is applied at four excitation points shown in the Figure 3.26 to obtain the forced response in terms of sinusoidal transverse-displacement of width-tapered laminated composite beams for simply-supported, clamped-clamped and clamped-free boundary conditions. Rayleigh-Ritz method is used to find the sinusoidal transverse displacement of width-tapered composite beams.

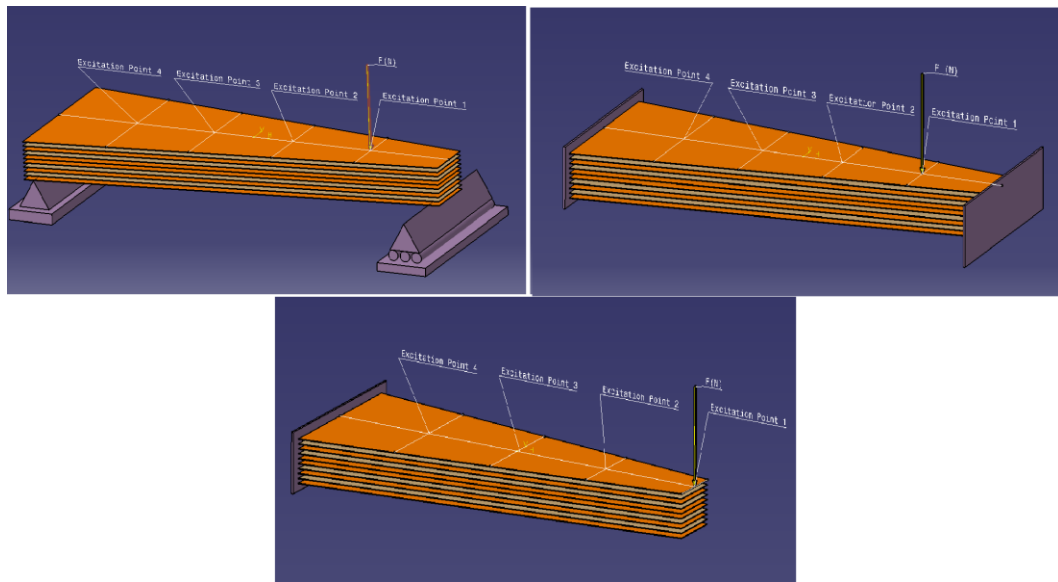


**Figure 3.26** Schematic illustration of linear width- tapered laminated composite beams showing the excitation points

Effects of width ratio ( $b_R/b_L$ ), laminate configuration, length ratio ( $L_1/L_3$ ), boundary condition, and static end-axial force on sinusoidal transverse displacement of width-tapered composite beams are discussed in the further sections.

### **3.7.1 Effect of width ratio ( $b_R/b_L$ ) on forced response in terms of sinusoidal transverse displacement**

To investigate the effect of width ratio ( $b_R/b_L$ ) on forced response in terms of transverse displacement, the linear width-tapered composite beam of clamped-free boundary condition at four excitation points as shown in the Figure 3.26 are considered. The width ratio ( $b_R/b_L$ ) values considered are 0.2, 0.5, and 1 to investigate the effect on transverse displacement. The plies of  $([0/90]_9)_s$  composite beam which is made up of NCT-301 graphite-epoxy is considered.

A sinusoidal force of magnitude 2N with excitation frequency  $\omega$  is applied at four excitation points. The sinusoidal force 2N is chosen based on the input force measured in experimental modal analysis using impact hammer technique as explained in section 4.7.2. By using the mechanical and geometrical properties given in the Tables 3.1, 3.2 and 3.3, the forced response in terms of transverse displacement obtained for clamped-free boundary condition corresponding to the four excitation points. The forced response in terms of sinusoidal transverse displacement is obtained using Rayleigh-Ritz method. The range of frequency in the x-axis is between 1 to 10000 Hz.

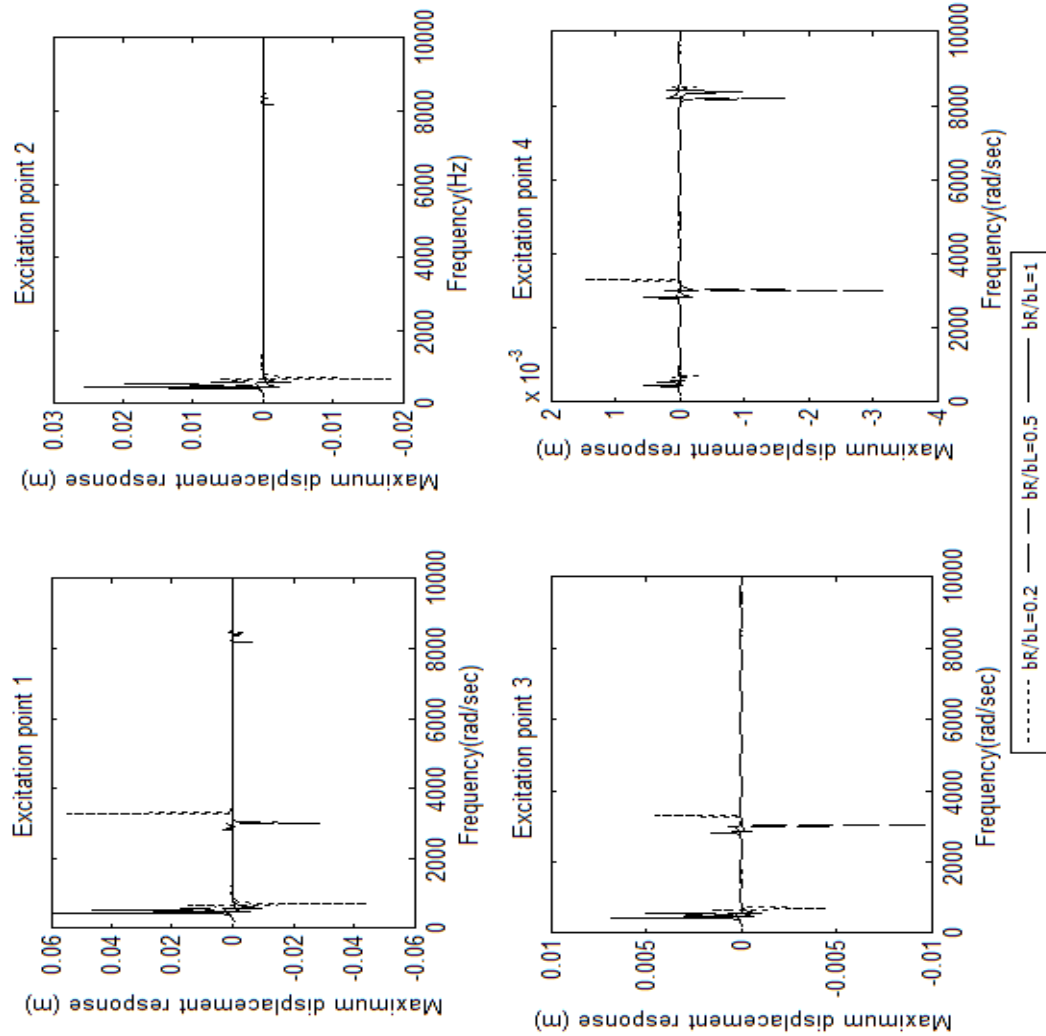


**Figure 3.27** Effect of width ratio ( $b_R/b_L$ ) on frequency-displacement response

Figure 3.27 shows the effect of width ratio ( $b_R/b_L$ ) on forced response in terms of transverse displacement amplitude with excitation frequency  $\omega$  applied at four excitation points for clamped-free (cantilever) boundary condition. The width ratio ( $b_R/b_L$ ) values of the beam considered are 0.2, 0.5 and 1. From the Figure 3.27, it can be observed that for

clamped-free boundary condition, transverse displacement amplitude is highest for width ratio ( $b_R/b_L$ ) value of 1, second highest for width ratio value of 0.5 and lowest for width ratio value of 0.2. This indicates that the transverse displacement amplitude is highest for higher width ratio values of the beam. As the width ratio value increases, transverse displacement amplitude increases. The transverse displacement amplitude is highest at excitation point 1 and lowest at excitation point 4. Another observation that can be made is that the transverse displacement amplitude is highest for mode 1 and lowest for mode 3 at excitation point 1, whereas for excitation point 4, the transverse displacement amplitude is highest for mode 1 and lowest for mode 2. This is same for all width ratio values of the beam.

### **3.7.2 Effect of laminate configuration on forced response in terms of sinusoidal transverse displacement**

To investigate the effect of laminate configuration on forced response in terms of transverse displacement, the linear width-tapered clamped-free beam with width ratio ( $b_R/b_L$ ) values of 0.2, 0.5, and 1 are considered. The laminate configurations are chosen differently to understand the effect of different fiber orientations on forced vibration response. The laminate configurations considered are: 1)  $([0/90]_9)_s$  denoted as ‘LC1’, 2)  $([\pm 45]_9)_s$  denoted as ‘LC2’, 3)  $([0_4/\pm 45_7])_s$  denoted as ‘LC3’, and 4)  $([0/\pm 60]_6)_s$  denoted as ‘LC4’. The different laminate

A sinusoidal force of magnitude  $2N$  with excitation frequency  $\omega$  is applied at four excitation points as shown in the Figure 3.26. By using the properties given in the Tables 3.1, 3.2 and 3.3, the effect of laminate configuration on forced responses in terms of sinusoidal transverse displacements are obtained for clamped-free boundary condition at four excitation points for width ratio ( $b_R/b_L$ ) values of 0.2, 0.5, and 1. The forced responses in terms of sinusoidal transverse displacement are obtained using Rayleigh-Ritz method.

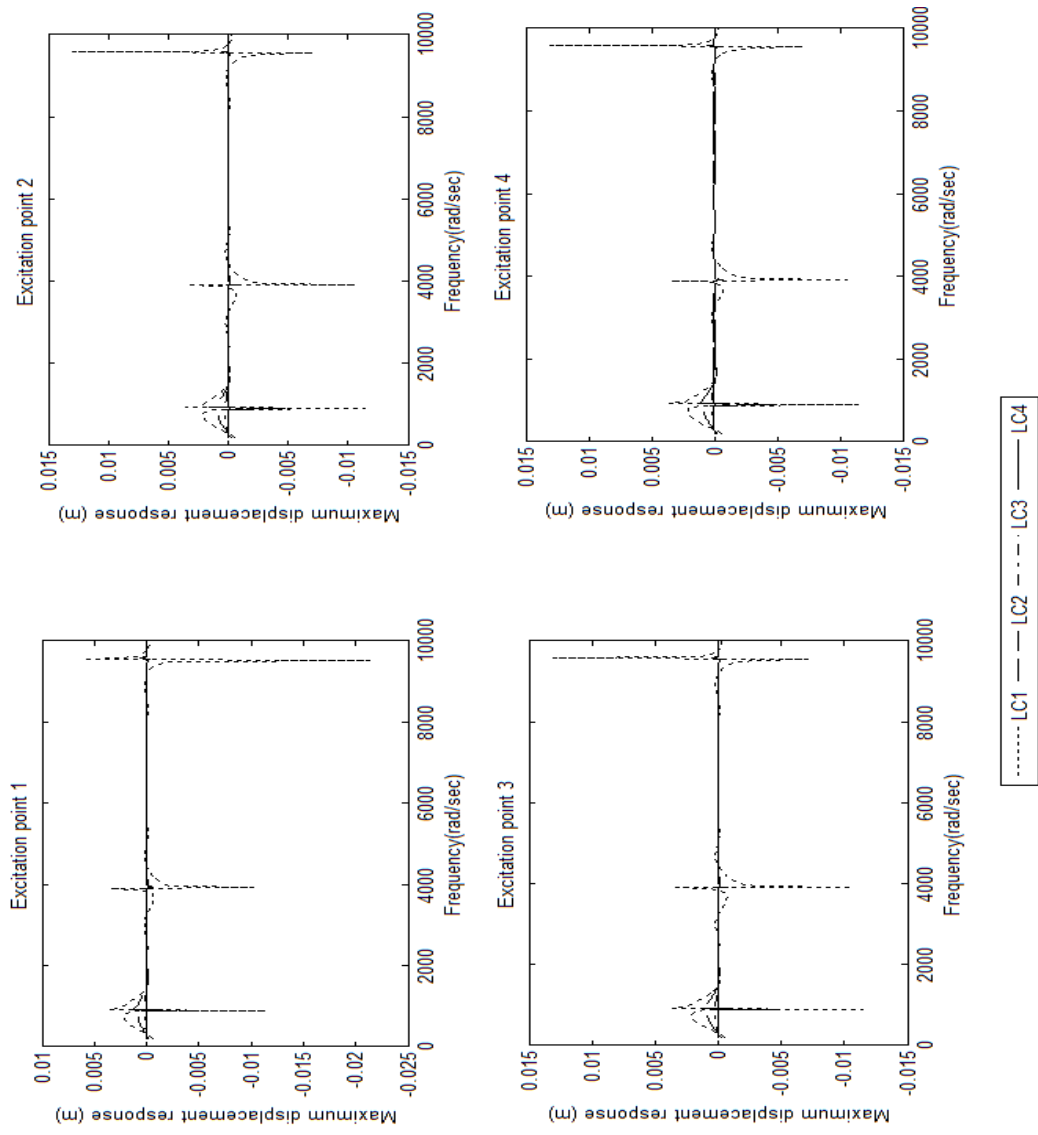


**Figure 3.28** Effect of laminate configurations on frequency-amplitude response for width-ratio ( $b_R/b_L$ ) value of 0.2

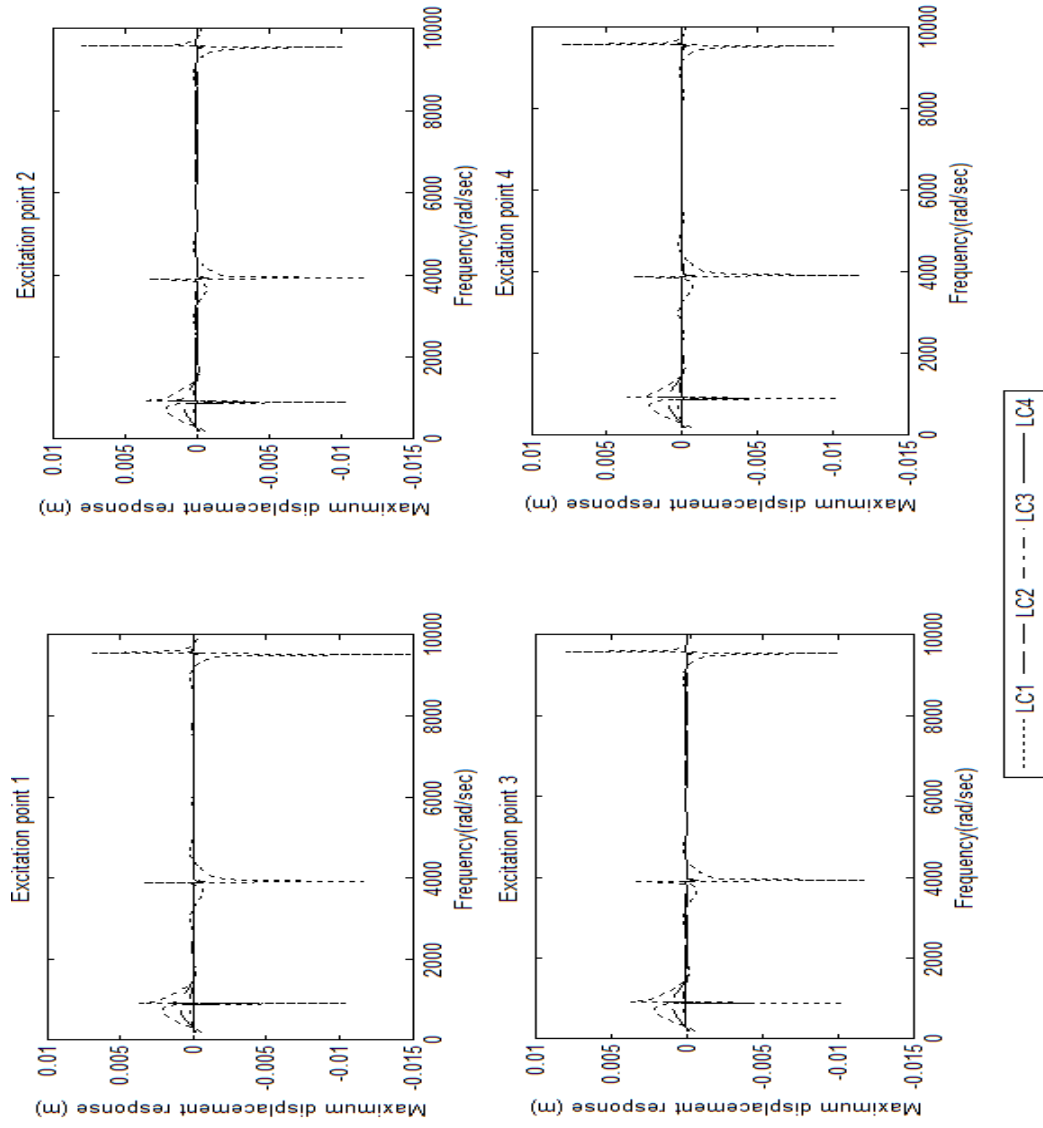


**Figure 3.29** Effect of laminate configurations on frequency-amplitude response for width-ratio ( $b_R/b_L$ ) value of 0.5

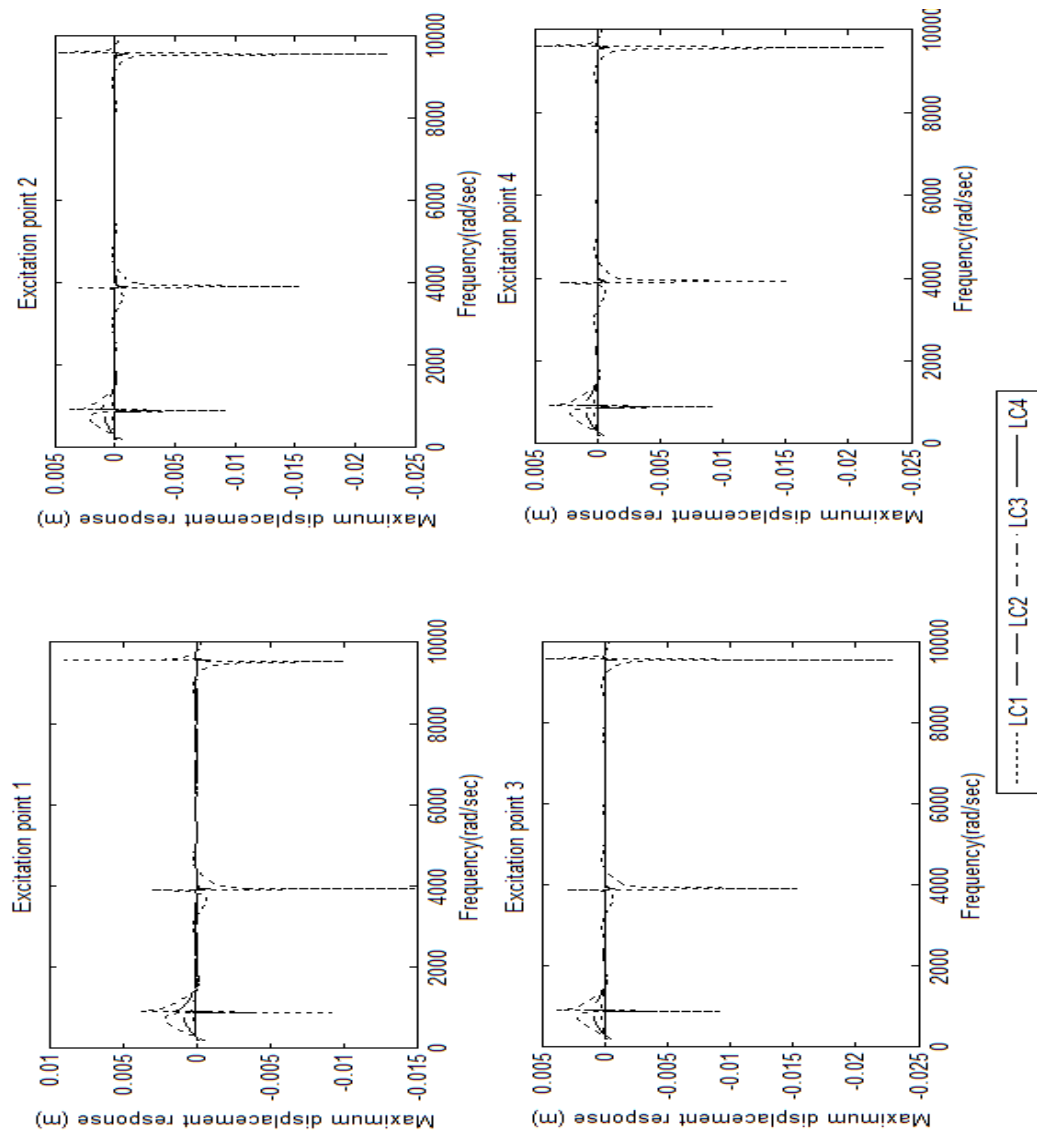


**Figure 3.30** Effect of laminate configurations on frequency-amplitude response for width-ratio ( $b_R/b_L$ ) value of 1

Figures 3.28-3.30 shows the effect of laminate configuration on forced response in terms of sinusoidal transverse displacement amplitude for width ratio ( $b_R/b_L$ ) values of 0.2, 0.5, and 1 with excitation frequency  $\omega$  applied at four excitation points for clamped-free boundary condition as shown in the Figure 3.26. From the Figures 3.28-3.30, it can be observed that the transverse displacement amplitude is largest for laminate configuration LC2, second largest for laminate configuration LC1, third largest for LC4 and lowest for laminate configuration LC3. This is common at all the excitation points on the beam. The transverse displacement amplitude is largest for angle ply laminate LC2 because the fibers are oriented along  $+45^0$  and  $-45^0$ , which has lower extensional and bending stiffness but higher shear modulus.

Another observation that can be made is the transverse displacement amplitude is largest when the width ratio ( $b_R/b_L$ ) value of the beam is 1. The transverse displacement amplitude reduces as the width ratio ( $b_R/b_L$ ) values reduce. Different laminate configurations of composite beams give the different stiffness according to ply orientations in the laminate.

### **3.7.3 Effect of length ratio ( $L_1/L_3$ ) on forced response in terms of sinusoidal transverse displacement**

To study the effect of length ratio ( $L_1/L_3$ ) on forced response in terms of sinusoidal transverse displacement, the width-tapered composite beams of width ratio

$(b_N/b_w)$  with Length ratio  $(L_1/L_3)$  shown in the Figure 3.12 for clamped-free boundary condition is considered. The laminate configuration considered is  $([0/90]_9)_s$  and each ply of composite beam is made of NCT-301 graphite-epoxy. The geometric properties of the beam are: the beam is considered with 36 plies, the height of the beam is 0.0045 m, and individual ply thickness  $(t_k)$  is 0.000125 m. A sinusoidal force of magnitude 2N with excitation frequency  $\omega$  is applied at four excitation points. By using the properties given in the Tables 3.1, 3.2 and 3.3, the effect of length ratio  $(L_1/L_3)$  on forced response in terms of sinusoidal transverse displacement with width ratios  $(b_N/b_w)$  values of 0.2, 0.5, and 1 for clamped-free boundary condition is carried out in the current section. The forced response in terms of sinusoidal transverse displacements is obtained using Rayleigh-Ritz method.

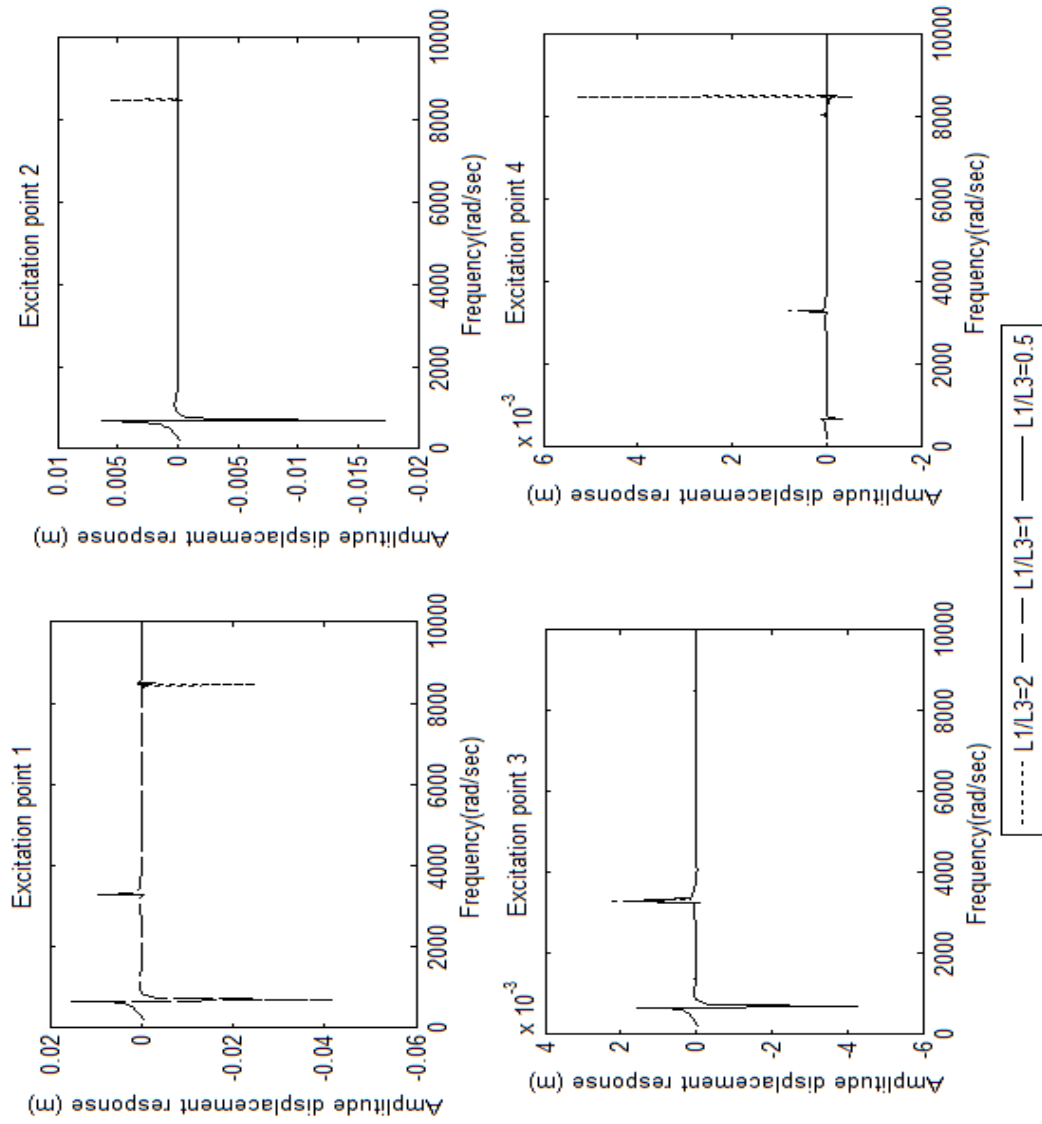


**Figure 3.31** Effect of length ratio ( $L_1/L_3$ ) on frequency-amplitude response for width-ratio ( $b_N/b_w$ ) value of 0.2

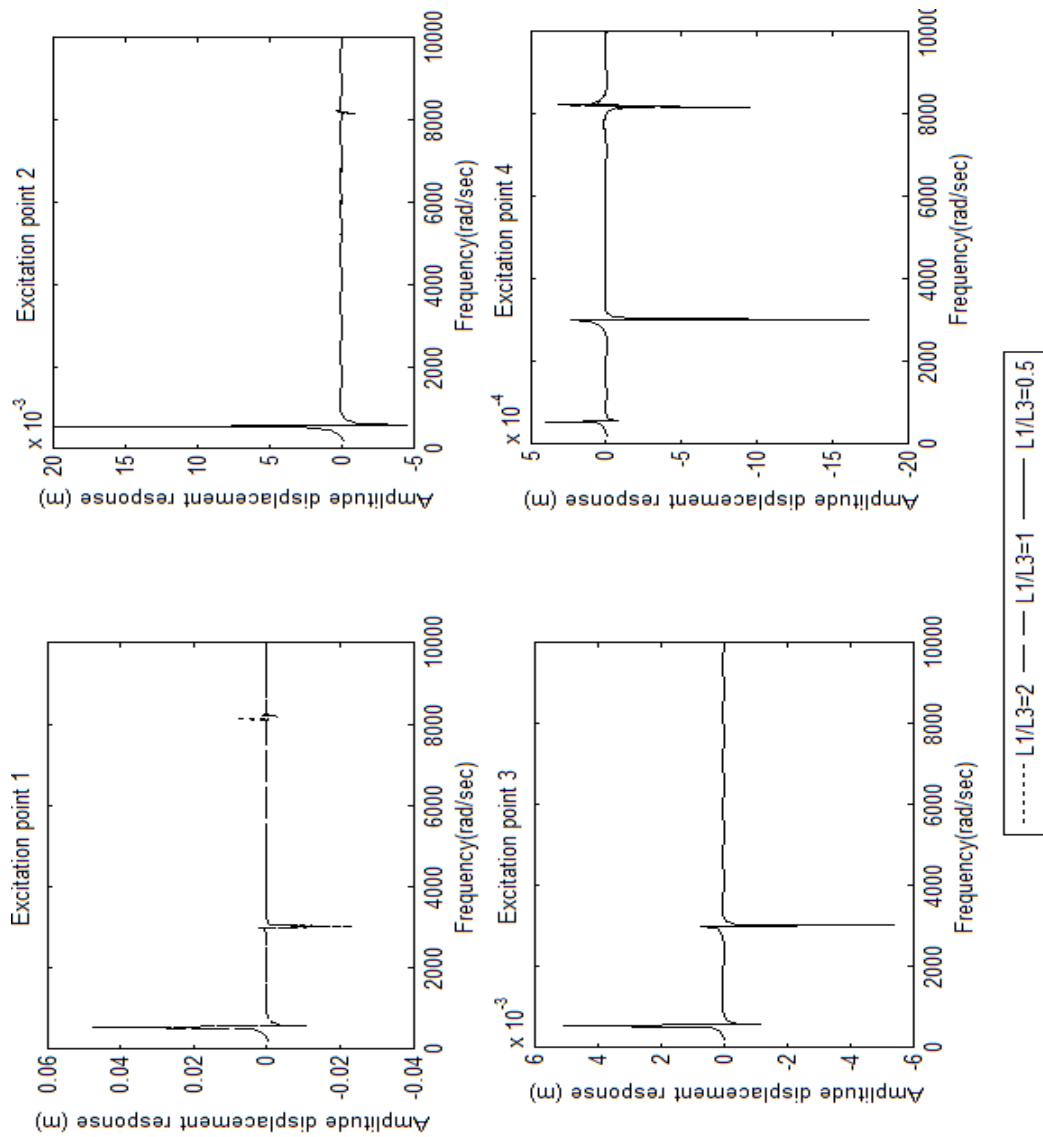


**Figure 3.32** Effect of length ratio ( $L_1/L_3$ ) on frequency-amplitude response for width-ratio ( $b_N/b_w$ ) value of 0.5

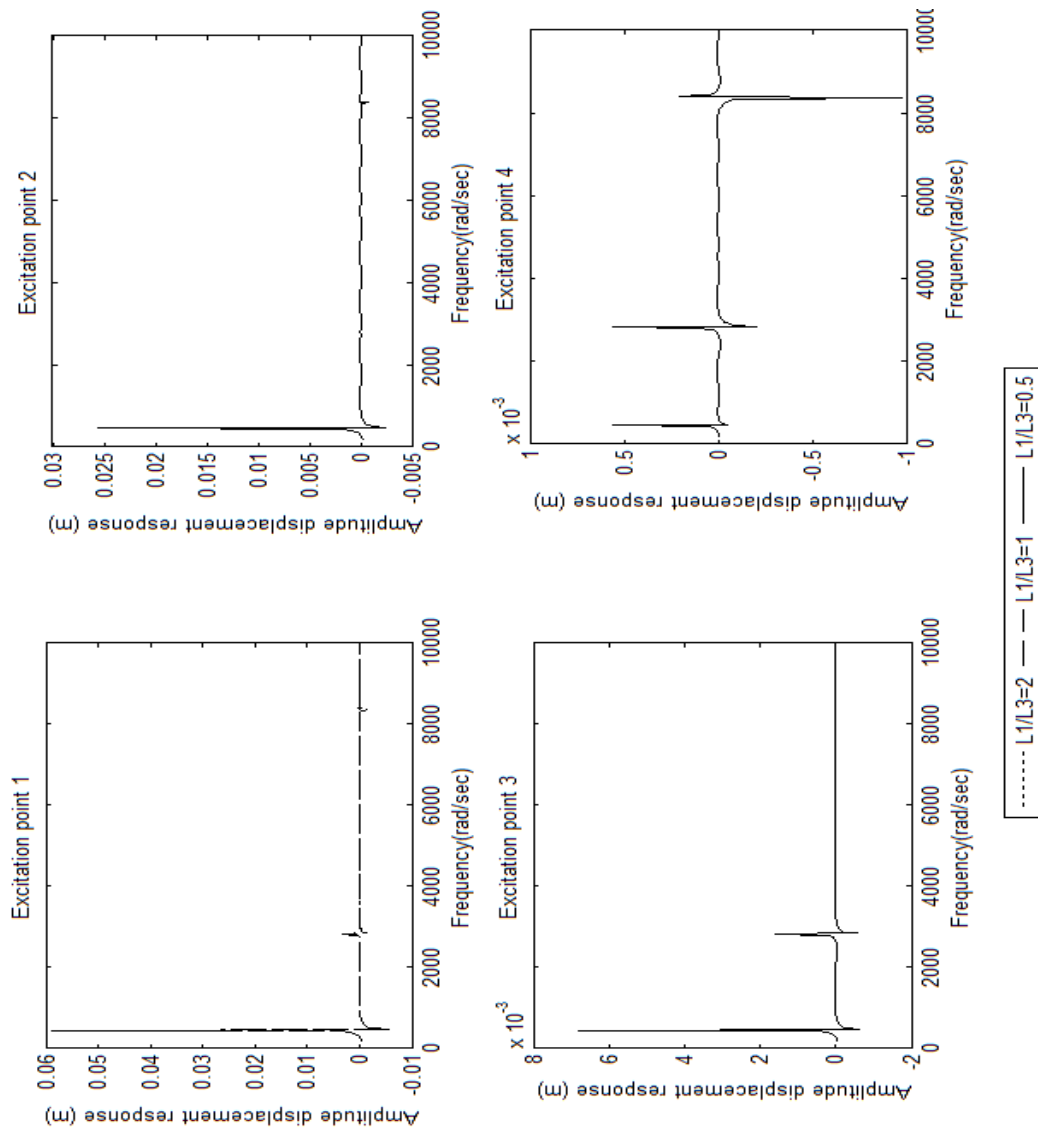


**Figure 3.33** Effect of length ratio ( $L_1/L_3$ ) on frequency-amplitude response for width-ratio ( $b_N/b_w$ ) value of 1

Figures 3.31-3.33 shows the effect of length ratio ( $L_1/L_3$ ) on forced response in terms of transverse amplitude displacements with excitation frequency  $\omega$  applied at four excitation points for clamped-free boundary condition. From the Figures 3.31-3.33, it can

be observed that the transverse displacement amplitude is largest for length ratio ( $L_1/L_3$ ) value of 0.25 and lowest for length ratio ( $L_1/L_3$ ) value of 2. The transverse displacement decrease with increase in length ratio because for largest length ratio values, the length of wider section of the beam increases, which makes the beam stiff that results in lower response in terms of transverse displacement, lower length ratio value of the beam results in increase in transverse amplitude displacement.

Another important observation that can be made is the transverse displacement amplitude is largest at excitation points 1 and 2 for clamped-free boundary condition.

#### **3.7.4 Effect of boundary conditions on forced response in terms of sinusoidal transverse displacement**

To study the effect of boundary conditions on forced response in terms of transverse displacement, the width ratio ( $b_R/b_L$ ) values of 0.2, 0.5, and 1 of width-tapered composite beams with four excitation points are considered. Simply-supported, clamped-clamped and clamped-free boundary conditions are considered. The laminate configuration considered is  $([0/90]_9)_s$  and each ply of composite beam is made of NCT-301 graphite-epoxy.

A sinusoidal force of magnitude 2N with excitation frequency  $\omega$  is applied at four excitation points shown in Figure 3.26. By using the properties given in the Tables 3.1, 3.2 and 3.3, the effect of boundary conditions on forced response in terms of sinusoidal

transverse displacement is presented in the current section. The forced response in terms of sinusoidal transverse displacement is obtained using Rayleigh-Ritz method. The range of frequency is between 1 to 10000 Hz.

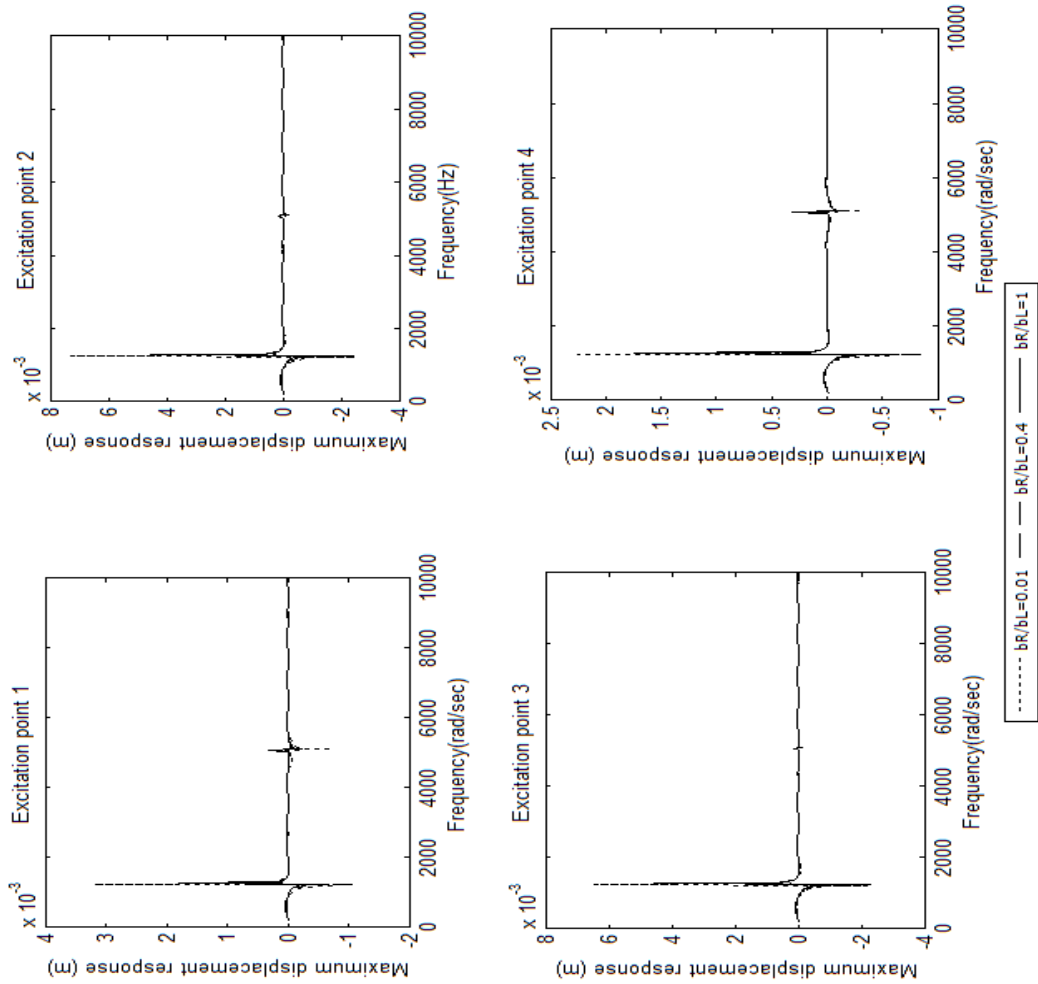


**Figure 3.34** Effect of simply-supported boundary condition on frequency-amplitude response

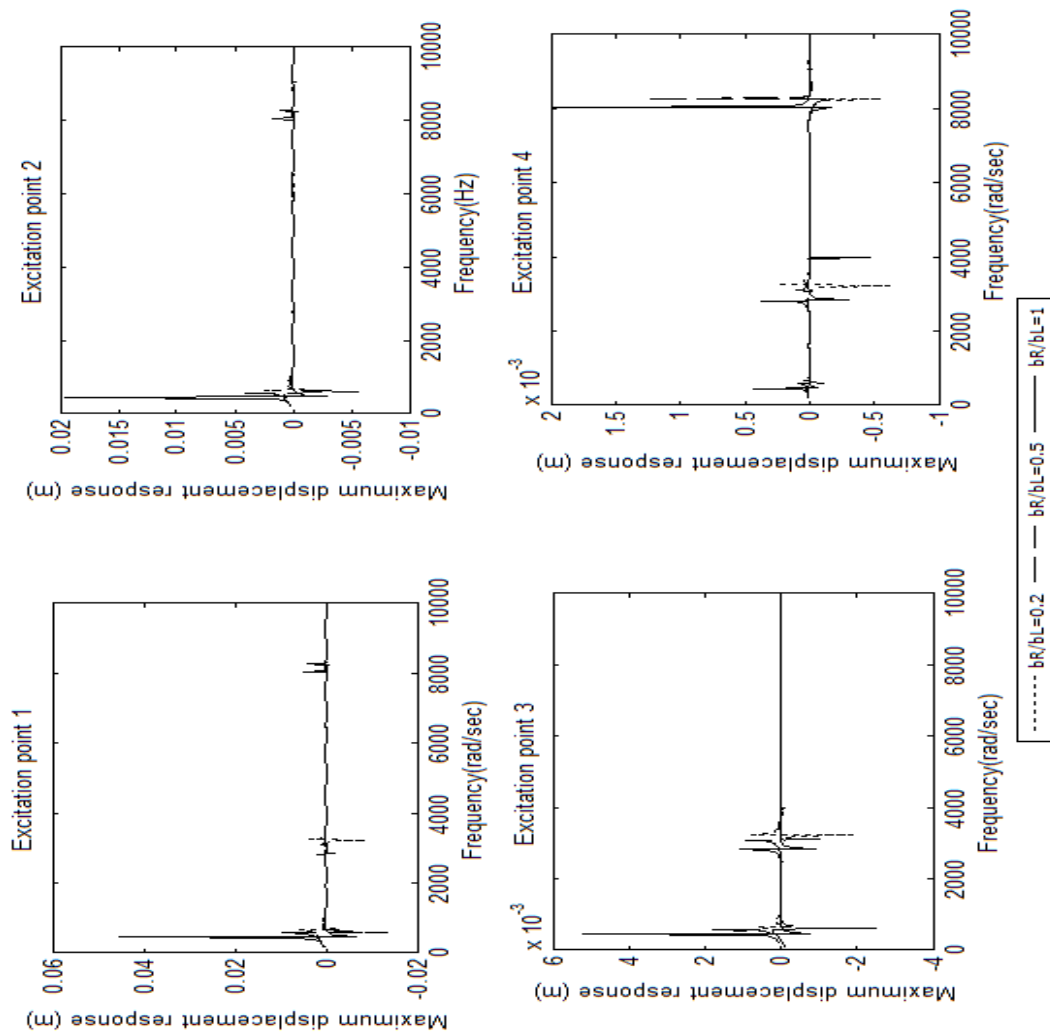


**Figure 3.35** Effect of clamped-free boundary condition on frequency-amplitude response

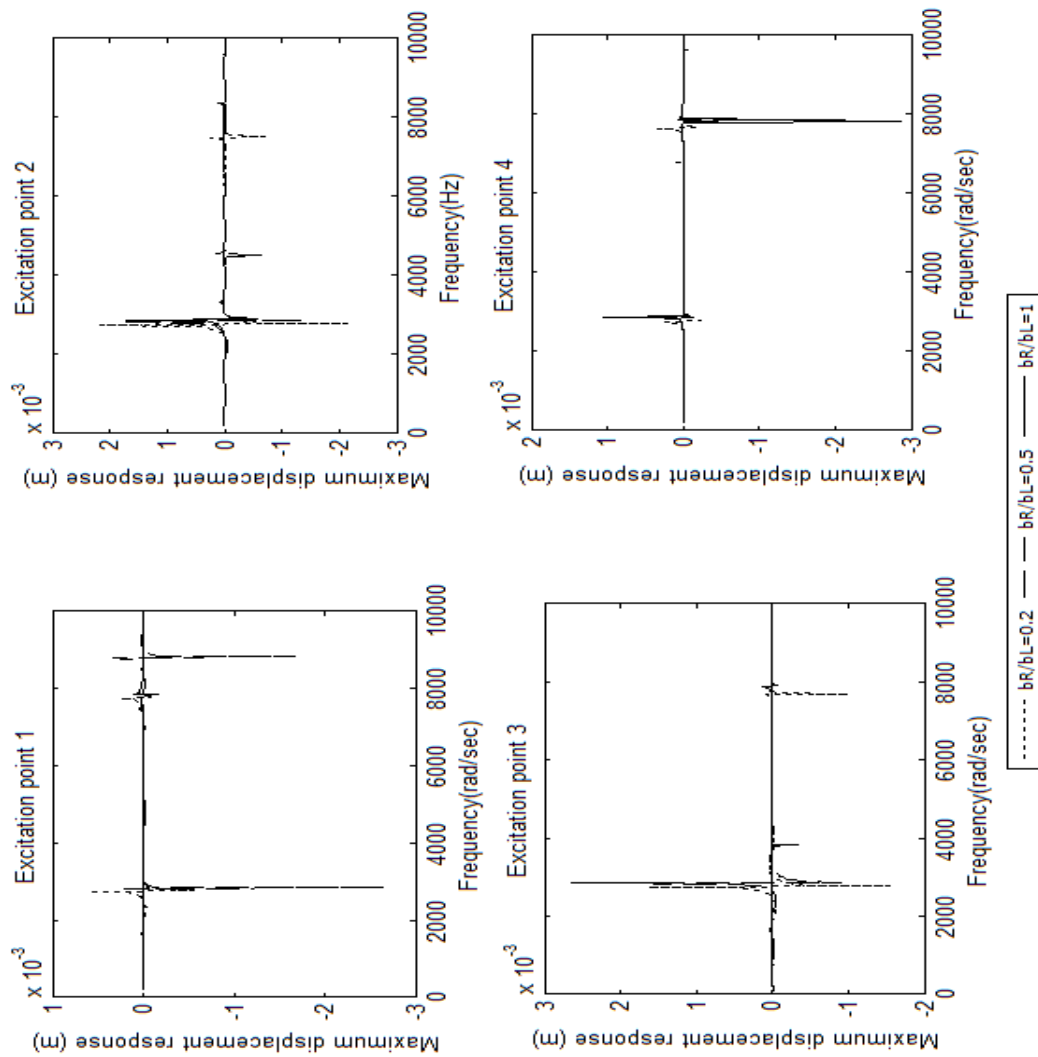


**Figure 3.36** Effect of clamped-clamped boundary condition on frequency-amplitude response

Figures 3.34-3.36 show the effect of boundary conditions on forced response in terms of transverse displacement amplitude with excitation frequency  $\omega$  applied at four excitation points. From the Figures 3.34-3.36, one can be observe that the forced

response in terms of transverse displacement amplitude is largest for clamped-free boundary condition and lowest for clamped-clamped boundary condition. This is because at clamped-free boundary condition of the beam, since the stiffness of the beam is low, the transverse displacement amplitude is high, and for clamped-clamped boundary condition since the beam is stiffest the transverse displacement amplitude is low.

The transverse displacement amplitude is largest for clamped-free boundary condition at excitation point 1, second highest for simply-supported at excitation points 2 & 3 and lowest for clamped-clamped boundary condition at excitation points 2 and 3. Another observation that can be made that is the transverse displacement amplitude is lowest for width ratio ( $b_R/b_L$ ) value of 0.2 for simply supported and clamped-clamped boundary conditions, for clamped-free boundary condition as the width ratio ( $b_R/b_L$ ) values increase from 0.2 to 1, the transverse displacement amplitude increases since the beam is less stiff at the free end of the beam.

### **3.7.5 Effect of axial forces on forced response in terms of sinusoidal transverse displacement**

To investigate the effects of applied end-axial (static) tensile and compressive loads on forced response in terms of transverse displacement, the linear width-tapered composite beams with width ratio ( $b_R/b_L$ ) values of 0.2, 0.5, and 1 for clamped-free boundary condition with four excitation points are considered. The ply of composite

beam is made up of NCT-301 graphite-epoxy and the laminate consists of 36 plies. The length ( $L$ ) of the beam is 0.25 m, the height of the beam ( $H$ ) = 0.0045 m and individual ply thickness ( $t_k$ ) is 0.000125 m. Concentrated end-axial compressive and tensile loads as the % of critical buckling load and tensile first-ply failure load respectively are applied respectively as shown in the Figure 3.37.

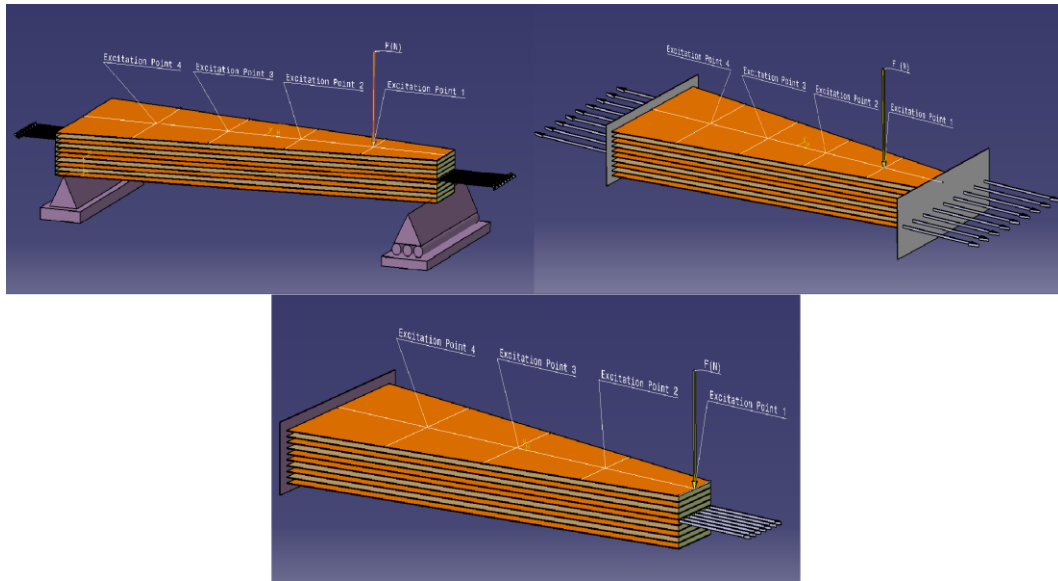


**Figure 3.37** Schematic illustration of linear width- tapered laminated composite beams with end-axial static load

A sinusoidal force of magnitude 2N with excitation frequency  $\omega$  is applied at four excitation points shown in the Figure 3.37. By using the properties given in the Tables 3.1, 3.2 and 3.3, the effect of applied end-axial (static) load on forced response in terms of sinusoidal transverse displacement obtained using Rayleigh-Ritz method is presented in the current section. The range of frequency in the x-axis is between 1 to 10000 Hz.

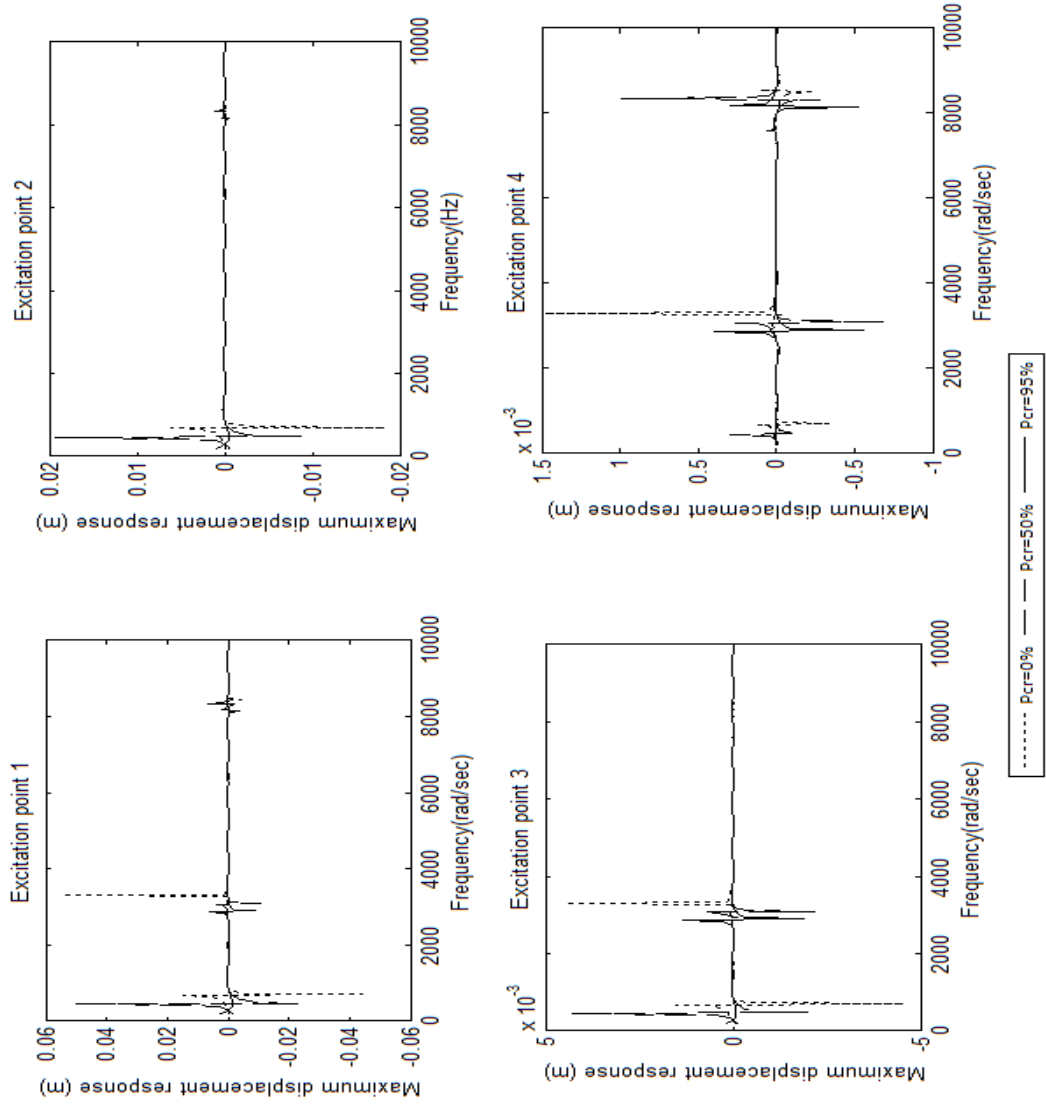


**Figure 3.38** Effect of compressive end-axial static load on frequency-amplitude response for clamped-free boundary condition for width-ratio ( $b_R/b_L$ ) value of 0.2

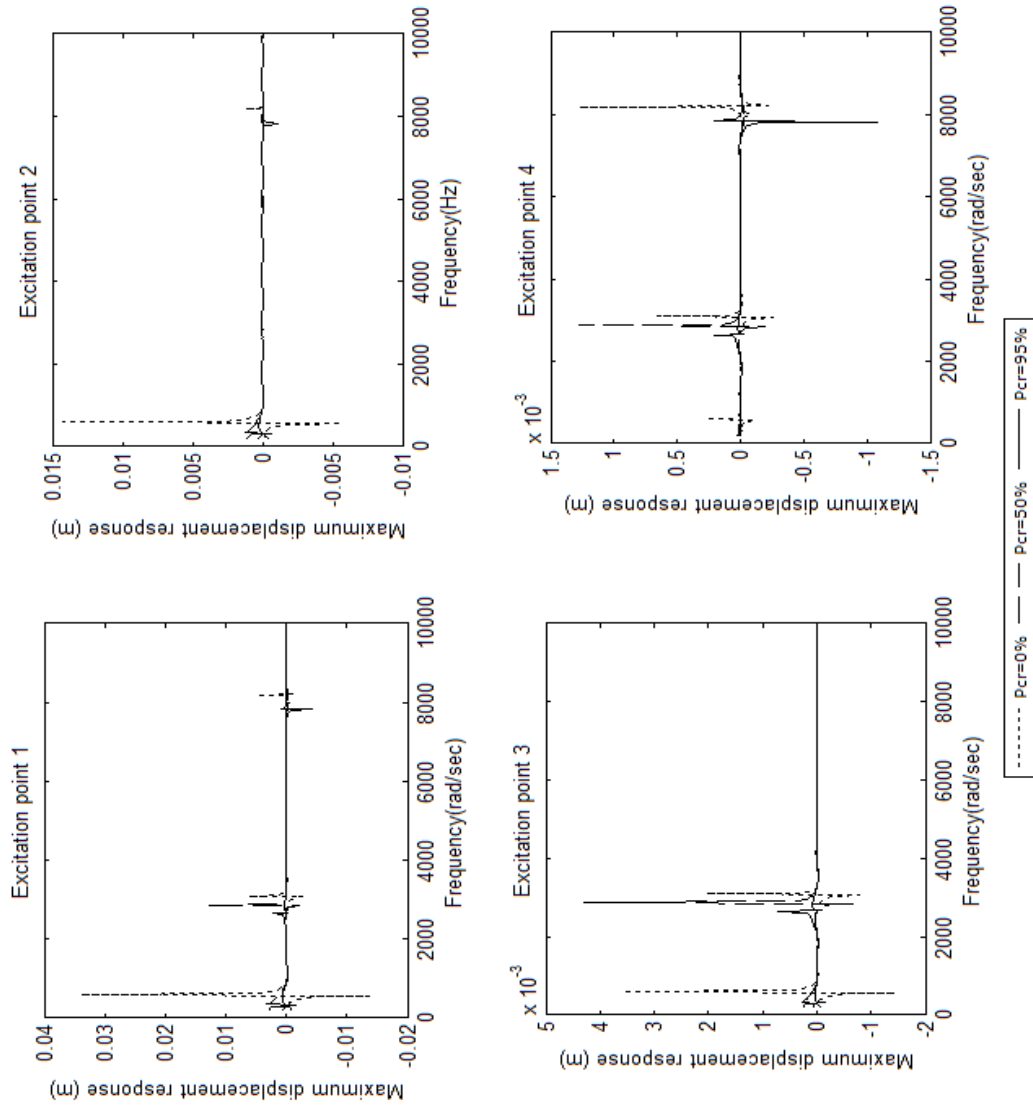


**Figure 3.39** Effect of compressive end-axial static load on frequency-amplitude response for clamped-free boundary condition for width-ratio  $(b_R/b_L)$  value of 0.5

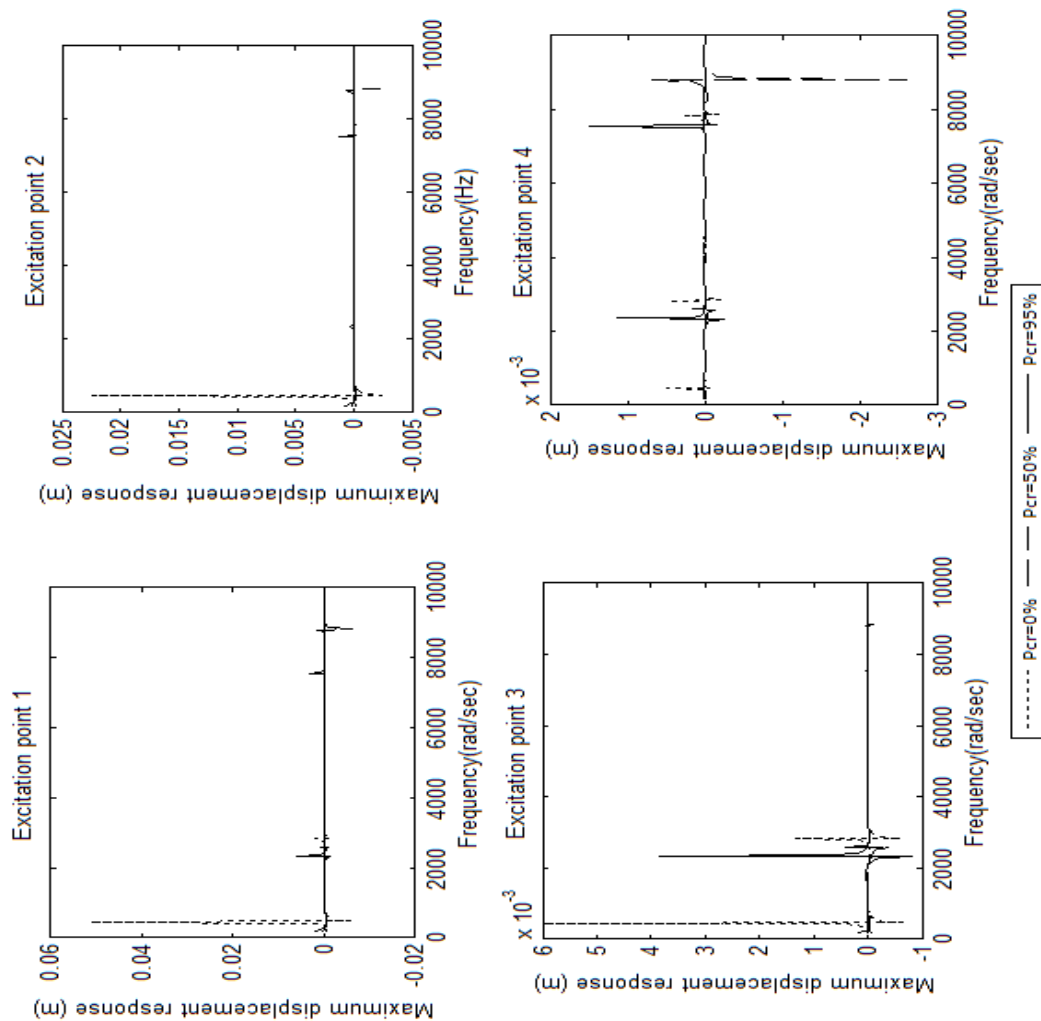


**Figure 3.40** Effect of compressive end-axial static load on frequency-amplitude response for clamped-free boundary condition for width-ratio ( $b_R/b_L$ ) value of 1

Figures 3.38-3.40 show the effects of end-axial compressive load applied as percentage of critical buckling load on forced response in terms of transverse displacement amplitude for width ratio ( $b_R/b_L$ ) values of 0.2, 0.5, and 1 with excitation frequency  $\omega$  applied at four excitation points for four boundary conditions. From the Figures 3.38-3.40, it can be observed that the forced response in terms of transverse displacement amplitude is largest for axial load equal to 95% of critical buckling load for simply supported boundary condition at excitation points 2 and 3. For clamped-free boundary condition the transverse displacement amplitude is largest at excitation point 3, since the beams gets lowest stiffness at this boundary condition.

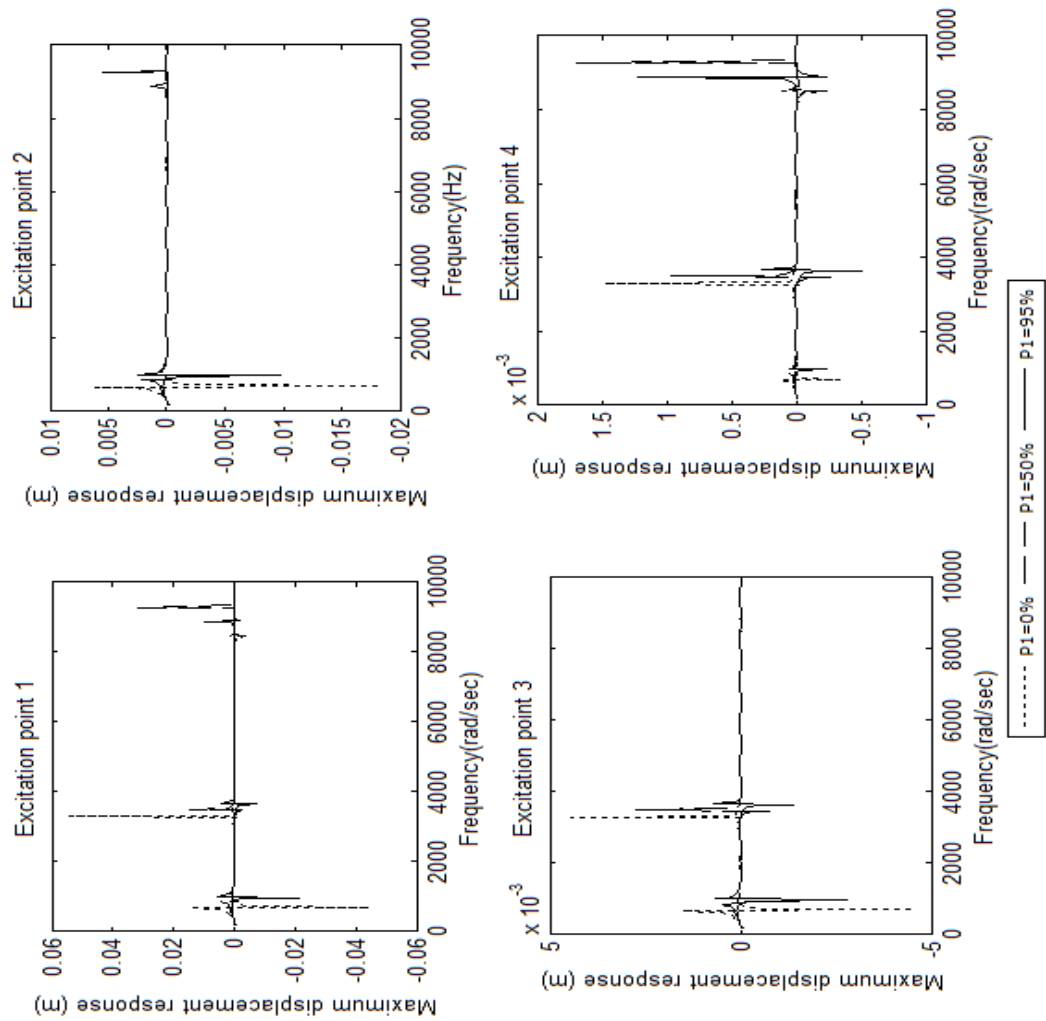


**Figure 3.41** Effect of tensile end-axial static load on frequency-amplitude response for clamped-free boundary condition for width-ratio ( $b_R/b_L$ ) value of 0.2

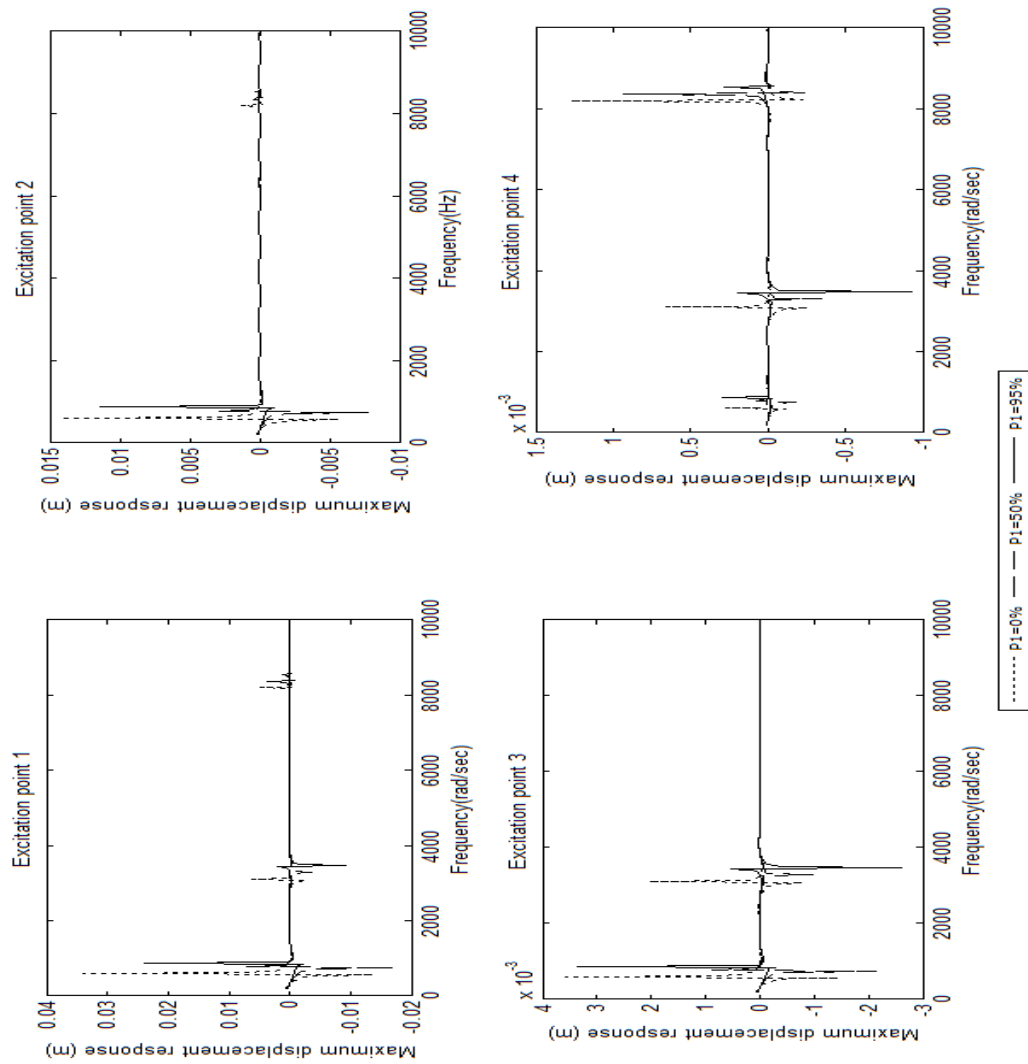


**Figure 3.42** Effect of tensile end-axial static load on frequency-amplitude response for clamped-free boundary condition for width-ratio ( $b_R/b_L$ ) value of 0.5

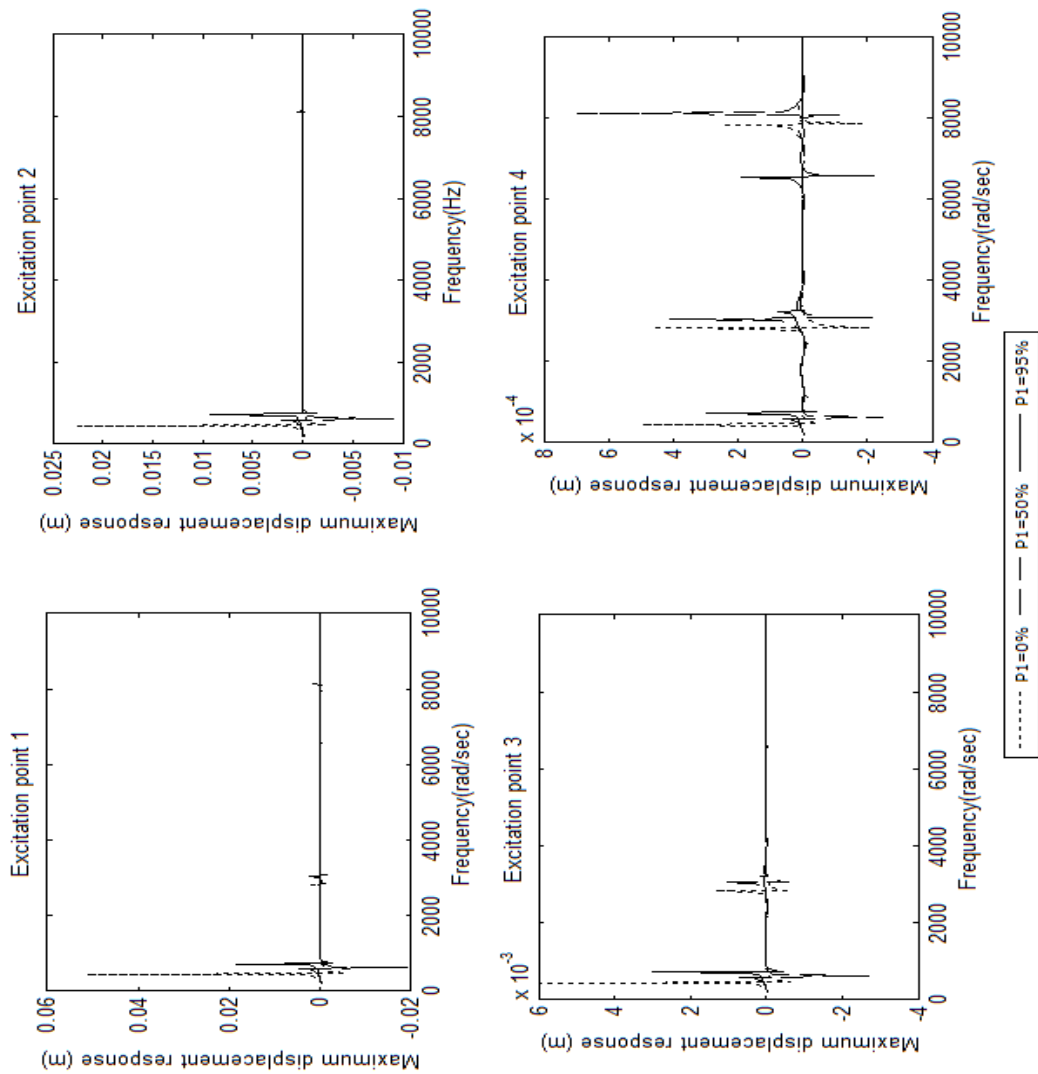


**Figure 3.43** Effect of tensile end-axial static load on frequency-amplitude response for clamped-free boundary condition for width-ratio ( $b_R/b_L$ ) value of 1

Figures 3.41-3.43 show the effects of end-axial tensile load applied as percentage of tensile first-ply failure load on forced response in terms of transverse displacement amplitude for width ratio ( $b_R/b_L$ ) values of 0.2, 0.5, and 1 with excitation frequency

$\omega$  applied at four excitation points for clamped-free boundary condition. From the Figures 3.41-3.43, it can be observed that the transverse displacement amplitude for clamped-free boundary condition is largest at excitation points 1 and 2. The transverse displacement amplitude is largest for beams that have low stiffness. The transverse displacement amplitude decreases as increase in percentage of tensile failure load because the beam becomes stiffer by applying more axial tensile load.

### **3.8 Comparison of forced response in terms of sinusoidal transverse displacement between Rayleigh-Ritz method and conventional finite element method.**

By using the properties given in the Tables 3.1, 3.2 and 3.3, the current section presents the comparison of forced response in terms of sinusoidal transverse displacement for clamped-free simply-supported and clamped-clamped boundary conditions of width-tapered composite beams obtained by using Rayleigh-Ritz method with that obtained using conventional finite element method [81]. The compared results are presented in the Figures 3.44-3.46 below.

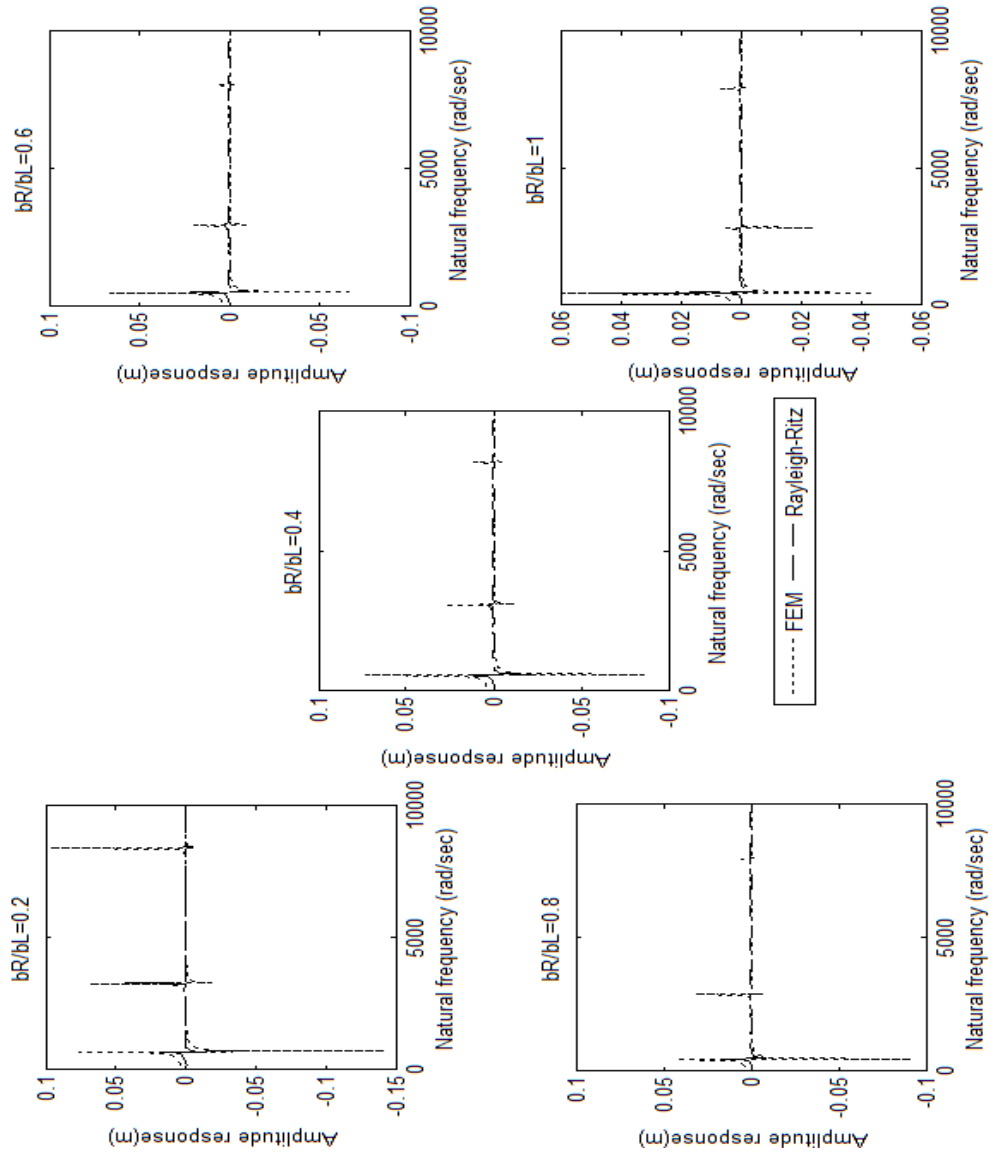


**Figure 3.44** Comparison of forced response in terms of sinusoidal transverse displacement- clamped-free boundary condition

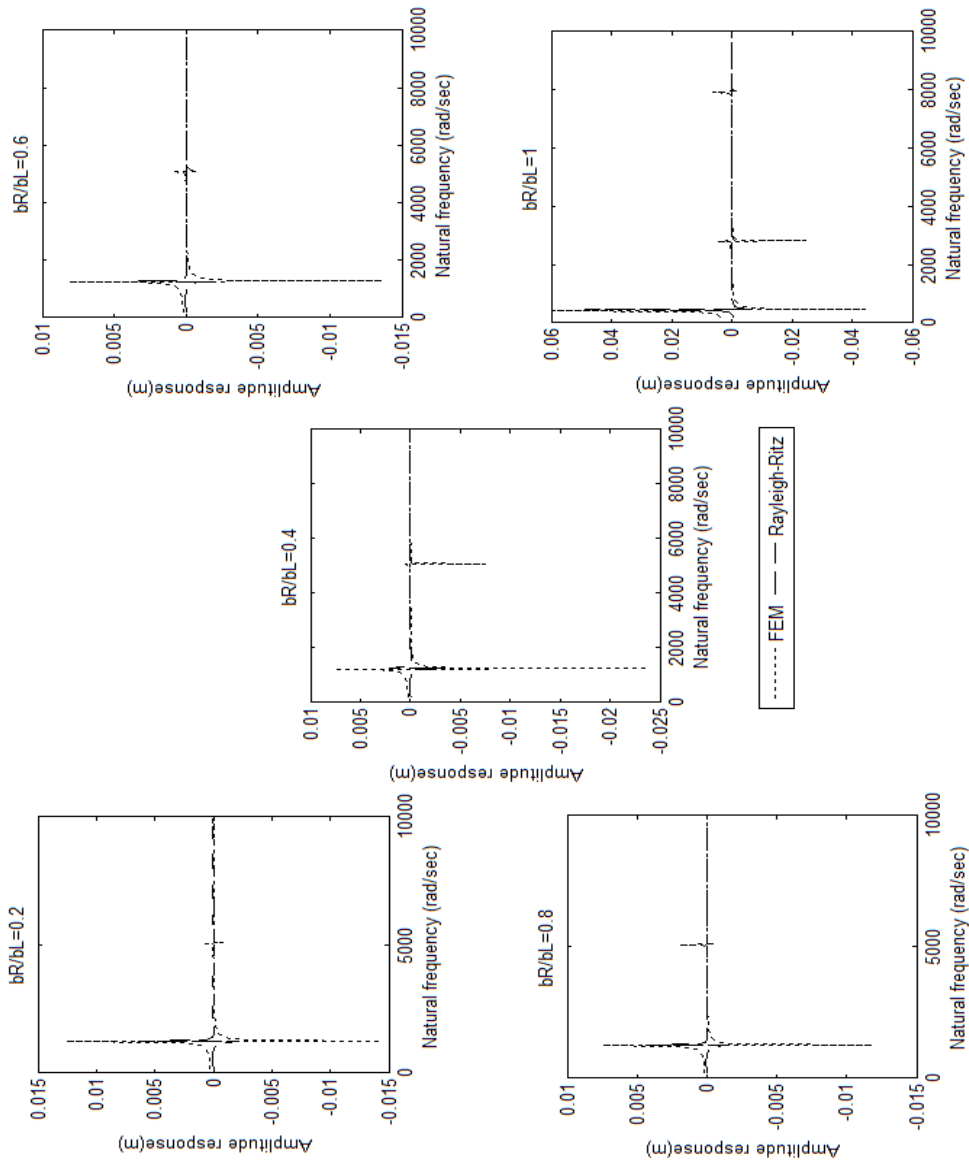


**Figure 3.45** Comparison of forced response in terms of sinusoidal transverse displacement- simply-supported boundary condition

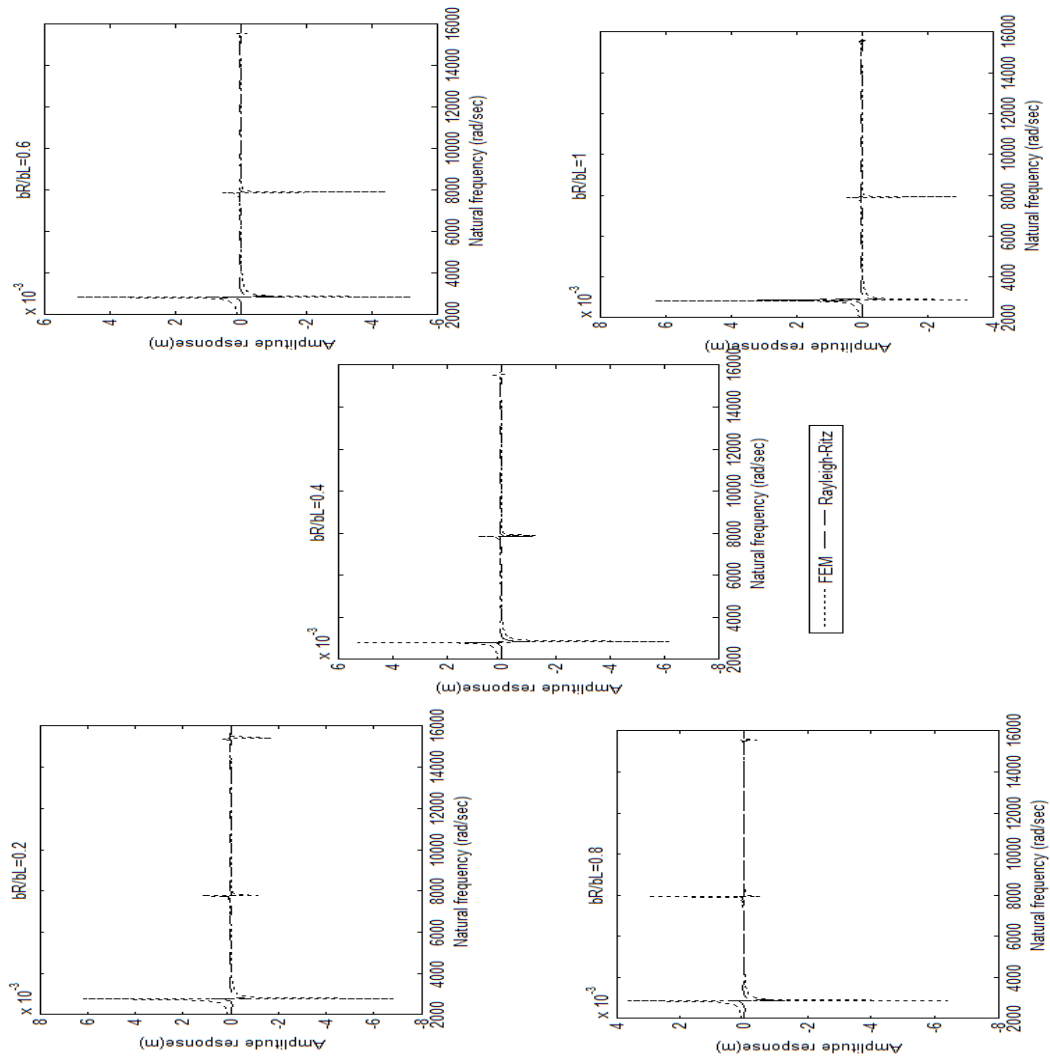


**Figure 3.46** Comparison of forced response in terms of sinusoidal transverse displacement- clamped-clamped boundary condition

Figures 3.44-3.46 show the comparison of forced response in terms of sinusoidal transverse displacement for clamped-free simply-supported and clamped-clamped boundary conditions of width-tapered composite beams for width-ratio values of 0.2, 0.4, 0.6, 0.8 and 1. From the Figures 3.44-3.46, the comparison differences for simply-supported boundary condition is between 3- 4%, for clamped-clamped boundary

condition it is between 2-4% and for clamped-free boundary condition it is between 2-4.5%. The comparison differences in transverse displacement from the above Figures 3.44-3.46 are well accepted. Also the differences in transverse displacements is because of no damping is considered.

### 3.9 Summary

In this chapter, dynamic analyses of width-tapered laminated composite beams are considered. In the present case, Rayleigh-Ritz method is used to find the natural frequencies, forced response and critical buckling load ( $P_{cr}$ ) for width-tapered laminated composite beams. The extensional and flexural stiffness distributions for linear width-tapered composite beams are shown. The previous sections show the effect of different width ratio values, laminate configurations, length ratios, and boundary conditions on natural frequencies, forced response and critical buckling load ( $P_{cr}$ ). The effects of applied end-axial static force and damping on natural frequencies and forced response of width-tapered composite beams have been investigated. The first-ply failure load of width-tapered beam is obtained to find the effects of end-axial compressive and tensile load on natural frequencies. From the figures given in different sections, one can conclude the following:

- The laminate configuration LC1 is strongest in terms of extensional stiffness  $A_{11}$  and  $A_{22}$ . The extensional stiffness is second highest for laminate configuration LC2, third for LC3 and least for LC4 for all the extensional stiffnesses. The laminate configuration

LC2 is strongest in terms of extensional stiffness coefficients  $A_{12}$  and  $A_{66}$ . The laminate configuration LC3 is second largest for extensional stiffness coefficients  $A_{11}$ ,  $A_{12}$  and  $A_{66}$  and least for  $A_{22}$ . The laminate configuration LC4 is third largest for extensional stiffness coefficients  $A_{11}$ ,  $A_{12}$  and  $A_{66}$  but second largest for  $A_{22}$ .

- The laminate configuration LC3 is strongest in terms of flexural stiffness coefficient  $D_{11}$ . The laminate configuration LC1 is second largest, LC4 is third largest and LC2 is fourth largest. The laminate configuration LC2 is strongest in terms of flexural stiffness coefficients  $D_{12}$ ,  $D_{22}$ ,  $D_{26}$  and  $D_{66}$ . But the laminate configuration LC1 is largest in terms of flexural stiffness coefficient  $D_{12}$ , the laminate configuration LC2 is strongest in terms of flexural stiffness coefficient  $D_{16}$ .

- As the width ratio  $(b_R/b_L)$  value increases, all three natural frequencies increase for simply-supported, clamped-clamped and free-clamped boundary conditions. Increasing the width ratio  $(b_R/b_L)$  results in increase in the value of bending stiffness

term  $\left( \frac{1}{D_{11}^*(x)} \right)$ , which in turn results in increase in stiffness matrix coefficients. But all

three natural frequencies decrease for clamped-free boundary condition as the width ratio  $(b_R/b_L)$  value is increased.

- The first natural frequency is largest for clamped-clamped boundary condition of beam constant width compared to the width-tapered beam. The change in the fundamental natural frequency corresponds to different ply orientations of the laminate.

The fundamental natural frequency is second largest for simply-supported, third largest for clamped-free and fourth largest for free-clamped boundary conditions.

- For the effect of laminate configuration on first three natural frequencies of width-tapered composite beams, the natural frequencies are largest for laminate configuration LC3, second largest for LC1, third largest for LC4 and fourth largest for LC2. The

stiffness of the beam depends on  $\left( \frac{1}{D_{11}^*(x)} \right)$  which is directly related with  $Q_{11}$  of the ply.

As the width ratio ( $b_R/b_L$ ) value increases from 0.01 to 1, the natural frequencies increase for simply-supported, clamped-clamped and free-clamped boundary conditions. But they decrease for clamped-free boundary condition.

- As the length ratio ( $L_1/L_3$ ) value increases, all the three natural frequencies increase. Also the three natural frequencies increase as the width ratio ( $b_R/b_L$ ) increases for SS, CC and FC boundary conditions, but decrease for CF boundary condition. The first, second and third natural frequencies increase for width ratio ( $b_R/b_L$ ) values from 0.2 to 0.4 but the natural frequencies remain unchanged with the increase in width ratio ( $b_R/b_L$ ) values upto 1.

- The natural frequencies increase as the width ratio ( $b_R/b_L$ ) values increase from 0.01 to 1 for SS, CC and FC boundary conditions, but decrease for CF boundary condition. Clamped-clamped boundary condition beam has largest natural frequencies compared to other boundary conditions whereas free-clamped boundary condition has

lowest natural frequencies. The beam with simply-supported and clamped-free boundary conditions is second highest and third highest in natural frequencies respectively.

- As the axial load is increased from 0 to 95 % of critical buckling load, the natural frequencies decrease. This is because the beam becomes less stiff which results in decrease in the natural frequencies. As the tensile axial load is increased from 0% to 95 % of tensile failure load, the natural frequencies increase because the beam becomes stiffer thereby increasing the natural frequencies.
- The natural frequencies decrease for damped condition compared to un-damped condition. The difference between the undamped and damped natural frequencies is small because of low values of damping.
- The comparisons of natural frequencies were made between Rayleigh-Ritz method and conventional finite element method. From the observations, the comparison differences for simply-supported boundary condition is <0.2%, for clamped-clamped boundary condition it is <1.5%, for clamped-free boundary condition it is <0.15% and for free-clamped boundary condition it is <0.7%.
- As the width ratio values increase the critical buckling load increase for SS, CC and FC boundary conditions, but decrease for CF boundary condition. The critical buckling load is highest for clamped-clamped boundary condition and least for free-clamped boundary condition.
- The critical buckling load for variation of width ratio ( $b_R/b_L$ ) values is largest for laminate configuration LC3, second largest for LC1, third largest for LC4 and fourth

largest for LC2. This difference in critical buckling load is expected for different laminate configurations because the stiffness of the column depends on  $\left( \frac{1}{D_{11}^*} \right)$  which are directly related with  $Q_{11}$  of the ply. The critical buckling load increases for SS, CC and FC boundary condition, but decreases for CF boundary condition.

The critical buckling load is largest for length ratio ( $L_1/L_3$ ) of 2 and least for length ratio 0.25. As the width ratio ( $b_R/b_L$ ) values increase from 0.2 to 1, the critical buckling load increases for simply-supported, clamped-clamped and free-clamped boundary condition but decreases for clamped-free boundary condition.

- The critical buckling load is largest for clamped-clamped boundary condition since the column is stiffer and least for free-clamped boundary condition. As the width ratio  $b_R/b_L$  values increase from 0.01 to 1, the critical buckling load increase for SS, CC and FC boundary conditions, but decreases for CF boundary condition.
- The first-ply failure load varies for different width ratio values of width-tapered composite beams. From the Tables 3.14-3.15 using the Tsai-Wu theory it can be found that the failure load is minimum for the  $90^\circ$  ply compared to  $0^\circ$  ply. The failure load (tensile and compressive) for both  $0^\circ$  and  $90^\circ$  plies are least for width ratio value of 0.01 and highest for 1. The first-ply failure load is used to find the natural frequencies and forced response with respect to displacement with effect of static end-axial load.

- The transverse displacement amplitude is largest for width ratio ( $b_R/b_L$ ) value of 1, second largest for width ratio value of 0.5 and lowest for width ratio value of 0.2 for clamped-free boundary condition. The transverse displacement amplitude is largest for higher width ratio values of the beam. As the width ratio value increase, transverse displacement amplitude increases.
- The transverse displacement amplitude is largest for laminate configuration LC2, second largest for laminate configuration LC1, third largest for LC4 and lowest for laminate configuration LC3. The transverse displacement amplitude is largest for laminate configuration LC2 because the fibers are oriented along  $+45^0$  and  $-45^0$ , which has lower extensional and bending stiffness but higher shear stiffness. Another observation that can be made is the transverse displacement amplitude is largest when the width ratio ( $b_R/b_L$ ) value of the beam is 1. The transverse displacement amplitude reduces as the width ratio ( $b_R/b_L$ ) values reduce.
- The transverse displacement amplitude is largest for length ratio ( $L_1/L_3$ ) value of 0.25 and lowest for length ratio ( $L_1/L_3$ ) value of 2 for all four boundary conditions. The transverse displacement decrease with increase in length ratio of the beam because for larger length ratio values, the length of wider section of the beam increases, which makes the beam stiff that results in lower response in terms of transverse displacement, lower length ratio value of the beam results in increase in transverse amplitude displacement. Another important observation that can be made is the transverse displacement amplitude is largest at excitation points 1 and 2 for clamped-free boundary condition.

- The forced response in terms of transverse displacement amplitude is largest for clamped-free boundary condition and lowest for clamped-clamped boundary condition. The transverse displacement amplitude is largest for clamped-free boundary condition at excitation point 1, second largest for free-clamped boundary condition at excitation point 1, third highest for simply-supported at excitation points 2 and 3 and lowest for clamped-clamped boundary condition at excitation points 2 and 3.
- Another observation can be made that is the transverse displacement amplitude is lowest for width ratio ( $b_R/b_L$ ) value of 0.2 for simply supported and clamped-clamped boundary condition, for clamped-free and free-clamped boundary conditions as the width ratio ( $b_R/b_L$ ) values increase from 0.2 to 1, the transverse displacement amplitude increases since the beam is less stiff at the free end of the beam.
- The forced response in terms of transverse displacement amplitude is largest for axial load equal to 95% of critical buckling load for clamped-free boundary condition at excitation point 1, since the beams gets lowest stiffness at this boundary condition.
- Another observation that can be made is the transverse displacement is largest for lower width ratio ( $b_R/b_L$ ) values of the beams as the beams is less stiff and as the width ratio values increases the beams becomes more stiffer and hence the transverse displacement decreases.
- The transverse displacement amplitude for clamped-free boundary condition is largest at excitation points 1 and 2. The transverse displacement amplitude is largest for beams that have low stiffness. The transverse displacement amplitude decreases as increase in the percentage of tensile failure load because the beams become stiffer by

applying more axial tensile load. The transverse displacement is largest for lower width ratio ( $b_R/b_L$ ) values of the beams.

- The comparisons of transverse displacement between Rayleigh-Ritz method and conventional finite element method show the difference in transverse displacement for simply-supported boundary condition is between 3- 4%, for clamped-clamped boundary condition it is between 2-4% and for clamped-free boundary condition it is between 2-4.5%. The comparison differences in transverse displacement are well accepted.

## **CHAPTER 4**

### **EXPERIMENTAL VALIDATION FOR WIDTH-TAPERED COMPOSITE BEAMS**

#### **4.1 Introduction**

The laminated composite beams are basic structural components used in a variety of engineering structures such as airplane wings, helicopter blades and turbine blades as well as many others applications in the aerospace, mechanical and civil industries. This is due to their excellent features, such as high strength-to-weight and stiffness-to-weight ratios, the ability of being different strengths in different directions and the nature of being tailored to satisfy the strength and stiffness requirements in practical designs. An important element in the dynamic analysis of composite beams is the computation of natural frequencies. This is important because composite beam structures often operate in complex environmental conditions and are frequently exposed to a variety of dynamic excitations.

In this chapter, detailed procedures of manufacturing and modal analysis of composite beams for evaluating the structural properties are described. Pre-impregnated NCT-301 graphite/epoxy material supplied by NEWPORT Company, USA is used in the present thesis for all experiments and analysis. The mechanical properties (longitudinal modulus  $E_1$ , transverse modulus  $E_2$ , shear modulus  $G_{12}$ , Poisson's ratio  $\nu_{12}$ ) of the ply of

composite laminate has been tested according to ASTM specification D 3039 M-00 and ASTM specification D 3518-94-01 in a previous work [24].

The composite laminates are manufactured using the fabrication of fiber reinforced with polymer matrix which are placed or shaped into a structural form. Vacuum bag is prepared for laminate curing. The laminate which is prepared using vacuum bag is cured using autoclave.

Modal testing is the process of determining the modal parameters of the structure for all modes in the frequency range of interest. The most popular technique used for modal testing is impact or hammer excitation technique [65].

The frequency response measurements are made by using PULSE<sup>TM</sup> system, the multi-analyzer system type 3560 from Bruel and Kjaer and a four-channel signal analyzer. The excitation force from the impact hammer is measured from the force transducer mounted at the tip of the hammer and resulting response is supplied to one of the inputs of signal analyzer to amplify the input signals. The response is measured by an accelerometer and the resulting signal is supplied to another input of signal analyzer to amplify the output signals. The frequency response obtained here represents the structure's accelerance, since the measured quantity is the complex ratio of the acceleration to force in the frequency domain. For impact hammer excitation, the accelerometer response position is fixed and used as a reference position. The hammer is used to excite the beam at every translational degree of freedom corresponding to the degrees of freedom in the model.

## **4.2 Manufacturing of composite laminate**

The multitude of tasks involved in the manufacturing of composite laminates can be categorized into two phases:

- 1) Fabrication
- 2) Processing

### **4.2.1 Fabrication**

In the fabrication phase the fiber reinforcement and matrix material are placed or shaped into a structural form. In the present work a flat plate is manufactured from layers or plies of pre-impregnated NCT-301 graphite/epoxy material.

*Tooling:* All fabrication methods require tools to provide the shape of the composite structure/laminate during the processing. In this case a flat aluminum tool is used to manufacture flat composite plate.

*Secondary materials for laminate curing preparation:* Many secondary or specialty materials are used in composite manufacturing such as release agent, release films, bleeder plies, breather plies, vacuum bag and sealant tape. Each of these materials provides specific function. A typical lay-up of a composite structure prepared for autoclave processing is shown in Figure 4.1.

*Hand lay-up:*

The hand lay-up of pre-impregnated materials is the oldest and most commonly used method where the production volume is low and other forms of production would prove to be expensive. Each step in hand lay-up of a flat composite laminate must follow in successive fashion in order to obtain a high quality composite laminate after final processing. The major steps that are followed in the hand lay-up of prepreg are briefly highlighted:

- At first, the surface of the plate is cleaned and a release agent is applied followed by one layer of the release film as shown in Figure 4.2 a. This allows the part to easily separate from the mold after curing.
- The preimpregnated material is cut from the prepreg roll according to the required dimension of respective specimen.
- A ply is oriented and placed upon the tool and subsequent plies are placed on top of the lamina according to the laminate configuration. Compaction pressure is applied by the use of a roller device as shown in Figure 4.2 b to adhere the plies and remove entrapped air that could lead to voids or delamination in between the layers.
- After completing the ply gathering, a sheet of porous release film, the bleeder ply, the breather plies and vacuum valve are placed on the top of the laminate one after the as shown in the Figures 4.2 c- 4.2 g.

- After completing all the lay-up of all the secondary material plies, the sealant tape is placed around the periphery of the laid laminate and the vacuum bag is placed over the entire lay-up as shown in Figure 4.2 h and Figure 4.2 i.
- The entire assembly is placed inside an autoclave and the vacuum is connected to vacuum pump of the autoclave to check the leaks between sealant and vacuum bag before starting the autoclave for processing as shown in Figure 4.2 j.

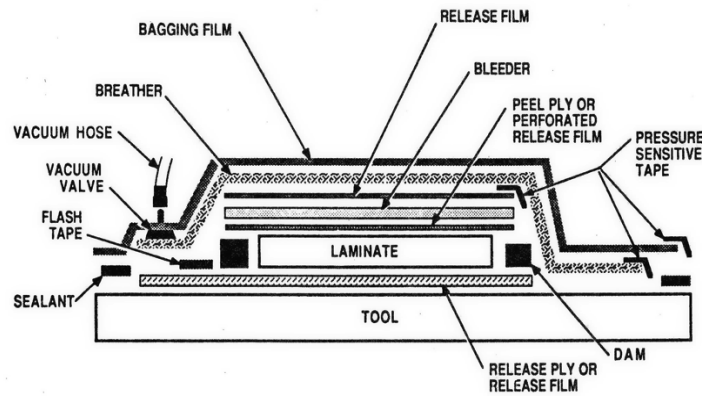
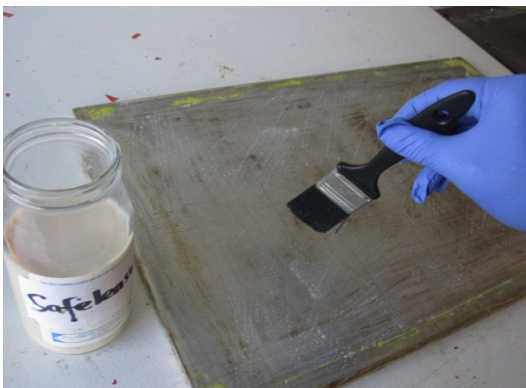
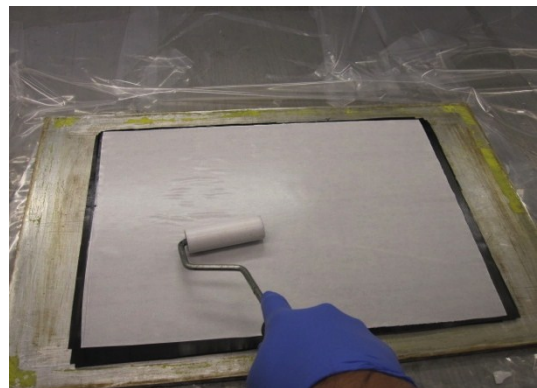


**Figure 4.1** Typical autoclave layup (Source: Carbonfiberguru.com)



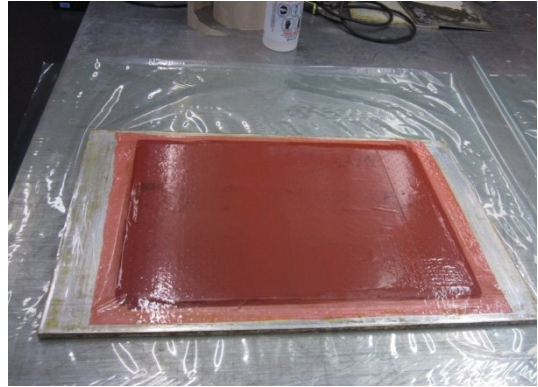
**a** (Hand layup)



**b** (Compaction pressure using roller)



**c** (porous release film)



**d** (vacuum bag sheet)



**e** (breather and bleeder plies)



**f** (vacuum valve)



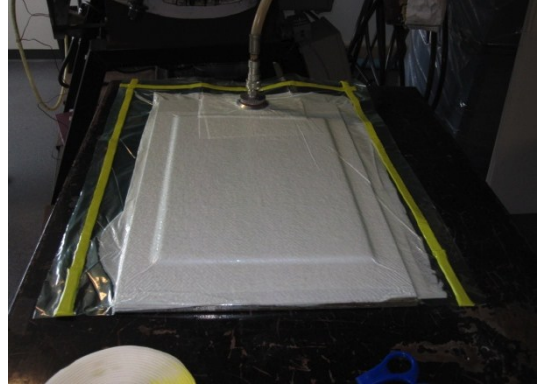
**g** (vacuum valve fixed)



**h** (application of sealant tape)



**i** (vacuum bag prepared)



**j** (vacuum valve fixed to the autoclave)

**Figure 4.2** Hand layup process of NCT-301 graphite/epoxy composite laminate

#### 4.2.2 Processing

##### *Autoclave curing:*

The autoclave shown in the Figure 4.3 is used to provide the necessary heat and pressure required to consolidate and cure the composite laminate. The major advantages of the autoclave are that it represents a flexible method to apply required pressure and temperature to a composite part, which is controlled by the numeric controller.



**Figure 4.3** Photograph of typical Autoclave for curing composite materials

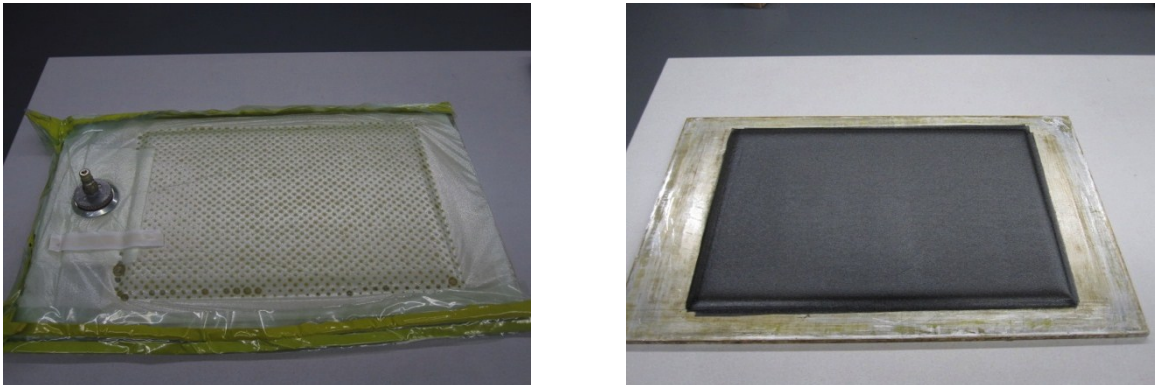


**Figure 4.4** Photograph of NCT-301 graphite/epoxy composite laminate post autoclave curing

The cure temperature and pressure are selected to meet the following requirements:

- To cure the resin uniformly and to attain a specified degree of cure in the shortest possible time.
- To maintain the temperature of any part inside the prepreg this should not exceed a prescribed limit during the cure.
- To have sufficient pressure to squeeze out all the excess resin from every ply before the resin becomes gel at any location inside the prepreg.
- Pressurization also helps to bond layers and remove persistent voids in the matrix.

In autoclave the temperature plays an important role in initiation of cross-linking and acceleration of curing process. This cure cycle was given by NEWPORT Company, USA for the current batch of pre-impregnated NCT-301 graphite/epoxy material.

In the cure cycle the laminate is heated from room temperature (RT) to 135<sup>0</sup> C at constant rate in 70 minutes and it is held at this temperature for a period of 60 minutes. There is a single dwell in the current cure cycle. A constant pressure of 55-psi is maintained inside the autoclave throughout the processing time. Then the laminate is cooled to room temperature at constant rate. A typical cure cycle for NCT-301 graphite/epoxy composite is shown in the Figure 4.5.

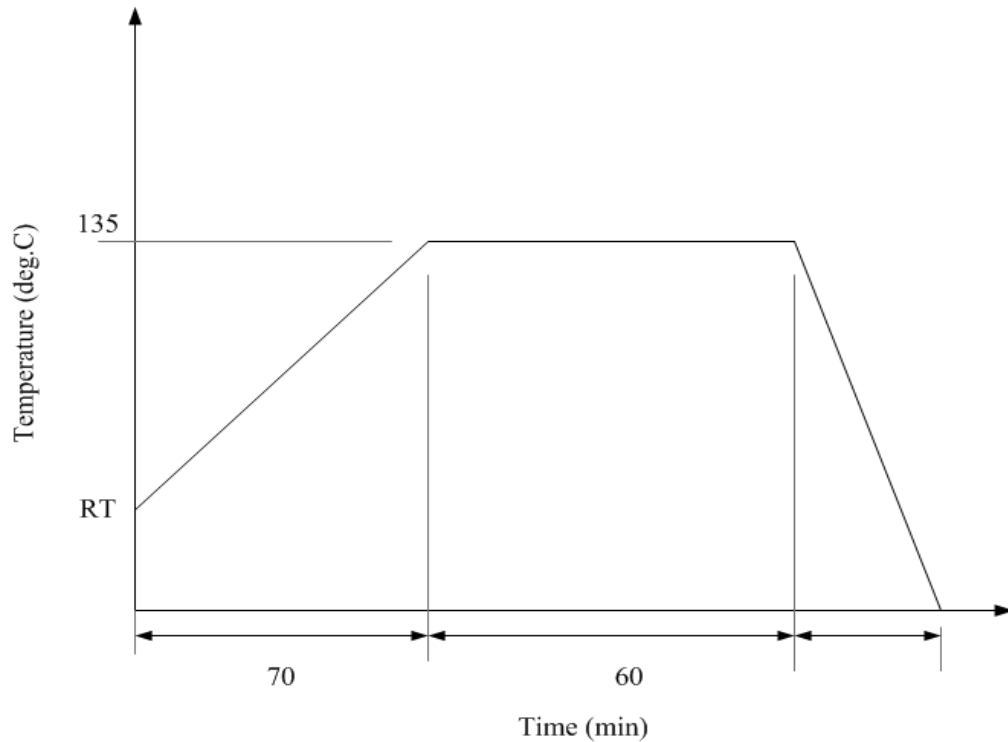


**Figure 4.5** Cure cycle for NCT-301 graphite/epoxy composite material

### **4.3 Inspection of NCT-301 graphite/epoxy panel by Laser ultrasonic**

Ultrasonics is based on the principle of transmitting high frequency sound into a test part and monitoring the received ultrasonic energy. This novel technology is based on the use of lasers for the generation and detection of ultrasound and can be used to measure thicknesses, detect and image surface or bulk flaws in complex structures, and characterize material microstructure in service or during processing as explained in Refs. [72] and [73].



**Figure 4.6** Photograph of NCT-301 graphite/epoxy panel in a fixture

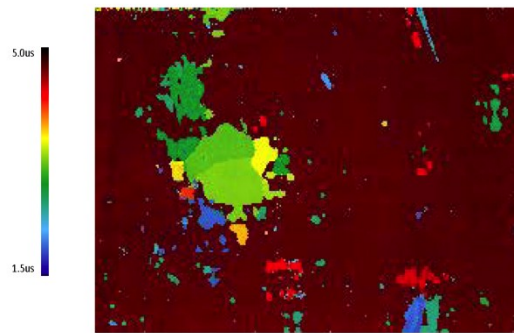


**Figure 4.7** Photograph of NCT-301 graphite/epoxy panel - C scan (different colors show the variation in time (thickness) in the sample)

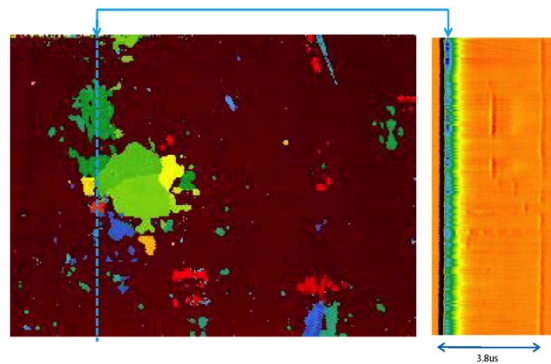


**Figure 4.8** Photograph of NCT-301 graphite/epoxy panel- BY-Scan #59

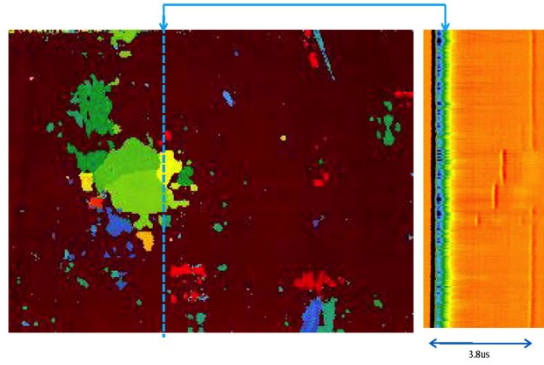


**Figure 4.9** Photograph of NCT-301 graphite/epoxy panel- BY-Scan #111

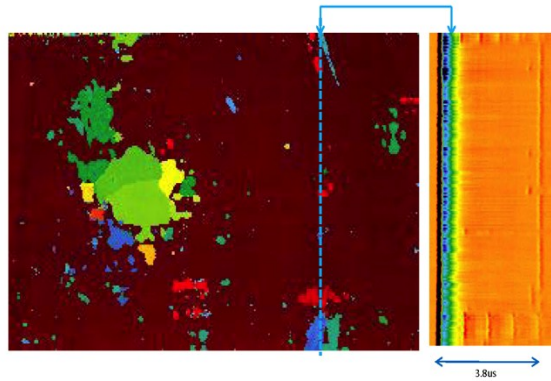


**Figure 4.10** Photograph of NCT-301 graphite/epoxy panel- BY-Scan #220

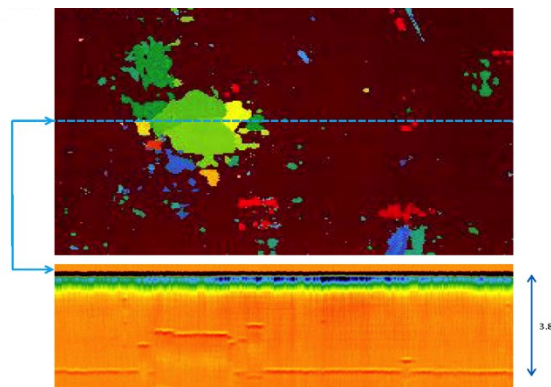


**Figure 4.11** Photograph of NCT-301 graphite/epoxy panel- BX-Scan #91

The NCT-301 graphite/epoxy composite laminate made by using autoclave curing is inspected for detection of flaws and defects using laser ultrasonic method. The laser ultrasonic inspection was done with the help of National Research Council of Canada's (CNRC) Industrial Materials Institute. The flaws or defects in the composite laminate may be due to voids, when prepregs are not fully impregnated, inadequate vacuum may result in internal defects such as delamination.

Ultrasonic data can be collected and displayed in a number of different formats. The three most common formats are A-scan, B-scan and C-scan presentations. Each presentation mode provides a different way of looking at and evaluating the region of material being inspected. In the current tests, B and C-scan are conducted.

The B-scan presentations are a profile (cross-sectional) view of the test specimen. In the B-scan, the time-of-flight (travel time) of the sound energy is displayed along the vertical axis and the linear position of the transducer is displayed along the horizontal axis. From the B-scan, the depth of the reflector and its approximate linear dimensions in the scan direction can be determined. The C-scan presentation provides a plan-type view of the location and size of test specimen features. The plane of the image is parallel to the scan pattern of the transducer. The C-scan presentation provides an image of the features that reflect and scatter the sound within and on the surfaces of the test piece.

From the Figure 4.7, it can be observed from the C-scan presentation, the green and yellow patches represent the defects as delaminations in the laminate. From the Figures 4.8 - 4.11, the B-scan presentations are a profile (cross-sectional) view of the test

specimen. The different colours show the variation in the thickness at different positions in x- and y-axis respectively. Care is exercised to discard the areas where defects are present by cutting the laminate using water-cooled rotary-type diamond cutter. The portions which are intact are only used for modal testing of composite beams as discussed in section 4.4.

#### 4.4 Water-cooled rotary-type diamond cutter

After the autoclave cure process and laser ultrasonic inspection, NCT-301 graphite/epoxy composite laminate is cut to the required size by using water-cooled rotary-type diamond cutter shown in Figure 4.12. The laminate is cut in to five specimens of beams of  $([0/90]_9)_s$  laminate configuration with the geometric specification given in Table 4.1. All the test specimens are finished by abrading the edges on a fine carborundum paper.

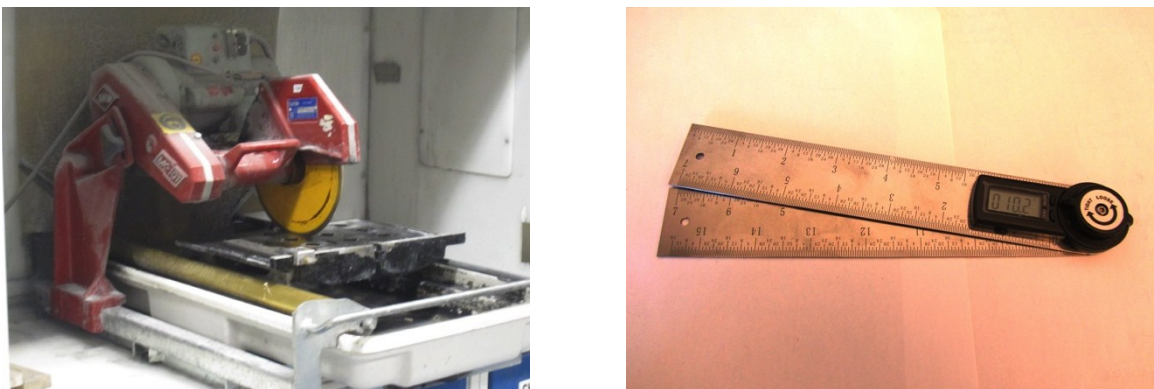


**Figure 4.12** Pictorial representation of water cooled-rotary type diamond cutter and digital protractor

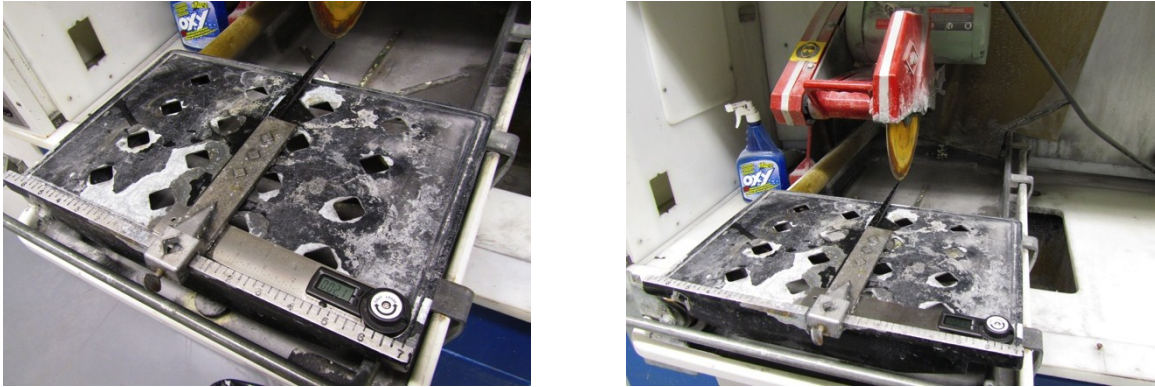


**Figure 4.13** Pictorial representation of composite beam fixture table and cutting position

The taper profiles of the composite beams are cut using the digital protractor shown in the Figure 4.12. The composite beams are clamped on the fixture table with desired taper angle measured using the digital protractor as shown in the Figure 4.13. The composite beam is cut using the cutter manually following all the safety measures.

As water-cooled rotary-type diamond cutting is a hand operation, the quality of the cut is strongly depends on the skill of the operator. The cost and maintenance of the process is economical. Factors like quality, speed and feed rate of the cutter depend on the quality of the cut specimen. Traditional mechanical cutting methods destroy the structural integrity of such materials. Abrasive water jet trimming has emerged as the preferred method for trimming cured composite laminates. The advantages of abrasive water jet cutting are that consistent delamination-free edges are produced and the tooling requirements are simpler because the cutting path is numeric controlled. However to process using abrasive water jet, large expensive numeric controlled machine tools are required [78].

## 4.5 Experimental modal analysis

Most practical noise and vibration problems are related to resonance phenomena, where the operational forces excite one or more of the modes of vibration. Modes of vibration which lie within the frequency range of the operational dynamic forces represent potential problems.

An important property of modes is that any free or forced dynamic response of a structure can be reduced to a discrete set of modes.

The standard modal parameters are:

- Modal frequency
- Modal damping and
- Mode shape

The modal parameters of all the modes, within the frequency range of interest, constitute a complete dynamic description of the structure. Hence the modes of vibration represent the inherent dynamic properties of a free structure (a structure on which there are no forces acting). In this thesis the modal parameters such as modal frequency and modal damping are determined. The mode shapes are not found out due to non-availability of post-processing software.

Through an impact hammer experimental test, determined are the FRF's (Frequency Response Functions) which relate to the response given by the specimen when loaded

with a signal, allowing for determination of the natural frequencies and damping factors, as shown in the Figure 4.14 as block diagram of experimental testing. This was done by fixing the beam specimen in a rigid support with one of its sides free to vibrate, as a cantilever beam. The impact hammer is used to give the input load (pulse) to the specimen, and the signal analyzer is set from 0 Hz to 1600 Hz. This output was captured by the accelerometer and together with input signal were amplified using Bruel and Kjaer's (B&K) 4-channel portable PULSE™ 3560 multi-analyzer system giving the FRF known as accelerance that is given by acceleration/force.

The dynamic behavior of the composite beams can be viewed as a set of individual modes of vibration, each having a characteristic natural frequency, damping and mode shape. The modal parameters are determined from a set of frequency response measurements between a reference point and a number of measurement points. The modal frequencies and damping can be found from all frequency response measurements on the beams (except those for which the excitation or response measurement is in a nodal position, that is, where the displacement is zero). The experimental results were used to validate the analytical results obtained using Rayleigh-Ritz method as shown in Chapter 03.

In the experimental work, the composite beam specimens shown in the Figure 4.15 are prepared from the NCT-301 graphite/epoxy beams of laminate configuration  $([0/90]_9)_s$  and geometric configurations given in the Table 4.1. The composite beam is mounted on a corner of a big rigid table with vice/fixture providing sufficient clamp force at the root of the beam to simulate fixed end, similar to cantilevered boundary condition

as shown in Figure 4.23. The beam is excited by the impact hammer and provides signal to the amplifier. Response accelerometer is attached at the free end of the beam with bees' wax glue and provides response to the amplifier. Dual mode amplifier is used to amplify the signals from the transducers (hammer and response) and they are supplied to the 4-channel portable PULSE™ 3560 multi-analyzer system. It is determined that the beam specimen is divided in equal lengths into four points where the roving hammer is excited at these points marked on the beam specimen as shown in Figure 4.23. The point of excitation is made such that it does not coincide with nodal point.

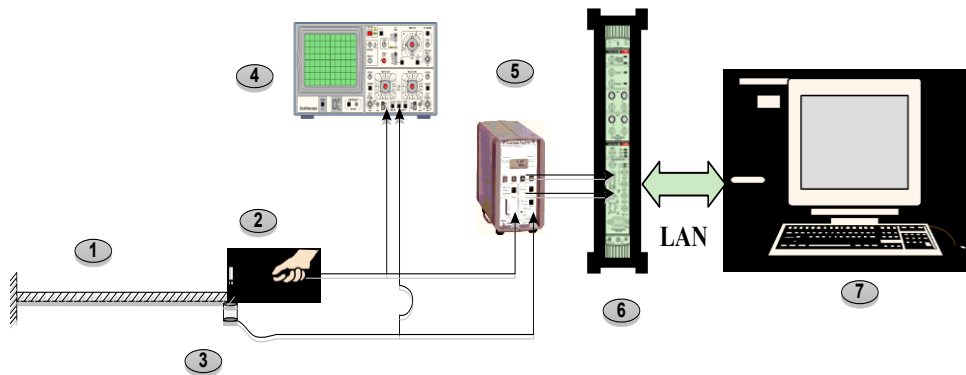


**Figure 4.14** Block diagram of experimental modal analysis instrumentation

From the Figure 4.14, 1 represents: Fixed-free (cantilever) composite beam, 2: Impact hammer with transducer at the tip, 3: Response transducer (accelerometer), 4: Oscilloscope, 5: Dual mode charge amplifier, 6: 4-channel Portable PULSE, 3560 multi-analyzer system, 7: Personal computer.

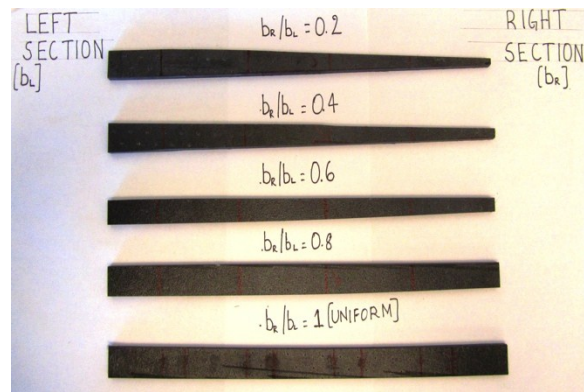


**Figure 4.15** Photographs of NCT-301 graphite/epoxy composite beam specimens

**Table 4.1** Specifications of width-tapered composite beams

| Specimen | Length, L<br>(m) | Width, (m) |       | Width<br>ratio | Height, H<br>(m) | Mass, m<br>(g) |
|----------|------------------|------------|-------|----------------|------------------|----------------|
|          |                  | $b_L$      | $b_R$ | $b_R/b_L$      |                  |                |
| 1        | 0.25             | 0.015      | 0.003 | 0.2            | 0.0045           | 26.87          |
| 2        | 0.25             | 0.016      | 0.006 | 0.4            | 0.0045           | 27.03          |
| 3        | 0.25             | 0.016      | 0.009 | 0.6            | 0.0045           | 27.66          |
| 4        | 0.25             | 0.015      | 0.012 | 0.8            | 0.0045           | 37.46          |
| 5        | 0.25             | 0.016      | 0.016 | 1              | 0.0045           | 38.36          |

## **4.5.1 Measurement equipments and apparatus**

The experimental set-up used for mobility measurement is explained below. There are three major items: (i) Excitation mechanism, (ii) Transducer system and (iii) An analyzer, to extract the desired information.

### **4.5.1.1 Test fixture**

The test fixture consists of a rigid mounting support which provides a clamp for the root of the beam.

### **4.5.1.2 Signal analyzer**

PULSE<sup>TM</sup>, the multi-analyzer system type 3560, is used as a data acquisition front-end hardware as shown in Figure 4.16. The Pulse analyzer is connected to the computer for real-time signal processing. An oscilloscope of type 54624 A from Agilent technologies shown in Figure 4.17, is used to monitor the quality of the signals from impact hammer and accelerometer.



**Figure 4.16** Photograph of B & K's PULSE™ front-end multi-analyzer type 3560



**Figure 4.17** Photograph of typical oscilloscope

### 4.5.1.3 Charge amplifiers

The role of the amplifier is to strengthen the signals generated by the transducers so that they can be fed to the analyzer for measurement. The charge amplifiers used in this experiment are Kistler's three channels - Dual mode amplifier type-5804 A and Intertechnology's PCB 482A 04 piezoelectric amplifier as shown in Figures 4.18 and 4.19 respectively. These amplifiers are used for conditioning of signals from piezoelectric

transducers, such as charge accelerometer, and impact hammer to Pulse multi-analyzer system.



**Figure 4.18** Photograph of typical Dual mode amplifier



**Figure 4.19** Photograph of piezoelectric charge amplifier

#### 4.5.1.4 Impact hammer

The specification of the impact hammer used in the experiment is as shown in the Figure 4.20. Impact force: 0 to 222.5N, sensitivity: ( $\pm 20\%$ ) (22.5 mV/N), measurement range: 222 N pk, hammer mass: 4.8 g.

The hammer consists of an integral integrated circuit piezoelectric quartz force sensor mounted on the striking end of the hammer head. The sensing element functions to transfer impact force into electrical signal for display and analysis. The hammer is connected to PCB 482A 04 piezoelectric amplifier to amplify the piezoelectric signals to Pulse multi-analyzer system.



**Figure 4.20** Photograph of typical impact hammer

#### 4.5.1.5 Accelerometer

For response measurement, the transducer used in the experiment is type 4381-piezoelectric accelerometer as shown in Figure 4.21. When the response transducer is chosen, the structural loading caused by mounting the transducer must be taken into consideration. Loading the structure may alter the modal parameters. The mass loading effect should be minimal [69]. The accelerometer is mounted to the beam specimen by applying a thin layer of beeswax. The specifications of the accelerometer used in the experiment are: Frequency: 0.1 - 4800 Hz, temperature: -74 - 250 °C (-101.2 - 482.0 °F), Weight: 43 grams, Sensitivity: 100 pC/g, Maximum Operational Level (peak): 2000 g.

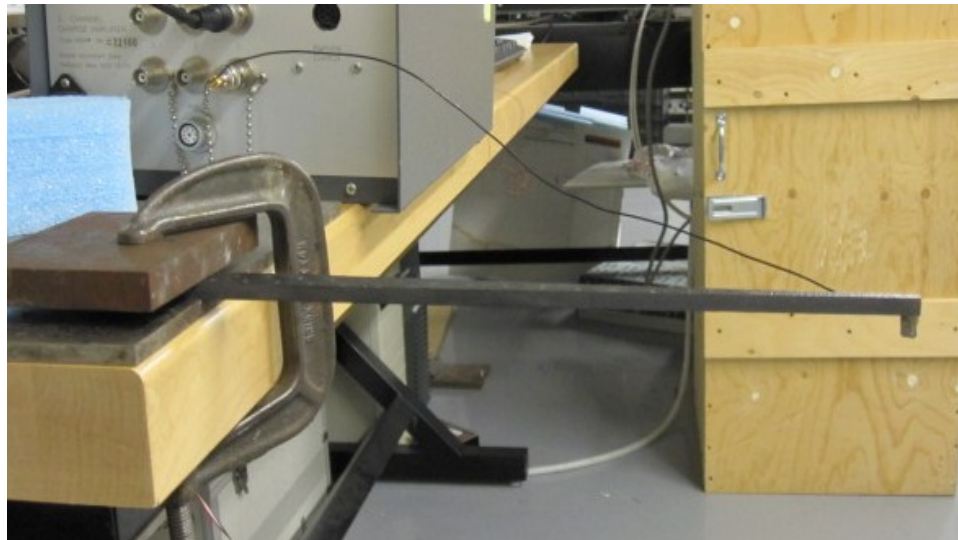


**Figure 4.21** Photograph of typical response transducer mounted below width-tapered beam

#### 4.5.2 Impact excitation

For mobility measurements the structure must be excited by a measured dynamic force. The waveform produced by an impact is a transient (short duration) energy transfer event. The spectrum is continuous, with a maximum amplitude at 0 Hz and decaying amplitude with increasing frequency.

The duration, and thus the shape of the spectrum, of an impact are determined by the mass and stiffness of both the impact and the structure. Advantages of hammer testing are that they are fast as only few averages of impact measurements are required, no elaborate fixtures are required, there is no variable mass loading of the structure, and it is portable and relatively inexpensive.



**Figure 4.22** Photograph of experimental modal analysis test set-up

### 4.5.3 Impact testing requirements

Even though impact testing is fast and convenient, there are several important considerations that must be taken into account in order to obtain accurate results. They include:

*Pre-Trigger delay:* Because the impulse signal exists for such a short period of time, it is important to capture all of it in the sampling window of FFT analyzer. To ensure that the entire signal is captured, the analyzer must be able to capture the impulse and impulse response signals prior to the occurrence of the impulse.

*Force and exponential windows:* The force window is used to remove noise from the impulse (force) signal. The force window preserves the samples in the vicinity of the impulse, and removes the noise from all of the other samples in the force signal by making them zero. The exponential window is used to reduce leakage in the spectrum of the response.

*Accept/reject capability:* Since accurate impact testing results depend on the skill of one doing the impacting, FRF measurements should be made with spectrum averaging. In this experiments, 10-sampling size is selected for the accurate measurements. If in case one or two of the impacts during the measurement process may be bad hits, an FFT analyzer designed for impact testing will have the ability to accept or reject the result of each impact.

#### 4.5.4 Response transducer calibration

Most commercial transducers are supplied with calibration certificates, but a calibration test before every mobility measurement is strongly recommended [57]:

- To check the integrity of the transducers, to detect any errors in the cables, connectors, conditioning and analyzers, to check that all gain, polarity and attenuator settings in the system are correct.
- To check the pair of transducers being used, are matched in the frequency band of interest.
- To calibrate the entire system is to measure the mobility of the structure. Generally the known mass is used as reference.

From Newton's second law:

Force = mass × acceleration

Therefore, Accelerance is given as:

$$A(\omega) = \frac{\textit{acceleration}}{\textit{force}} = \frac{1}{\textit{mass}} \quad (4.1)$$

A known mass suspended so that it moves in only one direction, with an accelerometer attached to detect the motion, can be used for hammer techniques. This gives a ratio calibration, ensuring correct mobility measurements, rather than an absolute calibration of the individual transducers. For this purpose, even a hand-held mass is

adequate. If the calibration mass is considered to be absolutely rigid, in the frequency range of interest, the force and acceleration waveforms are equal.

#### **4.6 Modal testing for damping factor**

Damping characteristics in composite materials is an important factor of the dynamic behavior of structures, controlling the resonant and near resonant vibrations and thus prolonging the structure service life under fatigue and impact loading. Generally composite materials have more damping capacity than metals. Damping in vibrating composite structures refers to a complex physical dynamic nature including from both constituent level (visco-elastic behavior of matrix, damping at fiber-matrix interface) and laminate level (layer orientation, inter-laminar effects, stacking sequence, etc) [65].

It is difficult to determine accurately the damping parameters by an analytical approach. The experimental method is very desirable.

##### **4.6.1 Damping loss factor**

The methodology of calculating damping loss factor using half-power bandwidth technique is explained in detail in the Ref. [65].

From the experimental modal testing , the extracted values of damping loss factor ( $\eta$ ), damping ratio ( $\xi$ ), mass proportional damping constant ( $\alpha$ ) and stiffness

proportional damping constant ( $\beta$ ) from three specimens are obtained using half-power bandwidth technique [65] which are presented in the Table 4.2.

**Table 4.2** Damping loss factor measurements

|                           | $\eta_1$ | $\xi_1$ | $\eta_2$ | $\xi_2$ | $\alpha$ | $\beta$                |
|---------------------------|----------|---------|----------|---------|----------|------------------------|
| Specimen-1 (Uniform beam) |          |         |          |         |          |                        |
| Exci-1                    | 0.0378   | 0.0189  | 0.0220   | 0.0110  | 2.611    | $3.44 \times 10^{-05}$ |
| Exci-2                    | 0.0094   | 0.0047  | 0.0185   | 0.0093  | 0.497    | $3.59 \times 10^{-05}$ |
| Exci-3                    | 0.0200   | 0.0100  | 0.0160   | 0.0080  | 1.343    | $2.73 \times 10^{-05}$ |
| Specimen-2 (Uniform beam) |          |         |          |         |          |                        |
| Exci-1                    | 0.0412   | 0.0206  | 0.0152   | 0.0076  | 3.082    | $1.86 \times 10^{-05}$ |
| Exci-2                    | 0.0420   | 0.0212  | 0.0131   | 0.0065  | 3.208    | $1.31 \times 10^{-05}$ |
| Exci-3                    | 0.0414   | 0.0207  | 0.0207   | 0.0103  | 2.835    | $3.06 \times 10^{-05}$ |
| Specimen-3 (Uniform beam) |          |         |          |         |          |                        |
| Exci-1                    | 0.0318   | 0.0159  | 0.0170   | 0.0085  | 2.162    | $2.65 \times 10^{-05}$ |
| Exci-2                    | 0.0345   | 0.0172  | 0.0166   | 0.0083  | 2.361    | $2.44 \times 10^{-05}$ |
| Exci-3                    | 0.0193   | 0.0097  | 0.0103   | 0.0052  | 1.203    | $3.77 \times 10^{-05}$ |

In the Table 4.2, Exci-1 stands for first excitation and so on. The calculated damping properties are used to calculate average proportional mass and stiffness constants to form a Rayleigh's damping matrix  $[C]$  as a linear combination of mass and stiffness matrices for free and forced vibrations determined using Rayleigh-Ritz method

#### 4.7 Experimental modal analysis results

This section presents the results from experimental investigation, where impact testing at different excitation points as shown in Figure 4.23 with cantilevered boundary condition was carried out. The output data from the modal testing namely coherence function, time and auto spectrum for hammer impact and transducer response and Frequency Response Functions are presented.

The experimental modal analysis test was carried out at Concordia Centre for Composites (CONCOM) testing laboratory. The measured modal parameters are served as a reference for further comparison with solution obtained from Rayleigh-Ritz method.

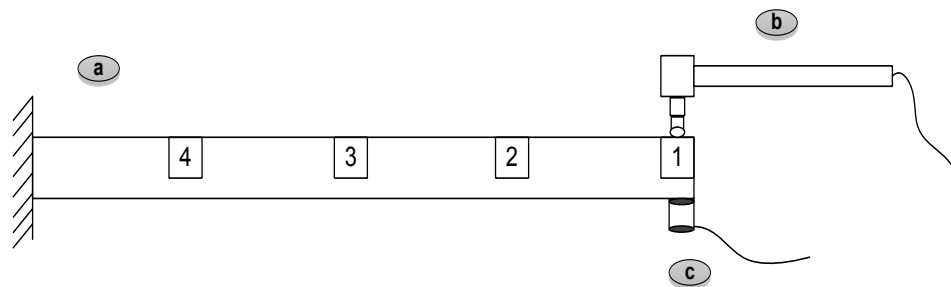


**Figure 4.23** Schematic illustrations of composite beam with excitation points

From the Figure 4.23-a) Fixed-free (cantilever) composite beam, b) Impact hammer with transducer at the tip, c) Response transducer (accelerometer).

#### **4.7.1 Coherence function at different excitation points for width-tapered composite beam**

The coherence function provides a means for assessing the degree of linearity between the input and output signals. The coherence function is defined as follows [72]:

$$\gamma(\omega)^2 \equiv \frac{|G_{XF}(\omega)|^2}{G_{XX}(\omega) \cdot G_{FF}(\omega)}, 0 \leq \gamma(\omega)^2 \leq 1 \quad (4.2)$$

where  $G_{XF}$  is the cross-spectrum between the force and response and  $G_{XX}$  and  $G_{FF}$  are the autospectra of the response and force respectively. In experimental modal testing, the coherence function at each excitation point is obtained with the help of PULSE software rather than by the direct use of Equation (4.2) given above.

The bounds for coherence function are 1, for no noise in the measurements, and 0 for pure noise in the measurements. The interpretation of coherence function is that for each frequency  $\omega$  it shows the degree of linear relationship between the measured input and output signals. The coherence function is used to detect possible errors, during mobility measurements.

By using the impact excitation technique described in the Section 4.5.2, test specimens of NCT-301 graphite/epoxy beam with laminate configuration  $([0/90]_9)_s$  and geometric specification given in Table 4.1 are used to find the coherence function for different width ratio ( $b_R/b_L$ ) values for fixed-free (cantilever) boundary condition of width--tapered composite beam at four excitation points as shown in Figure 4.23.

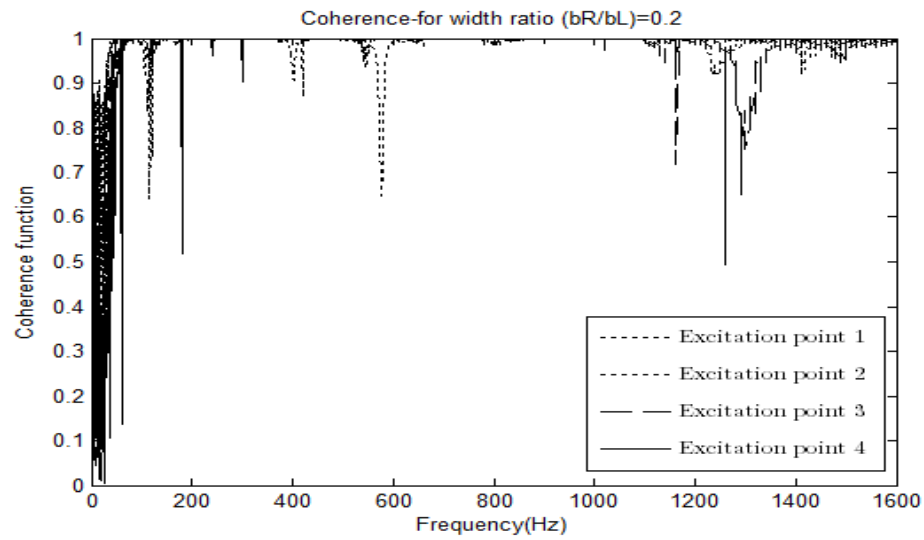


**Figure 4.24** Coherence function for width ratio ( $b_R/b_L$ ) of 0.2 at four excitation points

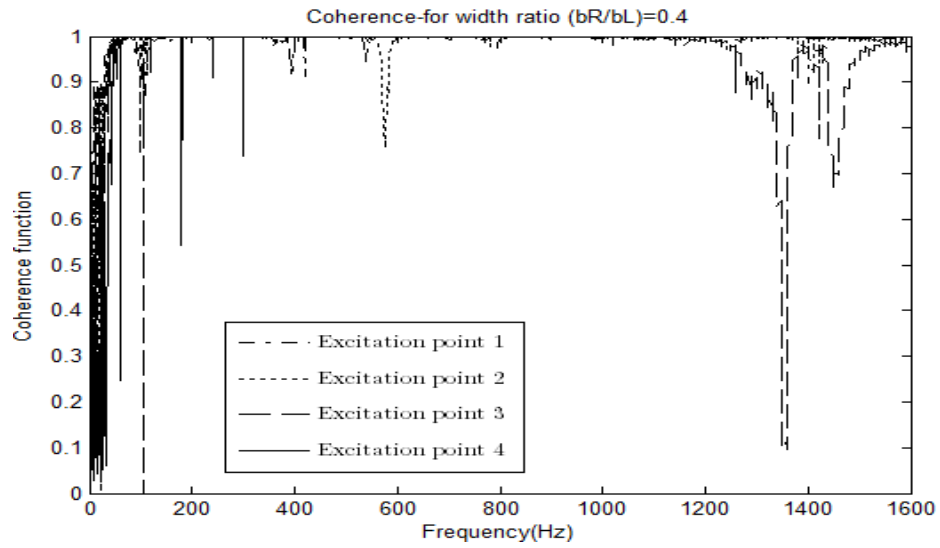


**Figure 4.25** Coherence function for width ratio ( $b_R/b_L$ ) of 0.4 at four excitation points

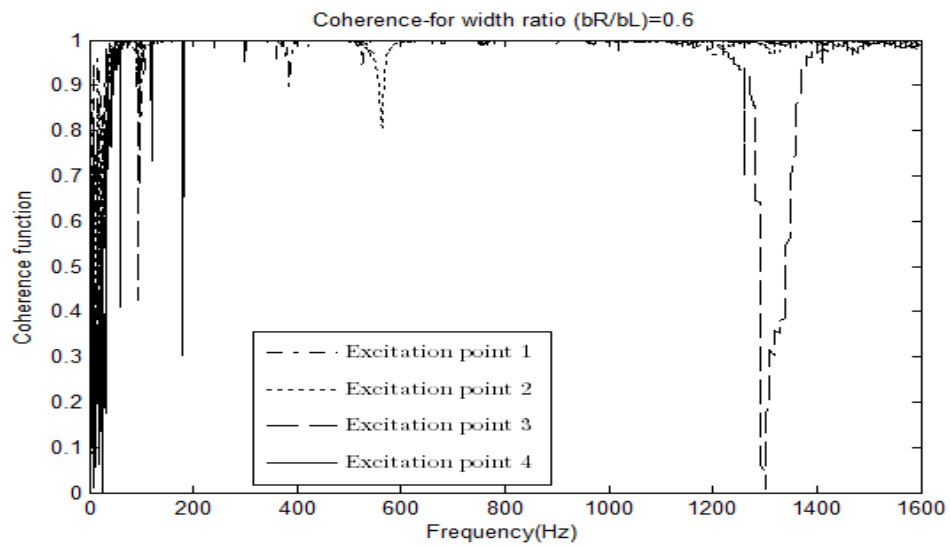


**Figure 4.26** Coherence function for width ratio ( $b_R/b_L$ ) of 0.6 at four excitation points

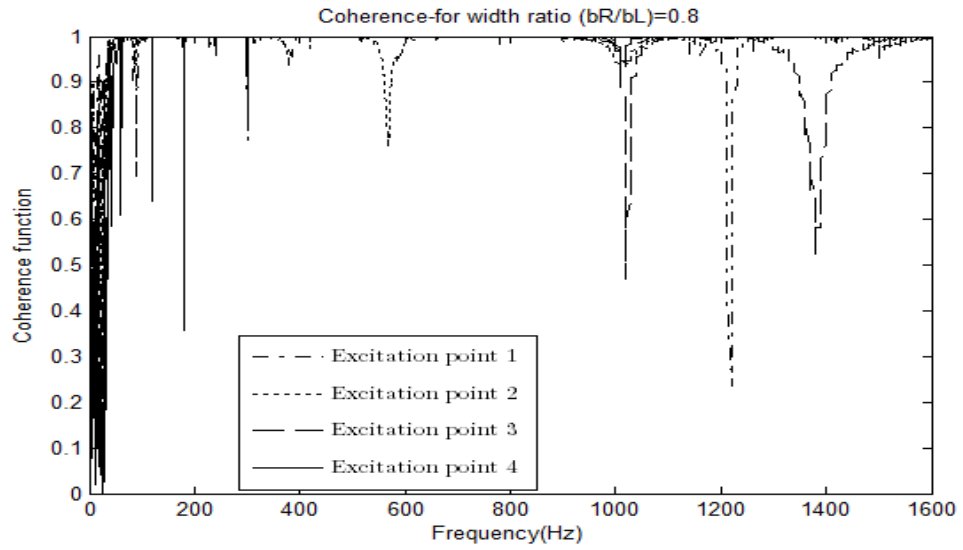


Figure 4.27 Coherence function for width ratio ( $b_R/b_L$ ) of 0.8 at four excitation points

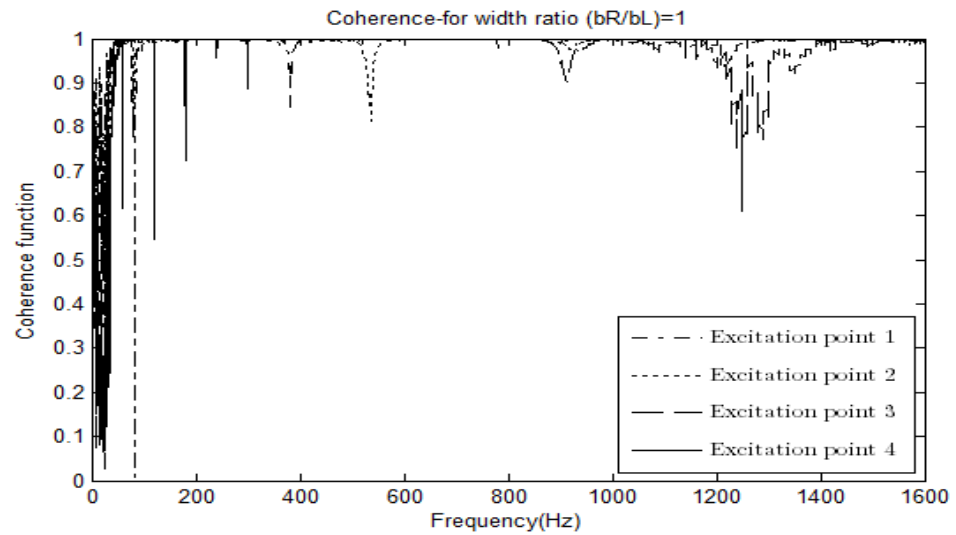


Figure 4.28 Coherence function for width ratio ( $b_R/b_L$ ) of 1 at four excitation points

Figures 4.24-4.28 show the coherence functions obtained through impact testing for fixed-free (cantilever) boundary condition for width--tapered composite beam at four excitation points. One can observe from the Figures 4.24 - 4.28 that for all width ratio ( $b_R/b_L$ ) values of the beams, the coherence function is poor at the initial frequency values. This is because of initial disturbance during impact excitation. By using the force windowing technique these signal values are tailored for good input signal values for FRF calculations. Another observation made is that at excitation point 3 for width ratio ( $b_R/b_L$ ) values of 0.4 and 0.6, the coherence values are less than 0.5. This is because the excitation point is close to a node point, coherence may be extremely low. This is acceptable however, since the modal strength at this point is weak and not important for the analysis [69].

#### **4.7.2 Time response and autospectrum response at different excitation points for width-tapered composite beam**

An autospectrum is calculated by multiplying a spectrum by its complex conjugate (opposite phase sign), and by averaging a number of independent products. When the complex conjugate of one spectrum is multiplied by a different spectrum we obtain the cross-spectrum. The cross-spectrum is complex, showing the phase shift between the output and input, and a magnitude representing the coherent product of power in the input and output.

The duration of an impact is usually very short compared to the record length. The window used is the transient window, this takes the data unweighted during the period of contact, and sets it to zero for the remaining record. If we observe the time history of the impact force, negative signals can be observed. In a physical sense this is prohibited, but since we are measuring the force within a limited frequency range (truncation), this short ringing is a correct representation in the particular frequency range (leakage) [70]. The length of the force window must be chosen such that the entire signal is included. The response to an impact is a free decay of all the modes of vibration. The exponential window is used when there is a leakage error or poor signal-to-noise ratio in the measured data. In the case of leakage error, the response is forced to decay completely within the record so that leakage due to truncation is avoided. For poor signal-to-noise ratio, the noise is attenuated by the window [70].

By using the impact excitation technique described in the Section 4.5.2, test specimens of NCT-301 graphite/epoxy beam with laminate configuration  $([0/90]_9)_s$  and geometric specification given in Table 4.1 are used to find the time response and FRF autospectra for input 1 and input 2, which are for impact hammer transducer and response accelerometer respectively for different width ratio  $(b_R/b_L)$  values of width-tapered composite beam at four excitation points as shown in Figure 4.23.

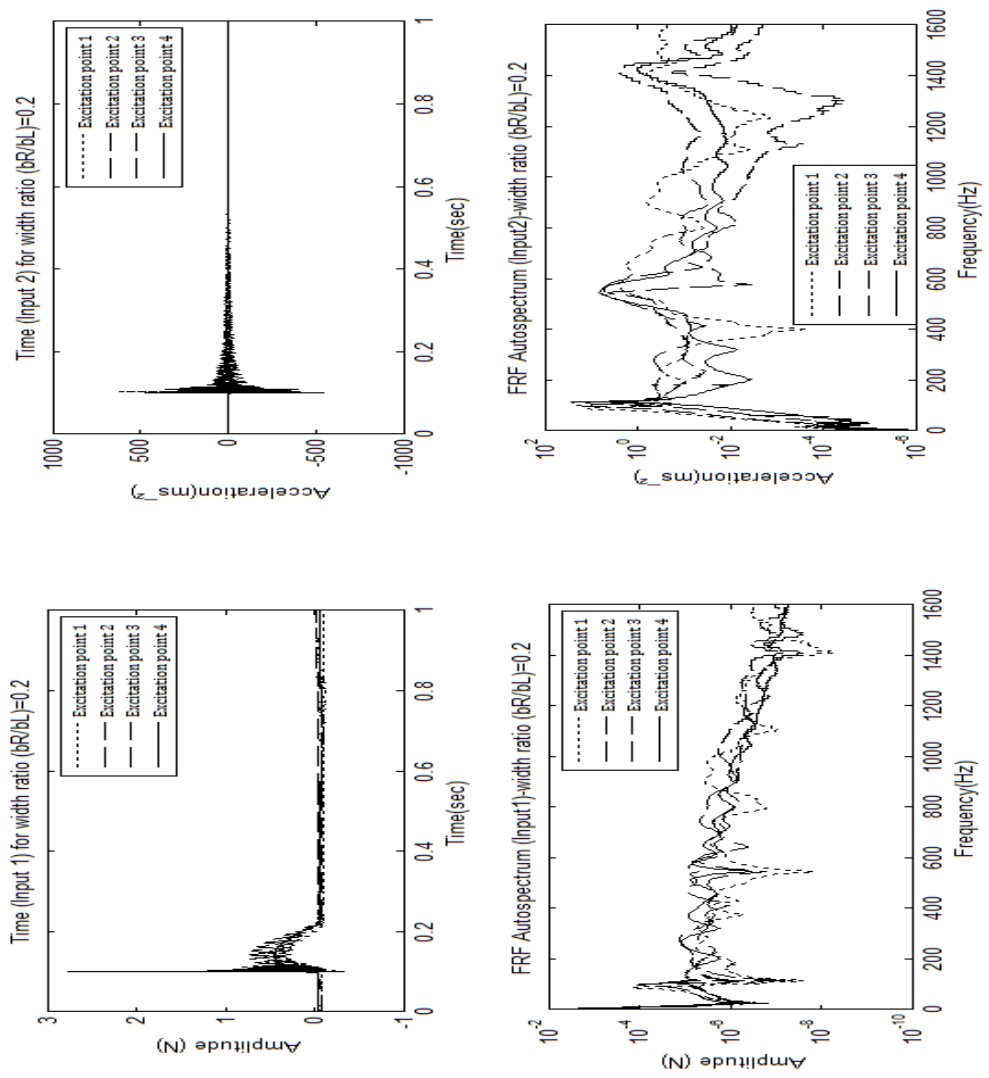


**Figure 4.29** Time response and autospectrum response for width ratio  $(b_R/b_L)$  of 0.2 at four excitation points

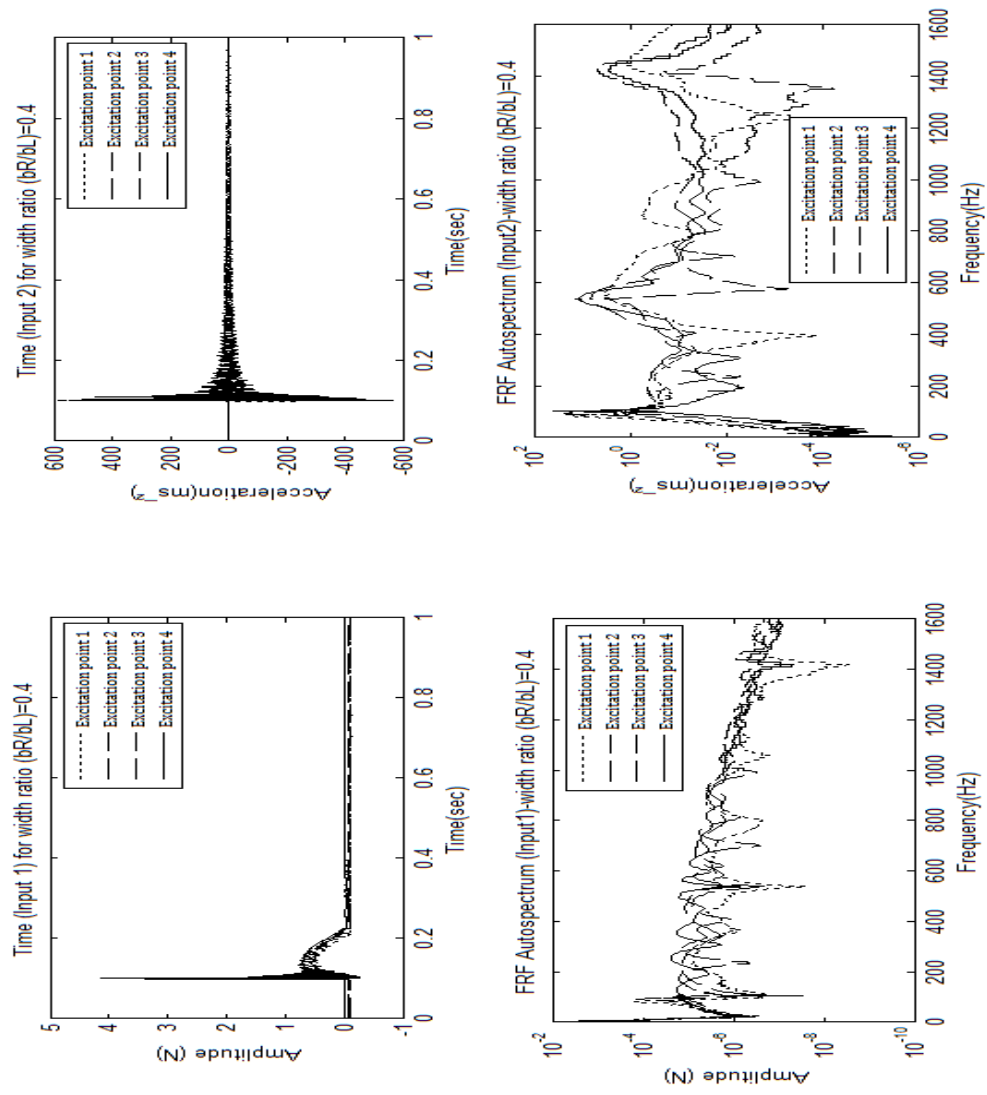


**Figure 4.30** Time response and autospectrum response for width ratio  $(b_R/b_L)$  of 0.4 at four excitation points

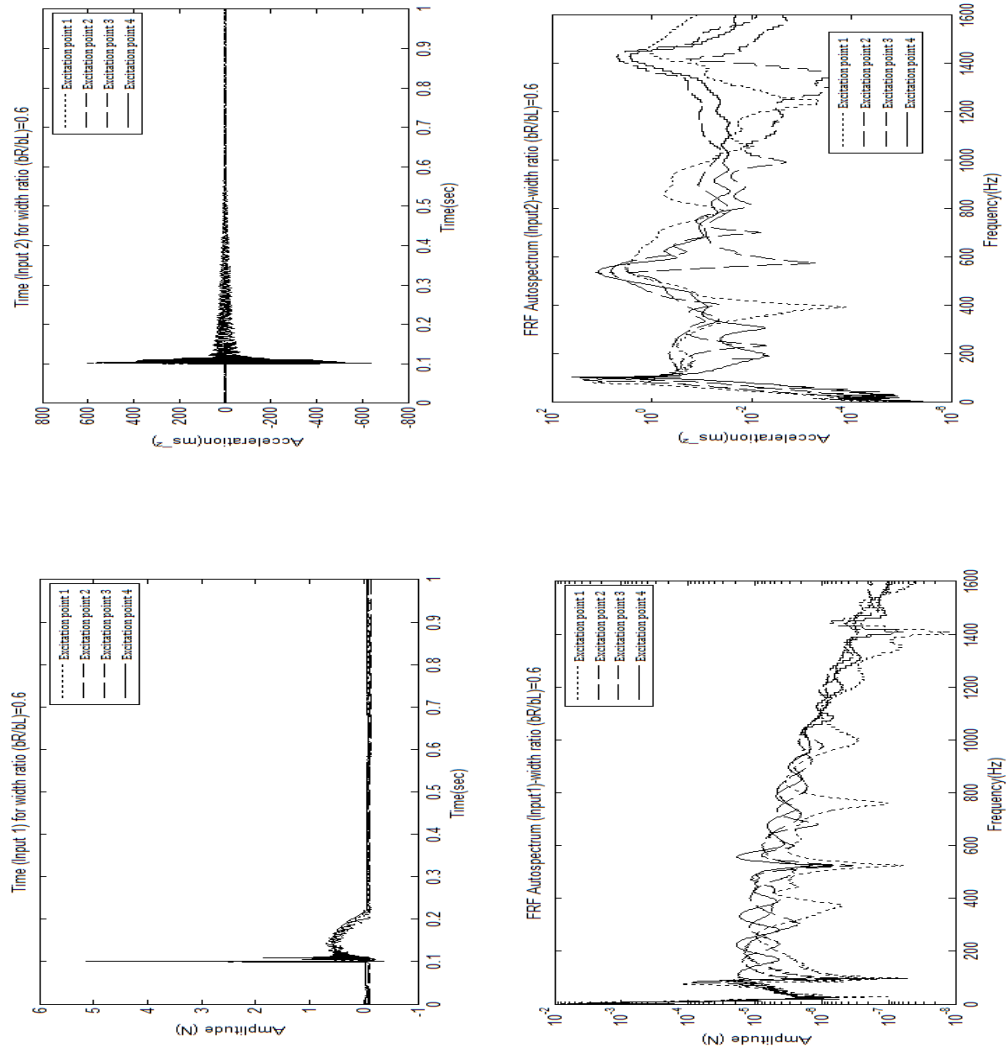


**Figure 4.31** Time response and autospectrum response for width ratio  $(b_R/b_L)$  of 0.6 at four excitation points

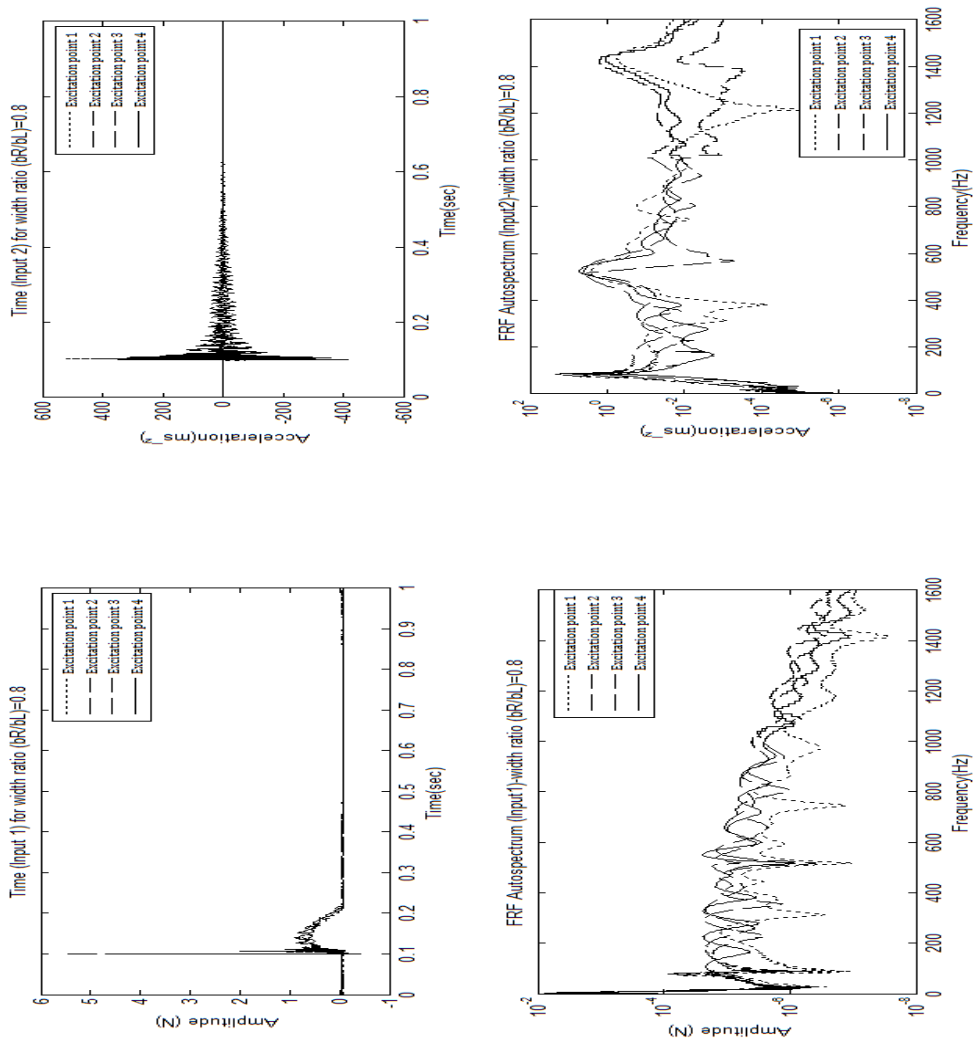


**Figure 4.32** Time response and autospectrum response for width ratio  $(b_R/b_L)$  of 0.8 at four excitation points

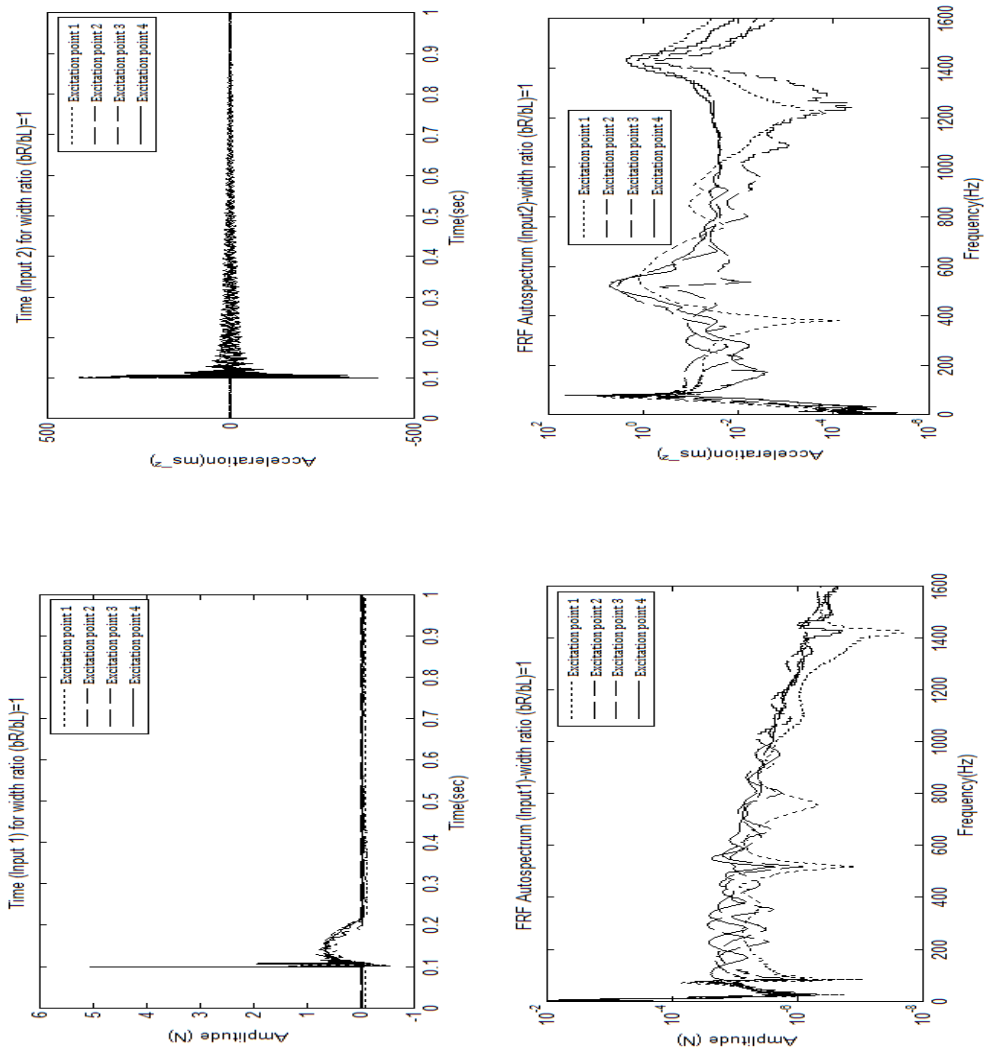


**Figure 4.33** Time response and autospectrum response for width ratio ( $b_R/b_L$ ) of 1 at four excitation points

Figures 4.29 - 4.33 show the time response and autospectrum obtained by impact testing for different width ratio ( $b_R/b_L$ ) values for fixed-free (cantilever) boundary condition of width-tapered composite beam at four excitation points. It is observed from the Figures 4.29 - 4.33 that for all width ratio ( $b_R/b_L$ ) values of the beams, the impulse force is highest at excitation point 4 since the stiffness of the beam is higher at this point. The time response and autospectra of inputs 1 and 2 are for impact hammer transducer and response accelerometer respectively. In the time and auospectrum response of Figures 4.29-4.33, it is important to ensure that the data captured during the excitation is free from unacceptable sources of error like double hit of the impact hammer, capture of noise in the output signal due to instrumentation and environmental vibrations, etc. The data captured as observed from Figures 4.29-4.33 are satisfactory [69].

### **4.7.3 Frequency Response Function (FRF- $H_1$ ) at different excitation points for width-tapered composite beam**

One very efficient model of a linear system is a frequency domain model, where the output spectrum is expressed as the input spectrum weighted by a system descriptor,

$$X(\omega) = H(\omega).F(\omega) \quad (4.3)$$

This system descriptor  $H(\omega)$  is called the Frequency Response Function (FRF), defined as:

$$H(\omega) = \frac{X(\omega)}{F(\omega)} \quad (4.4)$$

The physical interpretation of the FRF is that a sinusoidal input force, at a frequency, will produce a sinusoidal output motion at the same frequency. The basis for one specific class of experimental modal analysis is the measurement of a set of frequency response functions. The mobility measurement used here to describe the FRF is ‘accelerance’, where the motion is described in terms of acceleration/force. For impact excitation and pseudo-random excitation,  $H_1$  and  $H_2$  will generally be equal at resonances.  $H_1$  is preferred since it is the best estimator at antiresonances [69].

By using the impact excitation technique described in the Section 4.5.2, test specimens of NCT-301 graphite/epoxy beam with laminate configuration  $([0/90]_9)_s$  and geometric specification given in Table 4.1 are used in the current section to find the Frequency Response Function (FRF- $H_1$ ) which is computed as the ratio of the cross spectrum to the input autospectrum for different width ratio ( $b_R/b_L$ ) values for fixed-free (cantilever) boundary condition of width-tapered composite beam at four excitation points.

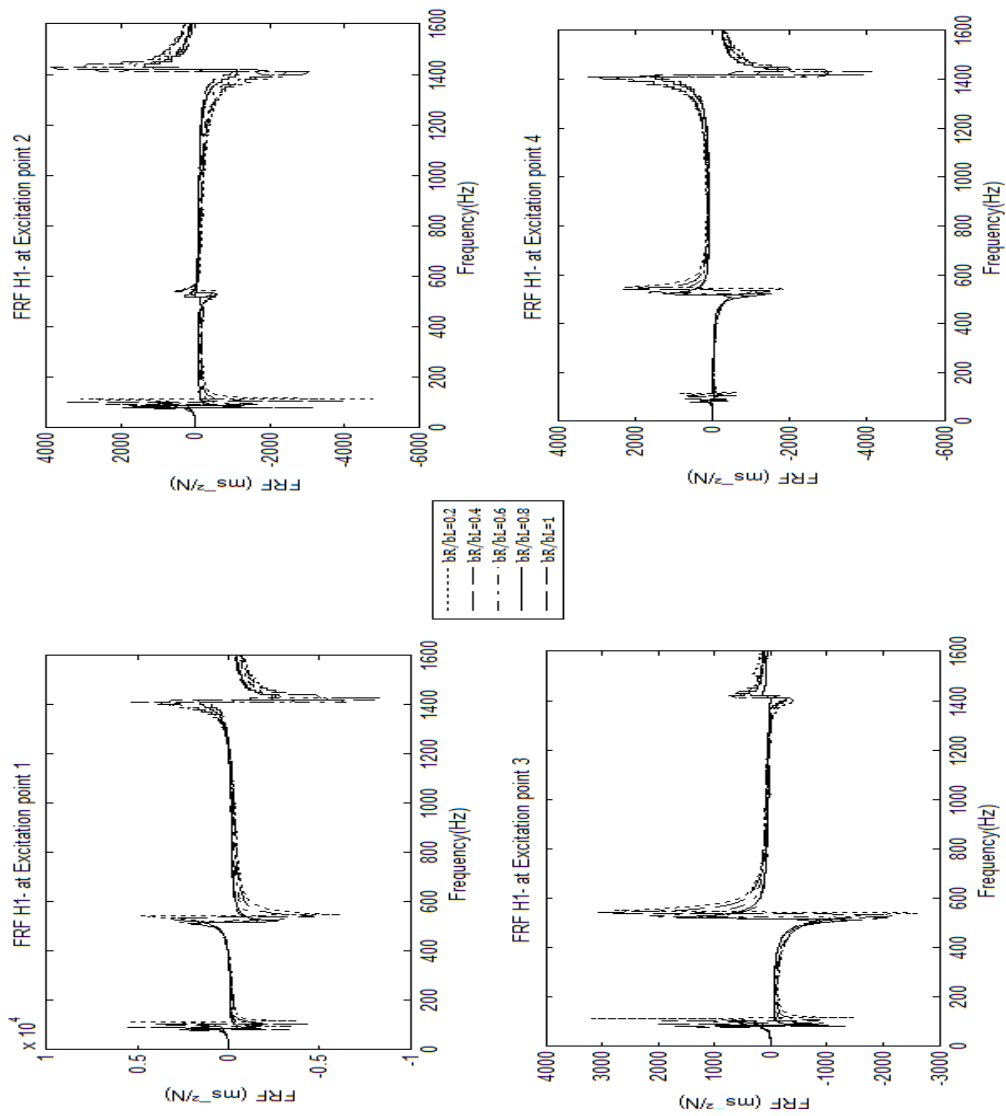


**Figure 4.34** FRF  $-H_1$  at four excitation points for width ratio ( $b_R/b_L$ ) values of 0.2, 0.4, 0.6, 0.8 and 1

Figures 4.34 show the Frequency Response Function (FRF- $H_1$ ) obtained by impact testing for different width ratio ( $b_R/b_L$ ) values for fixed-free (cantilever) boundary

condition of width-tapered composite beam at four excitation points. Figure 4.34 shows the FRF which is measured for first three natural frequencies (Hz) with amplitude measured as accelerance ( $\text{ms}^{-2}/\text{N}$ ) for individual excitation points. It is observed that the natural frequencies are highest for width ratio ( $b_R/b_L$ ) of 0.2 and gradually decreases as width ratio ( $b_R/b_L$ ) values increases for fixed-free (cantilever) boundary condition. This is because the stiffness of the beam is highest for width ratio ( $b_R/b_L$ ) of 0.2. Another observation that can be made is that at excitation point 1, the amplitude at first mode is highest whereas lowest at mode three. But in the case at excitation point 4, the amplitude at third mode is highest whereas it is lowest at first mode. This is because the beam at excitation point 1, it is more flexible at the free end of the beam.

#### **4.7.4 Comparison of natural frequencies between experimental modal testing and Rayleigh-Ritz method for width-tapered composite beam**

The analytical and the experimental modal analysis results for linear width-tapered beam with different width ratio ( $b_R/b_L$ ) values, for fixed-free (cantilever) boundary condition, are compared in the current section for validation purpose.

By using the impact excitation technique described in the Section 4.5.2, test specimens of NCT-301 graphite/epoxy beam with laminate configuration  $([0/90]_9)_s$  and geometric specification given in Table 4.1 are used in the current section to find the % difference for three natural frequencies between the experimental modal testing and

Rayleigh-Ritz method, for different width ratio ( $b_R/b_L$ ) values of width-tapered composite beam at four excitation points as shown in Figure 4.23.

**Table 4.3** Comparison of natural frequencies for width-tapered composite beams at four excitation points

| width ratio ( $b_R/b_L$ )           | 0.2   | 0.4   | 0.6  | 0.8   | 1     |
|-------------------------------------|-------|-------|------|-------|-------|
| $\omega_1$ (R-R), Hz                | 110   | 99.4  | 90.1 | 83.4  | 77.8  |
| $\omega_1$ (Excitation point 1), Hz | 114   | 103   | 93   | 86    | 80    |
| % difference                        | 3.6   | 3.6   | 3.2  | 3.1   | 2.8   |
| $\omega_1$ (Excitation point 2), Hz | 114   | 104   | 93   | 86    | 80    |
| % difference                        | 3.5   | 3.5   | 3.3  | 3.3   | 3.2   |
| $\omega_1$ (Excitation point 3), Hz | 114   | 103   | 93   | 86    | 80    |
| % difference                        | 3.6   | 3.5   | 3.3  | 3.2   | 3.1   |
| $\omega_1$ (Excitation point 4), Hz | 114   | 104   | 93   | 86    | 80    |
| % difference                        | 3.6   | 3.5   | 3.4  | 3.3   | 3.3   |
| $\omega_2$ (R-R), Hz                | 525.5 | 512.5 | 500  | 492.5 | 488.5 |
| $\omega_2$ (Excitation point 1), Hz | 543   | 532   | 520  | 513   | 506   |
| % difference                        | 3.3   | 3.8   | 4    | 4.2   | 3.6   |
| $\omega_2$ (Excitation point 2), Hz | 550   | 541   | 528  | 522   | 522   |

|                                     |      |      |      |      |      |
|-------------------------------------|------|------|------|------|------|
| % difference                        | 4.2  | 3.8  | 4    | 4.5  | 3.5  |
| $\omega_2$ (Excitation point 3), Hz | 550  | 543  | 529  | 523  | 523  |
| % difference                        | 4.2  | 3.9  | 4.4  | 4.4  | 3.8  |
| $\omega_2$ (Excitation point 4), Hz | 550  | 541  | 528  | 522  | 523  |
| % difference                        | 4.2  | 3.9  | 4.4  | 4.3  | 3.8  |
| $\omega_3$ (R-R), Hz                | 1346 | 1354 | 1354 | 1356 | 1372 |
| $\omega_3$ (Excitation point 1), Hz | 1400 | 1410 | 1400 | 1400 | 1420 |
| % difference                        | 4    | 4.1  | 3.4  | 3.2  | 3.5  |
| $\omega_3$ (Excitation point 2), Hz | 1420 | 1430 | 1420 | 1430 | 1430 |
| % difference                        | 5.5  | 3    | 3.5  | 3.4  | 3.1  |
| $\omega_3$ (Excitation point 3), Hz | 1420 | 1420 | 1410 | 1430 | 1430 |
| % difference                        | 5.5  | 3.6  | 4.9  | 3.8  | 3.1  |
| $\omega_3$ (Excitation point 4), Hz | 1400 | 1410 | 1400 | 1400 | 1410 |
| % difference                        | 4    | 3.5  | 4.4  | 3.3  | 3.4  |

Table 4.3 shows the comparison of natural frequencies between the results from experimental modal testing and Rayleigh-Ritz method for linear width-tapered composite beam with different width ratio ( $b_R/b_L$ ) values for fixed-free (cantilever) boundary condition. It can be observed from the Table 4.3 that the % difference between the natural frequencies is lowest as for mode 1 and highest for mode 3. The % difference is lowest for width ratio ( $b_R/b_L$ ) value of 1 and increases as the width ratio ( $b_R/b_L$ ) value of decreases until 0.2. The % difference is lowest at excitation point 1 and highest at

excitation point 4 for modes 1 and 3 but for mode 3, the % difference is highest at excitation points 2 and 3 and lowest at excitation points 1 and 4. The results show good agreement between the theoretical predictions and the experimental values of the natural frequencies. The natural frequencies are compared for the effect of width-ratio for different boundary condition in section (3.5) obtained using Rayleigh-Ritz method with that obtained using conventional finite element method [81]. The % difference is less than 1 % and shows good agreement between the two methods.

#### **4.8 Summary**

In this chapter, experimental validation for width-tapered composite beams has been carried out. The manufacturing of composite laminate is discussed with fabrication and processing. The composite laminate manufactured is inspected using laser ultrasonic technique and the results are discussed. The composite laminate is cut with the geometric shape of width-tapered beams using water-cooled rotary-type diamond cutter. Experimental modal analysis is conducted using impact hammer excitation. The measurement equipments and apparatus used are explained. Modal testing for damping factor for finding out the damping in the beams is conducted using half-power bandwidth method [24]. The experimental modal analysis results like Coherence function, time response and auto response function and Frequency Response Function (FRF) of different width ratio values of width-tapered composite beams are shown through graphical plots. Comparison of experimental modal analysis results and theoretical results

for width-tapered composite beams are discussed. From the figures and analyses the following conclusions are drawn:

- The coherence function is obtained through impact testing for different width ratio ( $b_R/b_L$ ) values of width-tapered composite beams. The coherence function is poor at the initial frequency values because of initial disturbance during impact excitation. By using the force windowing technique these signal values are tailored for good input signal. At excitation point 3 for width ratio ( $b_R/b_L$ ) values of 0.4 and 0.6, the coherence values are less than 0.5.
- The time response and autospectrum response is obtained through impact testing for different width ratio ( $b_R/b_L$ ) values for fixed-free (cantilever) boundary condition of width-tapered composite beam at four excitation points. For all width ratio ( $b_R/b_L$ ) values of the beams, the impulse force is highest at excitation point 4. This is because the beam is stiff at excitation point 4.
- The Frequency Response Function (FRF- $H_1$ ) by impact testing is analyzed for different width ratio ( $b_R/b_L$ ) values of width-tapered composite beams. The fundamental natural frequency is highest for width ratio ( $b_R/b_L$ ) value of 0.2 and it gradually decreases as width ratio ( $b_R/b_L$ ) values increases. At excitation point 1 that is at the free end of the beam, the amplitude at first mode is highest whereas it is lowest at mode three.
- The % difference between the natural frequencies is lowest as for mode 1 and highest for mode 3. The % difference is lowest for width ratio ( $b_R/b_L$ ) value of 1 and increases as the width ratio ( $b_R/b_L$ ) value decreases until 0.2. The % difference is lowest

at excitation point 1 and highest at excitation point 4 for modes 1 and 3 but for mode 3, the % difference is highest at excitation points 2 and 3 and lowest at excitation points 1 and 4. The results show good agreement between the analytical predictions and the experimental values of the natural frequencies.

## CHAPTER 5

### DYNAMIC RESPONSE OF THICKNESS- AND WIDTH-TAPERED LAMINATED COMPOSITE BEAMS USING RAYLEIGH-RITZ METHOD

#### 5.1 Introduction

Mechanical vibration deals with the interaction of inertia and restoring forces. The former is due to the effect of mass of an object, while the latter is due to the elastic deformation capability of the object. The inertia force tends to maintain the current state of the object. The restoring force tends to push the object back to its equilibrium position. Undesired vibrations in equipment cause loss of accuracy as in the case of measuring equipment, fatigue failure and discomfort for human beings as in the case of aircrafts and cars. If the frequency of exciting force gets close to the frequency band of the natural frequencies of the structure, the mechanical component experiences severe vibration due to resonance. The resonance will decrease the lifetime of the structure and causes unpredictable failures. Dynamic analyses in mechanical design are of great importance to control the vibration in order to maintain the operating performance and to prevent sudden failures in structures.

In this chapter, free and forced vibration response of thickness- and width-tapered laminated composite beams and buckling response of thickness- and width-

tapered laminated composite columns are conducted using Rayleigh-Ritz method. In section 5.2, energy formulation for dynamic response of thickness- and width-tapered laminated composite beams based on one-dimensional laminated beam theory is developed. In section 5.2.1 system matrices are formed for thickness- and width-tapered laminated beams. Properties of the ply in the tapered laminate are shown in the section 5.2.1.1. In section 5.2.2 Rayleigh-Ritz method for free and forced vibration and buckling response is formed. In section 5.3 dynamic response of thickness- and width-tapered laminated composite beams is shown. In sections 5.3.1- 5.3.5 free vibration response of thickness- and width-tapered laminated composite beams with effects of angle of thickness-taper ( $\phi$ ) and width ratio ( $b_R/b_L$ ), laminate configuration, boundary condition, end-axial forces, and damping are presented. In section 5.4 comparisons of natural frequencies obtained using Rayleigh-Ritz method with that obtained using conventional finite element method [81] are made. In sections 5.5.1-5.5.3 buckling response of thickness- and width-tapered laminated composite columns with effects of angle of thickness-taper ( $\phi$ ) and width ratio ( $b_R/b_L$ ), laminate configuration, boundary condition are presented. In section 5.4 comparisons of forced response in terms of sinusoidal transverse displacement obtained using Rayleigh-Ritz method with that obtained using conventional finite element method are made. In section 5.6 the summary is provided that serve as factors to be considered in calculating the optimal results. These conclusions can guide the designer on the choice of different parameters involved in the analysis.

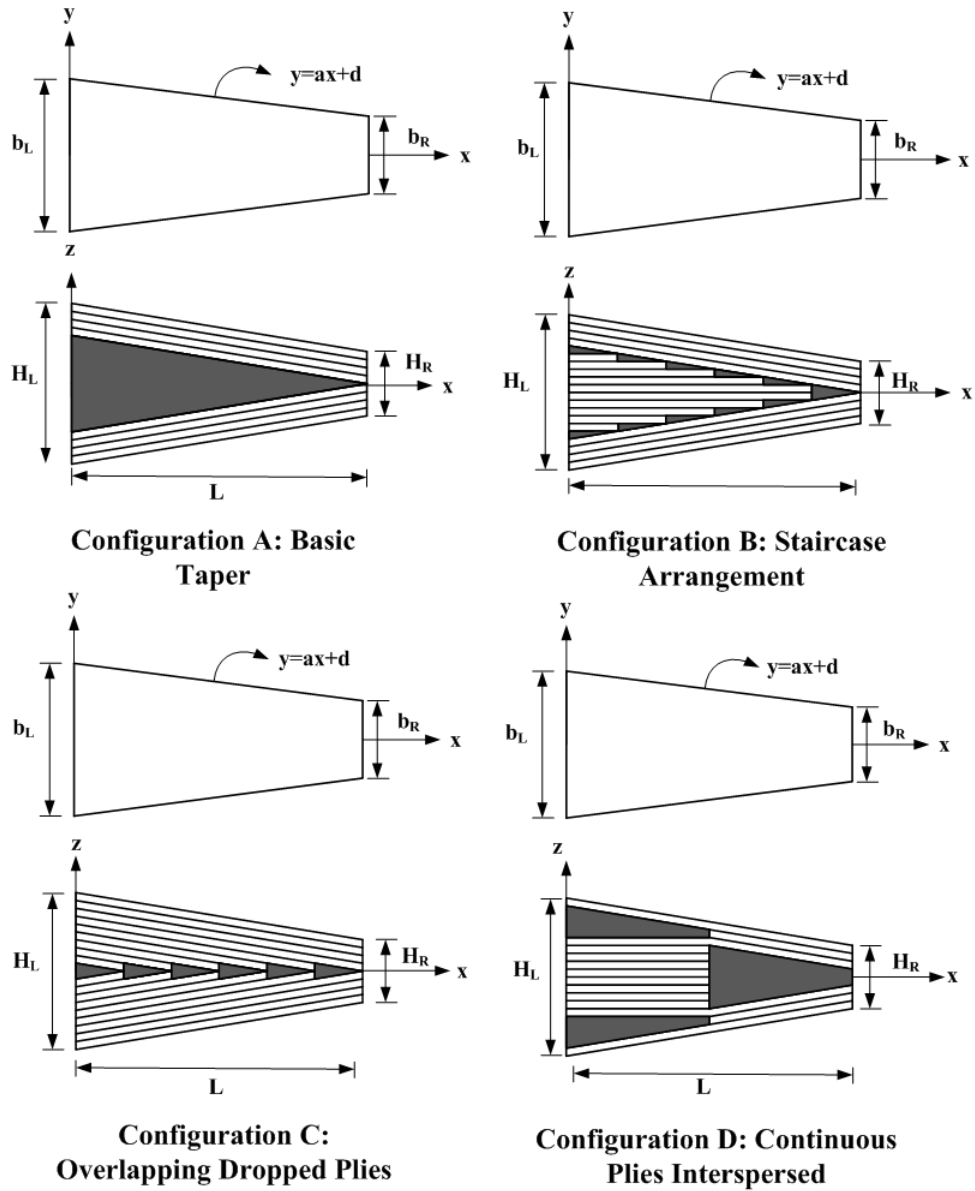


**Figure 5.1** Schematic illustration of thickness- and width-tapered composite beam configurations

## **5.2 Energy formulation for dynamic response of thickness- and width-tapered laminated composite beams based on one-dimensional laminated beam theory**

Euler-Bernoulli beam theory is also defined as classical beam theory. This beam model accounts for bending moment effects on stress and deformation. Transverse shear forces are recovered from equilibrium but their effect on beam deformation is neglected [24].

### **5.2.1 System matrices**

Classical Laminated Plate Theory (CLPT) is considered for the bending of symmetrically laminated thickness- and width-tapered laminated beams [5].

The equation for first co-efficient of the bending stiffness matrix for uniform-thickness and uniform-width beam is shown in the equation (2.2c). One should note that in the thickness-tapered beam as shown in the reference [22], the cross-section area and the value of  $D_{11}$  are not constant through the length of the beam.  $D_{11}$  for a mid-plane thickness-tapered uniform-width beam is explained in the section 5.2.1.1

### 5.2.1.1 Properties of ply in the tapered laminate

In the case of thickness-tapered composite laminate, as shown in the Figure 5.2, the cross section area and the value of  $D_{11}(x)$  are not constant throughout the length in the tapered section and there are ply drop offs at specific distances [22].

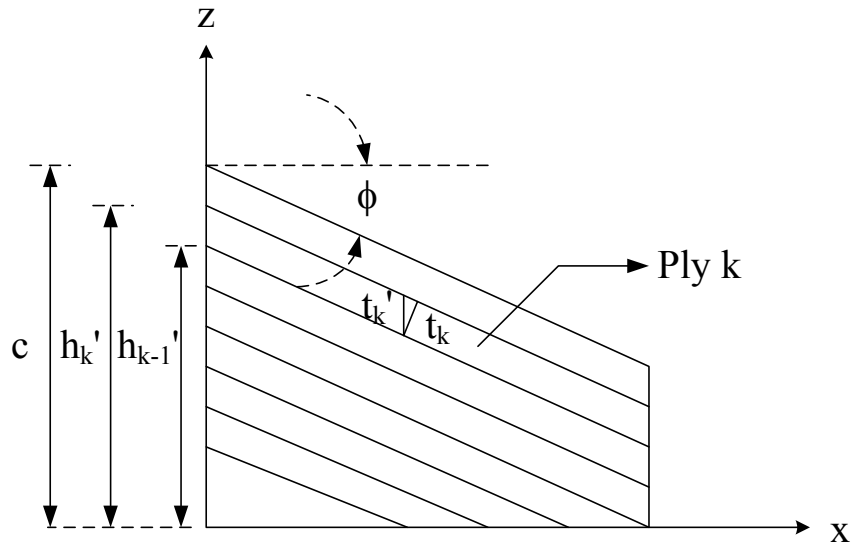


**Figure 5.2** Schematic illustration of properties of typical thickness-tapered laminate

Based on the classical laminate theory, the bending or flexural laminate stiffness of the tapered beam can be written as:

$$D_{11}(x) = \sum_{k=1}^n \left[ t_k' \cdot \bar{z}_k^2 + \frac{t_k^3}{12} \right] (\bar{Q}_{11})_k \quad (5.1)$$

where,

$$t_k' = h_k' - h_{k-1}' = \frac{t_k}{\cos(\phi)} \quad (5.2)$$

From the equation (5.1),  $\bar{z}_k$  is the distance between the centerline of the inclined ply and the mid-plane of the laminate for the  $k^{\text{th}}$  ply which is given as [22]:

$$\bar{z}_k = Sx + c \quad (5.3)$$

where,

$$S = -\tan(\phi) \quad (5.4)$$

Equation (5.1) is rewritten as:

$$D_{11}(x) = \sum_{k=1}^n \left[ \frac{t_k (Sx + c)_k^2}{\cos(\phi)} + \frac{t_k^3}{12 \cos^3(\phi)} \right] (\bar{Q}_{11})_k \quad (5.5)$$

The above equation (5.5), is the first co-efficient of the bending stiffness element for thickness-tapered and uniform-width beam of unit width. The  $D_{11}(x)$  from the equation (5.5) is plugged in the equation (2.7) after multiplying with the term  $b(x)$ . Based on one-dimensional laminated beam theory, equations (2.9) to (2.11) remain the same.

The strain energy due to flexure of the beam which is given in equation (2.13) for width-tapered laminated composite beam based on one-dimensional beam theory remains the same for thickness- and width-tapered composite beam with the properties of thickness-taper and width-taper in the beam is considered.

The work done due to applied static end-axial load for the width-tapered laminated beam which is shown in equation (2.14) is the same for the present case. Hence, the total strain energy  $U_{total}$  which is the sum of  $U_{flexure}$  and  $U_{axialload}$  is given in the equation (2.15) remains the same for thickness- and width-tapered laminated composite beams.

The kinetic energy for uniform-thickness and width-tapered laminated beam is given in equation (2.19).

But for the thickness- and width-tapered beam, the height is not constant across the length of the beam as shown in the Figure (5.2).

Therefore, the kinetic energy for thickness-tapered and width-tapered laminated beam is given as:

$$T = \frac{1}{2} \int_0^L \rho_c \cdot b(x) \cdot H(x) \cdot \left( \frac{\partial w}{\partial t} \right)^2 dx \quad (5.6)$$

## 5.2.2 Analysis using Rayleigh-Ritz method

The formulations based on Rayleigh-Ritz method for width-tapered laminated composite beams which are derived using classical laminate theory in section (2.3.1.1) are followed the same way here to find the natural frequencies and forced response of thickness- and width-tapered laminated composite beams and critical buckling load of thickness- and width-tapered laminated composite columns.

From the section (2.3.1.1), the co-efficients of the stiffness and geometric stiffness which are given in equations (2.24) and (2.25) remains the same.

But it should be noted that the co-efficient of mass for width-tapered laminated beam is shown in the equation (2.26). To construct mass matrix for a thickness-tapered beam, one should consider the decreasing value of area due to the ply drop-off. Therefore the equation (2.26) is changed for thickness-tapered and width-tapered laminated beam which is given as:

$$M_{ij} = \int_0^L \rho_c \cdot b(x) \cdot H(x) \cdot \phi_i(x) \cdot \phi_j(x) dx \quad (5.7)$$

The rest of the equations from (2.27) to (2.33) remain unchanged.

The co-efficients of stiffness, geometric stiffness and mass matrices for thickness-taper configurations A, B, C and D which were formulated in the reference [22] using finite element modeling are used after considering width-taper of the beam. The individual routines for different thickness- and width-taper configurations have been developed using MATLAB<sup>®</sup> software to calculate the stiffness and mass matrices. The resulting beams with thickness- and width-taper configurations A-D which are shown in Figure 5.1 are analyzed for the dynamic response. The detail steps followed in numerical computations of these thickness- and width-tapered composite beams for their dynamic response are shown in Appendix B.

### **5.2.3 Dynamic response of thickness- and width-tapered laminated composite beams**

The formulations that were done on free and forced vibration response of width-tapered laminated composite beams considering static end-axial force and damping in sections 2.3.2, 2.3.3 and 2.3.4 and buckling response of width-tapered laminated columns in the section 2.3.5, will remain the same for free and forced vibration response of thickness- and width-tapered laminated composite beams considering static end-axial force and damping and buckling response of thickness- and width-tapered laminated composite columns.

### **5.3 Free vibration response of thickness- and width-tapered laminated composite beams**

In this section, free vibration response of thickness- and width-tapered laminated composite beams is considered for simply-supported, clamped-clamped, and clamped-free boundary conditions. The mechanical properties of NCT-301 graphite-epoxy prepreg fiber and resin that are given in the Tables 3.1 and 3.2 respectively are used to find the natural frequencies. The geometric properties of the beam are given in the Table 5.1. The configuration of the beam considered is  $([0/90]_9)_s$  which has 36 plies.

Rayleigh-Ritz method is used to find the natural frequencies of thickness- and width-tapered laminated composite beams. Comprehensive parametric studies for natural

frequencies of thickness- and width-tapered composite beams have been shown through plots.

**Table 5.1** Geometric properties of thickness- and width-tapered composite beam

|   |                          |
|---|--------------------------|
| Width at left section ( $b_L$ )               | 0.015 m                  |
| Width ratio ( $b_R/b_L$ )                     | 0.2, 0.4, 0.6, 0.8 and 1 |
| Individual ply thickness (t)                  | 0.000125 m               |
| Height of the laminate on left side ( $H_L$ ) | 0.0045 m                 |

**Table 5.2** Angle of thickness-taper, length, length/height ratio and length/width at left section ratio

|  |       |      |       |      |
|--|-------|------|-------|------|
| Angle of thickness-taper ( $\phi$ ), degrees | 0.344 | 0.43 | 0.573 | 0.86 |
| L,m  | 0.25  | 0.2  | 0.15  | 0.1  |
| L/H  | 56    | 44   | 33    | 22   |
| L/ $b_L$                                     | 17    | 13   | 10    | 7    |

**Table 5.3** Cases for different thickness- and width-taper configurations

| Case | Angle of thickness-taper ( $\phi$ ), degrees | Width-taper ( $b_R/b_L$ ) |
|------|--|---------------------------|
| 1a   | 0.344 to 0.86                                | 1                         |
| 1b   | 0.344 to 0.86                                | 0.5                       |
| 1c   | 0.344 to 0.86                                | 0.2                       |
| 2    | 0.573  | 0.2 to 1                  |

**5.3.1 Effect of angle of thickness-taper ( $\phi$ ) and width ratio ( $b_R/b_L$ ) on natural frequencies**

To study the effects of angle of thickness-taper ( $\phi$ ) and width ratio ( $b_R/b_L$ ) on the first four natural frequencies, the thickness- and width-tapered laminated composite beams of simply-supported, clamped-clamped, and clamped-free boundary conditions are considered for free vibration response. The results are summarized in Figures 5.3-5.8. Different cases of thickness- and width-taper configurations which are shown in the Table 5.3 are considered to study the effect of angle of thickness-taper ( $\phi$ ) and width ratio ( $b_R/b_L$ ) on the natural frequencies.

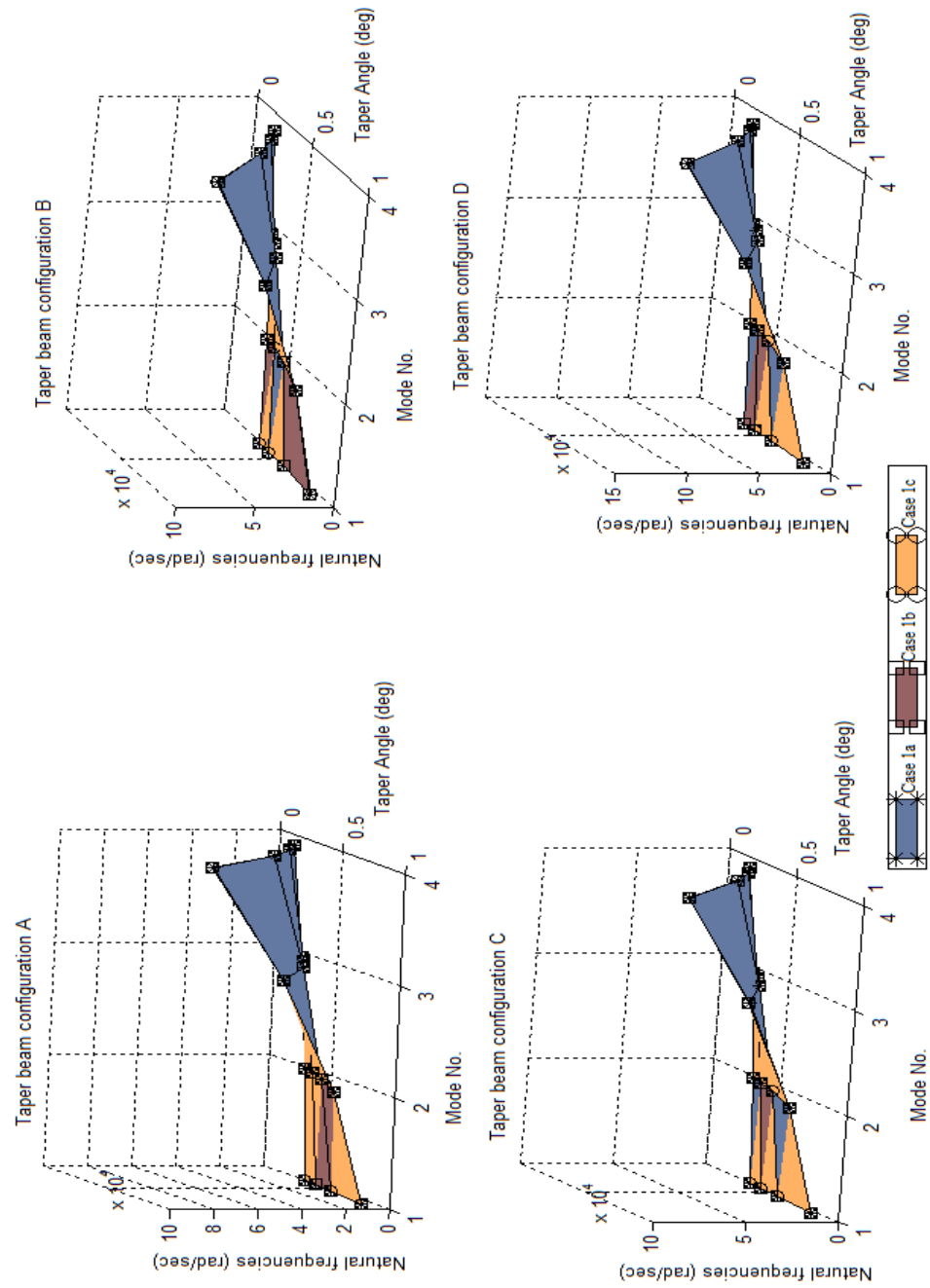


**Figure 5.3** Effect of angle of thickness-taper and width ratio on the natural frequencies for simply-supported composite beam

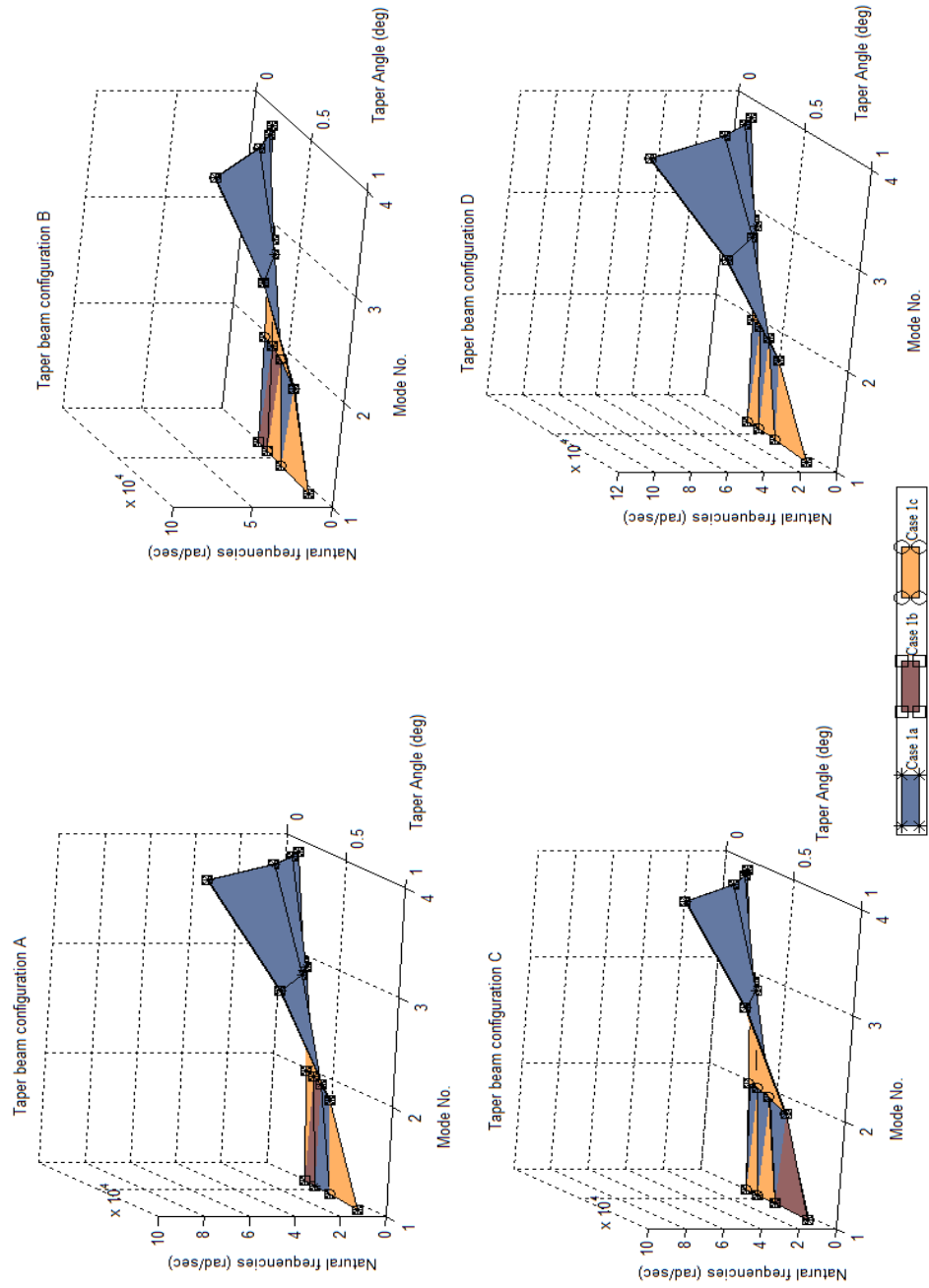


**Figure 5.4** Effect of angle of thickness-taper and width ratio on the natural frequencies for clamped-clamped composite beam

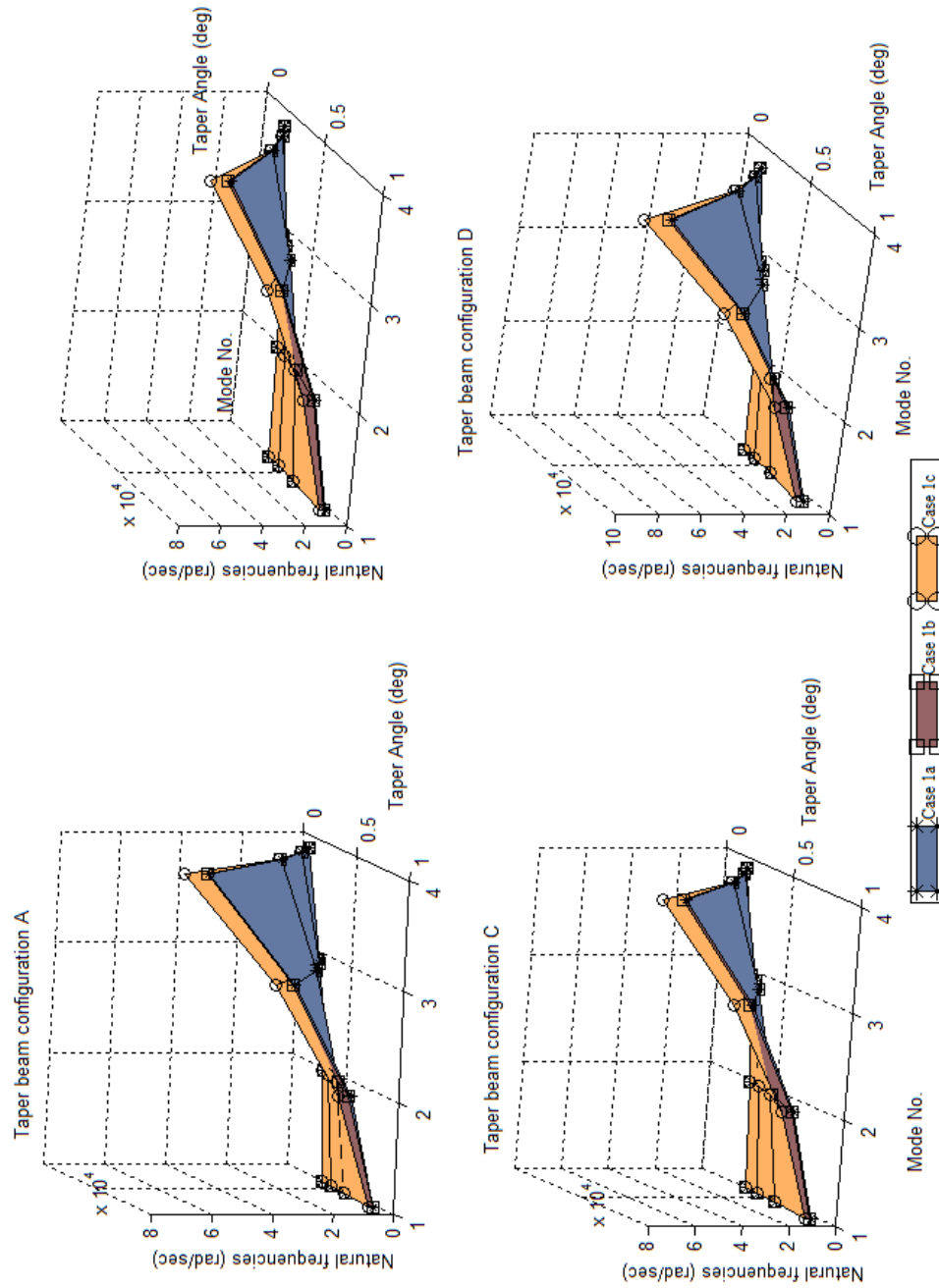


**Figure 5.5** Effect of angle of thickness-taper and width ratio on the natural frequencies for clamped-free composite beam

Figures 5.3-5.5 show the effects of angle of thickness-taper ( $\phi$ ) and width ratio ( $b_R/b_L$ ) on the first four natural frequencies for simply-supported, clamped-clamped, and clamped-free boundary conditions of thickness- and width-tapered composite beams for different thickness- and width-taper configurations as shown in the Figure 5.1. It can be observed from the Figures 5.3-5.5 that as the angle of thickness-taper ( $\phi$ ) and width ratio ( $b_R/b_L$ ) increase, all four modes of natural frequencies increase for all three boundary conditions. From Figures 5.3-5.5, one can observe that the natural frequencies are highest for case 1c, second highest for case 1b and lowest for case 1a for all the thickness- and width-taper configurations for all three boundary conditions. This is because as the width ratio ( $b_R/b_L$ ) values decrease with increase in thickness-taper ( $\phi$ ), the beam becomes more stiff thus results in increase in all four natural frequencies. For clamped-free boundary condition, the natural frequencies are highest for case 1c and lowest for case 1a and second highest for case 1b. The natural frequencies are highest for configuration D, second highest for configuration B, third highest for configuration C and the lowest for configuration A. This indicates that as the width ratio ( $b_R/b_L$ ) value decrease the beam becomes stiffer for clamped-free boundary condition. Increasing the width ratio ( $b_R/b_L$ ) directly affects the value of bending stiffness term  $\left(\frac{1}{D_{11}^*(x)}\right)$ . The stiffness depends on  $Q_{11}$  of the ply.

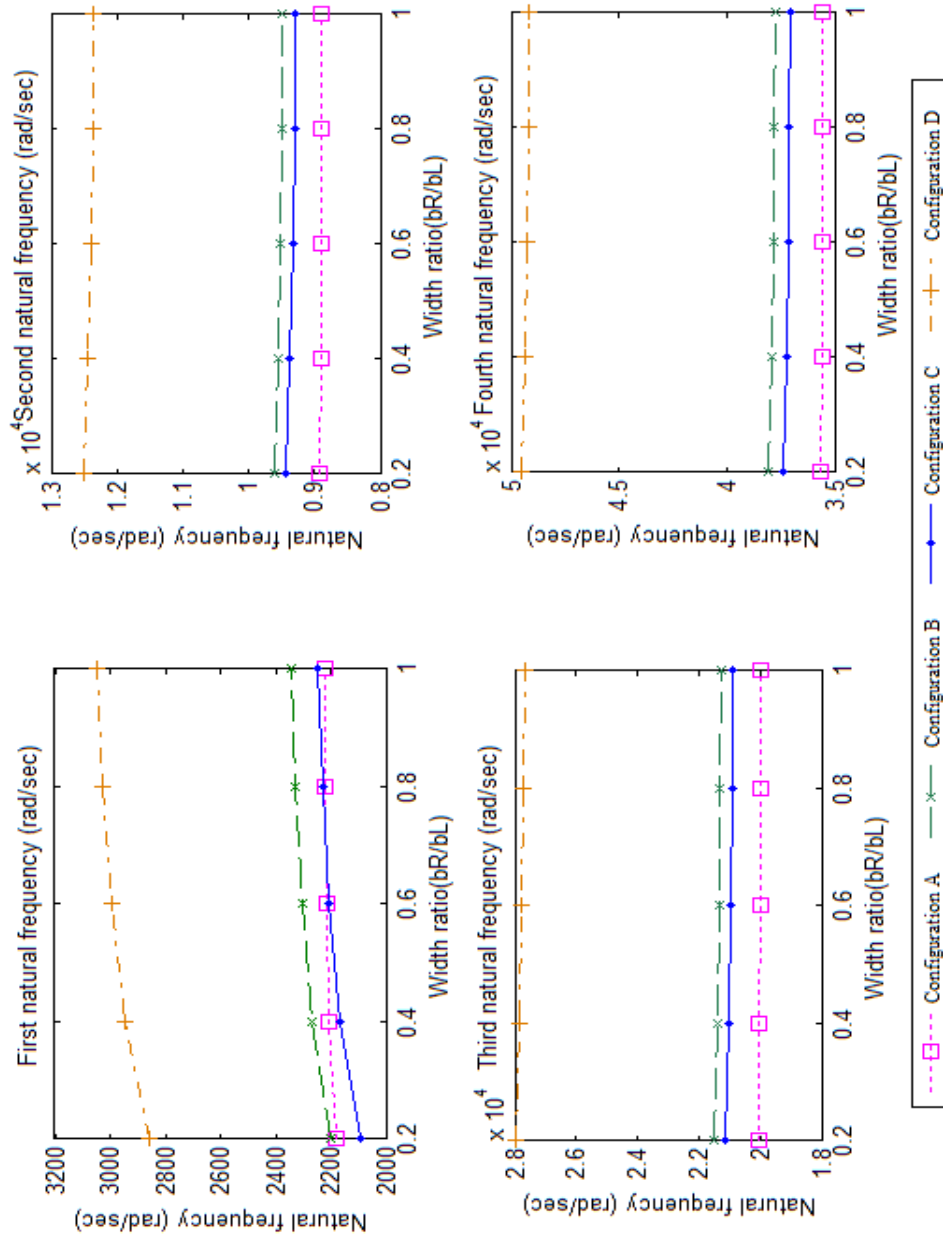


**Figure 5.6** Effect of width ratio for angle of thickness-taper ( $\phi$ ) of  $0.57^0$  on natural frequencies (case 2) – simply-supported boundary condition

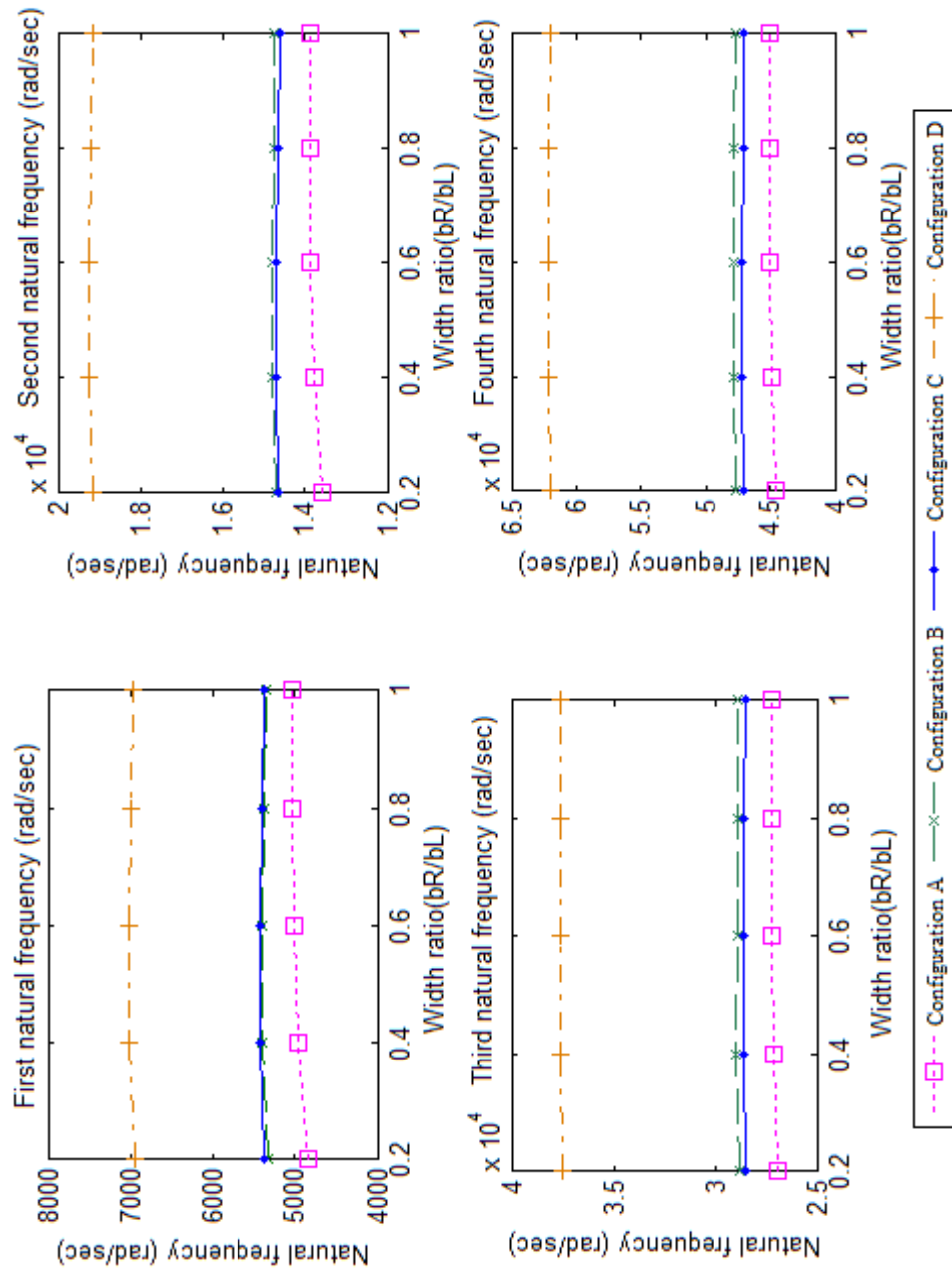


**Figure 5.7** Effect of width ratio for angle of thickness-taper ( $\phi$ ) of  $0.57^\circ$  on natural frequencies (case 2) - clamped-clamped boundary condition

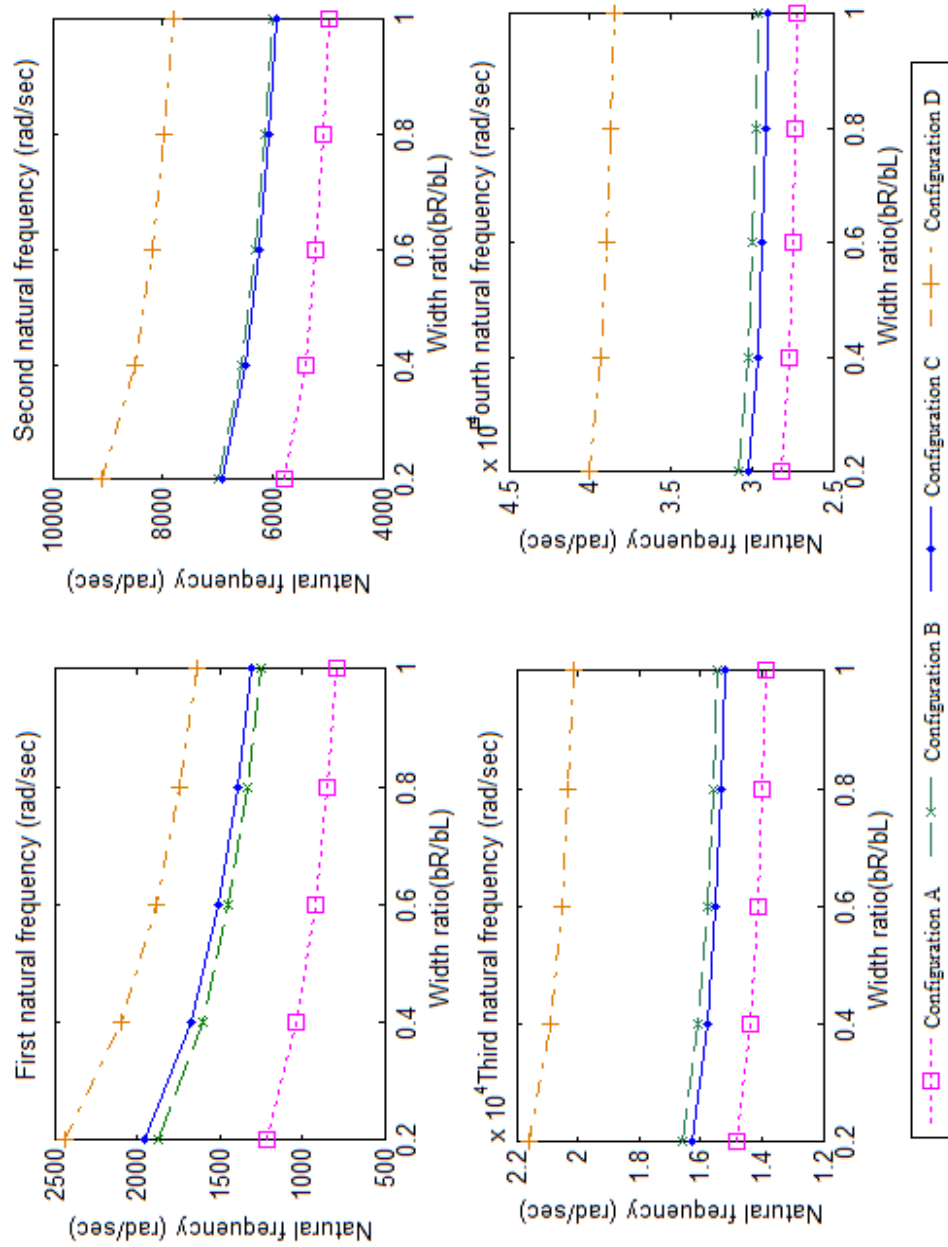


**Figure 5.8** Effect of width ratio for angle of thickness-taper ( $\phi$ ) of  $0.57^0$  on natural frequencies (case 2) - clamped-free boundary condition

Figures 5.6-5.8 show the effect of variation of width ratio ( $b_R/b_L$ ) with constant angle of thickness-taper ( $\phi$ ) of  $0.57^\circ$  on first four natural frequency of the thickness- and width-tapered composite beam. In the current case, for simply-supported boundary condition as the width ratio ( $b_R/b_L$ ) value increase, the first natural frequency increase for all the thickness- and width-taper beam configurations. One can also observe from the Figure 5.6 for simply-supported boundary condition, that the first natural frequency for configuration C is lower than that of configuration A until the width ratio ( $b_R/b_L$ ) value increases from 0.2 to 0.6. But as the width ratio value increases from 0.6 to 1, the first natural frequency for configuration C is higher than that for configuration A. This is because of the change in the stiffness characteristics in the beam configuration. The configuration C has ply drop-off near mid-plane due to a resin pocket. Configuration A has a large resin pocket leading to low stiffness. The second, third and fourth natural frequencies decrease as the width ratio value increases. From the Figure 5.7 for clamped-clamped boundary condition, all four modes of natural frequencies increase with highest natural frequencies for configuration D, second highest for configuration B, third highest for configuration C and lowest for configuration A. From the Figure 5.8 for the clamped-free boundary condition, as the width-ratio ( $b_R/b_L$ ) value increase from 0.2 to 1 with constant angle of thickness-taper ( $\phi$ ) of  $0.57^\circ$ , all four modes of natural frequencies decrease.

### 5.3.2 Effect of laminate configurations on natural frequencies

In this section the effect of laminate configurations on natural frequencies for thickness- and width-tapered laminated composite beams are obtained using Rayleigh-Ritz method. The angle of thickness-taper ( $\phi$ ) value of  $0.57^\circ$  and width ratio ( $b_R/b_L$ ) value of 0.5 is considered to find the natural frequencies. The Tables 5.4-5.6 below show the variation of natural frequencies for different laminate configurations for simply-supported, clamped-clamped and clamped-free boundary conditions. The laminate configurations considered are: 1)  $([0/90]_9)_s$  denoted as 'LC1', 2)  $([\pm 45]_9)_s$  denoted as 'LC2', 3)  $([0_4/\pm 45_7])_s$  denoted as 'LC3'.

**Table 5.4** Comparison of natural frequencies for the effect of laminate configuration - Simply-supported boundary condition

| Beam configuration | Laminate Configuration | $\omega_1$<br>(rad/sec) | $\omega_2$<br>(rad/sec) | $\omega_3$<br>(rad/sec) | $\omega_4$<br>(rad/sec) |
|--------------------|------------------------|-------------------------|-------------------------|-------------------------|-------------------------|
| A                  | LC1                    | 798                     | 3208                    | 7216                    | 12825                   |
|                    | LC2                    | 578                     | 2326                    | 5232                    | 9299                    |
|                    | LC3                    | 724                     | 2913                    | 6553                    | 11647                   |
| B                  | LC1                    | 824                     | 3438                    | 7698                    | 13647                   |
|                    | LC2                    | 599                     | 2501                    | 5600                    | 9928                    |
|                    | LC3                    | 746                     | 3111                    | 6967                    | 12352                   |
| C                  | LC1                    | 788                     | 3369                    | 7554                    | 13398                   |

|   |     |      |      |       |       |
|---|-----|------|------|-------|-------|
|   | LC2 | 563  | 2414 | 5412  | 9599  |
|   | LC3 | 721  | 3077 | 6900  | 12237 |
| D | LC1 | 1072 | 4475 | 10018 | 17762 |
|   | LC2 | 643  | 2687 | 6022  | 10682 |
|   | LC3 | 809  | 3372 | 7556  | 13402 |

**Table 5.5** Comparison of natural frequencies for the effect of laminate configuration – Clamped-clamped boundary condition

| Beam configuration | Laminate Configuration | $\omega_1$<br>(rad/sec) | $\omega_2$<br>(rad/sec) | $\omega_3$<br>(rad/sec) | $\omega_4$<br>(rad/sec) |
|--------------------|------------------------|-------------------------|-------------------------|-------------------------|-------------------------|
| A                  | LC1                    | 1801                    | 4985                    | 9791                    | 16199                   |
|                    | LC2                    | 1306                    | 3614                    | 7098                    | 11744                   |
|                    | LC3                    | 1635                    | 4527                    | 8891                    | 14710                   |
| B                  | LC1                    | 1945                    | 5330                    | 10422                   | 17207                   |
|                    | LC2                    | 1417                    | 3880                    | 7584                    | 12520                   |
|                    | LC3                    | 1759                    | 4823                    | 9432                    | 15574                   |
| C                  | LC1                    | 1955                    | 5298                    | 10307                   | 16978                   |
|                    | LC2                    | 1404                    | 3801                    | 7391                    | 12170                   |
|                    | LC3                    | 1783                    | 4835                    | 9410                    | 15502                   |
| D                  | LC1                    | 2533                    | 6939                    | 13565                   | 22393                   |
|                    | LC2                    | 1526                    | 4180                    | 8171                    | 13489                   |
|                    | LC3                    | 1911                    | 5239                    | 10245                   | 16914                   |

**Table 5.6** Comparison of natural frequencies for the effect of laminate configuration – Clamped-free boundary condition

| Beam configuration | Laminate configuration | $\omega_1$<br>(rad/sec) | $\omega_2$<br>(rad/sec) | $\omega_3$<br>(rad/sec) | $\omega_4$<br>(rad/sec) |
|--------------------|------------------------|-------------------------|-------------------------|-------------------------|-------------------------|
| A                  | LC1                    | 350                     | 1909                    | 5130                    | 9939                    |
|                    | LC2                    | 254                     | 1384                    | 3720                    | 7206                    |
|                    | LC3                    | 318                     | 1734                    | 4659                    | 9026                    |
| B                  | LC1                    | 546                     | 2308                    | 5729                    | 10826                   |
|                    | LC2                    | 400                     | 1682                    | 4171                    | 7877                    |
|                    | LC3                    | 492                     | 2086                    | 5184                    | 9797                    |
| C                  | LC1                    | 568                     | 2285                    | 5625                    | 10621                   |
|                    | LC2                    | 411                     | 1639                    | 4031                    | 7609                    |
|                    | LC3                    | 517                     | 2085                    | 5137                    | 9701                    |
| D                  | LC1                    | 711                     | 3001                    | 7451                    | 14078                   |
|                    | LC2                    | 416                     | 1782                    | 4456                    | 8444                    |
|                    | LC3                    | 522                     | 2239                    | 5596                    | 10601                   |

Tables 5.4-5.6 show the effect of laminate configuration on natural frequencies with angle of thickness-taper ( $\phi$ ) of  $0.57^\circ$  and width ratio ( $b_R/b_L$ ) value of 0.5 for three boundary conditions. One can observe from the Tables 5.4-5.6 that the results obtained for different laminate configurations show that the natural frequencies is largest for laminate configuration LC1, second largest for laminate configuration LC3 and lowest for laminate configuration LC2. This difference in natural frequencies is due to the variation of stiffness in the beam. This is because in the laminate configuration LC1,

most of the  $0^\circ$  fibers are oriented along the length of the beam.  $0^\circ$  fibers have highest  $E_1$  compared to other fiber direction which is the direction of the bending loads. Also the natural frequencies is largest for configuration D of the taper configuration with second largest for configuration B, third largest for configuration C and lowest for configuration A. These differences in natural frequencies for different taper configurations are expected because of the variation of stiffness in the tapered beam configuration.

### 5.3.3 Effect of boundary condition on natural frequencies

In this section the effect of boundary condition on natural frequencies for thickness- and width-tapered beam are obtained using Rayleigh-Ritz method. The angle of thickness-taper ( $\phi$ ) value of  $0.57^\circ$  and width ratio ( $b_R/b_L$ ) value of 0.5 is considered to find the natural frequencies. Simply-supported, clamped-clamped and clamped-free boundary conditions are considered. The natural frequencies for all three boundary conditions are obtained using Rayleigh-Ritz method.

**Table 5.7** Comparison of natural frequencies-Simply-supported boundary condition

| Beam configuration | $\omega_1$ (rad/sec) | $\omega_2$ (rad/sec) | $\omega_3$ (rad/sec) | $\omega_4$ (rad/sec) |
|--------------------|----------------------|----------------------|----------------------|----------------------|
| A                  | 798                  | 3208                 | 7216                 | 12825                |

|   |      |      |       |       |
|---|------|------|-------|-------|
| B | 824  | 3438 | 7698  | 13647 |
| C | 788  | 3369 | 7554  | 13398 |
| D | 1072 | 4475 | 10018 | 17762 |

**Table 5.8** Comparison of natural frequencies-Clamped-clamped boundary condition

| Beam configuration | $\omega_1$ (rad/sec) | $\omega_2$ (rad/sec) | $\omega_3$ (rad/sec) | $\omega_4$ (rad/sec) |
|--------------------|----------------------|----------------------|----------------------|----------------------|
| A                  | 1801                 | 4985                 | 9791                 | 16199                |
| B                  | 1945                 | 5330                 | 10422                | 17207                |
| C                  | 1955                 | 5298                 | 10307                | 16978                |
| D                  | 2533                 | 6939                 | 13565                | 22393                |

**Table 5.9** Comparison of natural frequencies-Clamped-free boundary condition

| Beam configuration | $\omega_1$ (rad/sec) | $\omega_2$ (rad/sec) | $\omega_3$ (rad/sec) | $\omega_4$ (rad/sec) |
|--------------------|----------------------|----------------------|----------------------|----------------------|
| A                  | 350                  | 1909                 | 5130                 | 9939                 |
| B                  | 546                  | 2308                 | 5729                 | 10826                |
| C                  | 568                  | 2285                 | 5625                 | 10621                |
| D                  | 711                  | 3001                 | 7451                 | 14078                |

Tables 5.7-5.9 show the effect of boundary conditions on four natural frequencies for thickness- and width-tapered laminated composite beam. From the Tables 5.7-5.9, one can observe that the natural frequencies are largest for clamped-clamped boundary condition because the stiffness of the beam is largest. Beam with clamped-free (cantilever) boundary condition has lowest natural frequencies this is because of lower stiffness. The natural frequencies are second largest for simply-supported boundary condition. Also, one can observe natural frequencies are largest for taper configuration D and lowest for configuration A, second largest for configuration B and third largest for configuration C.

#### **5.3.4 Effects of end-axial forces on natural frequencies**

By using the mechanical and geometric properties described in section 5.3.1, the effect of applied static end-axial tensile and compressive forces on the first four natural frequencies for simply-supported, clamped-clamped, and clamped-free boundary conditions of thickness- and width-tapered composite beams are carried out in the current section. The angle of thickness-taper ( $\phi$ ) of  $0.57^\circ$  and width ratio ( $b_R/b_L$ ) value of 0.5 are considered for the analysis. Concentrated end-axial compressive and tensile forces which are applied as the percentage of critical buckling load and first-ply tensile failure loads respectively are applied on both ends of the beam to determine the natural frequencies due to the effect of axial forces.

The critical buckling load is determined in the section 5.5.1 for thickness- and width tapered composite columns and first-ply tensile failure loads are determined in the section 3.6.1. The results are presented in the plots in Tables 5.10-5.15 which are obtained using Rayleigh-Ritz method.

**Table 5.10** Effect of end-axial compressive force on natural frequencies -Simply supported boundary condition

| % Pcr | Beam configuration | $\omega_1$ (rad/sec) | $\omega_2$ (rad/sec) | $\omega_3$ (rad/sec) | $\omega_4$ (rad/sec) |
|-------|--------------------|----------------------|----------------------|----------------------|----------------------|
| 0     | A                  | 798                  | 3208                 | 7216                 | 12825                |
|       | B                  | 824                  | 3438                 | 7698                 | 13647                |
|       | C                  | 788                  | 3369                 | 7554                 | 13398                |
|       | D                  | 1072                 | 4475                 | 10018                | 17762                |
| 50    | A                  | 678                  | 2951                 | 7000                 | 12697                |
|       | % decrease         | 15                   | 8                    | 3                    | 1                    |
|       | B                  | 700                  | 3163                 | 7467                 | 13511                |
|       | % decrease         | 15                   | 8                    | 3                    | 1                    |
|       | C                  | 670                  | 3099                 | 7328                 | 13264                |
|       | % decrease         | 15                   | 8                    | 3                    | 1                    |
|       | D                  | 911                  | 4117                 | 9717                 | 17584                |
|       | % decrease         | 15                   | 8                    | 3                    | 1                    |

|    |            |     |      |      |       |
|----|------------|-----|------|------|-------|
| 95 | A          | 542 | 2630 | 6783 | 12440 |
|    | % decrease | 15  | 8    | 3    | 1     |
|    | B          | 560 | 2819 | 7236 | 13238 |
|    | % decrease | 15  | 8    | 3    | 1     |
|    | C          | 536 | 2762 | 7101 | 12996 |
|    | % decrease | 15  | 8    | 3    | 1     |
|    | D          | 729 | 3669 | 9417 | 17229 |
|    | % decrease | 15  | 8    | 3    | 1     |

**Table 5.11** Effect of end-axial compressive force on natural frequencies- Clamped-clamped boundary condition

| % Pcr | Beam configuration | $\omega_1$ (rad/sec) | $\omega_2$ (rad/sec) | $\omega_3$ (rad/sec) | $\omega_4$ (rad/sec) |
|-------|--------------------|----------------------|----------------------|----------------------|----------------------|
| 0     | A                  | 1801                 | 4985                 | 9791                 | 16199                |
|       | B                  | 1945                 | 5330                 | 10422                | 17207                |
|       | C                  | 1955                 | 5298                 | 10307                | 16978                |
|       | D                  | 2533                 | 6939                 | 13565                | 22393                |
| 50    | A                  | 1477                 | 4387                 | 8910                 | 15389                |
|       | % decrease         | 18                   | 12                   | 9                    | 5                    |
|       | B                  | 1595                 | 4690                 | 9484                 | 16347                |
|       | % decrease         | 18                   | 12                   | 9                    | 5                    |
|       | C                  | 1603                 | 4662                 | 9379                 | 16129                |

|    |            |      |      |       |       |
|----|------------|------|------|-------|-------|
|    | % decrease | 18   | 12   | 9     | 5     |
|    | D          | 2077 | 6106 | 12344 | 21273 |
|    | % decrease | 18   | 12   | 9     | 5     |
| 95 | A          | 1224 | 4088 | 9203  | 15713 |
|    | % decrease | 18   | 12   | 9     | 5     |
|    | B          | 1322 | 4371 | 9797  | 16691 |
|    | % decrease | 18   | 12   | 9     | 5     |
|    | C          | 1329 | 4344 | 9689  | 16469 |
|    | % decrease | 18   | 12   | 9     | 5     |
|    | D          | 1722 | 5690 | 12751 | 21721 |
|    | % decrease | 18   | 12   | 9     | 5     |

**Table 5.12** Effect of end-axial compressive force on natural frequencies- Clamped-free boundary condition

| % Pcr | Beam configuration | $\omega_1$ (rad/sec) | $\omega_2$ (rad/sec) | $\omega_3$ (rad/sec) | $\omega_4$ (rad/sec) |
|-------|--------------------|----------------------|----------------------|----------------------|----------------------|
| 0     | A                  | 350                  | 1909                 | 5130                 | 9939                 |
|       | B                  | 546                  | 2308                 | 5729                 | 10826                |
|       | C                  | 568                  | 2285                 | 5625                 | 10621                |
|       | D                  | 711                  | 3001                 | 7451                 | 14078                |
| 50    | A                  | 305                  | 1737                 | 4976                 | 9840                 |
|       | % decrease         | 13                   | 9                    | 3                    | 1                    |
|       | B                  | 475                  | 2100                 | 5557                 | 10718                |
|       | % decrease         | 13                   | 9                    | 3                    | 1                    |
|       | C                  | 495                  | 2079                 | 5456                 | 10515                |
|       | % decrease         | 13                   | 9                    | 3                    | 1                    |
|       | D                  | 618                  | 2731                 | 7227                 | 13937                |
|       | % decrease         | 13                   | 9                    | 3                    | 1                    |
| 95    | A                  | 256                  | 1623                 | 4874                 | 9741                 |
|       | % decrease         | 13                   | 9                    | 3                    | 1                    |
|       | B                  | 398                  | 1962                 | 5443                 | 10609                |
|       | % decrease         | 13                   | 9                    | 3                    | 1                    |
|       | C                  | 415                  | 1942                 | 5344                 | 10409                |
|       | % decrease         | 13                   | 9                    | 3                    | 1                    |

|  |            |     |      |      |       |
|--|------------|-----|------|------|-------|
|  | D          | 519 | 2551 | 7078 | 13796 |
|  | % decrease | 13  | 9    | 3    | 1     |

Tables 5.10-5.12 show the effect of applied end-axial (static) compressive forces on first four natural frequencies for simply-supported, clamped-clamped, and clamped-free boundary conditions of thickness- and width-tapered composite beams. It can be observed from the Tables 5.10-5.12 that as the magnitude of end axial compressive force is increased all the four natural frequencies decrease for all three boundary conditions. This is because as the axial compressive force is applied, the beam becomes less stiff thereby decrease in the natural frequencies. One can also observe from the Tables 5.10-5.12 that the percentage of decrease between the modes 1-4 varies in the same taper beam configurations.

**Table 5.13** Effect of end-axial tensile force on natural frequencies -Simply supported boundary condition

| % P <sub>1</sub> | Beam configuration | $\omega_1$ (rad/sec) | $\omega_2$ (rad/sec) | $\omega_3$ (rad/sec) | $\omega_4$ (rad/sec) |
|------------------|--------------------|----------------------|----------------------|----------------------|----------------------|
| 0                | A                  | 798                  | 3208                 | 7216                 | 12825                |
|                  | B                  | 824                  | 3438                 | 7698                 | 13647                |
|                  | C                  | 788                  | 3369                 | 7554                 | 13398                |
|                  | D                  | 1072                 | 4475                 | 10018                | 17762                |

|    |            |        |       |       |       |
|----|------------|--------|-------|-------|-------|
| 50 | A          | 5010.5 | 10558 | 16970 | 24496 |
|    | % increase | 528    | 229   | 135   | 91    |
|    | B          | 5077.1 | 10776 | 17350 | 25024 |
|    | % increase | 516    | 213   | 125   | 83    |
|    | C          | 5074.7 | 10791 | 17377 | 25034 |
|    | % increase | 544    | 220   | 130   | 87    |
|    | D          | 5131.4 | 11221 | 18655 | 27714 |
|    | % increase | 379    | 151   | 86    | 56    |
| 95 | A          | 6849.3 | 14128 | 22084 | 30967 |
|    | % increase | 759    | 340   | 206   | 141   |
|    | B          | 6948.6 | 14423 | 22597 | 31697 |
|    | % increase | 743    | 320   | 194   | 132   |
|    | C          | 6947.1 | 14440 | 22642 | 31759 |
|    | % increase | 782    | 329   | 200   | 137   |
|    | D          | 6989.1 | 14774 | 23671 | 33976 |
|    | % increase | 552    | 230   | 136   | 91    |

**Table 5.14** Effect of end-axial tensile force on natural frequencies- Clamped-clamped boundary condition

| % P <sub>1</sub> | Beam configuration | $\omega_1$ (rad/sec) | $\omega_2$ (rad/sec) | $\omega_3$ (rad/sec) | $\omega_4$ (rad/sec) |
|------------------|--------------------|----------------------|----------------------|----------------------|----------------------|
|                  | A                  | 1801                 | 4985                 | 9791                 | 16199                |
|                  | B                  | 1945                 | 5330                 | 10422                | 17207                |
|                  | C                  | 1955                 | 5298                 | 10307                | 16978                |
|                  | D                  | 2533                 | 6939                 | 13565                | 22393                |

|    |            |        |       |       |       |
|----|------------|--------|-------|-------|-------|
| 50 | A          | 5614.7 | 11819 | 18952 | 27238 |
|    | % increase | 212    | 137   | 94    | 68    |
|    | B          | 5780   | 12146 | 19392 | 27778 |
|    | % increase | 197    | 128   | 86    | 61    |
|    | C          | 5827.4 | 12227 | 19478 | 27832 |
|    | % increase | 198    | 131   | 89    | 64    |
|    | D          | 6085.9 | 13071 | 21429 | 31478 |
|    | % increase | 140    | 88    | 58    | 41    |
| 95 | A          | 7426.2 | 15316 | 23943 | 33540 |
|    | % increase | 312    | 207   | 145   | 107   |
|    | B          | 7631.9 | 15761 | 24579 | 34340 |
|    | % increase | 292    | 196   | 136   | 100   |
|    | C          | 7682.3 | 15858 | 24709 | 34477 |
|    | % increase | 293    | 199   | 140   | 103   |
|    | D          | 7909.2 | 16565 | 26333 | 37549 |
|    | % increase | 212    | 139   | 94    | 68    |

**Table 5.15** Effect of end-axial tensile force on natural frequencies- Clamped-free boundary condition

| % $P_1$ | Beam configuration | $\omega_1$ (rad/sec) | $\omega_2$ (rad/sec) | $\omega_3$ (rad/sec) | $\omega_4$ (rad/sec) |
|---------|--------------------|----------------------|----------------------|----------------------|----------------------|
| 0       | A                  | 350                  | 1909                 | 5130                 | 9939                 |
|         | B                  | 546                  | 2308                 | 5729                 | 10826                |
|         | C                  | 568                  | 2285                 | 5625                 | 10621                |
|         | D                  | 711                  | 3001                 | 7451                 | 14078                |
|         | A                  | 2983.3               | 8247.2               | 14302                | 21321                |

|    |            |        |        |       |       |
|----|------------|--------|--------|-------|-------|
| 50 | % increase | 752    | 332    | 179   | 115   |
|    | B          | 3339.5 | 8882.3 | 15282 | 22662 |
|    | % increase | 512    | 285    | 167   | 109   |
|    | C          | 3368.1 | 8954.3 | 15382 | 22760 |
|    | % increase | 493    | 292    | 173   | 114   |
|    | D          | 3439.8 | 9301.2 | 16371 | 24876 |
|    | % increase | 384    | 210    | 120   | 77    |
| 95 | A          | 4048.3 | 11045  | 18760 | 27277 |
|    | % increase | 1056   | 479    | 266   | 174   |
|    | B          | 4484.1 | 11767  | 19855 | 28785 |
|    | % increase | 722    | 410    | 247   | 166   |
|    | C          | 4512.9 | 11845  | 19977 | 28936 |
|    | % increase | 694    | 418    | 255   | 172   |
|    | D          | 4580.3 | 12151  | 20830 | 30763 |
|    | % increase | 545    | 305    | 180   | 119   |

Tables 5.13-5.15 show the effect of applied end-axial (static) tensile force on first four natural frequencies for simply-supported, clamped-clamped, and clamped-free boundary conditions of thickness- and width-tapered composite beams. It can be observed from the Tables 5.13-5.15 that as the magnitude of end axial tensile force is increased all the four natural frequencies increase for all three boundary conditions. This is because as the axial tensile force is applied the beam becomes stiffer thereby increase in the natural frequencies. Once can observe from the Tables 5.13-5.15 that the % increase in the natural frequencies are high due to the application of high end-axial tensile load.

### 5.3.5 Effect of damping on natural frequencies

To study the effect of damping on the first four natural frequencies, the mechanical and geometric properties which are described in section 5.3.1 are used in the current section. The angle of thickness-taper ( $\phi$ ) value of  $0.57^\circ$  and width ratio ( $b_R/b_L$ ) value of 0.5 are considered for the effect of damping on natural frequencies of thickness- and width-tapered composite beams with simply-supported, clamped-clamped, and clamped-free boundary conditions.

**Table 5.16** Effect of damping on natural frequencies for simply-supported boundary condition.

| Condition | Beam configuration | $\omega_1$<br>(rad/sec) | $\omega_2$<br>(rad/sec) | $\omega_3$<br>(rad/sec) | $\omega_4$<br>(rad/sec) |
|-----------|--------------------|-------------------------|-------------------------|-------------------------|-------------------------|
| Undamped  | A                  | 798                     | 3208                    | 7216                    | 12825                   |
|           | B                  | 824                     | 3438                    | 7698                    | 13647                   |
|           | C                  | 788                     | 3369                    | 7554                    | 13398                   |
|           | D                  | 1072                    | 4475                    | 10018                   | 17762                   |
| Damped    | A                  | 780                     | 3135                    | 7052                    | 12534                   |
|           | B                  | 803                     | 3352                    | 7506                    | 13308                   |
|           | C                  | 768                     | 3282                    | 7360                    | 13054                   |
|           | D                  | 1045                    | 4363                    | 9769                    | 17320                   |

**Table 5.17** Effect of damping on natural frequencies for clamped-clamped boundary condition

| Condition | Beam configuration | $\omega_1$<br>(rad/sec) | $\omega_2$<br>(rad/sec) | $\omega_3$<br>(rad/sec) | $\omega_4$<br>(rad/sec) |
|-----------|--------------------|-------------------------|-------------------------|-------------------------|-------------------------|
| Undamped  | A                  | 1801                    | 4985                    | 9791                    | 16199                   |
|           | B                  | 1945                    | 5330                    | 10422                   | 17207                   |
|           | C                  | 1955                    | 5298                    | 10307                   | 16978                   |
|           | D                  | 2533                    | 6939                    | 13565                   | 22393                   |
| Damped    | A                  | 1778                    | 4921                    | 9666                    | 15992                   |
|           | B                  | 1829                    | 5013                    | 9802                    | 16183                   |
|           | C                  | 1795                    | 4865                    | 9464                    | 15589                   |
|           | D                  | 2322                    | 6361                    | 12435                   | 20527                   |

**Table 5.18** Effect of damping on natural frequencies for clamped-free boundary condition

| Condition | Beam configuration | $\omega_1$<br>(rad/sec) | $\omega_2$<br>(rad/sec) | $\omega_3$<br>(rad/sec) | $\omega_4$<br>(rad/sec) |
|-----------|--------------------|-------------------------|-------------------------|-------------------------|-------------------------|
| Undamped  | A                  | 350                     | 1909                    | 5130                    | 9939                    |
|           | B                  | 546                     | 2308                    | 5729                    | 10826                   |
|           | C                  | 568                     | 2285                    | 5625                    | 10621                   |

|        |   |     |      |      |       |
|--------|---|-----|------|------|-------|
|        | D | 711 | 3001 | 7451 | 14078 |
| Damped | A | 265 | 1442 | 3876 | 7509  |
|        | B | 453 | 1914 | 4751 | 8977  |
|        | C | 481 | 1933 | 4761 | 8989  |
|        | D | 589 | 2490 | 6180 | 11678 |

Tables 5.16-5.18 show the effect of damping on first four natural frequencies for all three boundary conditions of thickness- and width- tapered laminated composite beams. The mass proportional constant ( $\alpha$ ) and stiffness proportional constant ( $\beta$ ) are 3.753 and  $4.83 \times 10^{-5}$  respectively are considered to study for the effects of damping obtained through experimental modal testing. One can observe from the Tables 5.16-5.18, that the natural frequencies of un-damped beam are higher than the natural frequencies with damping for all boundary conditions. Another important observation is that the difference between the natural frequencies of un-damped and damped beam is largest for beam configuration D for simply-supported boundary condition. For clamped-clamped boundary condition the highest difference between un-damped and damped natural frequencies is for configuration D and least for configuration A.

#### 5.4 Comparison of natural frequencies between Rayleigh-Ritz method and conventional finite element method

By using the mechanical and geometric properties given in section 5.3.1, the current section presents the comparison of first four natural frequencies for simply-supported, clamped-clamped, and clamped-free boundary conditions of thickness-and width-tapered composite beams obtained using Rayleigh-Ritz method with that obtained using conventional finite element method [81]. The angle of thickness-taper ( $\phi$ ) value is increased from  $0.344^\circ$  to  $0.86^\circ$  with keeping constant width ratio ( $b_R/b_L$ ) value of 0.5 which is the case 2 as shown in the Table 5.3 is considered to compare the natural frequencies.

**Table 5.19** Comparison of natural frequencies for configuration A-Simply supported boundary condition

|                  |       |      |       |       |
|------------------|-------|------|-------|-------|
| Angle (deg)      | 0.344 | 0.43 | 0.573 | 0.86  |
| L,m              | 0.25  | 0.2  | 0.15  | 0.1   |
| L/H              | 56    | 44   | 33    | 22    |
| $\omega_1$ (R-R) | 780   | 1219 | 2165  | 4868  |
| $\omega_1$ (FEM) | 760   | 1187 | 2109  | 4744  |
| % difference     | 2.61  | 2.57 | 2.55  | 2.53  |
| $\omega_2$ (R-R) | 3244  | 5068 | 8999  | 20219 |

|                  |      |       |       |       |
|------------------|------|-------|-------|-------|
| $\omega_2$ (FEM) | 3221 | 5032  | 8948  | 20133 |
| % difference     | 0.70 | 0.71  | 0.57  | 0.42  |
| $\omega_3$ (R-R) | 7297 | 11402 | 20245 | 45482 |
| $\omega_3$ (FEM) | 7178 | 11216 | 19940 | 44866 |
| % difference     | 1.63 | 1.63  | 1.50  | 1.35  |

**Table 5.20** Comparison of natural frequencies for configuration A-Clamped-clamped boundary condition

|                  |       |       |       |       |
|------------------|-------|-------|-------|-------|
| Angle (deg)      | 0.344 | 0.43  | 0.573 | 0.86  |
| L,m              | 0.25  | 0.2   | 0.15  | 0.1   |
| L/H              | 56    | 44    | 33    | 22    |
| $\omega_1$ (R-R) | 1821  | 2845  | 5051  | 11349 |
| $\omega_1$ (FEM) | 1808  | 2825  | 5024  | 11302 |
| % difference     | 0.71  | 0.69  | 0.55  | 0.41  |
| $\omega_2$ (R-R) | 5041  | 7876  | 13985 | 31420 |
| $\omega_2$ (FEM) | 4947  | 7729  | 13741 | 30917 |
| % difference     | 1.87  | 1.86  | 1.74  | 1.60  |
| $\omega_3$ (R-R) | 9901  | 15470 | 27468 | 61711 |
| $\omega_3$ (FEM) | 9664  | 15101 | 26847 | 60405 |
| % difference     | 2.39  | 2.38  | 2.26  | 2.12  |

**Table 5.21** Comparison of natural frequencies for configuration A-Clamped-free boundary condition

|                  |       |      |       |       |
|------------------|-------|------|-------|-------|
| Angle (deg)      | 0.344 | 0.43 | 0.573 | 0.86  |
| L,m              | 0.25  | 0.2  | 0.15  | 0.1   |
| L/H              | 56    | 44   | 33    | 22    |
| $\omega_1$ (R-R) | 563   | 878  | 1552  | 3520  |
| $\omega_1$ (FEM) | 582   | 913  | 1617  | 3682  |
| % difference     | 3.53  | 4.01 | 4.20  | 4.60  |
| $\omega_2$ (R-R) | 2212  | 3457 | 6137  | 13918 |
| $\omega_2$ (FEM) | 2274  | 3553 | 6317  | 14217 |
| % difference     | 2.79  | 2.79 | 2.93  | 2.15  |
| $\omega_3$ (R-R) | 5238  | 8184 | 14530 | 32646 |
| $\omega_3$ (FEM) | 5463  | 8536 | 15176 | 34146 |
| % difference     | 4.29  | 4.30 | 4.44  | 4.60  |

**Table 5.22** Comparison of natural frequencies for configuration B-Simply-supported boundary condition

|                  |       |       |       |       |
|------------------|-------|-------|-------|-------|
| Angle (deg)      | 0.344 | 0.43  | 0.573 | 0.86  |
| L,m              | 0.25  | 0.2   | 0.15  | 0.1   |
| L/H              | 56    | 44    | 33    | 22    |
| $\omega_1$ (R-R) | 820   | 1281  | 2276  | 5115  |
| $\omega_1$ (FEM) | 837   | 1307  | 2322  | 5230  |
| % difference     | 2.14  | 2.02  | 1.98  | 2.25  |
| $\omega_2$ (R-R) | 3654  | 5695  | 10120 | 22740 |
| $\omega_2$ (FEM) | 3733  | 5833  | 10368 | 23327 |
| % difference     | 2.15  | 2.41  | 2.45  | 2.58  |
| $\omega_3$ (R-R) | 8125  | 12680 | 22540 | 50548 |
| $\omega_3$ (FEM) | 8347  | 13042 | 23187 | 52166 |
| % difference     | 2.73  | 2.86  | 2.87  | 3.20  |

**Table 5.23** Comparison of natural frequencies for configuration B-Clamped-clamped boundary condition

|                  |       |       |       |       |
|------------------|-------|-------|-------|-------|
| Angle (deg)      | 0.344 | 0.43  | 0.573 | 0.86  |
| L,m              | 0.25  | 0.2   | 0.15  | 0.1   |
| L/H              | 56    | 44    | 33    | 22    |
| $\omega_1$ (R-R) | 2135  | 3322  | 5897  | 13225 |
| $\omega_1$ (FEM) | 2178  | 3404  | 6050  | 13619 |
| % difference     | 2.02  | 2.47  | 2.60  | 2.98  |
| $\omega_2$ (R-R) | 5716  | 8910  | 15810 | 35548 |
| $\omega_2$ (FEM) | 5837  | 9121  | 16215 | 36482 |
| % difference     | 2.13  | 2.37  | 2.56  | 2.63  |
| $\omega_3$ (R-R) | 11092 | 17283 | 30643 | 68897 |
| $\omega_3$ (FEM) | 11322 | 17691 | 31451 | 70762 |
| % difference     | 2.08  | 2.37  | 2.64  | 2.71  |

**Table 5.24** Comparison of natural frequencies for configuration B-Clamped-free boundary condition

|                  |       |       |       |       |
|------------------|-------|-------|-------|-------|
| Angle (deg)      | 0.344 | 0.43  | 0.573 | 0.86  |
| L,m              | 0.25  | 0.2   | 0.15  | 0.1   |
| L/H              | 56    | 44    | 33    | 22    |
| $\omega_1$ (R-R) | 733   | 1139  | 2024  | 4540  |
| $\omega_1$ (FEM) | 751   | 1170  | 2080  | 4693  |
| % difference     | 2.54  | 2.71  | 2.78  | 3.36  |
| $\omega_2$ (R-R) | 2643  | 4129  | 7337  | 16477 |
| $\omega_2$ (FEM) | 2710  | 4233  | 7526  | 16939 |
| % difference     | 2.51  | 2.52  | 2.58  | 2.80  |
| $\omega_3$ (R-R) | 6276  | 9803  | 17417 | 39122 |
| $\omega_3$ (FEM) | 6420  | 10031 | 17832 | 40122 |
| % difference     | 2.29  | 2.32  | 2.38  | 2.55  |

**Table 5.25** Comparison of natural frequencies for configuration C-Simply-supported boundary condition

|                  |       |       |       |       |
|------------------|-------|-------|-------|-------|
| Angle (deg)      | 0.344 | 0.43  | 0.573 | 0.86  |
| L,m              | 0.25  | 0.2   | 0.15  | 0.1   |
| L/H              | 56    | 44    | 33    | 22    |
| $\omega_1$ (R-R) | 809   | 1268  | 2246  | 5053  |
| $\omega_1$ (FEM) | 827   | 1296  | 2299  | 5175  |
| % difference     | 2.16  | 2.21  | 2.35  | 2.41  |
| $\omega_2$ (R-R) | 3493  | 5456  | 9699  | 21821 |
| $\omega_2$ (FEM) | 3589  | 5609  | 9970  | 22433 |
| % difference     | 2.75  | 2.79  | 2.79  | 2.80  |
| $\omega_3$ (R-R) | 7840  | 12238 | 21740 | 48911 |
| $\omega_3$ (FEM) | 8013  | 12521 | 22259 | 50080 |
| % difference     | 2.20  | 2.32  | 2.39  | 2.39  |

**Table 5.26** Comparison of natural frequencies for configuration C-Clamped-clamped boundary condition

|                  |        |        |        |       |
|------------------|--------|--------|--------|-------|
| Angle (deg)      | 0.344  | 0.43   | 0.573  | 0.86  |
| L,m              | 0.25   | 0.2    | 0.15   | 0.1   |
| L/H              | 56     | 44     | 33     | 22    |
| $\omega_1$ (R-R) | 1950.3 | 3046.4 | 5412.2 | 12154 |
| $\omega_1$ (FEM) | 2031   | 3174   | 5641   | 12693 |
| % difference     | 4.15   | 4.19   | 4.24   | 4.44  |
| $\omega_2$ (R-R) | 5286   | 8257   | 14671  | 32946 |
| $\omega_2$ (FEM) | 5540   | 8656   | 15388  | 34623 |
| % difference     | 4.80   | 4.83   | 4.89   | 5.09  |
| $\omega_3$ (R-R) | 10525  | 16456  | 29242  | 65697 |
| $\omega_3$ (FEM) | 10811  | 16892  | 30031  | 67566 |
| % difference     | 2.72   | 2.65   | 2.70   | 2.85  |

**Table 5.27** Comparison of natural frequencies for configuration C-Clamped-free boundary condition

|                  |       |      |       |       |
|------------------|-------|------|-------|-------|
| Angle (deg)      | 0.344 | 0.43 | 0.573 | 0.86  |
| L,m              | 0.25  | 0.2  | 0.15  | 0.1   |
| L/H              | 56    | 44   | 33    | 22    |
| $\omega_1$ (R-R) | 651   | 1025 | 1806  | 4092  |
| $\omega_1$ (FEM) | 680   | 1069 | 1890  | 4269  |
| % difference     | 4.57  | 4.29 | 4.66  | 4.31  |
| $\omega_2$ (R-R) | 2436  | 3805 | 6761  | 15182 |
| $\omega_2$ (FEM) | 2564  | 4006 | 7123  | 16026 |
| % difference     | 5.24  | 5.28 | 5.35  | 5.56  |
| $\omega_3$ (R-R) | 5833  | 9112 | 16343 | 36699 |
| $\omega_3$ (FEM) | 6122  | 9566 | 17008 | 38265 |
| % difference     | 4.96  | 4.99 | 4.07  | 4.27  |

**Table 5.28** Comparison of natural frequencies for configuration D-Simply-supported boundary condition

|                  |       |       |       |       |
|------------------|-------|-------|-------|-------|
| Angle (deg)      | 0.344 | 0.43  | 0.573 | 0.86  |
| L,m              | 0.25  | 0.2   | 0.15  | 0.1   |
| L/H              | 56    | 44    | 33    | 22    |
| $\omega_1$ (R-R) | 1065  | 1665  | 2958  | 6646  |
| $\omega_1$ (FEM) | 1019  | 1590  | 2826  | 6365  |
| % difference     | 4.31  | 4.44  | 4.48  | 4.23  |
| $\omega_2$ (R-R) | 4454  | 6958  | 12364 | 27776 |
| $\omega_2$ (FEM) | 4581  | 7157  | 12724 | 28629 |
| % difference     | 2.84  | 2.87  | 2.92  | 3.07  |
| $\omega_3$ (R-R) | 9971  | 15577 | 27677 | 62179 |
| $\omega_3$ (FEM) | 10351 | 16172 | 28750 | 64684 |
| % difference     | 3.81  | 3.82  | 3.88  | 4.03  |

**Table 5.29** Comparison of natural frequencies for configuration D-Clamped-clamped boundary condition

|                  |       |       |       |       |
|------------------|-------|-------|-------|-------|
| Angle (deg)      | 0.344 | 0.43  | 0.573 | 0.86  |
| L,m              | 0.25  | 0.2   | 0.15  | 0.1   |
| L/H              | 56    | 44    | 33    | 22    |
| $\omega_1$ (R-R) | 2523  | 3941  | 7003  | 15733 |
| $\omega_1$ (FEM) | 2570  | 4015  | 7140  | 16066 |
| % difference     | 1.87  | 1.89  | 1.96  | 2.12  |
| $\omega_2$ (R-R) | 6908  | 10792 | 19176 | 43080 |
| $\omega_2$ (FEM) | 6859  | 10717 | 19052 | 42865 |
| % difference     | 0.71  | 0.69  | 0.64  | 0.50  |
| $\omega_3$ (R-R) | 13503 | 21093 | 37478 | 84198 |
| $\omega_3$ (FEM) | 13725 | 21446 | 38126 | 85779 |
| % difference     | 1.65  | 1.68  | 1.73  | 1.88  |

**Table 5.30** Comparison of natural frequencies for configuration D-Clamped-free boundary condition

|                  |       |       |       |       |
|------------------|-------|-------|-------|-------|
| Angle (deg)      | 0.344 | 0.43  | 0.573 | 0.86  |
| L,m              | 0.25  | 0.2   | 0.15  | 0.1   |
| L/H              | 56    | 44    | 33    | 22    |
| $\omega_1$ (R-R) | 850   | 1326  | 2355  | 5294  |
| $\omega_1$ (FEM) | 869   | 1357  | 2411  | 5425  |
| % difference     | 2.22  | 2.33  | 2.39  | 2.47  |
| $\omega_2$ (R-R) | 3088  | 4825  | 8567  | 19262 |
| $\omega_2$ (FEM) | 3154  | 4927  | 8761  | 19711 |
| % difference     | 2.13  | 2.11  | 2.26  | 2.34  |
| $\omega_3$ (R-R) | 7422  | 11594 | 20601 | 46280 |
| $\omega_3$ (FEM) | 7582  | 11847 | 21061 | 47386 |
| % difference     | 2.16  | 2.19  | 2.24  | 2.39  |

Tables 5.19-5.30 show the comparison of first four natural frequencies for simply-supported, clamped-clamped, and clamped-free boundary conditions of thickness-and width-tapered composite beams for case 2. The comparisons of natural frequencies were made between Rayleigh-Ritz method and conventional finite element method. From the above tables, the comparison differences for configuration A <5%, for configuration B it

is <4%, for configuration C it is <6% and for configuration D it is <4.5%. This difference in natural frequencies is expected from the inside geometry variation; the location of plies drop-off, because frequencies calculated for different taper configurations depend on the stiffness of the beam. From the above tables, the comparisons the difference in natural frequencies are well accepted.

## **5.5 Buckling response of thickness- and width-tapered laminated composite columns**

In this section buckling response of thickness- and width-tapered laminated composite columns are considered for simply-supported, clamped-clamped and clamped-free boundary conditions. The taper configurations shown in Figure 5.1 are used for buckling response. Rayleigh-Ritz method is used to find the critical buckling load of thickness- and width-tapered composite columns. Comprehensive parametric studies have been shown through plots.

### **5.5.1 Effect of angle of thickness-taper ( $\phi$ ) and width ratio ( $b_R/b_L$ ) on critical buckling load**

To investigate effects of angle of thickness-taper ( $\phi$ ) and width ratio ( $b_R/b_L$ ) on critical buckling load, the thickness- and width-tapered laminated composite columns of simply-supported, clamped-clamped, and clamped-free boundary conditions are

considered for buckling response. The results are summarized in the Figures 5.9-5.12. Different cases of thickness- and width-taper configurations as shown in the Table 5.3 are considered to study the angle of thickness-taper ( $\phi$ ) and width ratio ( $b_R/b_L$ ) on critical buckling load.

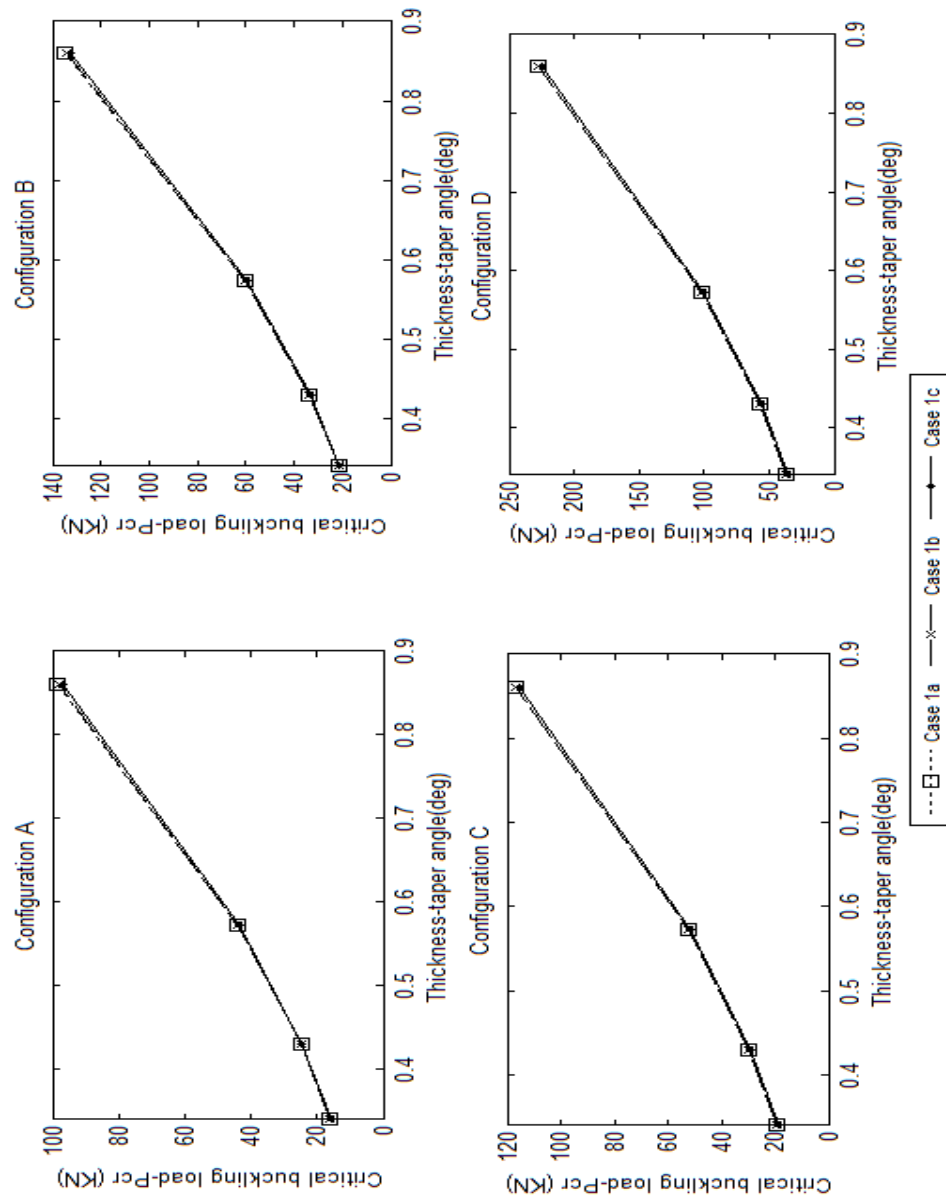


**Figure 5.9** Effect of angle of thickness-taper ( $\phi$ ) and width ratio ( $b_R/b_L$ ) on critical buckling load for simply-supported boundary condition

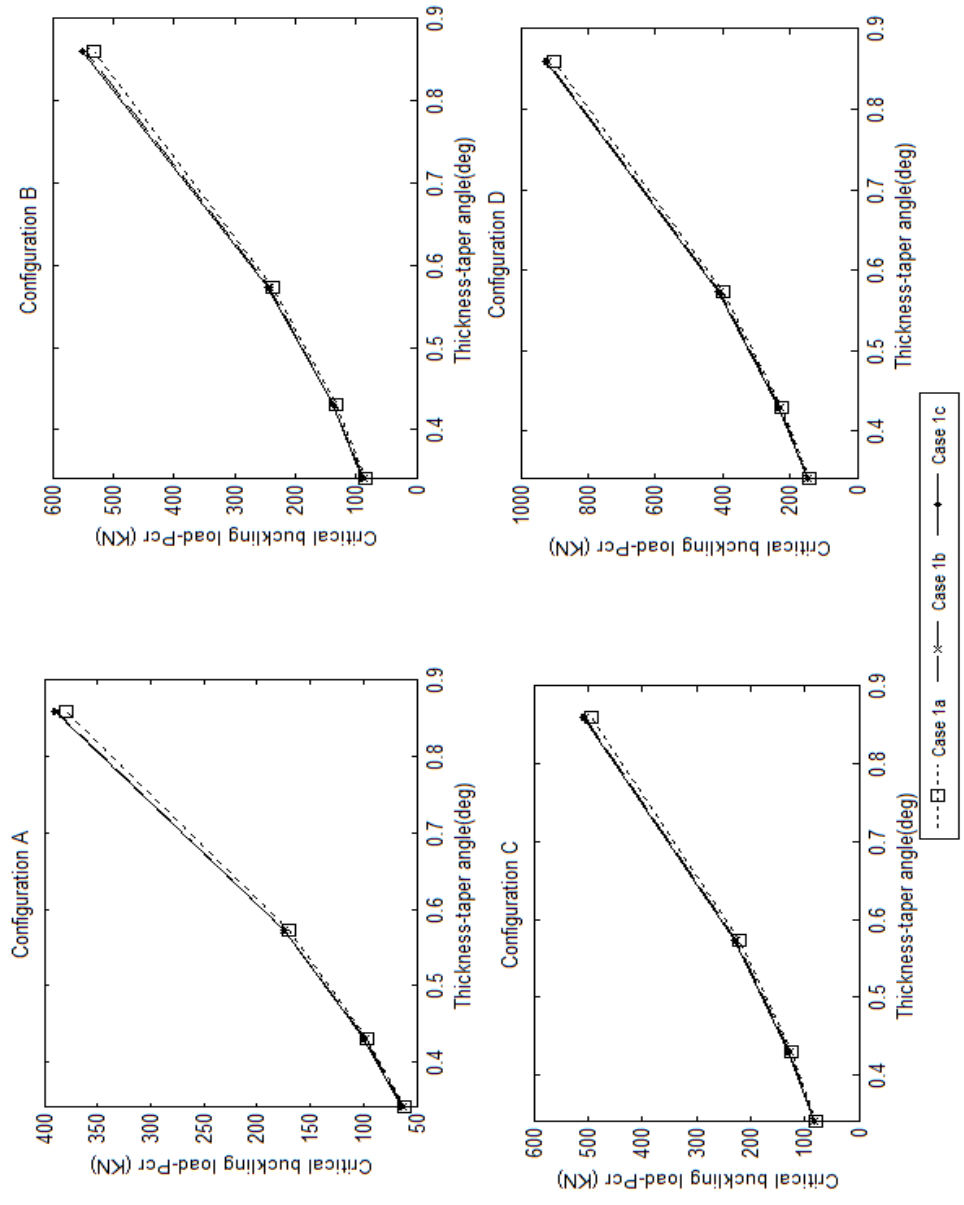


**Figure 5.10** Effect of angle of thickness-taper ( $\phi$ ) and width ratio ( $b_R/b_L$ ) on critical buckling load for clamped-clamped boundary condition

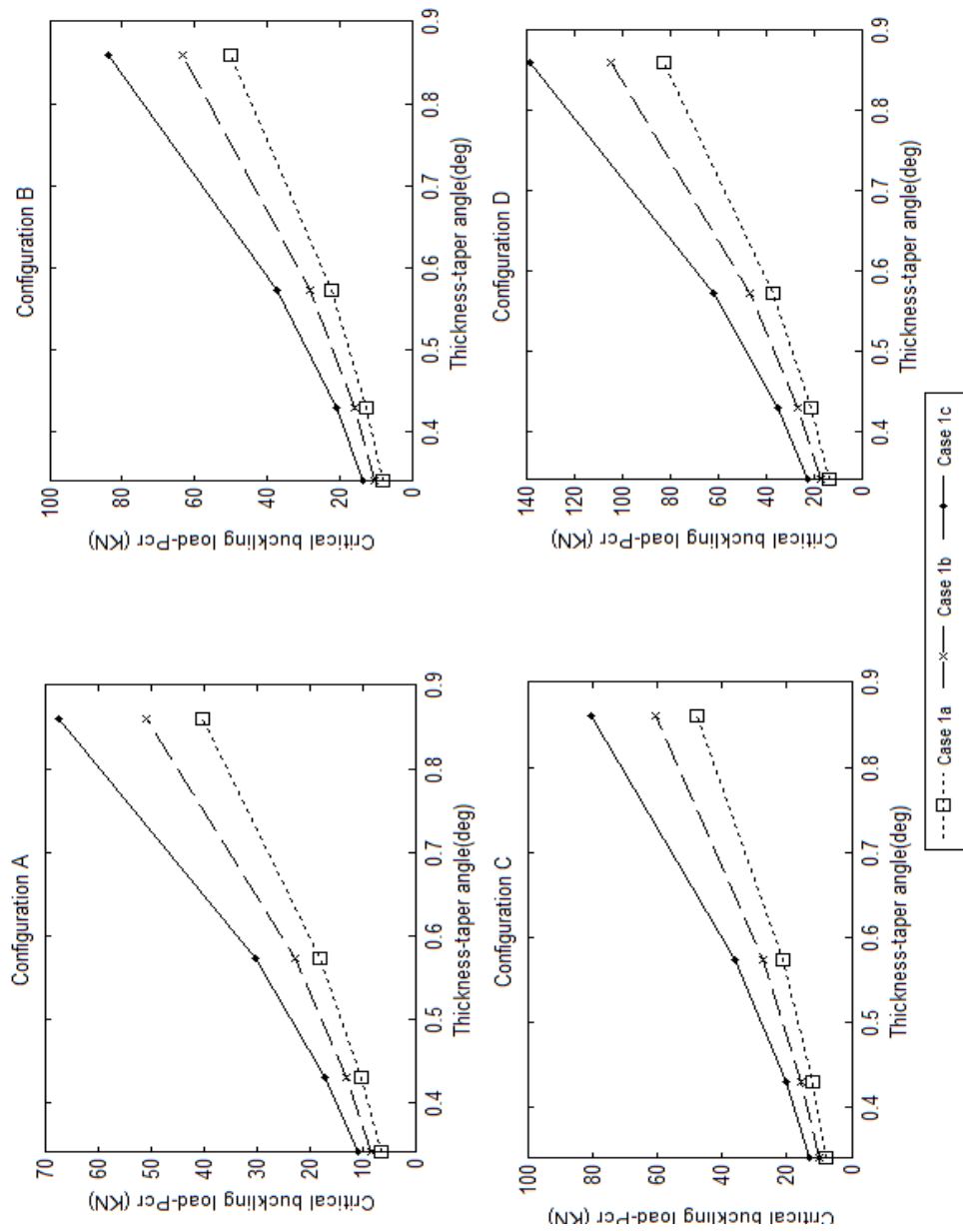


**Figure 5.11** Effect of angle of thickness-taper ( $\phi$ ) and width ratio ( $b_R/b_L$ ) on critical buckling load for clamped-free boundary condition

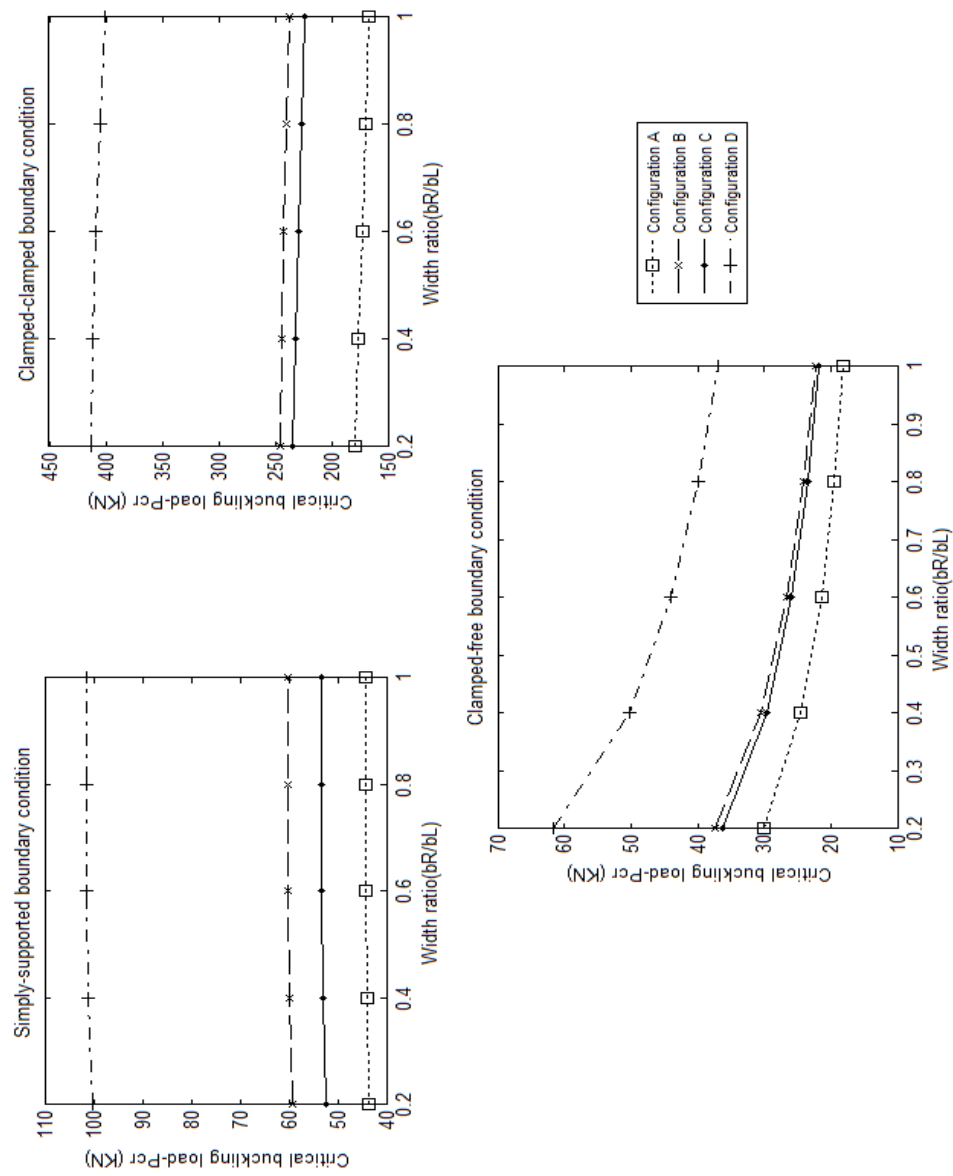


**Figure 5.12** Effect of constant angle of thickness-taper ( $\phi$ ) of  $0.57^\circ$  and width ratio ( $b_R/b_L$ ) (case 2) on critical buckling load

Figures 5.9-5.12 show the effect of angle of thickness-taper ( $\phi$ ) and width ratio ( $b_R/b_L$ ) on critical buckling load ( $P_{cr}$ ) for simply-supported, clamped-clamped, and clamped-free boundary conditions of thickness- and width-tapered laminated composite columns. It can be observed from the Figures 5.9-5.12, that the critical buckling load ( $P_{cr}$ ) is highest for case 1c, second highest for case 1b and lowest for case 1a for all the three boundary conditions. This indicates that as the angle of thickness-taper ( $\phi$ ) is increased and width ratio ( $b_R/b_L$ ) value is decreased, the stiffness of the column increases for all three boundary conditions. Also one can observe from the Figure 5.9 that the difference in the critical buckling loads between case 1a, 1b and 1c for clamped-free boundary condition are largest compared to other boundary conditions. Figure 5.12 shows the effect of variation of width ratio ( $b_R/b_L$ ) with constant angle of thickness-taper ( $\phi$ ) of  $0.57^\circ$  on critical buckling load ( $P_{cr}$ ) of thickness- and width-tapered composite column. One can observe from the Figure 5.12 that the critical buckling load ( $P_{cr}$ ) is largest for configuration D, because the stiffness of the beam is largest compared to the other configurations. Second largest is configuration B, third largest and fourth largest are configurations C and A respectively for all three boundary conditions. It can also be observed that as the width ratio ( $b_R/b_L$ ) values increase for constant angle of thickness-taper ( $\phi$ ) of  $0.57^\circ$ , the critical buckling load ( $P_{cr}$ ) is increased for simply-supported boundary condition, but for clamped-clamped boundary the critical buckling load ( $P_{cr}$ ) increase until width ratio ( $b_R/b_L$ ) value is increased from 0.2 upto 0.4, but decrease as the width ratio value increase from 0.6 to 1. For the case of clamped-free boundary condition, the critical buckling load ( $P_{cr}$ ) decreases as the width ratio ( $b_R/b_L$ ) value increase from 0.2 to 1.

### 5.5.2 Effect of laminate configuration on critical buckling load

In this section the effect of laminate configurations on critical buckling load ( $P_{cr}$ ) for thickness- and width-tapered laminated composite columns are obtained using Rayleigh-Ritz method. The Tables 5.31-5.33 show the variation of critical buckling load ( $P_{cr}$ ) for simply-supported, clamped-clamped and clamped-free boundary conditions. The laminate configurations considered are: 1)  $([0/90]_9)_s$  denoted as 'LC1', 2)  $([\pm 45]_9)_s$  denoted as 'LC2', 3)  $([0_4/\pm 45_7])_s$  denoted as 'LC3'.

**Table 5.31** Comparison of critical buckling load-Simply-supported boundary condition

| Beam configuration | Laminate configuration | Pcr (KN) |
|--------------------|------------------------|----------|
| A                  | LC1                    | 28.9     |
|                    | LC2                    | 15.5     |
|                    | LC3                    | 23.6     |
| B                  | LC1                    | 21.6     |
|                    | LC2                    | 11.4     |
|                    | LC3                    | 17.7     |
| C                  | LC1                    | 19.1     |
|                    | LC2                    | 9.7      |
|                    | LC3                    | 16.1     |
| D                  | LC1                    | 36.5     |
|                    | LC2                    | 13.7     |
|                    | LC3                    | 21.5     |

**Table 5.32** Comparison of critical buckling load -Clamped-clamped boundary condition

| Beam configuration | Laminate configuration | Pcr (KN) |
|--------------------|------------------------|----------|
| A                  | LC1                    | 114.9    |
|                    | LC2                    | 62.2     |
|                    | LC3                    | 93.7     |
| B                  | LC1                    | 87.8     |
|                    | LC2                    | 45.3     |
|                    | LC3                    | 71.8     |
| C                  | LC1                    | 83.2     |
|                    | LC2                    | 41.3     |
|                    | LC3                    | 69.4     |
| D                  | LC1                    | 147.8    |
|                    | LC2                    | 55.2     |
|                    | LC3                    | 87.7     |

**Table 5.33** Comparison of critical buckling load - Clamped-free boundary condition

| Beam configuration | Laminate configuration | Pcr (KN) |
|--------------------|------------------------|----------|
| A                  | LC1                    | 9.4      |
|                    | LC2                    | 5.1      |
|                    | LC3                    | 7.7      |
| B                  | LC1                    | 10.2     |
|                    | LC2                    | 5.4      |
|                    | LC3                    | 8.3      |
| C                  | LC1                    | 9.9      |
|                    | LC2                    | 5.1      |

|   |     |      |
|---|-----|------|
|   | LC3 | 8.3  |
| D | LC1 | 16.8 |
|   | LC2 | 6.0  |
|   | LC3 | 9.5  |

Tables 5.31-5.33 show the effect of laminate configuration on critical buckling load ( $P_{cr}$ ) with angle of thickness-taper ( $\phi$ ) value of  $0.57^\circ$  and width ratio ( $b_R/b_L$ ) value of 0.5 for three boundary conditions. One can observe from the Tables 5.31- 5.33 that the results obtained for different laminate configuration show that critical buckling load ( $P_{cr}$ ) is largest for laminate configuration LC1, second largest for laminate configuration LC3 and lowest for laminate configuration LC2. This difference in critical buckling load ( $P_{cr}$ ) is due to the variation of stiffness in the column. Also the critical buckling load ( $P_{cr}$ ) is largest for beam configuration D of the taper configuration with second largest for model B, third largest for model C and lowest for beam configuration A. This difference in critical buckling load for different beam configuration is expected because of the variation of stiffness in the tapered model.

### 5.5.3 Effect of boundary condition on critical buckling load

In this section the effect of boundary condition on critical buckling load ( $P_{cr}$ ) for thickness and width- tapered column are obtained using Rayleigh-Ritz method. The

angle of thickness-taper ( $\phi$ ) value of  $0.57^\circ$  and width ratio ( $b_R/b_L$ ) value of 0.5 is considered to find the critical buckling load for simply-supported, clamped-clamped and clamped-free boundary conditions. The critical buckling load ( $P_{cr}$ ) for all three boundary conditions is obtained using Rayleigh-Ritz method.

**Table 5.34** Comparison of critical buckling load -Simply-supported boundary condition

| Beam configuration | Laminate configuration | $P_{cr}$ (KN) |
|--------------------|------------------------|---------------|
| A                  | LC1                    | 28.9          |
| B                  | LC1                    | 21.6          |
| C                  | LC1                    | 19.1          |
| D                  | LC1                    | 36.5          |

**Table 5.35** Comparison of critical buckling load -Clamped-clamped boundary condition

| Beam configuration | Laminate configuration | $P_{cr}$ (KN) |
|--------------------|------------------------|---------------|
| A                  | LC1                    | 114.9         |
| B                  | LC1                    | 87.8          |
| C                  | LC1                    | 83.2          |
| D                  | LC1                    | 147.8         |

**Table 5.36** Comparison of critical buckling load -Clamped-free boundary condition

| Beam configuration | Laminate configuration | $P_{cr}$ (KN) |
|--------------------|------------------------|---------------|
| A                  | LC1                    | 9.4           |
| B                  | LC1                    | 10.2          |
| C                  | LC1                    | 9.9           |
| D                  | LC1                    | 16.8          |

Tables 5.34-5.36 show the effect of boundary conditions on critical buckling load ( $P_{cr}$ ) for thickness- and width- tapered laminated composite column. From the Tables 5.34-5.36, one can observe that the critical buckling load ( $P_{cr}$ ) is largest for clamped-clamped boundary condition because the stiffness of the column is largest. Column with clamped-free (cantilever) boundary condition has lowest critical buckling load ( $P_{cr}$ ) this is because of lower stiffness. The critical buckling load ( $P_{cr}$ ) is second largest for simply-supported boundary condition. Also, one can observe the critical buckling load ( $P_{cr}$ ) is largest for beam configuration model D and lowest for beam configuration A, second largest for beam configuration B and third largest for beam configuration C.

## **5.6 Comparison of forced response in terms of sinusoidal transverse displacement between Rayleigh-Ritz method and conventional finite element method**

By using the mechanical and geometric properties given in section 5.3.1 and considering case 2 from Table 5.3, the current section presents the comparison of forced response in terms of sinusoidal transverse displacement for simply-supported, clamped-free and clamped-clamped boundary conditions of thickness- and width-tapered laminated composite beams obtained by using Rayleigh-Ritz method with that obtained using conventional finite element method [81]. A sinusoidal force of magnitude 2N with excitation frequency  $\omega$  is applied at the maximum excitation point conditions. For simply-supported boundary and clamped-clamped boundary condition the excitation point applied at the centre of the tapered composite beam, while for clamped-free boundary condition the excitation point is applied on the free end of the beam. The compared results are presented in the Figures 5.13-5.15 below.

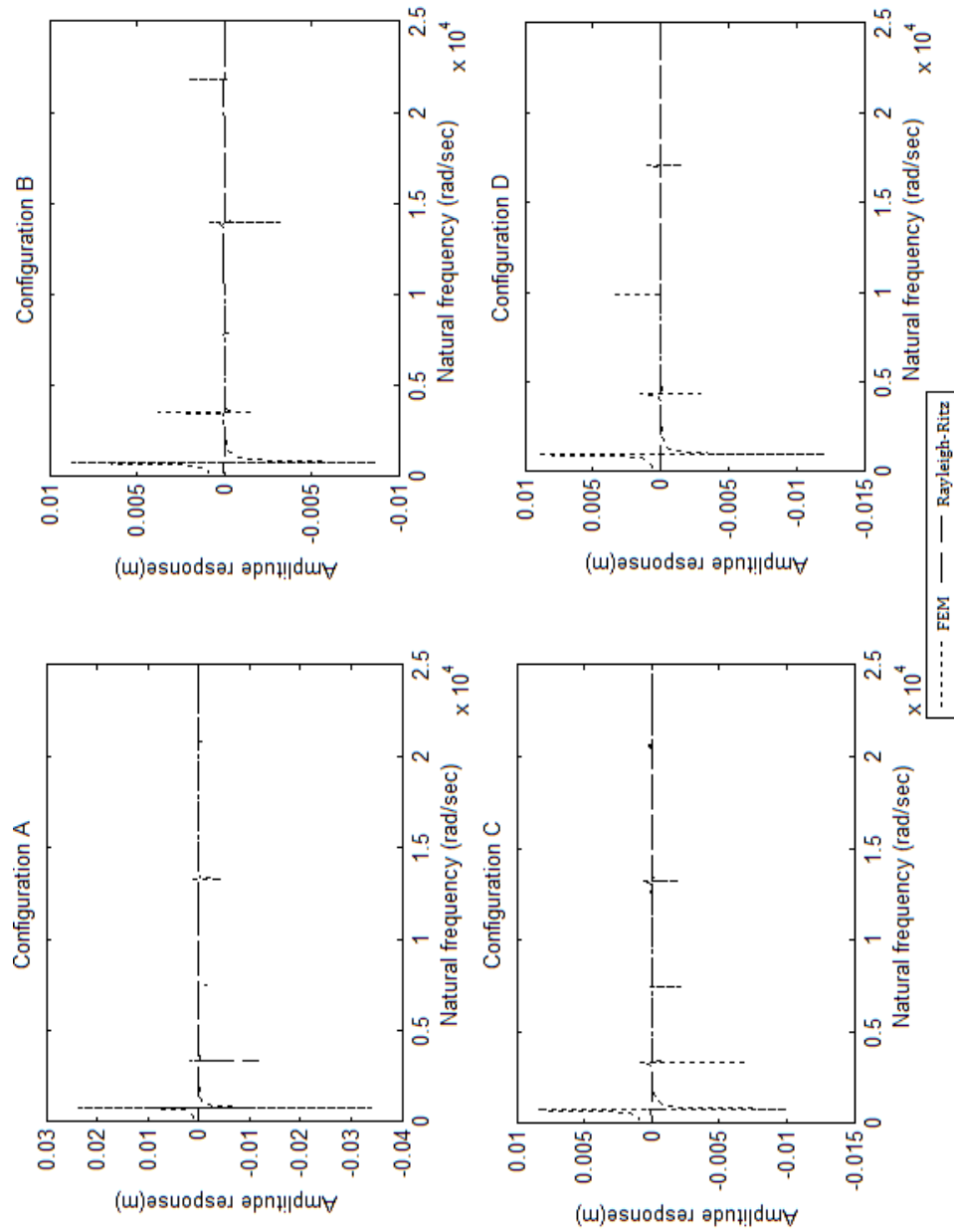


**Figure 5.13** Comparison of forced response in terms of sinusoidal transverse displacement- simply-supported boundary condition

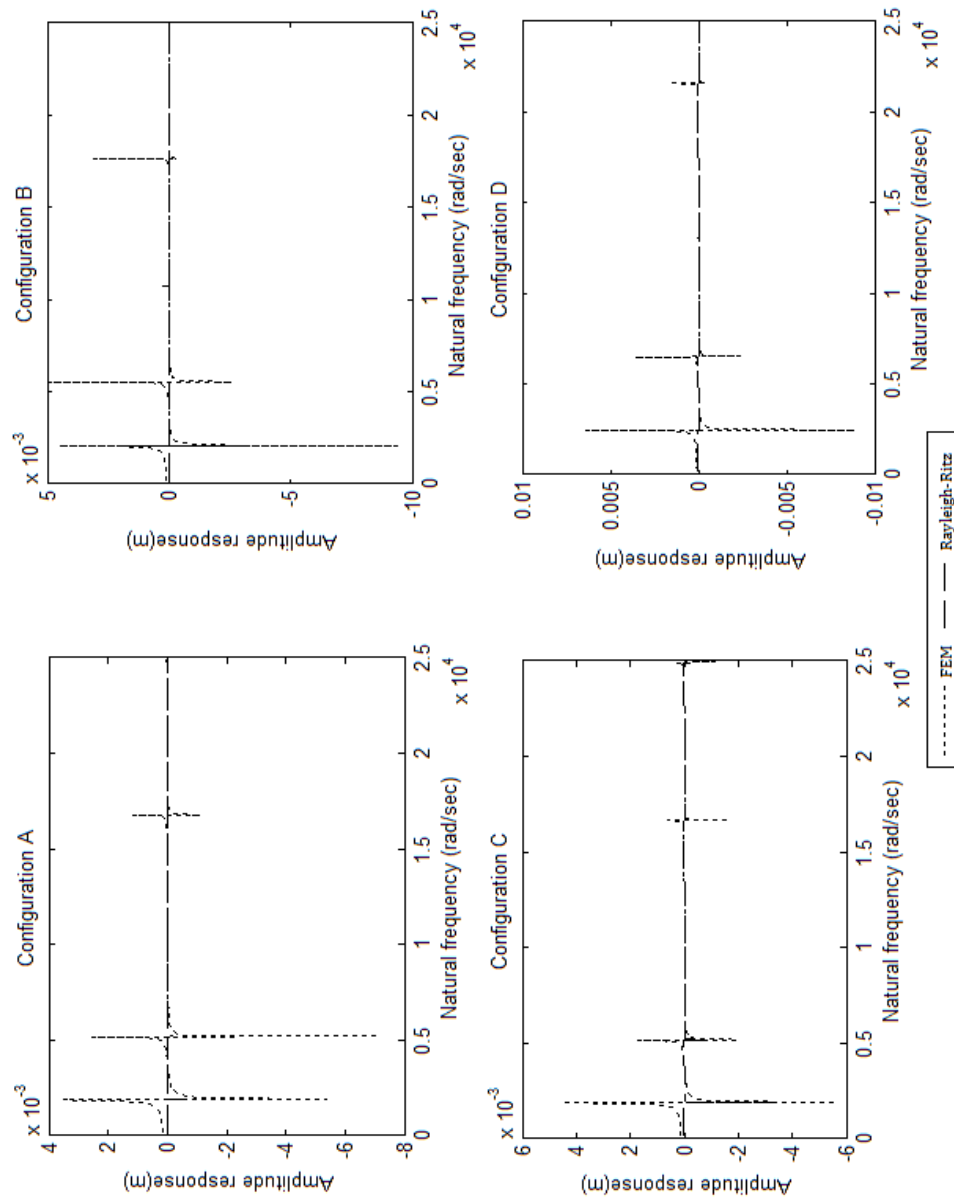


**Figure 5.14** Comparison of forced response in terms of sinusoidal transverse displacement- clamped-clamped boundary condition

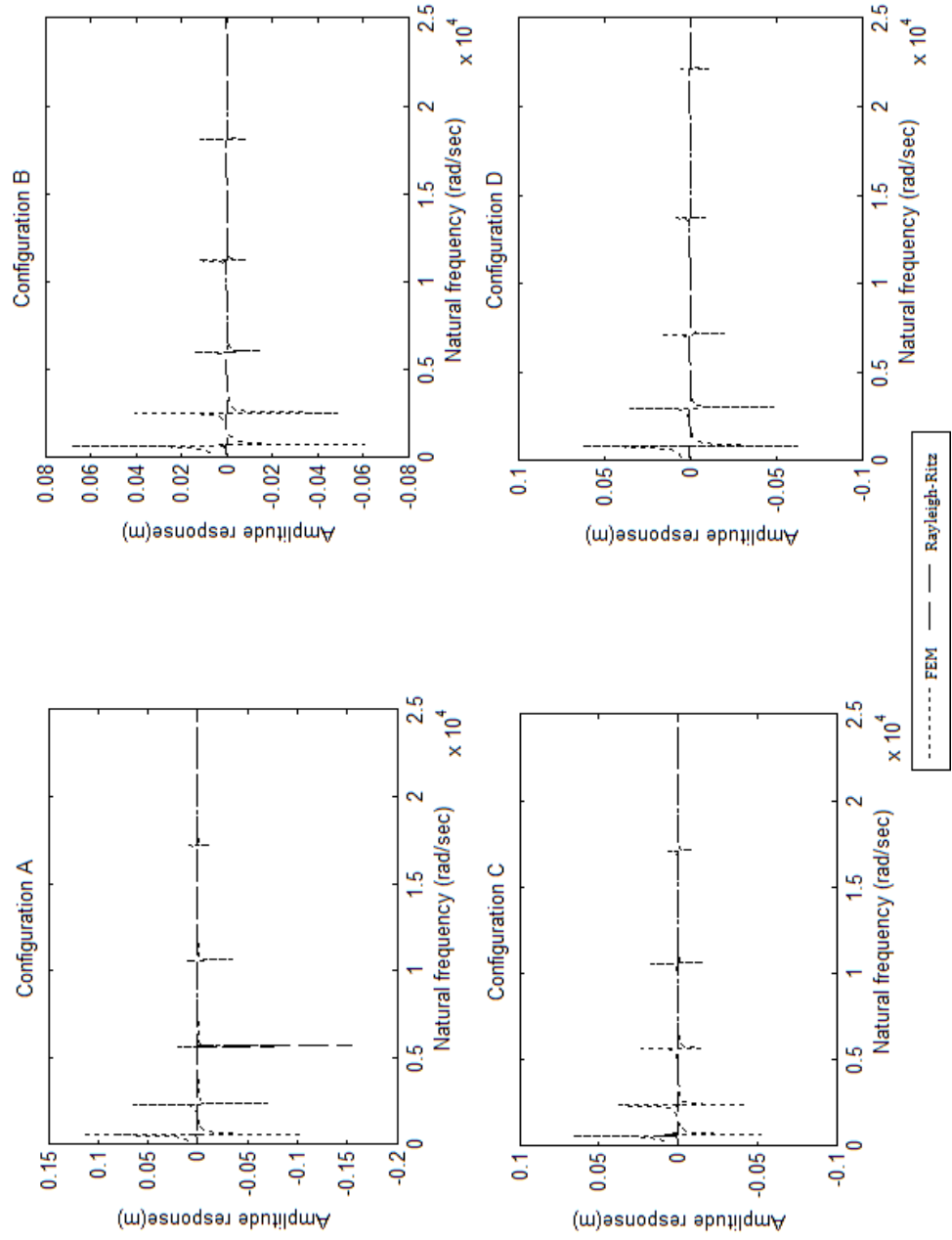


**Figure 5.15** Comparison of forced response in terms of sinusoidal transverse displacement- clamped-free boundary condition

Figures 5.13-5.15 show the comparison of forced response in terms of sinusoidal transverse displacement for simply-supported, clamped-clamped and clamped-free boundary conditions for thickness-and width-tapered composite beams with angle of thickness-taper ( $\phi$ ) value of  $0.57^\circ$  and width ratio ( $b_R/b_L$ ) value of 0.5. From the Figures 5.13-5.15, the comparison difference for simply-supported boundary condition is between 5-7%, for clamped-clamped boundary condition it is between 4-6% and for clamped-free boundary condition it is between 5-7%. The comparison differences in transverse displacement from the above Figures 5.18-5.20 are well accepted.

## 5.7 Summary

In this chapter, the energy formulation for dynamic response of thickness- and width tapered laminated composite beams based on one-dimensional laminated beam theory is derived following Chapter-02. Rayleigh-Ritz method is used for dynamic response of thickness- and width-tapered laminated composite beams. From the numerical results through graphical plots and tables, the following conclusions are drawn:

- As the angle of thickness-taper ( $\phi$ ) and width ratio ( $b_R/b_L$ ) increase, all four modes of natural frequencies increase for all three boundary conditions. The natural frequencies are highest for case 1c, second highest for case 1b and lowest for case 1a. For clamped-free boundary condition, the natural frequencies are highest for case 1c and lowest for

case 1a and second highest for case 1b. The natural frequencies are highest for configuration D, second highest for configuration B, third highest for configuration C and the lowest for configuration A.

- In case 2, for simply-supported boundary condition as the width ratio ( $b_R/b_L$ ) value increase, the first natural frequency increases for all the thickness- and width-taper beam configurations. The second, third and fourth natural frequencies remain constant as the width ratio value increases. For clamped-clamped boundary condition, all four modes of natural frequencies increase with highest natural frequencies for configuration D, second highest for configuration B, third highest for configuration C and lowest for configuration A. For the clamped-free boundary condition, as the width-ratio ( $b_R/b_L$ ) value increase from 0.2 to 1 with constant angle of thickness-taper ( $\phi$ ) of  $0.57^\circ$ , the natural frequencies decrease.

- The natural frequencies are largest for laminate configuration LC1, second largest for laminate configuration LC3 and lowest for laminate configuration LC2. Also the natural frequencies is largest for beam configuration D, second largest for beam configuration B, third largest for beam configuration C and lowest for beam configuration A.

- The natural frequencies are largest for clamped-clamped boundary condition. Beam with clamped-free (cantilever) boundary condition has the lowest natural frequencies. The natural frequencies are second largest for simply-supported boundary condition. Also, one can observe natural frequencies are largest for beam configuration D and lowest for beam configuration A, second largest for beam configuration B and third largest for beam configuration C.

- The comparison between Rayleigh-Ritz method developed from the current thesis and conventional finite element method [81] is compared for four natural frequencies for thickness- and width-tapered composite beams for case 2. The differences between the two methods are well accepted.
- As end axial tensile force is increased the natural frequencies increase, but decrease for compressive force for all three boundary conditions.
- The natural frequencies of un-damped beam are higher than the natural frequencies with damping for all boundary conditions
- The critical buckling load ( $P_{cr}$ ) is highest for case 1c, second highest for case 1b and lowest for case 1a for all the three boundary conditions. For the effect of variation of width ratio ( $b_R/b_L$ ) with constant angle of thickness-taper ( $\phi$ ) of  $0.57^\circ$ , the critical buckling load ( $P_{cr}$ ), is largest for configuration D, second largest is configuration B, third largest and fourth largest are configurations C and A respectively for all three boundary conditions. As the width ratio ( $b_R/b_L$ ) values increase for constant angle of thickness-taper ( $\phi$ ) of  $0.57^\circ$ , the critical buckling load ( $P_{cr}$ ) is increased for simply-supported boundary condition, but for clamped-clamped boundary the critical buckling load ( $P_{cr}$ ) increase until width ratio ( $b_R/b_L$ ) value is increased from 0.2 upto 0.4, but decrease as the width ratio value increase from 0.6 to 1. For clamped-free boundary condition, the critical buckling load ( $P_{cr}$ ) decreases as the width ratio ( $b_R/b_L$ ) value increase from 0.2 to 1
- The critical buckling load ( $P_{cr}$ ) is largest for laminate configuration LC1, second largest for laminate configuration LC3 and lowest for laminate configuration LC2. This difference in critical buckling load ( $P_{cr}$ ) is due to the variation of stiffness in the

column. The critical buckling load ( $P_{cr}$ ) is largest for beam configuration D of the taper configuration with second largest for beam configuration B, third largest for beam configuration C and lowest for beam configuration A.

- The critical buckling load ( $P_{cr}$ ) is largest for clamped-clamped boundary condition because the stiffness of the column is largest. Column with clamped-free (cantilever) boundary condition has lowest critical buckling load ( $P_{cr}$ ) this is because of lower stiffness. The critical buckling load ( $P_{cr}$ ) is second largest for simply-supported boundary condition.

- The comparisons of transverse displacement for thickness- and width-tapered composite beams between Rayleigh-Ritz method and conventional finite element method show the difference in transverse displacement for simply-supported boundary condition is between 5-7%, for clamped-clamped boundary condition it is between 4-6% and for clamped-free boundary condition it is between 5-7%.

- The present study helps the designer in the selection of the angle of thickness-taper ( $\phi$ ) and width ratio ( $b_R/b_L$ ) so as to shift the natural frequencies as desired or to control the vibration level.

## CHAPTER 6

### CONCLUSIONS AND RECOMMENDATIONS

#### 6.1 Major contributions

The primary objectives of the research work are: (1) To investigate the free and forced vibration and buckling response of width-tapered and thickness- and width-tapered laminated composite beams obtained using Rayleigh-Ritz method, (2) To conduct a detailed parametric study on the effects of various material, geometric and structural properties on the dynamic response of tapered composite beams, (3) To conduct modal testing using impact hammer excitation to determine the Frequency Response Function (FRF) of width-tapered composite beams.

Following are considered to be the major contributions of the study:

- a) The Rayleigh-Ritz formulation has been used and the efficiency and accuracy are established very systematically. Formulations have been developed based on Kirchhoff one dimensional laminated beam theory for free and forced vibrations of width-tapered and thickness- and width-tapered composite beams including damping and end-axial force effects, and for buckling response of tapered composite columns.

- b) The first-ply failure analysis using Tsai-Wu failure criterion is conducted for  $[(0/90)_9]_s$  laminate and the results are used to determine the effect of static end-axial force on the free and forced vibration response of tapered laminated composite beams.
- c) Free and forced response results obtained using Rayleigh-Ritz method are compared with that obtained using conventional finite element formulation [81]. The free vibration response results are also validated using experimental modal testing.
- d) The codes of programming, involving numerical and symbolic computations are written in MATLAB software. The beam properties such as stiffness matrix, mass matrix and force matrix are computed numerically using individual sub-programs.
- e) A detailed parametric study has been conducted using the above mentioned theoretical and experimental developments to determine the influence of the material properties, geometric properties, structural properties and applied axial force on the natural frequencies and modal displacement response. The effects of width ratio, taper configuration, taper angle, length ratio, boundary conditions, laminate configurations, static end-axial force, and damping on natural frequencies and modal displacement response are studied.
- f) Experimental modal analysis is conducted for the determination of Coherence function, time and auto-response function and Frequency Response Function (FRF) of width-tapered laminated composite beams with different width ratios. The damping loss factor ( $\eta$ ) is extracted from FRF plots using half-power bandwidth method.

## 6.2 Conclusions

The most important and principal conclusions of the present thesis that provides insight on the dynamic behaviour of width-tapered and thickness- and width- tapered composite beams for design purpose are given in the following:

a) As the width ratio ( $b_R/b_L$ ) values of the beam increases, the natural frequencies increase for simply-supported, clamped-clamped and free-clamped boundary conditions, but decrease for clamped-free boundary condition. Increasing the width ratio ( $b_R/b_L$ )

results in increase in the value of bending stiffness term  $\left( \frac{1}{D_{11}^*(x)} \right)$ , which in turn results in

increase in stiffness matrix coefficients.

b) As for the effect of laminate configuration on the natural frequencies of width-tapered composite beams, the natural frequencies are largest for laminate configuration LC3 (laminate with  $([0_4/\pm 45_7])_s$  configuration), second largest for LC1 (laminate with  $([0/90]_9)_s$  configuration), third largest for LC4 (laminate with  $([0/\pm 60]_6)_s$  configuration) and fourth largest for LC2 (laminate with  $([\pm 45]_9)_s$  configuration).

c) As the length ratio ( $L_1/L_3$ ) increases, all the natural frequencies increase. Also the natural frequencies increase as the width ratio ( $b_R/b_L$ ) increases for simply-supported, clamped-clamped and free-clamped boundary conditions, but decrease for clamped-free boundary condition.

d) Observations for different boundary conditions show that the beam with clamped-clamped boundary condition has the largest natural frequencies whereas free-clamped boundary condition has the lowest natural frequencies. The beams with simply-supported and clamped-free boundary conditions are second highest and third highest in natural frequencies respectively. As the compressive axial load is increased from 0 to 95 % of critical buckling load, the natural frequencies decrease. As the tensile axial load is increased from 0% to 95 % of tensile failure load, the natural frequencies increase. The damped natural frequencies are less than that obtained without damping.

e) As the width ratio value increases the critical buckling load increases for simply-supported, clamped-clamped and free-clamped boundary conditions, but decrease for clamped-free boundary condition. The critical buckling load is largest for laminate configuration LC3, second largest for LC1, third largest for LC4 and fourth largest for LC2. The critical buckling load is largest for length ratio ( $L_1/L_3$ ) value of 2 and least for length ratio ( $L_1/L_3$ ) value of 0.25. For the effect of different boundary conditions, the critical buckling load is largest for clamped-clamped boundary condition since the column is stiffer and is smallest for free-clamped boundary condition.

f) The first-ply failure loads for  $[(0/90)_9]_s$  laminate are calculated using Tsai-Wu theory. It was observed that the failure loads (tensile and compressive) are the lowest and highest for width ratios of respectively 0.01 and 1, for both  $0^\circ$  and  $90^\circ$  plies. This is because of the change in the cross-sectional stiffness of the beam.

g) It is concluded from the parametric study on forced response that the transverse displacement amplitude is largest for width ratio ( $b_R/b_L$ ) value of 0.2, second largest for

width ratio value of 0.5 and lowest for width ratio value of 1. The transverse displacement amplitude is largest for laminate configuration LC2, second largest for laminate configuration LC1, third largest for LC4 and lowest for laminate configuration LC3. The transverse displacement amplitude is largest for length ratio ( $L_1/L_3$ ) value of 0.25 and lowest for length ratio ( $L_1/L_3$ ) value of 2 for all four boundary conditions.

h) The transverse displacement amplitude is largest for clamped-free boundary condition and lowest for clamped-clamped boundary condition. The transverse displacement amplitude is largest for clamped-free boundary condition at excitation point 1, second largest for free-clamped boundary condition at excitation point 1, third highest for simply-supported at excitation points 2 and 3 and lowest for clamped-clamped boundary condition at excitation points 2 and 3. The transverse displacement amplitude decreases with increase in the percentage tensile failure load because the beam becomes stiffer by applying axial tensile load. Similarly, the transverse displacement amplitude increases with increase in percentage compressive failure load because the beam becomes less stiff by applying axial compressive load.

i) From the comparison of results obtained using Rayleigh-Ritz method with that obtained using conventional finite element method, the differences in natural frequencies and transverse displacement obtained for all cases are less than 6%. The results found with 8 to 15 trial functions of Rayleigh-Ritz method matched well with the results calculated by using conventional finite element method for width-tapered and thickness- and width-tapered composite beams for all taper configurations and all boundary conditions.

- j) Experimental modal analysis is conducted using impact hammer excitation. Modal testing for damping factor for finding out the damping in the beams is conducted using half-power bandwidth method [12]. The Frequency Response Function (FRF) is highest for width ratio ( $b_R/b_L$ ) value of 0.2 and it gradually decreases as width ratio ( $b_R/b_L$ ) value increases.
- k) Comparison of experimental modal analysis results and theoretical results for width-tapered composite beams shows good agreement between the natural frequencies.
- l) The observations from thickness- and width-tapered composite beams were made that, the natural frequencies are highest for case 1c, second highest for case 1b and lowest for case 1a. For clamped-free boundary condition, the natural frequencies are highest for case 1c and lowest for case 1a and second highest for case 1b. The natural frequencies are highest for configuration D, second highest for configuration B, third highest for configuration C and the lowest for configuration A.
- m) For simply-supported boundary condition as the width ratio ( $b_R/b_L$ ) value increase, the first natural frequency increase for all the thickness- and width-taper beam configurations. The second, third and fourth natural frequencies remain constant as the width ratio value increases. For clamped-clamped boundary condition, all four modes of natural frequencies increase with highest natural frequencies for configuration D, second highest for configuration B, third highest for configuration C and lowest for configuration A.
- n) The natural frequencies are largest for laminate configuration LC1, second largest for laminate configuration LC3 and lowest for laminate configuration LC2.

- o) The natural frequencies are largest for clamped-clamped boundary condition. Beam with clamped-free (cantilever) boundary condition has the lowest natural frequencies. The natural frequencies are second largest for simply-supported boundary condition.
- p) The comparison between Rayleigh-Ritz method developed from the current thesis and conventional finite element method [81] is compared for four natural frequencies for thickness- and width-tapered composite beams for case 2. The differences between the two methods are well accepted.
- q) The natural frequencies increase with an increase in end axial tensile force but decrease with increasing compressive force for all the three boundary conditions. The natural frequencies of undamped beam are higher than those with damping for all boundary conditions.
- r) The critical buckling load ( $P_{cr}$ ) is highest for case 1c, second highest for case 1b and lowest for case 1a for all the three boundary conditions. For the effect of variation of width ratio ( $b_R/b_L$ ) with constant angle of thickness-taper ( $\phi$ ) of  $0.57^\circ$ , the critical buckling load ( $P_{cr}$ ), is largest for configuration D, second largest is configuration B, third largest and fourth largest are configurations C and A respectively for all three boundary conditions.
- s) The critical buckling load ( $P_{cr}$ ) is largest for laminate configuration LC1, second largest for laminate configuration LC3 and lowest for laminate configuration LC2. This difference in critical buckling load ( $P_{cr}$ ) is due to the variation of stiffness in the column.
- t) The critical buckling load ( $P_{cr}$ ) is largest for clamped-clamped boundary condition Column with clamped-free (cantilever) boundary condition has lowest critical

buckling load ( $P_{cr}$ ) this is because of lower stiffness. The critical buckling load ( $P_{cr}$ ) is second largest for simply-supported boundary condition.

u) The comparisons of transverse displacement for thickness- and width-tapered composite beams between Rayleigh-Ritz method and conventional finite element method show the difference in transverse displacement for simply-supported boundary condition is between 5-7%, for clamped-clamped boundary condition it is between 4-6% and for clamped-free boundary condition it is between 5-7%.

### **6.3 Recommendations for future work**

The present study is an attempt to evaluate the effects of different material, geometric and structural parameters on the dynamic response of width-tapered and thickness-and width-tapered composite beams obtained using Rayleigh-Ritz method. The study of free and forced vibration and buckling response of tapered composite beams can be continued in the future studies as given in the following recommendations:

a) The free and forced vibration and buckling analyses of width-tapered composite beams and columns respectively obtained using Rayleigh-Ritz method presented in this thesis can be extended further combining with other advanced finite element methods such as higher order and hierarchical finite element.

- b) The free and forced vibration and buckling response obtained using Rayleigh-Ritz method presented in this thesis can be extended for free and forced vibration and buckling response of curved beam, plates and shells.
- c) The free and forced vibration of width-tapered composite beams obtained using Rayleigh-Ritz method presented in this thesis can be extended to transient and random vibrations.
- d) The experimental modal analysis conducted in the present thesis can be extended to analyze the Frequency Response Function (FRF) for tapered beams using non-classical boundary conditions.
- e) The methodology from the present study can be taken forward to optimize the geometric and material configurations of the laminated beam to avoid design critical response.

## BIBLIOGRAPHY

- [1] S.S.Rao, *Vibration of continuous systems*, 2007, Hoboken, N.J. Wiley.
- [2] R.M.Jones, *Mechanics of Composite Materials*, 1999, Second edition, Taylor and Francis, Philadelphia, PA.
- [3] Bertholet, J.M., *Composite Materials-Mechanical Behavior and Structural Analysis*, 1999, Springer-Verlag, New York.
- [4] Thomson, W.T. and Dahleh, M.D., *Theory of vibration with Application*, 1998, Fifth edition, Prentice Hall, New Jersey.
- [5] J.N.Reddy., *An Introduction to the Finite Element Method*, 1993, Second edition, McGraw-Hill, Inc.
- [6] J.N. Reddy., *Mechanics of Laminated Composite Plates and Shells: Theory and Analysis*, 2003, Second Edition, CRC Press, Inc.
- [7] Abarcar, R.B. and P.F. Cunniff., “The vibration of cantilever beams of fiber reinforced material”. *Journal of Composite Materials*, 1972, pp. 504–517.
- [8] Miller, A.K. and Adams, D.F., “An analytic means of determining the flexural and torsional resonant frequencies of generally orthotropic beams”. *Journal of Sound and Vibration*, Vol. 41(4), 1975, pp. 433-449.

- [9] J.R.Vinson and R.L. Sierakowski, *The Behavior of Structures composed of Composite Materials*, 2002, Second edition, Kluwer Academic Publishers.
- [10] Roy, P.K. and N. Ganesan., “A technical note on the response of a tapered beam”. *Computers and Structures*, Vol.45, No.1, 1992, pp.185-195.
- [11] He, K. Hoa, S.V. and Ganesan, R., “The study of tapered laminated composite structures: a review”, *Composites Science and Technology*, 2000, 60 (14), pp.2643-2657.
- [12] Steeves, C. A. and Fleck, N.A., “The compressive strength of composite laminates with terminated internal plies”. *Composites: Part A: Applied Science and Manufacturing*, 36, 2005, pp. 798–805.
- [13] Aydogdu, M., “Vibration analysis of cross-ply laminated beams with general boundary conditions by Ritz method”. *International Journal of Mechanical Sciences* 47, 2005, pp.1740–1755.
- [14] Boay, C.G. and Wee, Y.C., “The Coupling effects in bending, buckling and free vibration of generally laminated composite beams”. *Composites Science and Technology*, Vol. 68, Issues 7-8, June 2000, 60 (14), 1664–1670.
- [15] Hasan, O. and Sabuncu, M., “Stability analysis of a cantilever composite beam on elastic supports”. *Composites Science and Technology*, 65, 2005, pp.1982–1995.
- [16] Teoh, L.S. and Huang, C-C., “The vibration of beams of fibre reinforced materials”. *Journal of Sound and Vibration*, 1977, 51(4), pp.467–73.

- [17] Krishnaswamy, Chandrashekhara, K. and Wu, W.Z.B., “Analytical solutions to vibration of generally layered composite beams”. *Journal of Sound and Vibration* 1992; 159(1): pp.85–99.
- [18] Khdeir, A.A. and Reddy, J.N., “Free vibration of cross-ply laminated beams with arbitrary boundary conditions”. *International Journal of Engineering Sciences* 1994; 32(12): pp.1971–80.
- [19] Abromivich, H. and Livshits, A., “Free Vibration of Non-symmetric Cross-ply Laminated Composite beams”, *Journal of Sound and Vibration*, Vol.176 (5), 1994, pp.596-612.
- [20] Houmat, A., “Vibration of Timoshenko Beams by Variable order Finite Elements”, *Journal of Sound and Vibration*, Vol.187, 1995, pp.841-849.
- [21] Singh, M.P. and Abdelnassar, A.S., “Random response of Symmmetric Cross-ply Composite beams with arbitrary Boundary Conditions”, *AIAA Journal*, Vol.30 (4), 1992, pp.1081-1088.
- [22] Ganesan, R. and Zabihollah, A., “Vibration Analysis of Tapered Composite Beams using a Higher-order Finite Element; Part I: Formulation,” *Journal of Composite Structures*, vol. 77, pp. 309-318, 2007.
- [23] Ganesan, R. and Zabihollah, A., “Vibration Analysis of Tapered Composite Beams using a Higher-order Finite Element; Part II: Parametric Study, *Journal of Composite Structures*, vol.77, pp.319-330, 2007.

- [24] Ahmed, H.E.U., "Free and Forced Vibrations of tapered composite beams including the effects of axial force and damping", M.A.Sc.Thesis, 2008, Concordia University, Montreal, Canada.
- [25] Chen, L., "Free vibration analysis of tapered composite beams using Hierarchical finite element method", M.A.Sc.Thesis, 2004, Concordia University, Montreal, Canada.
- [26] Amit, K.O. and Yadav, D., "Forced nonlinear vibration of laminated composite plate with random material properties", Journal of Composite Structures, Vol.70, 2005, pp.334-342.
- [27] Asghar, N. Rakesh, K.K. and Reddy, J.N., "Forced vibration of low-velocity impact of laminated composite plates" Journal of Computational Mechanics, Vol.13, 1994, pp.360-379.
- [28] Cheung, Y.K. and Zhou, D., "Vibration analysis of symmetrically laminated rectangular plates with intermediate line supports", Journal of Computers and Structures, Vol. 79, 2001, pp.33-41
- [29] Kadivar, M.H. and Bohebpour, S.R., "Forced vibration of unsymmetrical laminated composite beams under the action of moving loads", Journal of Composites Science and Technology, Vol.58, 1998, pp.1675-1684.
- [30] Beytullah, T. Farouck, F.C. and Naki,T., "Forced vibration of composite cylindrical helical rods", International Journal of Mechanical Science, Vol.45, 2005, pp. 998-1022.

- [31] Azrar, I. Benamar, R. and White, R.G., "A Semi-analytical approach to the non-linear dynamic response problem of S-S and C-C beams at large vibration amplitudes Part I: General theory and Application to the single mode approach to free and forced vibration analysis", *Journal of Sound and Vibration*, Vol.224 (2), 1999, pp.183-207.
- [32] Farouk, F.C., "Free and forced vibrations of non-uniform composite beams", *Journal of Composite Structures*, 2008, 88 (2009), pp. 413–42.
- [33] Khdeir, A.A. and Reddy, J.N., "Buckling and Vibration of Laminated Composite Plates using Various Plate Theories", *AIAA Journal*, Vol.27 (12), 1989, pp.1808-1817.
- [34] Banerjee, J.R. and Williams, F.W., "The effect of Shear Deformation on the Critical Buckling of Columns", *Journal of Sound and Vibration*, Vol.174 (5), 1994, pp.607-616.
- [35] Khdeir, A.A. and Reddy, J.N., "Buckling of Cross-ply Laminated Beams with Arbitrary Boundary Conditions", *Composite Structures*, Vol.37 (1), 1997, pp.1-3.
- [36] Song, S.J. and Waas, A.M., "Effects of Shear Deformation on Buckling and Free Vibration of Laminated Composite Beams", *Composite Structures*, Vol. 37 (1), 1997, pp. 33-43.
- [37] Chen, L.W. and Peng, W.K., "The Stability Behavior of Rotating Composite Shafts under Axial Compressive Loads", *Composite Structures*, Vol.41 (3), 1998, pp.253-263.

- [38] Kim, C.G. Kyoung, W.M. and Hong, C.S., “Buckling and Post Buckling Behavior of Composite Cross-ply Laminates with Multiple Delaminations”, *Composite Structures*, Vol.43 (4), 1998, pp.257-274.
- [39] Matsunaga, H., “Vibration and Buckling of Deep Beam-Columns in Two-Parameter Elastic Foundations”, *Journal of Sound and Vibration*, Vol. 228(2), 1999, pp-359-376.
- [40] Lee, J. Kim, S.E. and Hong, K., “Lateral Buckling of I-section Composite Beams, *Engineering Structures*, Vol. 24 (7), 2002, pp-954-964.
- [41] Whitney, J.M., *Structural Analysis of Laminated Anisotropic Plates*, 1987, Technomic Publishing Company, Lancaster, Pa.
- [42] Abd EL-Maksoud , Mohamed, A., “Dynamic Analysis and Buckling of Variable-Thickness Laminated Composite Beams using Conventional and Advanced Finite Element Formulations”, M.A.Sc. Thesis, 2000, Concordia University, Montreal, Canada.
- [43] Cortinez, V.H. and Piovan, M.T., “Vibration and Buckling of Thin-walled Beams with Shear Deformability”, *Journal of Sound and Vibration*, Vol. 258 (4), 2002, pp-701-723.
- [44] Lee, J. and Kim, S.E., “Lateral Buckling Analysis of Thin-walled Laminated Channel-section Beams”, *Composite Structures*, Vol.56 (4), 2002, pp.391-399.

- [45] Ibrahim, M.D., "Effect of notch size on the reliability of composite laminates based on stochastic finite element analysis and experimental investigation", M.A.Sc. Thesis, 2000, Concordia University, Montreal, Canada.
- [46] Suarez, S.A. Gibson, R.F. and Deobald, L.R., "Random and impulse techniques for measurement of damping in composite materials", *Experimental Techniques*, 1984, pp.19-24.
- [47] Morison, W.D., "The prediction of material damping of laminated composites", *Journal of Canadian Aeronautics and Space*, 28(4), 1982, pp.372-382.
- [48] Hoa, S.V. and Ouellette, P., "Damping of composite materials", *Polymer Composite*, 5(4) 1984, pp.334-337.
- [49] Gibson, R.F., "Dynamical mechanical properties of advanced composite materials and structures: A review", *Shock and Vibration Digest*, 19(7), 1978, pp.13-22.
- [50] Adams, R.D. and Bacon, D.G.C., "Effect of fiber orientation and laminate geometry on the dynamic properties of CFRP", *Journal of Composite Materials*, 7(4), 1973, pp.402-428.
- [51] Zabaraz, N. and Pervez, T., "Viscous damping approximation of laminated anisotropic composite plates using the finite element method". *Computer Methods in Applied Mechanics and Engineering*, Vol.81 1990, pp.291-316.

- [52] Wei, C.Y. and Kukureka, S.N., "Evaluation of Damping and Elastic Properties of Composite and Composite Structures by the Resonance Technique", *Journal of Material Science*, Vol.35, 2000, pp. 378-392.
- [53] Adams, R.D. and Maheri, M.R., "Damping in Advanced polymer-matrix composite", *Journal of Alloys and Composite*, Vol.355, 2003, pp.126-130.
- [54] Sefrani, Y. and Bertholet, J.M., "Temperature Effect on the Damping properties of Unidirectional Glass-fiber Composite", *Journal of Composite Part:B*, Vol.37, 2006, pp.346-355.
- [55] Colakoglu, M., "Damping and Vibration Analysis of Polyethylene Fiber Composite under varied Temperature", *Turkish Journal of Engineering and Environmental Science*, Vol.30, 2006, pp.351-357.
- [56] Eslimy-Isfahay, S.H.R. and Banerjee, J.R., "Dynamic response of composite beams with application to aircraft wings", *Journal of Aircraft*, Vol.34, 1997, pp. 785-791.
- [57] Ewins, D. J., "*Modal testing: theory and practice*", 1984, Research Studies Press Ltd, London.
- [58] He, L., Wang, I. and Tang, D., "Dynamic responses of aircraft wing made of composite materials", *Proceedings of the 11th IMAC (International Modal Analysis Conference)*, Kissimme, Vol. 2, 1993, pp.1342-1346.
- [59] Koo, K.N. and Lee, I., "Dynamic behavior of thick composite beams", *Journal of Reinforced Plastics and Composites*, Vol.14, 1995, pp.196-210.

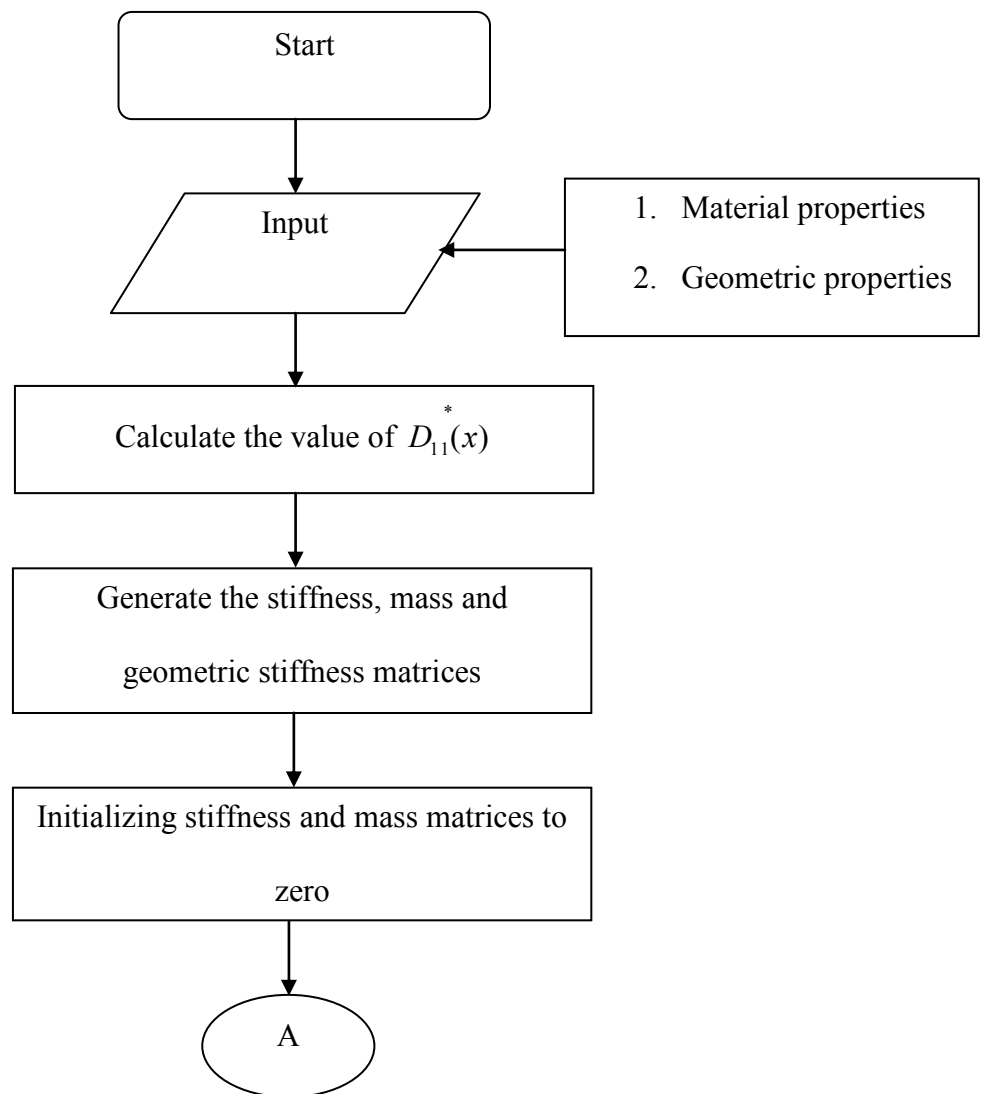
- [60] McConnel, K.G. and Varoto, P. S., *Vibration Testing: Theory and Practice*, 2<sup>nd</sup> edition, 2008, John Wiley & Sons, New York, NY.
- [61] Tsai, S. W. and Hahn, H. T., *Introduction to composite materials*, 1980, Technomic, Lancaster.
- [62] Halvorsen, W.G. and Brown, D.L., “Impulse Technique for Structural Frequency Response Testing”, *Journal of Sound and Vibration*, November, 1977, pp. 8-21
- [63] Klosterman, A., “On the Experimental Determination and Use of Modal Representations of Dynamic Characteristics”, Doctor of Philosophy Dissertation, Department of Mechanical Engineering, University of Cincinnati, 1971, pp. 184.
- [64] Potter, R.W., “A General Theory of Modal Analysis for Linear Systems”, *Shock and Vibration Digest*, November 1975, Volume 7.
- [65] Inman, D.J., *Engineering Vibration*, second edition, 2001, Prentice Hall, New York.
- [66] Nashif, A.D. Jones, D.I.G. and Henderson, J.P., *Vibration damping*, 1985, Wiley, New York.
- [67] Sodena, P.D. Kaddourb, A.S. and Hintonc, M.J., “Recommendations for designers and researchers resulting from the world-wide failure exercise”, *Composites Science and Technology*, 64, 2004, pp.589–604.
- [68] Zabihollah, H.E.U., “Vibration and buckling analyses of tapered composite beams using conventional and advanced finite element formulations”, M.A.Sc.Thesis, 2003, Concordia University, Montreal, Canada.

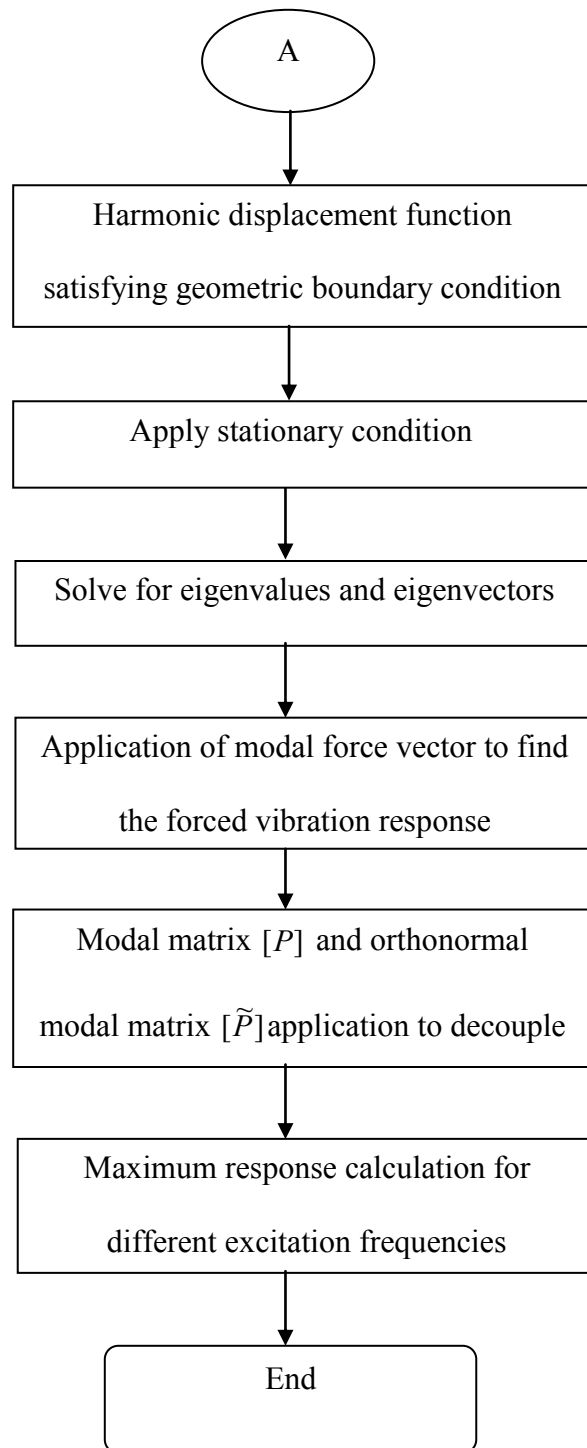
- [69] Ole Dossing, Bruel and Kjaer-Structural Testing-Part 1, April 1988.
- [70] Ole Dossing, Bruel and Kjaer-Structural Testing-Part 2, April 1988.
- [71] ASTM E 756-98, "Standard test method for measuring vibration-damping properties of materials".
- [72] Cawley, P., "Inspection of Composites – Current Status and Challenges", ECNDT 2006 - Mo.2.6.1.
- [73] National Research Council Canada (CNRC), "Laser Ultrasonic Inspection of Materials and Structures".
- [74] Krishnaswamy, S. Chandrashekhara, K. and Wu, W.Z.B., "Analytical solutions to Vibration of Generally Layered Composite Beams", Journal of Sound and Vibration, Vol.159 (1), 1992, pp.85-99.
- [75] Huebner, K.H., 1994, "*The finite element method for engineers*", J. Wiley, New York.
- [76] C. F. Beards, *Engineering Vibration Analysis with Application to Control Systems*, 1995, Edward Arnold.
- [77] Akhlaque-E-Rasul,S.M, "Buckling analysis of tapered composite plates using Ritz method based on classical and higher order theories", M.A.Sc.Thesis, 2005, Concordia University, Montreal, Canada.
- [78] S.K.Muzumdar., *Composites Manufacturing Materials, Product, and Process Engineering Method*, 2001, CRC Press.

- [79] A.K.Kaw., *Mechanics of Composite Materials*, Second Edition, 2005, CRC Press.
- [80] M.W.Hyer, *Stress Analysis of Fiber-Reinforced Composite Materials*, 2009, Destech Publications Inc.
- [81] Salajegheh, P., “Free and Forced Vibration response of internal width- and thickness-tapered composite beams using conventional and advanced finite element method”, M.A.Sc.Thesis, In Progress, Concordia University, Montreal, Canada.
- [82] Daniel, I.M and Ishai, O., *Engineering Mechanics of Composite Materials*, second edition, 2005, Oxford University Press, USA.

## APPENDIX-A

Flow chart for MATLAB<sup>®</sup> program for free and forced vibration and buckling response





The individual subroutine programs developed using MATLAB<sup>®</sup> software for free and forced vibration and buckling response of width-tapered and thickness- and width – tapered laminated composite beams with graphical plots for parametric studies are included in the *Vijay-thesis 2012 CD*<sup>®</sup> attached with this thesis.

**Trial functions used in Rayleigh-Ritz method for different boundary conditions**

| Boundary condition | Trial function   |
|--------------------|--|
| Simply Supported   | $w = \sum_{i=1}^n c_i \cdot \sin\left(\frac{i\pi x}{L}\right)$ |
| Fixed-Fixed        | $w = \sum_{i=1}^N c_i \cdot i \cdot x^i \cdot (L-x)^2$         |
| Fixed-Free         | $w = \sum_{i=1}^n c_i \cdot x^i$                               |
| Free- Fixed        | $w = \sum_{i=1}^n c_i \cdot (L-x)^i$                           |

## APPENDIX-B

### Derivation for orthonormal modal matrix $[\tilde{P}]$

#### Orthogonality of Eigenvectors

The normal modes, or the eigenvectors of the system, can be shown to be orthogonal with respect to the mass and stiffness matrices.

By using the notation  $\phi_i$  for the  $i^{\text{th}}$  eigenvector, the normal mode equation for the  $i^{\text{th}}$  mode is given as:

$$K\phi_i = \lambda_i M\phi_i \quad (1)$$

Pre-multiplying the  $i^{\text{th}}$  equation by the transpose  $\phi_j^T$  of the mode  $j$ , it is obtained as follows:

$$\phi_j^T K\phi_i = \lambda_i \phi_j^T M\phi_i \quad (2)$$

Also,

$$\phi_i^T K\phi_j = \lambda_j \phi_i^T M\phi_j \quad (3)$$

Because  $K$  and  $M$  are symmetric matrices, the following relationship are as follows:

$$\phi_j^T \begin{bmatrix} K \\ \text{or} \\ M \end{bmatrix} \phi_i = \phi_i^T \begin{bmatrix} K \\ \text{or} \\ M \end{bmatrix} \phi_j \quad (4)$$

Subtracting equation (3) from (2),

$$(\lambda_i - \lambda_j) \phi_i^T M \phi_j = 0 \quad (5)$$

If  $\lambda_i \neq \lambda_j$ , in the above equation (5), then equation (5) becomes,

$$\phi_i^T M \phi_j = 0, \quad i \neq j \quad (6)$$

It is also evident from equation (2) or equation (3) that as a consequence of equation (6),

$$\phi_i^T K \phi_j = 0, \quad i \neq j \quad (7)$$

Equations (6) and (7) define the orthogonal character of the normal modes.

If  $i = j$ ,

$$(\lambda_i - \lambda_j) = 0 \quad (8)$$

Equation (5) is satisfied for any finite value of the products given by equations (6) or (7),

$$\phi_i^T M \phi_i = M_{ii} \quad (9)$$

$$\phi_i^T K \phi_i = K_{ii} \quad (10)$$

From the equations (9) and (10),  $M_{ii}$  and  $K_{ii}$  are the generalized mass and generalized stiffness matrices.

**Orthonormal modes:**

If each of the normal modes  $\phi_i$  is divided by the square root of the generalized mass  $M_{ii}$ ,

It is evident from the equation (1), that the right side of the equation (9) will be unity.

The new normal mode is given as:

$$\frac{\phi_i}{\sqrt{M_{ii}}} = \tilde{\phi}_i \quad (11)$$

From the above equation (11),  $\tilde{\phi}_i$  is called the weighted normal mode or orthonormal mode.

It is also evident from equation (1), that the right side of the equation (10), will be eigenvalues  $\lambda_i$ .

Thus, the equations (9) and (10) can be written as:

$$\tilde{\phi}_i^T M \tilde{\phi}_i = 1 \quad (12)$$

$$\tilde{\phi}_i^T K \tilde{\phi}_i = \lambda_i \quad (13)$$

**Modal matrix  $[P]$  :**

When 'n' normal modes (eigenvectors) are assembled into a square matrix with each normal mode represented by a column, it is called the modal matrix  $[P]$

The modal matrix for a n- DOF system can appear as follows:

$$[P] = \left[ \begin{array}{cccc} \begin{Bmatrix} x_1 \\ x_2 \\ x_3 \end{Bmatrix}^1 & \begin{Bmatrix} x_1 \\ x_2 \\ x_3 \end{Bmatrix}^2 & \begin{Bmatrix} x_1 \\ x_2 \\ x_3 \end{Bmatrix}^3 & \dots, & \begin{Bmatrix} x_1 \\ x_2 \\ x_3 \end{Bmatrix}^n \end{array} \right] = [\phi_1 \quad \phi_2 \quad \phi_3 \dots \phi_n] \quad (14)$$

Also,

$$[P]^T = \left[ \begin{array}{cccc} \begin{Bmatrix} x_1 \\ x_2 \\ x_3 \end{Bmatrix}^1 & \begin{Bmatrix} x_1 \\ x_2 \\ x_3 \end{Bmatrix}^2 & \begin{Bmatrix} x_1 \\ x_2 \\ x_3 \end{Bmatrix}^3 & \dots, & \begin{Bmatrix} x_1 \\ x_2 \\ x_3 \end{Bmatrix}^n \end{array} \right]^T = [[\phi_1 \quad \phi_2 \quad \phi_3 \dots \phi_n]]^T \quad (15)$$

From the equation (14) and (15),

The results of  $P^T M P$  or  $P^T K P$ , will be diagonal matrix.

Thus,

$$P^T M P = \begin{bmatrix} M_{11} & 0 & 0 & 0 & 0 \\ 0 & M_{22} & 0 & 0 & 0 \\ 0 & 0 & M_{33} & 0 & 0 \\ 0 & 0 & 0 & \dots & 0 \\ 0 & 0 & 0 & 0 & M_{nn} \end{bmatrix} \quad (16)$$

$$P^T K P = \begin{bmatrix} K_{11} & 0 & 0 & 0 & 0 \\ 0 & K_{22} & 0 & 0 & 0 \\ 0 & 0 & K_{33} & 0 & 0 \\ 0 & 0 & 0 & \dots & 0 \\ 0 & 0 & 0 & 0 & K_{nn} \end{bmatrix} \quad (17)$$

Note from the above equations (16) and (17), the off-diagonal terms are zero, because of the orthogonality relationship.

The diagonal terms from equation (16) are generalized mass and from equation (17) are generalized stiffness.

If the normal modes  $\phi_i$  in the matrix  $[P]$  of equation (11) is replaced by the orthonormal modes  $\tilde{\phi}_i$ , the modal matrix is designated as  $[\tilde{P}]$

Thus, the orthogonality relationships are given as

$$[\tilde{P}]^T [M] [\tilde{P}] = [I] \quad (18)$$

$$[\tilde{P}]^T [K] [\tilde{P}] = [\Lambda] \quad (19)$$

where,  $[I]$  is the unit matrix and  $[\Lambda]$  is a diagonal matrix of the eigenvalues which is given as:

$$\Lambda = \begin{bmatrix} \omega_1^2 & & & \\ & \omega_2^2 & & \\ & & \dots & \\ & & & \omega_n^2 \end{bmatrix} \quad (20)$$

## **Contribution of numerical computation for dynamic response of thickness- and width-tapered laminated composite beams**

There is a significant contribution made in the numerical computation for the dynamic response of thickness- and width-tapered composite beams using the principle of superposition.

The steps followed are:

1. The detailed analysis for vibration response of uniform-width and thickness-tapered composite beams were made in the reference [68]
2. The stiffness, mass and geometric stiffness element matrices were determined for internally tapered composite beam for beam configurations A-D using finite element modeling.
3. Using the co-efficients of stiffness, mass and geometric stiffness matrices for uniform-width and thickness-tapered composite beams, and by using one-dimensional laminated beam theory the new co-efficients of stiffness, mass and geometric stiffness matrices for thickness- and width tapered composite beams are derived.
4. Individual subroutines programs using MATLAB<sup>®</sup> software were developed for dynamic response of thickness- and width tapered composite beams using R-R method.
5. The results obtained using Rayleigh-Ritz method were compared using conventional finite element method developed in [81] for validation purposes.

## APPENDIX-C

### Cost estimation report of width-tapered composite beams

Table 10.1 Manufacturing cost of width-tapered composite beams

| Sl.No.      | Description of materials                            | Cost        | Usage<br>(CAD \$) |
|-------------|---|-------------|-------------------|
| Fabrication |   |             |                   |
| 1           | NCT-301 graphite epoxy prepeg                       | \$25/lb     | 100               |
| 2           | Bleeder plies                                       | \$100       | 0                 |
| 3           | Breather plies                                      | \$148gallon | 20                |
| 4           | Vacuum or sealant tape                              | \$7/yard    | 25                |
| 5           | Aluminium flat plate                                | \$7/yard    | 25                |
| 6           | Brush   | \$5         | 5                 |
| 7           | Release agent                                       | \$5         | 5                 |
| 8           | Miscellaneous supplies (hand shovel, scissors etc.) | \$15        | 15                |
| Processing  |   |             |                   |
| 9           | Autoclave usage                                     | \$20/hr     | 30                |

|   |   |          |     |
|---|---|----------|-----|
| 10  | Manpower cost                           | \$50/day | 75  |
| 11  | Water cooled rotary type diamond cutter | \$10/hr  | 20  |
| Total usage cost/composite laminate plate |   |          | 320 |
| Total beams manufactured                  |   |          | 5   |
| Manufacturing cost of each beam           |   |          | 64  |

Laminate Configuration of composite laminate plate-  $([0/90]_9)_s$

Table 10.2 Dimension of composite laminate plate

| Sl.No. | Dimension | Size (inch) |
|--------|-----------|-------------|
| 1      | Length    | 16          |
| 2      | Width     | 11          |
| 3      | Height    | 0.1755      |

Table 10.3 Vibration testing cost of composite beams

| Sl.No.                         | Description of materials                               | Cost     | Usage<br>(CAD \$) |
|--------------------------------|--|----------|-------------------|
| 1                              | Clamping fixture                                       | \$40     | 100               |
| 2                              | Bees wax   | \$10     | 0                 |
| 3                              | Computer   |          | 0                 |
| 4                              | B & K's PULSE™ front-end multi-analyzer type 3560      |          | 0                 |
| 5                              | Charge amplifier (a) Dual mode amplifier               |          | 0                 |
|                                | (a) Piezoelectric charge amplifier                     |          | 0                 |
| 6                              | Impact hammer  |          | 0                 |
| 7                              | Accelerometer  |          | 0                 |
| 8                              | Impact excitation                                      |          | 0                 |
| 9                              | Miscellaneous supplies (cables, scissors, marker etc.) | \$50     | 50                |
| 10                             | Manpower cost  | \$50/day | 200               |
| Total vibration testing        |  |          | 350               |
| Vibration testing of each beam |  |          | 70                |